UiT The Arctic University of Norway

Faculty of health
Institute of Medial Biology

Novel screening methods for nanoscale changes in liver cell fenestrations elicited by pharmaceuticals

Application of super-resolution microscopy and advanced image analysis methods for development of new therapeutics against ageing and liver diseases

Karolina Szafranska

A dissertation for the degree of Philosophiae Doctor

August 2022

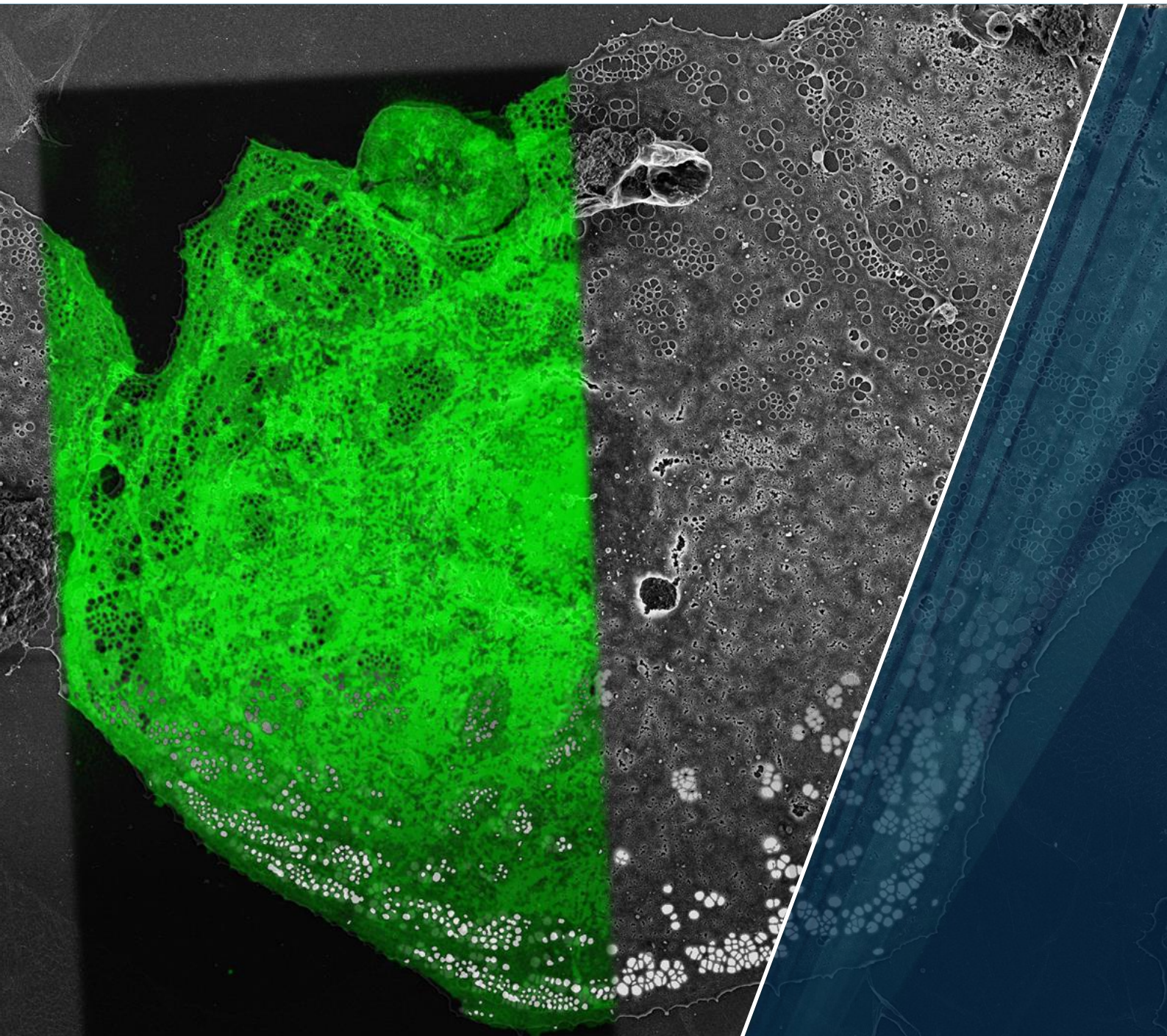

Novel screening methods for nanoscale changes in liver cell fenestrations elicited by pharmaceuticals

Application of super-resolution microscopy and advanced image analysis methods for development of new therapeutics against ageing and liver diseases

Karolina Szafrańska

A dissertation for the degree of Philosophiae Doctor

Vascular Biology Research Group
Department of Medical Biology
Faculty of Health Sciences
UiT – The Arctic University of Norway

August 2022

Table of Contents

Acknowledgements

The main funding for this project was received from the European Union's Horizon 2020 research and innovation programme under the Marie Skłodowska-Curie grant agreement no. 766181, project "DeLIVER". Parts of this work were also supported by the Research Council of Norway, Grant no. 288565 "NANO2021", Polish National Science Centre under the "SYMFONIA 3" project, grant agreement no. UMO-2015/16/W/NZ4/00070 and "SONATA 15" project, grant agreement no. UMO-2019/35/D/NZ3/01804.

This project was realised under the supervision of Prof. Peter McCourt, Prof. Karen Sørensen and Dr Bartłomiej Zapotoczny. I am deeply grateful for their guidelines and support in both scientific and personal life throughout the four years of my PhD. The PhD time is challenging even without the issues like the closure of UiT animal facility or a global pandemic but I believe that I was in the best possible place with the best people to overcome all of these obstacles.

First, I would like to thank my supervisor, Peter, who back in 2017 at the ISCHS conference in Galway, Ireland, met me – a random Polish master student – and offered me a PhD position (at the end of the world). I am so grateful for the warm welcome to Tromsø, I would never expect to be greeted by the institute leader! Thank you for believing in me and for dealing with my scepticism. I hope the next four years of our work together will be even better than the previous ones.

Next, but equally first, I would like to thank my mentor and scientific brother Bartek. I am so glad that we could continue working on LSEC together even after I left the country. Thank you for all the support, for all the long days in the lab and for constantly motivating me. Special thanks also to your wonderful family for coming to Tromsø. I know that whatever the future will bring we can always count on each other.

This project would not be possible without our McTeam of McKids – Larissa, Christopher, Tetyana, (and unofficial member Eike). I feel lucky to be able to collaborate with you all. We went together through all the good and horrible times, and I cannot imagine doing it with a different team. Thank you all for all the support inside and outside of work and for pushing some extra work-life balance onto me. Larissa and Eike – extra thanks for the constant supply of chocolate, Tetyana – thank you for looking at me like I know what I am doing even if I have absolutely no idea, Christopher – thank you for dealing with me 24/7 and support when I really needed it.

Special thanks to the whole Vascular Biology Research Group. It was a great experience to be a part of the VBRG family, even on Fridays without the cake meeting. I am extremely grateful to Prof. Karen Sørensen for the supervision, even if short our meetings always gave me so much precise and condensed knowledge that I regret not asking them years before. Many thanks to the technical team – Gianina, Ruomei and Jaione for your help especially with the animal experiments but also for sharing your knowledge of survival as foreigners in Norway. I would also like to thank our former group leader Prof. Bård Smedsrød for sharing his insight

into the LSEC world and coming to the office just to bring me copies of old german research articles. Thank you Ingelin, Sabin, Javier, Anett and Kjell for your support and creation of this warm, family-like atmosphere at VBRG. I would also like to thank Cristina for always constructive criticism and for sharing the knowledge and experience.

I would like to acknowledge all my co-authors, collaborators and colleagues. Special thanks for all ERSs from the DeLIVER ITN project. The survival of the Hurtigruten meeting in the middle of the storm will never be forgotten. I would like to acknowledge all the help I received from the Nanoscopy group at UiT, especially from Deanna who was always ready to help and save me, my samples and the microscope. I'd also like to extend my gratitude to Tom and Randi from the UiT core facility for sharing their knowledge and experience and guiding me through the world of electron microscopy. I am also grateful for all the opportunities from the research team at the Anzac Research Institute in Sydney and the Sydney University of Technology (UTS).

I also wish to thank everyone who I worked with in Poland for all the scientific and life experiences I brought with me to Tromsø. Especially colleagues from the Department of Physics of Nanostructures and Nanotechnology UJ and Jagiellonian Centre for Experimental Therapeutics.

I cannot begin to express my thanks to Christopher who lived with me through all the hardships of a PhD student life. Thank you for dealing with me both at work and at home and for supporting me on many days of late-night lab work.

Finally, getting to this point in my life would not be possible without my parents. I am grateful for all your support and for allowing me to pursue my goals.

Na koniec chciałabym podziekować moim rodzicom za wsparcie w całej mojej edukacji. Bez was i waszej cierpliwości do moich czasem szalonych pomysłow nie udało by mi się dotrzeć tu gdzie jestem. Zawsze będę wdzięczna za ogromne zaufanie którym obdarzaliście mnie od najmłodszych lat.

~~*“The easiest way to solve a problem is to deny it exists.”*~~

~~~ Isaac Asimov~~

“The most exciting phrase to hear in science, the one that heralds new discoveries, is not ‘Eureka!’ but ‘That’s funny…’”

~ Isaac Asimov
~~~

Summary

This thesis focuses on liver sinusoidal endothelial cells (LSEC) and their characteristic features called fenestrations. LSEC line the hepatic sinusoids and provide blood filtration. The bidirectional transport of solutes between the bloodstream and the interior of the liver is facilitated via transcellular nanopores called fenestrations. These structures are 50-350 nm in diameter, which is in large part below the resolution limit of conventional light microscopy. Fenestrations are dynamic structures that can react to various drugs and adapt their diameter and/or number within minutes or even seconds. Both the number and diameter of fenestrations are important for the maintenance of proper liver functions.

Various agents were shown to have an effect on LSEC fenestrations. Here we gathered the literature about existing drugs, both recreational and prescription ones, as well as other agents that influence fenestrations. This revision also contains/covers the description of different hypotheses about fenestration structure, regulation, and dynamics. Moreover, the analysis of previously used imaging techniques and image analysis methods allowed us to propose novel more efficient ways of studying LSEC. The application of machine learning and batch processing enabled the analysis of large datasets of hundreds or even thousands of images. Those methods were used in the next studies to quantitatively describe LSEC porous morphology.

The differences in the reported values of parameters describing fenestrations, such as fenestration diameter, fenestration frequency and porosity, depend mainly on the used imaging technique but also on sample preparation and image analysis method. Combination of different types of microscopies in a correlative manner allowed better understanding of those differences. Especially, the fenestration size can be influenced by the different types of fixations – wet, characteristic for optical techniques and dry for electron microscopy. The drying-related shrinkage of the cell body results in about 30% increase in the fenestration diameter. Also, various fixative agents influenced the measured diameter of fenestrations from atomic force microscopy images.

In the last part, the influence of xanthines was studied with the application of the previously optimized imaging techniques and image analysis methods. Xanthines such as caffeine and theobromine can be found in food and beverages but also in asthma medications – theophylline. The results of *in vitro* treatment of LSEC showed that in physiologically relevant concentrations (8-20 μg/ml, achievable by consumption of xanthines containing products) xanthines have no negative effects and theobromine increased the number of fenestrations. In high concentrations, all xanthines increased fenestration number which may find a future application using targeted delivery to avoid systemic side effects.

Paper I

Karolina Szafranska, Larissa D Kruse, Christopher F Holte, Peter AG McCourt, Bartlomiej Zapotoczny, **The wHole Story About Fenestrations in LSEC,** 2021, *Frontiers in Physiology*

https://doi.org/10.3389/fphys.2021.735573

Paper II

Karolina Szafranska, Tanja Neuman, Zbigniew Baster, Zenon Rajfur, Oskar Szelest, Christopher Holte, Agata Kubisiak, Edyta Kus, Deanna L. Wolfson, Stefan Chlopicki, Balpreet S. Ahluwalia, Malgorzata Lekka, Marek Szymonski, Peter McCourt, Bartlomiej Zapotoczny, **From fixed-dried to wet-fixed to live – comparative super-resolution microscopy of liver sinusoidal endothelial cell fenestrations**, 2022, *Nanophotonics*

https://doi.org/10.1515/nanoph-2021-0818

Paper III

Karolina Szafranska, Christopher F Holte, Larissa D Kruse, Hong Mao, Cristina Ionica Øie, Marek Szymonski, Bartlomiej Zapotoczny, Peter AG McCourt, **Quantitative analysis methods for studying fenestrations in liver sinusoidal endothelial cells. A comparative study**, 2021, *Micron*, vol 150

https://doi.org/10.1016/j.micron.2021.103121

Paper IV

Hong Mao, Karolina Szafranska, Larissa Kruse, Christopher Holte, Deanna L. Wolfson, Balpreet Singh Ahluwalia, Cynthia B. Whitechurch, Louise Cole, Glen P. Lockwood, Robin Diekmann, David Le Couteur, Victoria C. Cogger, Peter A.G. McCourt, **Effect of caffeine and other xanthines on liver sinusoidal endothelial cell ultrastructure**, 2022,

Under review

ABC - ATP-binding cassette

AFM - atomic force microscopy

BSE – backscattered electrons

CYP - Cytochrome P450 (enzymes)

DFC - defenestration centre(s)

dSTORM - direct stochastic optical reconstruction microscopy

EM – electron microscopy

FA – formaldehyde

FACR - fenestrae-associated cytoskeletal ring

FFC - fenestration forming centre(s)

FIB(-SEM) - focused ion beam (scanning electron microscopy)

FSA - formaldehyde-treated serum albumin

GA – glutaraldehyde

HDL – high-density lipoproteins

HMDS – hexamethyldisilazane

HSC - Hepatic stellate cells

LDL - low-density lipoproteins

LSEC – Liver Sinusoidal Endothelial Cell(s)

MLC – myosin light chain

MPC - mononuclear phagocyte system

NAFLD - Non-alcoholic fatty liver disease

NASH - non-alcoholic steatohepatitis

NL- SIM - non-linear Structured Illumination Microscopy

OTF - optical transfer function

PDE – phosphodiesterase

PKC - protein-kinase-C

PRR - pattern recognition receptor

PSF - point spread function

QPM - quantitative phase microscopy

RES - reticuloendothelial system

ROCK - Rho-associated protein kinase

SE – secondary electrons

SEM – scanning electron microscopy

SIM - Structured Illumination Microscopy

STED - stimulated emission depletion (microscopy)

TEM - transmission electron microscopy

TIRF - total internal reflection

TLR - toll-like receptor

VEGF - vascular endothelial growth factor

vWF - von Willebrand factor

This thesis is the result of interdisciplinary work connecting molecular and cell biology with physics, biophysics, and computational studies as a means to better understand medically relevant problems. This introduction may not contain all the available information required to fully comprehend the background but rather aims to fill the gaps between those disciplines and provide a better understanding for a reader from any related field of study.

1 Liver

The liver is the largest solid internal organ and is responsible for a variety of biological functions, such as blood clearance of metabolites, detoxification, protein synthesis and glucose metabolism regulation but it also has a role in immune reactions. Every few minutes the equivalent of the whole blood volume flows through the liver. There are two main blood sources for the liver (Figure 1): about 75% comes from the portal vein system, consisting of the low-oxygen/high nutrient venous blood and the remaining 25% comes from the hepatic artery as a high-oxygen systemic circulation arterial blood [1]. This structure has some important implications, especially for drug development and liver toxicity. The "first-pass" effect means that molecules absorbed via the gastrointestinal tract will first enter the liver before reaching the systemic circulation [2]. The low fraction of the arterial blood also indicates that hepatic cells are physiologically exposed to low oxygen levels (about 5%) *in vivo* [3].

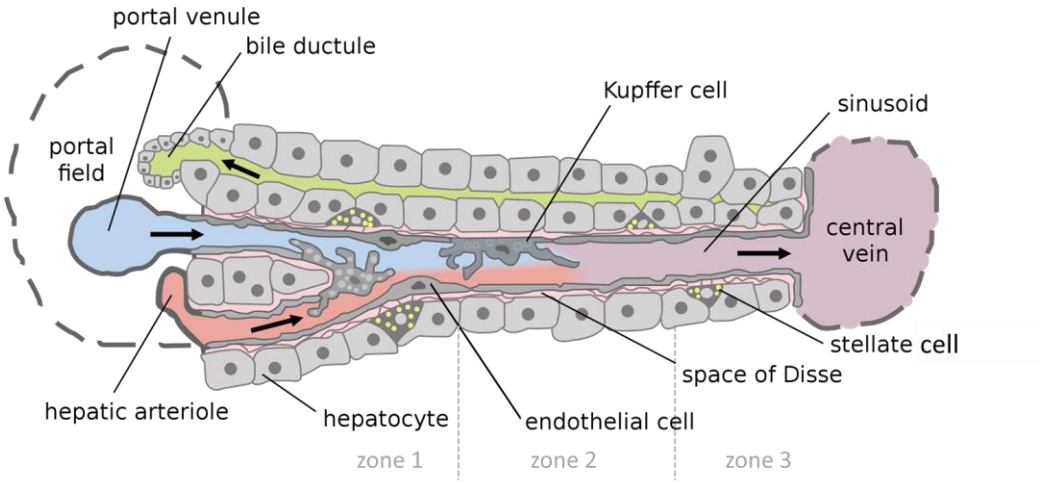

Figure 1 Schematic structure of the liver sinusoids. Reproduced from [253].

The internal structure of the liver is connected to its filtering function. The entering blood vessels branch forming small tubular channels, called sinusoids, with a mean diameter of about 8 µm – roughly the diameter of a red blood cell [4][5]. Sinusoids are lined with fenestrated endothelial cells (liver sinusoidal endothelial cells: LSEC) which regulate the active and passive transport between plasma and the space of Disse to which the hepatocytes are exposed. In the

middle of each lobule, the central vein collects blood from the sinusoids. About 85% of liver volume constitutes hepatocytes and other cells, while sinusoidal lumen and space of Disse occupy 10% and 5% respectively [6].

The phenotypes of both hepatocytes and LSEC change within their localization along with the sinuses, therefore establishing a defined zonation (Figure 1). Zone 1 (periportal) consists of the cells in the area close to the portal vein, then follows zone 2 (midzonal) then ends with zone 3 (centrilobular) around the central vein [2]. Between zone 1 and zone 3 the size of the sinusoids increases, changing from about 6.5 μm to > 8.5 μm [7][8], the pressure within sinusoids thus decreases [7] and blood flow increases [9][10], LSEC fenestration size slightly decreases while fenestration number increases [4][11][8]. The zonation reflects the gradual reduction of the available oxygen which influences the gene expression by hypoxia-inducible factors [12]. Hypoxia-inducible factors regulate major metabolic liver functions – gluconeogenesis, lipogenesis, insulin levels and protein degradation [13]. Moreover, many enzymes present graded expression across the lobules - β-oxidation enzymes decrease toward the central vein while enzymes involved in lipid synthesis are present mostly in the centrilobular region and gradually diminish toward the periportal zone [14].

Hepatocytes are the major cells in the liver and constitute 92% and 65% of the total cellular volume and number respectively [6]. They are also referred to as liver parenchymal cells and are responsible for many functions of the liver, such as glucose storage, lipid metabolism, production of albumin, bilirubin and many other molecules, as well as metabolism and elimination of various drugs and toxins via their CYP enzyme system [15]. The three other major cell types present in the liver sinusoids are Kupffer cells, hepatic stellate cells and LSEC with a cell number distribution of 20%, 10% and 70%, respectively [16]. Kupffer cells are located mainly in the luminal side of sinusoids and are responsible for the clearance of insoluble particles, pathogens, endotoxins and various other molecules. Hepatic stellate cells are pericytes residing in the space of Disse. They play a role in signalling between hepatic cells and remain mostly quiescent in the healthy liver but became activated in the progression of many liver diseases. LSEC line the hepatic sinusoids and regulate transport from the blood inside the liver (detailed description in the next section).

Other cells are also present in the liver – these are cholangiocytes (epithelial cells that line the bile ducts); liver-resident lymphocytes (multiple types involved in the maintenance of liver homeostasis); macrovascular endothelial cells (present in blood vessels before branching into

sinusoids); liver progenitor cells (dedifferentiated hepatocytes or cholangiocytes present during liver regeneration). All types of cells present in the liver have an important role on their own but also the cross-talk between them is crucial for the maintenance of the healthy state of the liver.

2 Liver sinusoidal endothelial cells (LSEC)

In LSEC research terms *in vitro* and *in vivo* are used to describe two main sample sourcing approaches (Figure 2). The experiments performed on the isolated cells are referred to as *in vitro*, Latin for "in/on the glass". Term *in vivo*, Latin for "within the living" refers to either experiment on animals treated with selected agents or in fenestration focused research it refers to the observation of tissue samples - both sections and tissue blocks.

2.1 A brief history of fenestration research

LSEC are a highly specialized type of endothelial cells with distinct morphological features – 50-350 nm transcellular pores called fenestrations (or fenestrae). The breakthrough in the history of hepatic sinusoid wall studies started in 1955/1956 when Fawcett [17] and Parks [18] challenged the wide acceptance of a continuous sinusoidal endothelial lining. Their electron micrographs showed regular gaps in the irregularly shaped endothelial cells. They did not find it compelling enough to announce as a new structure, but they distinguished them from other sample preparation artefacts. In 1958, Wassermann [19] revised the previous reports and stated that this regional discontinuity in the liver sinusoids may indeed contribute to a filtration function. Moreover, he suggested for the first time that these openings may be a flexible, dynamic structure. A year later, the final, widely accepted proof of fenestration existence came from Yamagishi [20], thanks to great improvements in sample preparation. Around the same time the term "liver fenestrations" came in use thanks to similarities to already known structures in the kidney and the parathyroid gland [21][17]. Further developments in liver perfusion and more complex fixation methods allowed better preservation of these delicate structures and enabled observation of fenestrations in a new, detailed way.

In 1970, Wisse's study [22] marked the next era of fenestration research and set directions for finding the ultrastructure of those pores as well as exploring various agents that influence them. At the same time, methods to isolate different liver cells, including LSEC, were developed. Thanks to these, *in vitro* studies gave complementary information to the previous

in vivo data. Until the late 1990s, electron microscopy remained the main technique used for the observation of LSEC morphology. Both scanning electron microscopy (SEM) and transmission electron microscopy (TEM) require extensive sample preparation that includes dehydration which can affect fenestrations, as reported in the early studies observing numerous artefacts [17][19]. To overcome these dehydration issues, atomic force microscopy (AFM) was applied to investigate the effects of both drying and different wet-fixation methods [23][24]. The development of AFM technology at that point in time allowed the visualisation of fenestrations, however, the interaction between the scanning probe and the sample proved to be destructive [25][26]. Later, attempts were made to observe live LSEC [27] but it was not possible without the further development of new, more gentle AFM technologies. In 2017, as a master student, I was a part of the team that using near forceless imaging, confirmed the dynamic nature of fenestrations [28] and estimated the fenestration lifespan to be about ~20 minutes [29].

In parallel, the development of optical microscopy occurred. The size of most fenestrations (50-350 nm) is below the resolution capabilities of regular light microscopy (about 200 nm). Therefore, super-resolution techniques are necessary to study LSEC morphology with optical methods. The first reported attempts were made in 1996, by Gatmaitan et al. [30]. The presented video-intensified fluorescence microscopy images showed some improvement in quality, but the resolution was still not optimal. Nevertheless, the authors performed image analysis on actin stained LSEC and showed some differences in size after treatments. This method did not stay within the field and electron microscopy (EM) and AFM remained the main fenestration visualization tools until the development of new types of super-resolution microscopy modalities in the early 2000s. In 2010, Cogger et al. [31] showed the possibilities to investigate LSEC with Structured Illumination Microscopy (SIM). Using cell membrane dyes the authors measured fenestration size distribution that was in agreement with the EM and AFM studies. Later other super-resolution techniques were also used to study the structure of fenestrations in LSEC – direct stochastic optical reconstruction microscopy (dSTORM) [32] and stimulated emission depletion (STED) microscopy [33]. In recent years, combinations of more than one imaging technique are becoming popular to further investigate fenestrations. Correlative SIM-dSTORM [32] and quantitative phase microscopy QPM-dSTORM [34] gave extra insights into the relationship between cytoskeleton and fenestrations and cell height, respectively. Recently, also nanophotonic chip-based approaches have been shown as a viable option to reduce the

costs of optical-super resolution imaging [35] and to effectively combine dSTORM and focused ion beam-scanning electron microscopy (FIB-SEM) to study LSEC.

2.2 Fenestrations

Fenestration size and number

LSEC facilitate passive transportation of particles below ~300 nm via transcellular pores called fenestrations gathered in groups of 5-100 pores, termed sieve plates [36]. The fenestration diameter – 50-350 nm, plays an important role in the selectivity of filtration. The actual size of fenestrations is not easy to determine due to large differences between reported values from different experiments [4][29]. Sample preparation, fixatives, imaging techniques and analysis methods can influence the obtained measurements **(Paper II)**[37]. In general, all holes in the sinusoids above 350 nm diameter are considered non-physiological gaps. The number of fenestrations per area (the parameter called fenestration frequency) varies between the species [4] but also between the cells in the liver due to the zonation (Figure 1)[38]. Normally, the mean fenestration frequency *in vitro* is in the range of about 2-10 per μm^2 and porosity (percentage of the cell area covered by fenestrations) of 4-8% [4][39].

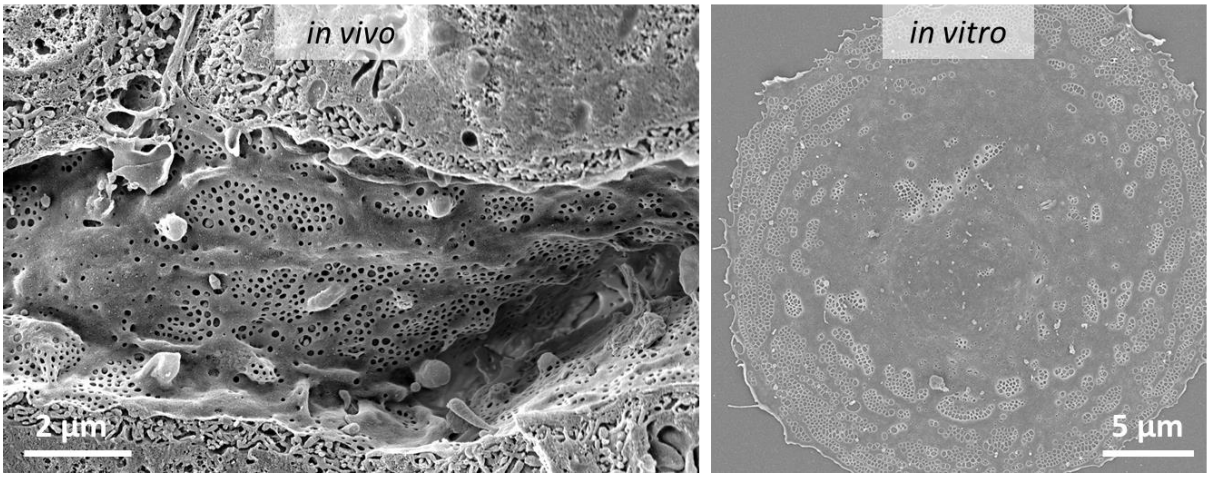

Figure 2 SEM images of the fenestrated morphology of mouse LSEC in tissue/in vivo and after isolation/in vitro. Left image reproduced from [42]. Courtesy of Karen K. Sørensen, UiT, Tromsø, Norway.

Fenestration structure

Up to date, the exact structure of fenestration remains unknown. The fenestrae-associated cytoskeletal ring (FACR) was proposed by Braet et al. [40] but its chemical composition has not been confirmed. Later, actin was shown to surround fenestrations, creating a mesh-like structure [32]. These findings support the results of the effects of multiple actin targeting agents on LSEC morphology [41][42]. Recently, spectrin has been shown to have a regulatory role in

the structural preservation of fenestration, supporting its open and closed state [43]. Little is known about other proteins building the fenestrations, but there have been several attempts to identify them based on similarities to other structures. Caveolae (Latin for "little caves") are 50-100 nm invaginations in the cell membrane, formed and maintained by the caveolin protein [44]. Considering that fenestrations resemble caveolae in both size and appearance and that caveolin-1 was found to colocalize with fenestrations, it became an interesting probable explanation of fenestration structure [45][46]. To investigate that, Warren et al. [47] used the caveolin-1 knockout mice but found no difference in the fenestration size or number in comparison to wild type mice. This result showed that fenestrations are not a form of caveolae nor are they dependent upon caveolin-1.

A relationship between lipid rafts and fenestrations was proposed by Svistounov [48] and Cogger [49]. Fenestrations appear to be formed in the membrane raft-free areas and disruption and induction of lipid rafts led to an increase and decrease in the fenestration number *in vitro*, respectively [48]. The interesting flat microdomains of non-raft membrane areas have been observed by both SIM and AFM [50] and may be connected with previously described fenestration forming centres (FFC) [51]. Moreover, there is a clear interdependence between fenestrations and cytoskeleton, however, not much is known about the way in which cell membrane connects to actin fibres in LSEC. There are various anchoring proteins that are good candidates for this role (such as adducins), and the lipid composition in the cell membrane would have an effect on the organisation and integration into bilayers, possibly affecting fenestrations.

Fenestra forming and defenestration centres (FFC and DFC)

The FFC structure is not well defined, but its appearance precedes rapid *de novo* formation of new fenestrations after treatment with some agents, mostly actin disruptors such as misakinolide [52] or jasplakinolide [29]. However, fenestrations can be also formed outside FFC. Another fenestration related structure is the defenestration centre (DFC), reported for the first time *in vivo* in tissue samples [53] and later *in vitro* using AFM [29]. In these areas, the whole sieve plates full of fenestrations rise above the cell body and then are expelled to quickly decrease the fenestration number. *In vitro* DFCs were only observed in the treated cells, never in *in vivo* conditions.

Fenestration dynamics

Wasserman [19] predicted early in 1958 that fenestrations should be dynamic structures to fully regulate the filtration in the liver. His hypothesis was confirmed almost 60 years later when live cell imaging became possible by AFM [50]. Fenestrations are dynamic structures that can open and close within seconds [43] and appear or disappear independently of each other [29]. There is no technique allowing to study of the dynamics of fenestrations *in vivo* but *in vitro* data suggest that isolated LSEC undergo quick morphological changes in the first hours in cell culture while spreading on the surface [29]. Fenestrations can form in the flat areas between the thicker actin stress fibres and move together with the cell body in the migrating cells. After a few hours of culture, primary LSEC morphology became more stable but remained responsive to stimuli, such as cytochalasin D [33].

Live imaging data showed that fenestrations can keep appearing and disappearing in minutes without the influence of any external stimuli. The mean lifespan of fenestrations was estimated to be about 18 minutes, but some holes can remain open for hours while some fractions can exist for only a few minutes at a time [29]. If those observations can be translated into *in vivo* conditions, it means that LSEC can rapidly adjust their filtering capabilities. Also, the large openings (>350 nm), normally considered gaps, showed similar dynamics as fenestrations. Some gaps can open and close or even fuse together while remaining functional, however, they have not been observed in tissue samples.

2.3 LSEC scavenging

In mammals, LSEC constitute the most efficient scavenger cell system [54], historically called “reticuloendothelial system” (RES) [55]. The term was first proposed by Aschoff in 1924 in relation to the cells accumulating some “vital stains” (colloidal lithium carmine)[56]. Later in the 1960s, as the phagocytic properties of RES and macrophages seemed the same, it was proposed to replace the term RES with mononuclear phagocyte system (MPC) [57]. Finally, in 1998, the novel cell isolation methods in combination with the original “vital dyes” identified LSEC as the main cells responsible for the dye uptake with just minor incorporation in Kupffer cells and monocytes [55].

The placement of LSEC, which uniquely expose them directly to nutrient and macromolecule rich blood from the portal vein, plays a crucial role in their filtering function. LSEC contribute to the filtering in the liver not only by forming the dynamic barrier but also

by active uptake of many blood-borne macromolecules via clathrin-mediated endocytosis [58][59][54][60][61]. Early studies revealed that the ultrastructure of LSEC is full of coated pits in the plasma membrane and intracellular vesicles suggesting a high endocytic capacity [62]. Later, several high-affinity endocytosis receptors, as well as a high-capacity lysosomal degradation system, have been described. This allows efficient uptake and elimination of circulating biomolecules such as hyaluronan [61], collagen alpha-chains [63], heparin [64], modified proteins and lipoproteins [65][66], soluble IgG complexes [67] but also viral pathogens [68]. This clearing function is especially important as many of these macromolecules are not taken up at all, or just to a small degree, by other cell types [58].

Clathrin-mediated endocytosis is the main scavenging mechanism in LSEC [69]. LSEC express many endocytosis receptors [70], however, when it comes to LSEC scavenger function, the most studied are the two members of scavenger receptor H family – stabilin 1 and 2 [71][72], the mannose receptor [63], and FcγRIIb2 [73]. In *in vitro* LSEC studies, the endocytic capacity can be used to assess the functional viability of the cells [74][75]. The best candidate for this assay is the high-affinity scavenger receptor ligand formaldehyde-treated serum albumin (FSA).

Serum albumin in its native form is cleared very slowly from the bloodstream, while denaturated forms such as FSA was shown to be removed rapidly (within minutes) [76][65]. FSA is a very stable soluble macromolecule taken up by LSEC via both stabilin-1 and -2 receptors [71][77] and can be easily labelled with fluorescent tags (for example with FITC or AlexaFluor dyes) or radioactive isotopes, such as ^{125}I.

2.4 Other functions of LSEC

The scavenging capacity of LSEC is closely related to their role in the immune response. The presence of pattern recognition receptors (PRRs), such as scavenging receptors or toll-like receptors, allows clearance of various pathogens, such as exogenous ligands, DNA fragments or endotoxins [54][78]. It is especially important as LSEC are constantly exposed to the blood flowing directly from the gastrointestinal tract [79]. PRRs can recognise lipopolysaccharides of Gram-negative bacteria (via toll-like receptor (TLR) 4) and CpG-motif DNA, which is abundant in microbial genomes (via TLR 9) [80]. FcγRIIb2 allows extensive recycling of small soluble IgG immune complexes [81] which play an important role in maintaining homeostasis within the liver. Scavenging receptors and toll-like receptors can also activate signalling

pathways within the cell promoting proinflammatory responses by expression of interleukin-6 and tumour necrosis factor α [82]. Under inflammatory conditions, LSEC can also act as an antigen presenting cell and activate immunogenic T cell responses and enhance leukocyte recruitment to the sinusoid [83][84]. Interestingly, the small size and low shear stress of the sinusoids resulted in the lack of rolling in the recruitment of leukocytes and therefore low levels of selectins [85]. Additionally, LSEC fenestration may regulate the communication between hepatocytes and other immune cells [86]. This probing of T cells through the fenestrations has an important role as it allows them to reach the hepatocytes presenting e. g. viral antigens [86].

LSECs are involved in blood clearance of virus and virus-like particles and were reported to be responsible for liver-mediated removal of adenoviruses [87], BK- and JC polyomavirus-like particles [68], HIV-like particles [88] as well as inhibition of replication of hepatitis C virus [89]. Interestingly, a preliminary study suggests that LSEC might have a key role in the liver injury caused by COVID-19. Infection with the SARS-CoV-2 virus causes activation and proinflammatory response in LSEC in human patients which creates a procoagulant phenotype that can trigger platelet aggregation [90].

2.5 LSEC in health and disease

In the healthy liver, LSEC present their characteristic fenestrated morphology, lack of basement membrane and thin cell body lining the sinusoids. There are many markers of LSEC in health-related to their functions: high scavenging activity, secretion of various molecules, regulation of immune homeostasis in the liver, and crosstalk with other liver cells [59][91]. Disturbance in any of these functions can lead to the development or progression of various liver diseases (reviewed in [92][93]). Also, with ageing, LSEC functions slowly deteriorate [94]. These age-related changes such as endothelium thickening and loss of fenestrations [95][96], decreased endocytic activity [74], and collagen deposition in the space of Disse [97], can have important systemic implications also for the development of other age-related diseases [98].

Both the size and number of fenestrations are important in maintaining proper liver functions. Chylomicron remnants, high- and low-density lipoproteins (HDL, LDL) are metabolised by hepatocytes but must first be transported to the space of Disse via the fenestrations [99]. Any disturbances in this process can lead to the accumulation of the particles in the bloodstream which may have severe health consequences leading to dyslipidaemia and

atherosclerosis [100][101]. These findings are in agreement with the observation of smaller fenestrations in rabbit and chicken and their high prevalence of hyperlipoproteinemia, as compared to the larger fenestrations in mice and rats which are less prone to develop atherosclerosis [102][103]. The number of fenestrations in LSECs is responsible for the filtration rate while the size of fenestrations has implications for filtration selectivity. For example, HDL and LDL have diameters below 100 nm, while chylomicron remnant size is usually above 100 nm [99]. Changes in the distribution of fenestration size such as a reduction in the number of holes >100 nm, can significantly reduce the clearance of chylomicrons [101][104]. Proper filtration of this cholesterol-rich fraction has important implications for cholesterol metabolism in parenchymal cells preventing the development of atherosclerosis lesions [101]. On the other hand, higher admission of fat into the space of Disse, due to increased size and/or number of fenestrations, may promote fatty liver [105].

LSEC capillarization and pseudocapillarisation

The loss of fenestrations and development of basement membrane is called capillarization, due to the resemblance in phenotype to common capillary endothelium [106](Figure 3). It compromises transportation through LSEC impeding oxygenation of hepatocytes, activating hepatic stellate cells and creating a proinflammatory environment [107]. Therefore, capillarization plays a key role in the majority of liver diseases as well as in acute or chronic liver injury [108], however, there is no consensus about the timing of capillarization in the development and/or progression of liver diseases. Pseudocapilarisation is a term used to describe the age-related loss of fenestrations which does not progress into fibrosis or cirrhosis [95].

Non-alcoholic fatty liver disease (NAFLD) is one of the most prevalent liver conditions in modern society, affecting up to 30% of the population of Western Europe and Eastern Asia [109]. NAFLD is a hepatic manifestation of metabolic syndrome and can have two distinct entities –simple steatosis, or non-alcoholic steatohepatitis (NASH) which can progress to liver cirrhosis or cancer [110]. In general, the development of NAFLD is associated with excessive triglyceride accumulation in the hepatocytes and LSEC defenestration (loss of fenestrated phenotype by LSEC) [111]. Interestingly, a recent report by Verhaegh et al. [112], analysing data from human liver samples, showed that fenestrations were still present in the patients with NASH in comparison to defenestrated samples from non-NASH/simple hepatic steatosis patients. The authors hypothesized the existence of potential protective mechanisms leading to

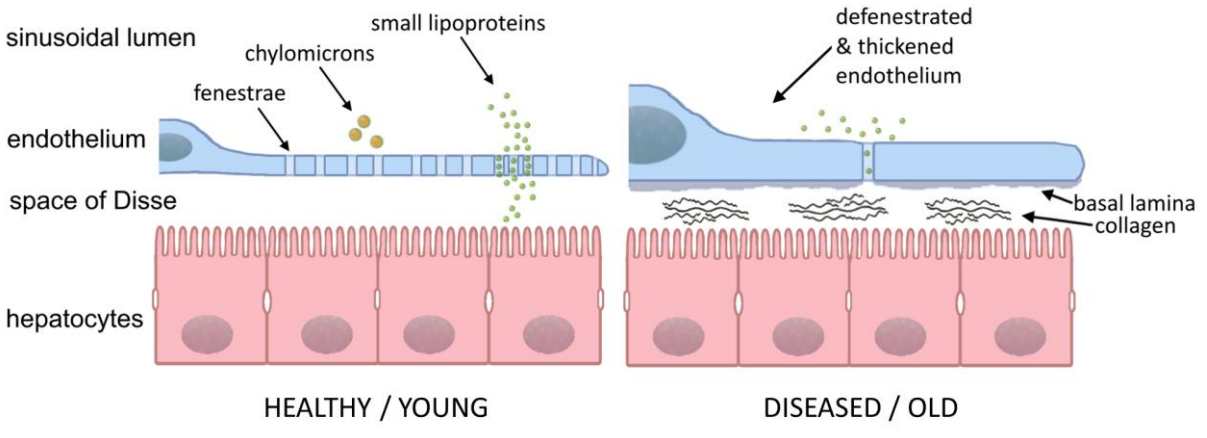

Figure 3 Changes in LSEC morphology between healthy and diseased states [42]

defenestration in simple steatosis that prevent the advancement of the disorder. Those observations are consistent with the *in vitro* studies of the high-fat diet-induced NAFLD development in mice [113]. In both the early and late stages of NAFLD, LSEC showed prominent adaptive capacity and preserved fenestrated morphology. Wisse et al. reported that enlarged fenestrations can return in NASH patients, however, details of this process remain without explanation [114].

On the other hand, capillarization is considered an integral part of the fibrotic process [106], however, it does not necessarily have to lead to fibrosis [112]. Further defenestration affects intrahepatic microcirculatory disturbances leading to the development of portal hypertension which in turn can lead to the progression from steatosis to NASH [115]. Also, capillarized LSEC lose the ability to keep HSC quiescent and prevent their activation, which promotes HSC activation and liver fibrosis [106].

Age-related defenestration is also called pseudocapillarization because of the lack of progression into fibrosis or HSC activation observed in the capillarization in chronic liver diseases [96][95]. Besides the markedly reduced size and number of fenestrations (studied in mouse [116], rat [95][117], baboon [118], and human [119]), LSEC also lose some of their endocytic capacity [74]. All of this affects chylomicron remnant clearance and post-prandial hyperglyceridaemia which may contribute to increased vascular risk in older people [120][98].

All those findings show the important role of fenestrations in both the development and progression of various liver conditions. A good understanding of the mechanisms behind the regulation of fenestration gives possibilities to design new therapeutics to prevent or reverse disease- or age-related defenestration.

2.6 LSEC and drugs

Ever since the first descriptions of fenestrations on the liver sinusoidal endothelium, the influence of various agents on LSEC morphology has been reported both *in vivo* and *in vitro*. Many of the studied compounds are already in use as medicines, some have other biological functions, and a large group consisting of toxic chemicals sometimes used to mimic the development of liver diseases. Many of those agents have known molecular mechanisms of action on LSEC or other endothelial cells, therefore we linked that their effects on fenestrations can help solve the mystery of fenestration structure (details can be found in **Paper I**, [42]).

Actin disrupting agents

As discussed in section 2.2, the cytoskeleton plays a major role in fenestration structure and regulation. Actin creates rings or a mesh surrounding fenestrations but also builds stress fibres and enables cell motility [121][122]. Various actin remodelling proteins keep the dynamic out-of-equilibrium state where constant polymerisation and depolymerisation occur. Agents affecting this process have been shown to influence LSEC morphology [41][4].

A large variety of toxins derived from moulds, marine sponges or mushrooms cause rapid increases in the number of fenestrations [123][52][124][29]. The main mechanism behind that is the shortening of actin fibres either by promotion of actin depolymerization, blockage of polymerization or fibre severing. The background of those processes is not yet fully understood but we hypothesized both the high availability of short actin fibres and the reduction in cell height are factors promoting fenestration formation [42]. Anti-actin drugs also revealed some new fenestration organization patterns. Misakinolide treatment created lines of very small holes emerging from small non-fenestrated areas, turning in time into fan-like patterns [41]. Similar non-fenestrated areas were observed after cytochalasin and jasplakinolide treatments [28][29] and later identified as fenestrae forming centres [52].

Treatment with an actin disrupting agent also provided an insight into the dynamics of fenestrations. Even without available super-resolution imaging techniques for live cells at the time, Spector et al. [41] described the fast formation of fenestrations within just 5 minutes after treatment. The time frame of these findings suggests that there is no *de novo* synthesis of proteins involved in fenestration formation but rather relocation of existing membrane domains [125][126].

Other non-medicinal agents

A significant group of mostly toxic compounds tested on LSEC is supposed to mimic the development of various liver diseases. In animal models, the administration of some chemicals is usually preferred for the development of pathological conditions. Spontaneous/genetic models or diet induction are closer to the real onset of the disease but are also more time and resource-consuming [127].

The most common toxic agents in use for the development of fibrosis are: carbon tetrachloride (CCl_4), thioacetamide, dimethyl- and diethylnitrosamine [128][129][130][131]. The route of admission, dosage, timing and even animal strain can influence the effect and needs to be carefully optimized. Monocrotaline is used for modelling sinusoidal obstruction syndrome and hepatic veno-occlusive disease [132][133]. Lipopolysaccharides, pyocyanin, C3-transferase and also other endotoxins are used to study liver inflammation and immune response [134][135][136]. In all these models of cirrhosis and/or fibrosis, LSEC lose their fenestrations. The exact cellular mechanisms are hard to pinpoint, and the overall in vivo effect depends largely on the disturbed crosstalk between different liver cells.

The knowledge about the specific molecular mechanisms and signalling pathways involved in the regulation of LSEC functions is growing rapidly in recent years. The development of new, more specific inhibitors and stimulators can “shut down” or divert some pathways allowing more precise detection of the involved mechanisms. Venkatraman and Tucker-Kellogg [137] showed elegantly that CD47 receptor activation stimulates signalling through the Rho-ROCK-myosin pathway inducing LSEC defenestration. They confirmed the exact mechanism by selective inhibition of various levels of signalling cascade and even the molecular fragment of thrombospondin 1 binding to CD47. In a similar manner de Zanger et al. [138] confirmed the involvement of protein-kinase-C (PKC), a molecule downstream in the cGMP/NO pathway, in the maintenance of fenestrations.

Medicinal drugs

The effects of drugs on the hepatic cells have always been of interest, especially in the field of pharmacology and drug development [139][140]. Over a third of drugs reaching clinical trials fails due to poor safety [141] and nearly 75% of all post-market drug withdrawals in the United States in 1975-2007 were due to liver and/or cardiovascular toxicity [142]. This data shows the challenges in the development of new therapeutics. Even though the majority of the drugs on the market are considered safe in use, side effects and overdosing can still affect the

liver. Unfortunately, for many medicines little is known about their direct effects on LSEC and other liver cells.

For some of the approved drugs, the effects on the unintended targets show an interesting opportunity. LSEC can be exposed to higher concentrations of drugs absorbed via the gastrointestinal tract, due to the first-pass effect, in comparison with the reported systemic/plasma levels [2]. Hunt et al. [143] showed that some already approved medicines for the treatment of high blood pressure, erectile dysfunction or diabetes have positive effects on LSEC porosity, leading to increased porosity, in both young and old mice. Metformin, sildenafil and simvastatin are examples of drugs that are shown to increase the number of fenestrations in LSEC [143][144]. On the other hand, almost all recreational drugs with reported effects on fenestrations (ethanol [145], cocaine [146], and nicotine [147]) showed clear negative effects on LSEC morphology, leading to the reduced number and/or diameter of the fenestrations. The only exception was DOI (2,5-dimethoxy-4-iodoamphetamine), a serotonin receptor agonist with hallucinogenic effects, which showed increased porosity in old mice [148][143] as well as improved the liver regeneration [149].

3 Microscopy

Achievable spatial resolution is one of the most important parameters when choosing an optimal microscopy technique for the observation of LSEC morphology. In light microscopy, the optical diffraction limit depends on the used objectives and wavelength and does not go below 200 nm [150]. For fenestration observation (size of 50 – 350 nm), it means that only holes larger than 200 nm can be detected. There are several ways to overcome the light microscopy limitations:

- Use the properties of light and/or fluorescent molecules to our advantage. Optical nanoscopy modalities, such as SIM, STED, dSTORM, overcome the diffraction limits in various ways.
- Use electrons instead of photons that interact with the matter in a different manner, and therefore have different resolution limits. Electron microscopy techniques, such as SEM and TEM, can achieve sub-nanometre resolution according to the applied electron energy.

- Use of physical scanning probes that allow for visualisation of the sample by "touch". AFM uses various imaging modes and resolution relies mainly upon the tip apex radius of the probe and the physical properties of the sample.

3.1 Atomic Force Microscopy (AFM)

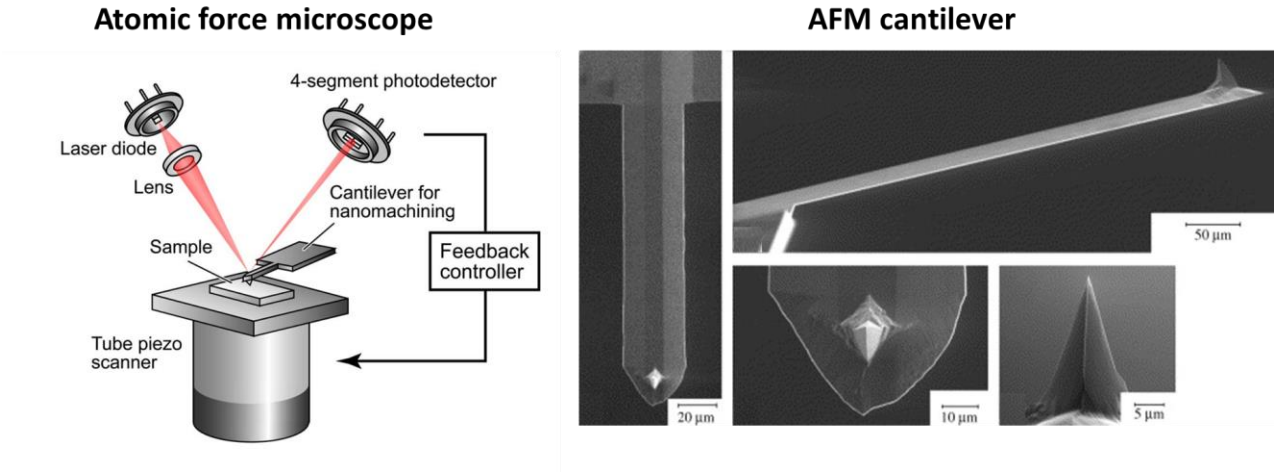

Figure 4 Schematic of the AFM microscope and SEM image of a representative AFM cantilever. Reproduced from [254] and [255].

Atomic force microscopy (AFM) is a part of the scanning probe microscopy family. Those techniques use a probe in the form of micrometre-sized cantilevers ended with a sharp needle with a nanometre size tip apex (Figure 4) [151][152]. It is commonly compared to "touching and feeling" as if the probe were a finger detecting both the topology and softness of the sample. The inventors of AFM, Gerd Binning and Heinrich Rohrer received a Nobel prize in 1986 for their findings [153].

AFM Imaging

There are several imaging modalities of AFM, but here only the two used in **Paper II** and **Paper III** will be discussed, namely contact mode and quantitative imaging™ (QI, JPK Instruments) mode. In the contact mode, an image is generated from the continuous scanning of the sample with a constant deflection of the cantilever (from a few nN to hundreds of pN) (Figure 5). The constant deflection is maintained via an electronic feedback loop. The precise, sub-nanometre movements of the probe and/or stage are facilitated by the piezoelectric motors [154]. The constant detection of the cantilever position is facilitated by a reflected laser signal allowing measurements of the sample topology (Figure 4). In the contact mode, the selection of a proper loading force is crucial. Overly low values hamper the detection of the signal

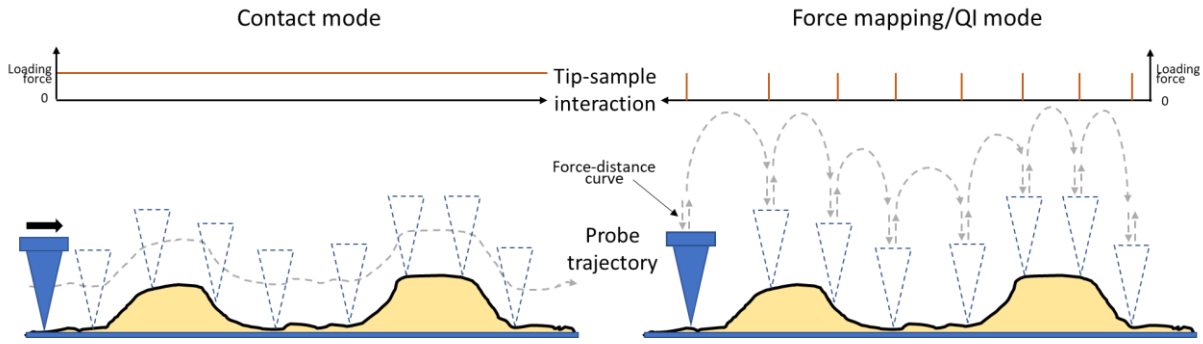

Figure 5 Selected imaging modes of AFM

corresponding to the detailed ultrastructure of investigated sample; overly high values can damage/alter the sample. The selection of cantilever is crucial for imaging, and it is highly dependent on the mechanical properties of sample. For soft samples, such as LSEC, the lowest possible spring constant must be selected. It allows for minimizing the deformation of the sample. If the sample is softer than the cantilever, the deformation of the sample, instead of deflection of the cantilever, occurs. At the same time, a low spring constant makes a cantilever prone to thermal drift that corresponds to uncontrolled large changes in the loading force during the scanning, so precise temperature control and system thermal stability is necessary [155][156]. In LSEC research, the contact mode is used only for fixed samples where fixed cells are significantly stiffer than live cells [155]. There have been attempts to image live LSEC using contact mode but the forces required to obtain good enough resolution were too high leading to the damage of cell membranes in the delicate areas with fenestrations [155][27][157].

Quantitative imaging (QI) is a commercial name for a mode originating from force mapping. In force mapping, independent force-distance curves are recorded and can be further translated into the images of topography (height), stiffness, adhesion, deformation or (visco)elasticity and other parameters. QI mode allows to greatly reduce the probe-to-sample interaction allowing for gentler imaging of biological samples such as LSEC. It is based on the collection of short (few hundred nanometres instead of a few micrometres for force mapping) force-distance curves in every pixel point of the image while the probe is moving between the pixel points without interacting with the sample (Figure 5,6), minimizing lateral forces [28]. The maximum loading force can be reduced providing minimum influence to the sample [158]. The topological data can be calculated either for the so-called contact point (zero loading force)

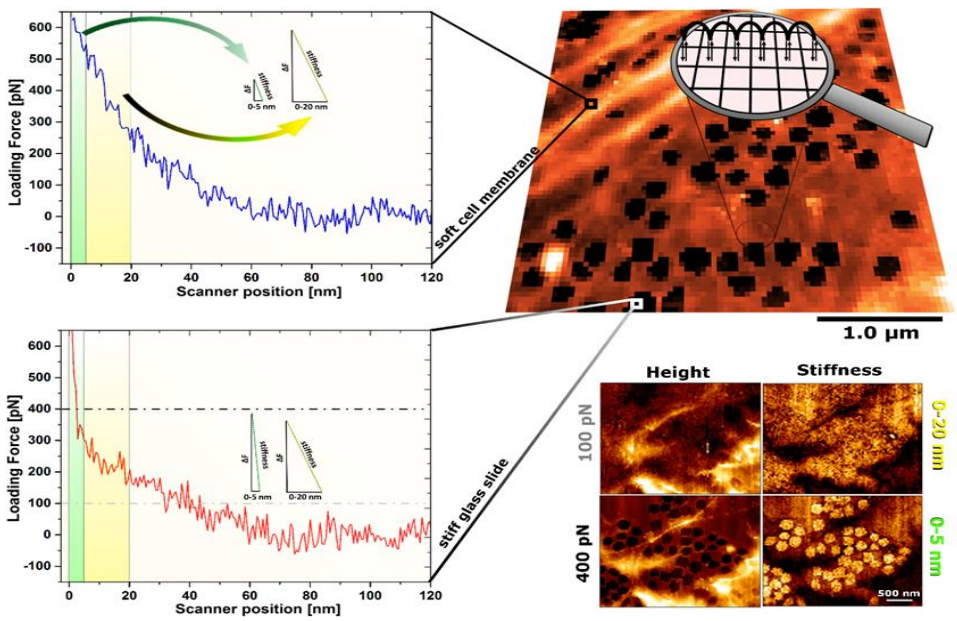

Figure 6 The principle of generating image in QI AFM mode using force-distance curves. Reproduced from [28].

to visualise the very surface of the cell, or for higher loading forces of <500 pN or >500 pN to reveal the cell cortex or deeper parts of the cells [159][160]. Also, the stiffness parameter (ratio of applied force to observed deformation) can be calculated for each pixel point creating a stiffness map which can be used for image analysis. For some samples, it may provide greater contrast between soft cell body vs hard substrate (Figure 6).

Force spectroscopy

Force-distance curves can be used not only for the force mapping but also to calculate more complex mechanical properties of cells (e.g. elastic modulus, shear modulus, storage and loss modulus [161]). Changes in mechanical properties can be used as markers of pathology [159]. Measurement of changes in elasticity after different kinds of fixation can also give extra information about the causes of some types of imaging artefacts (**Paper II**, [155]). Interestingly, the trends of induced changes in cell elasticity are preserved also after fixation, regardless of the over 10-fold increase in the elasticity parameter [162].

$$E = \frac{\sigma}{\epsilon} = const. \qquad \left[\frac{N}{m^2}\right] \tag{1}$$

E – Young modulus/modulus of elasticity, σ – tensile/compressive stress, ε – axial strain

The most common elasticity parameter used for biological samples is the Young modulus (E), based on Hook's law (1). It describes the constant ratio between stress (resulting from applied pressure) and measured deformation (indentation into the sample). Provided this

ratio is constant, the studied material is undergoing elastic deformation, which is true for biological samples such as cells if the indentations are small. Using Hook's law and some simple assumptions about the properties of the probe and the sample, Hertz proposed a model which can be fitted to the experimental data to calculate the Young modulus [163]. Measurements of the whole-cell elasticity have been successfully applied to, among others, distinguishing cancer cells from other cells [164], characterization of endothelial cell dysfunction [159], as well as for monitoring the progression of liver fibrosis [165]. Recently, elasticity changes have been described for LSEC [161] in the development of NAFLD [166] and under the influence of agents such as cytochalasin, and antimycin [158], iodoacetic acid and diamide [43].

3.2 Structured illumination microscopy (SIM)

Structured illumination microscopy (SIM) is a wide-field type of super-resolution microscopy that provides a two-fold improvement of resolution (to about 100-120 nm). The technique was first introduced by Heintzmann et al. in 1999 [167] in two dimensions and later in 2008 by Gustafsson et al. [168] in three dimensions. The SIM principle is based on the retrieving of super-resolution information from the sample (consisting of high-frequency components – details unresolvable by a regular microscope) using a well-defined illumination pattern. The grid-like pattern interferes with the sample moving high-frequency components into the resolvable range, resembling the Moiré fringes. Then, super-resolution information can be retrieved using reconstruction software. The data set for reconstruction requires several images made with different shifts in phase and angle of the grid pattern (usually, five phases and three angles are used) (Figure 7).

The SIM reconstruction process can be simply described based on the images transformed into Fourier space. This operation allows decomposing of the image information into some basic sinusoidal functions which are then plotted into a frequency domain (a detailed explanation can be found in [169]). Briefly, the centre of the image represents the low-frequency information (such as the general shape of the observed object), while points further away from the centre contribute to the high-frequency information (fine details of the image). In figure 7, the blue rings represent the limitation of the observable details due to the optical transfer function (OTF), which restricts the resolution. The yellow rings correspond to registered additional information, beyond the OTF, thanks to the illumination with different angles. Multiple angles provide isotropic resolution (even coverage of the frequency space).

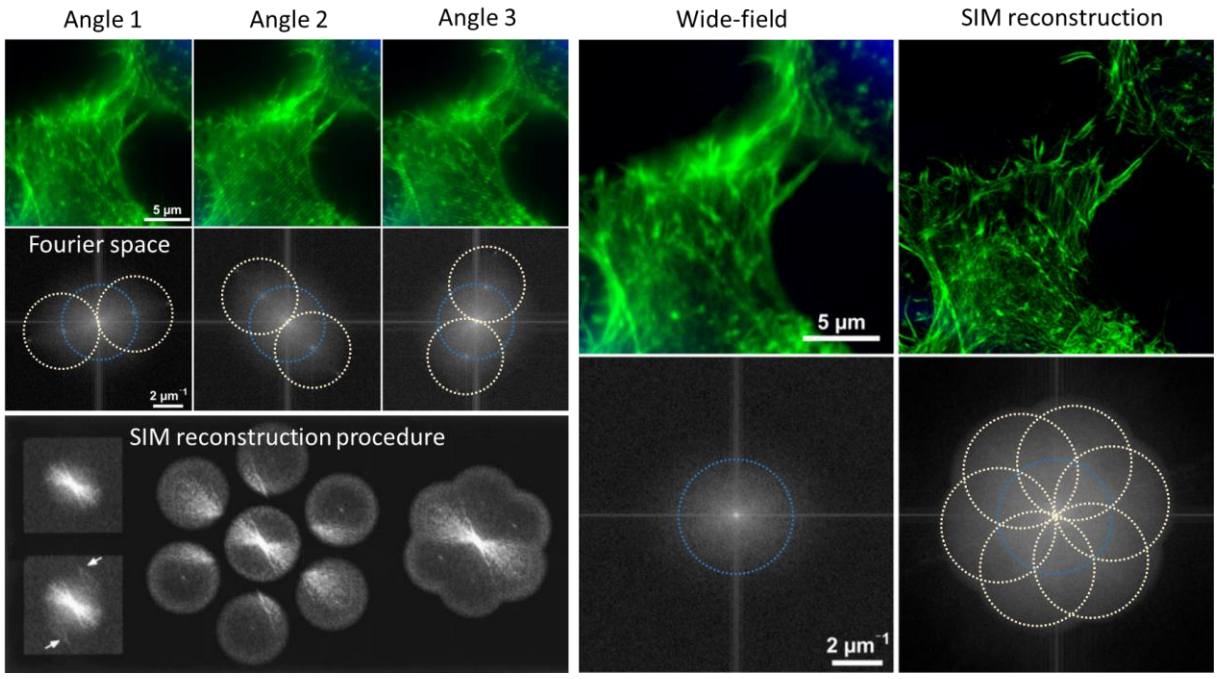

Figure 7 Image of U2OS cell with actin stain acquired using both 3D-SIM and wide-field microscopy. Images in three different angles of illumination patten and their representations in Fourier space are presented. Adapted from [223][231][253].

The different phase shifts are required for the reconstruction processes which solve numerous equations based on the image function (details are mathematically too advanced for the sake of this thesis but can be found in [167] and [168]). The graphical representation of that process in Fourier space is presented in Figure 7.

One of the greatest advantages of SIM is the possibility to use almost all types of fluorescent dyes developed for regular fluorescent microscopy. Techniques such as STED and dSTORM require specific fluorophores and/or additional buffer systems [170][171]. The wide variety of useful dyes and efficient multicolour imaging make SIM an excellent technique for biological samples. Moreover, SIM doesn't need high laser power to achieve a good signal to noise ratio, therefore reducing possible phototoxicity which is a limiting factor for live cell imaging. The image acquisition time for standard SIM is also relatively low, in the range of seconds per super-resolved image, compared to minutes for single molecule localization microscopies, and allows observation of dynamic processes [172]. Recently, the development of faster cameras and computing powers allow reducing the image acquisition even below 100 fps in a setup called "instant SIM", iSIM [173].

Further improvements in SIM resolution can be achieved using non-linear effects arising from fluorophore saturation. In regular SIM, the fluorescence signal responds linearly to

excitation power. With very high excitation intensity, the population of fluorophores in the excited state increases faster than the emission of the photons while the molecule returns to the ground state. This saturation effect leads to non-linearity in the fluorescent excitation, which can in principle be used to increase the resolution for non-linear SIM (NL-SIM). Gustafsson et al. showed as a proof of principle that NL-SIM can reach the resolution of 49 nm [174] but with the need for imaging at 12 different angles and nine phases (in comparison to three angles and five phases in regular SIM). The requirement of a high-intensity excitation beam and a large number of images significantly increases the light exposure of the sample. The high-intensity light can lead to phototoxicity in living cells and even the destruction of a biological sample. The optimization is needed to maintain the gain in resolution without inducing phototoxic effects. There are several approaches in the attempt to overcome this problem, such as using photo-switchable fluorophores that allow for lowering the excitation power [175][176].

3.3 STimulated-Emission-Depletion (STED) Microscopy

In 1994, Hell and Wichmann [177] proposed the concept of stimulated-emission-depletion (STED) microscopy, but it took another five years to be experimentally demonstrated [178]. The main principle of STED is presented in Figure 8; this technique requires 2 separate beams – first for the excitation of fluorophores, same as in regular fluorescent microscopy, and second for the stimulated emission depletion, which "switches off" the fluorophores by disabling their excitation. Stimulated depletion takes place before the fluorescence, so the fluorophores affected by the doughnut-shaped beam are never in the excited (S_1) state long enough for fluorescent emission. Thus, only the innermost region of the excitation beam contributes to the observed fluorescent signal. This effect is strictly localized to the centre of the beams, so imaging requires continuous or pulsed scanning of the whole sample with the combination of both beams.

The resolution depends on the thickness of the donut shape beam which in turn can be adjusted by increasing or decreasing laser power. In theory the achievable resolution is unlimited, however, the increase in resolution is linked with the reduction of fluorescent signal [177]. Therefore, the resolution becomes a tuneable parameter that must be optimized alongside the excitation laser power while imaging [179]. This has strong implications especially for

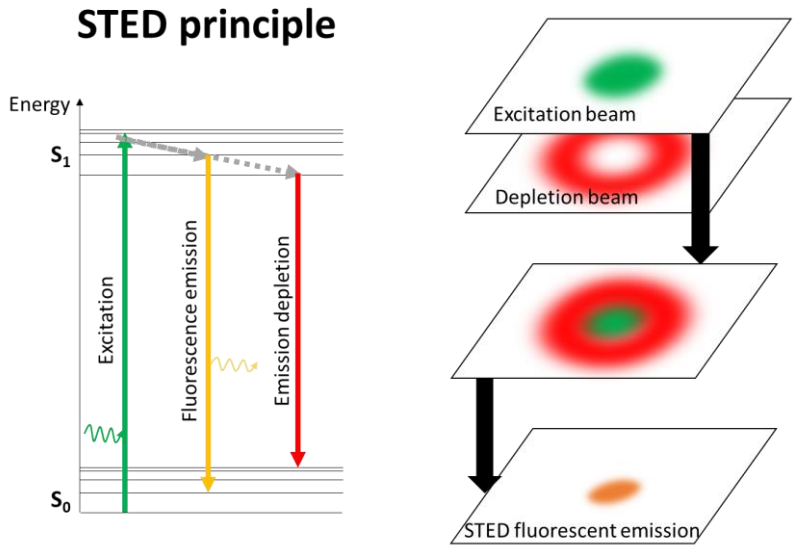

Figure 8 The principle of stimulated emission depletion. Fluorophores are excited from ground (S_0) into excited state (S_1) and either depleted by the donut shape depletion beam or spontaneously transferred with the emission of fluorescent photon.

fragile structures such as cells, as high laser intensity can contribute to phototoxicity in live cells or even thermal destruction in fixed cells [180].

The principle of work of STED microscopy limits the available number of fluorophores [170]. Moreover, multicolour imaging is challenging also because of the need for two laser beams for each colour. Recently, the search for new fluorophores with good properties for STED lead to the development of molecules with large Stokes shifts which can reduce the cross-talk between the imaging channels [170]. The tuneable resolution can be also used as an advantage of STED. Eggeling et al. showed the application of STED fluorescence correlation spectroscopy for studying diffusion rates of single molecules in the plasma membranes [181]. Another advantage of STED is no need for extra reconstruction as the super-resolved images are created directly during the imaging.

The use of STED for LSEC research concentrates now mostly on live imaging. Di Martino and co-workers established a fast and simple protocol for studying LSEC with STED, showing two colour staining as well as live cell imaging [33]. Later, they used STED to study cytochalasin induced refenestration of dedifferentiated LSEC after 3 days of cell culture [182].

3.4 Scanning Electron Microscopy (SEM)

The history of scanning electron microscopy dates back to the early 1930s when Ruska [183] and Knoll [184] independently worked on the development of the imaging technique for the surface of solid samples. In 1986, Ernst Ruska was awarded the Nobel prize in physics for his "fundamental work in electron optics, and for design of the first electron microscope"; he shared the prize with Binnig and Rohrer who designed the scanning tunnelling microscope (the precursor of AFM). After 1965, SEM started to be used in general research thanks to commercial development by two companies – the Cambridge Scientific Instrument Company in the U.K. and Japan Electron Optics Laboratory (JEOL) in Japan [185].

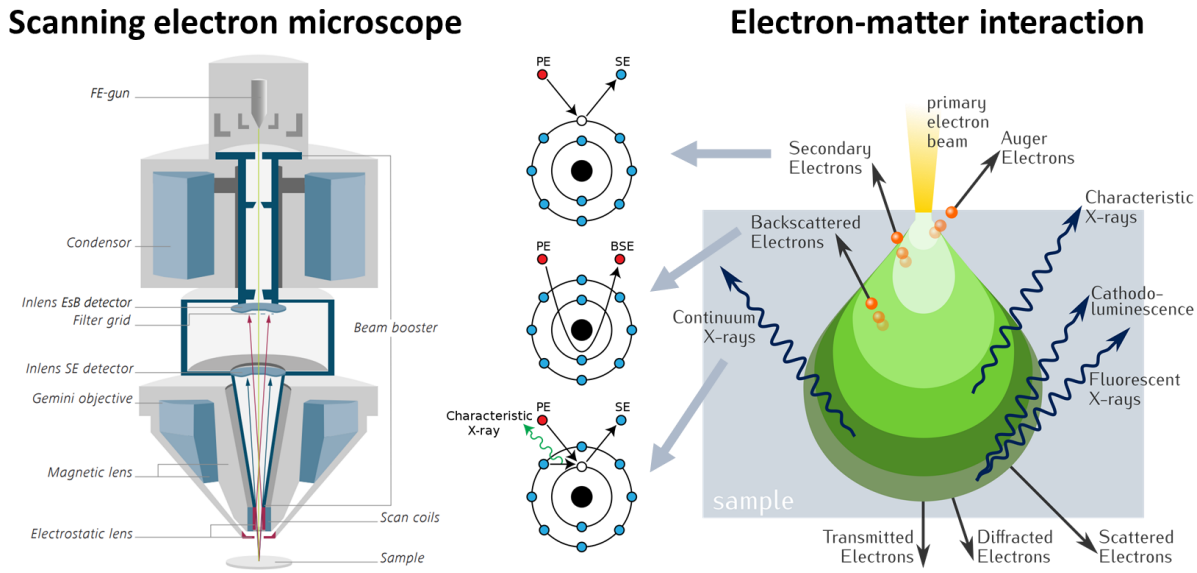

Figure 9 The schematic of SEM microscope based on Zeiss, Gemini model and diagram of electrons and matter interactions and types of detectable signals (Zeiss); PE, SE, BSE – primary, secondary, and backscattered electrons. Adapted from [257][258].

The principle of SEM is based on the interaction of a scanning electron beam with the atoms that build the sample. Depending on the depth within the observed object, different types of signals can be distinguished, such as secondary electrons (SE), reflected or backscattered electrons (BSE), and characteristic x-rays/light (Figure 9). Various types of detectors can be installed in the SEM chamber to detect these signals. The imaging of cells is mostly facilitated by the in-lens or backscattered detectors that register secondary or reflected electrons, respectively. SEs have low energy and originate from the first few nanometres within the sample. The image contrast is related to the number of emitted SE which in turn depends on the angle between the beam and the sample surface. The result is a high signal from the steep edges and a lower signal from the flat surface. For LSEC this mode provides great contrast as

fenestration edges appear as bright compared to the dark flat cell body (Figure 2, right). The BSE have high energy and come from the bent primary electron beam and the signal depends on the chemical composition as atoms with heavy nuclei strongly backscatter electrons. The position of the BSE detector on the side of the specimen limits the number of electrons that can be registered; therefore, the scanning speeds are usually slower than for SE to achieve a similar signal to noise ratio. For LSEC imaging, SE mode provides better contrast, so BSE backscattered electrons are rarely used.

The resolution of SEM can even go below 1 nm, but it depends highly on sample preparation which remains the main challenge for biological samples. The imaging chamber requires ultra-high vacuum conditions for uninterrupted use of the electron beam. Therefore, the preparation of samples such as cells must consist of dehydration and extensive chemical fixation to avoid structural damage. The surface of the sample must be coated with a conductive material to discharge the negatively charged electrons.

The standard protocol for sample preparation of LSEC culture starts with wet chemical fixation with a formaldehyde and glutaraldehyde mix, followed by incubation with tannic acid and osmium tetroxide (protein and lipid fixation, respectively) [186]. Then cells are dehydrated in an ethanol gradient with the final step of either hexamethyldisilazane (HMDS) or critically-point-drying [23]. SEM was also successfully applied for studying fenestrations *in vivo* in the liver tissue samples. Perfusion-fixation allows for observation of LSEC in their native environment among the other liver cells without altering the 3D liver structure (Figure 2, left).

3.5 Correlative techniques

Combinations of more than one type of imaging technique are becoming a steadily more popular approach. Various combinations of optical (both normal and super-resolution), electron, atomic force, phase and Raman microscopy have been reported to date. Correlative techniques can provide additional information that might be crucial for solving some scientific problems. A good example of the achievable benefits is the study of beta-amyloid aggregation, which is involved in the development of Parkinson's and Alzheimer's diseases. Cosentino et al. [187] used AFM to validate their STED results and found that only a fraction of aggregation could be detected using fluorescent microscopy. The cause was determined to be the protein-dye interaction that prevented some aggregation mechanisms. This example shows the strength of combination of label-free with dye-dependent techniques.

Correlative techniques can be useful not only for validation purposes but also to obtain extra information by taking advantage of the specific gains from each technique. For example, Butola et al. [34] combined dSTORM with quantitative phase microscopy for 3D LSEC imaging. Chip-based dSTORM provides a huge field of view (about 1 x 1 mm) and about 50 nm lateral resolution and QPM has nanometric sensitivity in axial dimension. This combination allows super-resolution imaging in x, y, and z directions.

The development of the chip-based methods allows for easy combinations of more than one type of microscopy. Helle et al. [188] showed that LSEC can be imaged on waveguides that provide total internal reflection (TIRF) illumination which allows the user to uncouple the excitation and collection light path. Later, Helle [189] and Diekmann [35] presented a super-resolution chip-based approach that allowed observation of large fields of view (up to 1 mm^2) with the nanometric resolution of dSTORM. These features made it a perfect setup for further combination with EM and waveguides can be also adjusted with additional landmarks for efficient co-localization of the regions of interest. Tinguely et al. [190] combined TIRF-dSTORM with FIB-SEM to study the fate of FSA in LSEC, as a proof of concept. Fluorescent microscopy allowed identification of the position of FSA inside the cell and additional high-resolution SEM data enabled the demonstration that it is inside endosomes and lysosomes.

4 Image analysis

Historically, microscopy techniques were developed to observe objects too small to be seen by the naked eye. In the fields of medicine and biology, it facilitated the detailed description of anatomical structures of many organisms which in turn helped to better understand their functions. Microscopy played a major role in those studies, but there are also two important aspects that deserve credit – sample preparation and image analysis.

Image analysis provides meaningful, qualitative and quantitative information from images. In the beginning, it was performed mostly manually but recent developments in the computational sciences enable the acquisition, storage, and analysis of large quantities of data. Microscopy images can be analysed in various ways to extract specific information. For scientific studies, it is important that these methods are unbiased, reproducible and give meaningful measurements describing what is observed. It is also crucial to understand that image analysis is the final step after acquisition and sample preparation and all preceding steps can influence the final result and have to be taken into consideration.

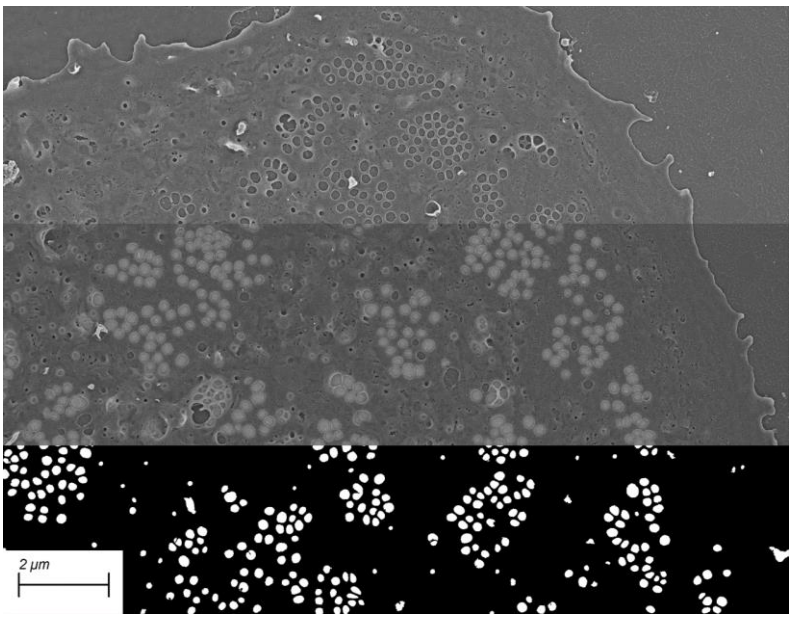

Figure 10 An example of segmentation of SEM image of LSEC. Top part present raw data, bottom part a segmentation mask and middle part an overlap mask over the raw image [Paper IV]

The main interests of LSEC studies described in this project are segmentation and object classification. In modern digital microscopes, images are just graphic representations of the recorded numerical data. Each pixel carries information about its position and intensity of the detected signal (often described as brightness). All image analysis steps are mathematical operations on those numbers that can be displayed on the screen for our better understanding and possible optimization and evaluation [191]. Segmentation is a process that separates the image into distinct parts, called objects, based on selected parameters. One of the basic segmentation methods is thresholding, where objects are detected based on the intensity difference between them and the image background [192]. This type of separation is easy to accomplish for images with good contrast where objects are clearly distinguishable. A good example is fluorescent images where certain structures of interest can be directly stained to increase the intensity contrast. Thresholding can be applied manually by the user or with the use of an algorithm that adjusts the cut off values to different image parameters (percentage of maximum intensity, mean intensity, signal to noise ratio etc). Threshold-base segmentation can be done in any graphic software such as ZEN (Zeiss) or Fiji/ImageJ [193] manually or by integrated automated algorithms.

Another approach for segmentation is based on machine learning. This method allows the training of a neural network algorithm on a small dataset of images and batch processing of the large quantitates of data. This enables great efficiency but requires good image quality among all images, and also is highly dependent on the available processing capabilities [194]. There

are several available free software with user-friendly interfaces, so it does not require programming skills anymore. Weka Segmentation [195] is open access plugin for Fiji/ImageJ [193] that allows training on a single image and later processing of multiple images. Ilastik [196] is another independent, open-access software that can be easily applied for segmentation. It allows training on several images in a graphical user-friendly way and is being constantly developed to match the needs of the scientific community. CellProfiler [197] is a more complicated program than Weka and Ilastik so the entrance barrier for a novice user is significant. Nevertheless, it enables complex multi-modular image analysis and contains some built-in options optimized for certain types of experiments.

Segmentation turns an image into a binary mask where the background is assigned with the value “0” and all detected objects with “1” (Figure 10). To obtain quantitative data, all objects must be analysed and assigned some numerical parameters. For studies of LSEC fenestrations, this part contains several following steps. To remove detected objects that are not fenestrations a size/shape filter can be applied so that only objects with a diameter of 50-350 nm and roundness above 0.5 remain (roundness is a ratio between the major and minor axis of an ellipse fitted to each object). Depending on the image, other processing steps may also be needed – if the objects are clustered together (such as merged fenestrations) the watershed function allows the detection of the border between them. Removal of objects touching the edges of the image is also necessary to avoid the measurement of only partially detected structures. After processing, final binary masks can be statistically analysed to obtain quantitative data with parameters such as the number of detected objects, their size descriptors (area, min- max- mean- diameters), shape descriptors (roundness, circularity), spatial distribution/clustering. All those parameters can be then used in the analysis of biological samples.

Aim of the study

The development of new therapeutics can be approached from two different angles – "top-down" by drug testing performed on the whole organism, mostly animals, to observe potential improvements in the studied disease models or "bottom-up" by trying to pinpoint the molecular mechanisms at the cellular level responsible for the disease onset and then finding ways to resolve this. The first approach is becoming outdated as new technologies are being developed to give us a better insight into the causes of many pathological conditions. The second approach allows the reduction of the animal suffering by selecting agents that have promising *in vitro* results.

In this study, we establish and standardize the methodologies for studying fenestrations in primary LSEC *in vitro*, with an emphasis on drug screening. Different imaging techniques are discussed and developed for the purpose of high quality and high quantity LSEC imaging, especially the correlative approaches that combine more than one microscopy modality. We also establish new quantitative image analysis methods and guidelines for the most efficient but also most precise measurements. The results will enable other scientists to choose the most optimal methods based on their research plans but also based on the available resources, such as microscope platforms or feasible timeframes.

To date, the complete molecular structure of LSEC fenestration remains unsolved. By analysing the existing reports on the effects of various agents, we were able to combine proposed hypotheses and propose both new possible therapeutics to improve LSEC porosity in ageing and disease, but also to set new directions for future research to get closer to the mystery of the mechanisms behind the structure and regulation of fenestrations in LSEC.

This project was divided into the following subprojects, based on the discussed above research questions:

1. Gathering the existing knowledge about the reported effects of various agents on LSEC fenestrations (**Paper I**)
2. Finding problems in the old methodologies and based on these proposing novel imaging approaches (**Paper II**) and image analysis methods (**Paper III**)
3. Exploration of the mechanisms behind LSEC fenestration regulation, structure, and dynamics based on the previous studies (**Paper I**)
4. Proposing novel refenestration approaches based on the studied mechanisms (**Paper IV**)

Paper I

Review: The wHole story about fenestrations in liver sinusoidal endothelial cells

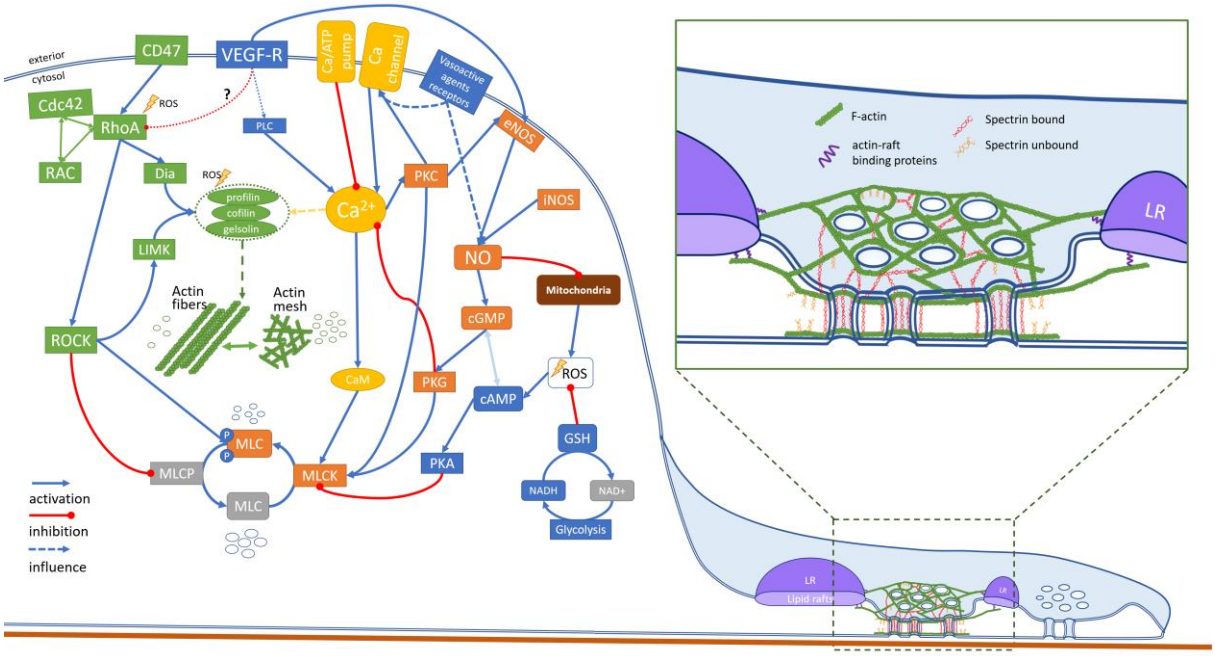

This scheme represents an attempt to unify the proposed hypotheses of mechanisms behind the structure and dynamics of fenestrations. Various signalling pathways involved in the regulation of fenestrations in LSEC are based on studies of LSEC (or other endothelial cells). LR – lipid raft, MLC – myosin light chain, CaM – calmodulin.

Objectives: Liver fenestrations have been studied extensively since the early 1970s and many agents affecting LSEC morphology have been described. In this review, we focused on systematizing the effects of medicines, recreational drugs, hormones, and laboratory tools (including toxins) on fenestrations. Also, various experimental models of liver diseases are described with an emphasis on changes in fenestrations.

Methods: Subgroups of agents are discussed and their reported effects on fenestration diameter, porosity and frequency are summarised. The references were selected in a non-systematic manner which allowed us to include many reports from non-indexed sources such as conference proceedings. All the data was then combined and discussed in terms of different mechanisms behind the fenestration regulation, structure, and function.

Results: The first section identifies commonly used medicines and recreational drugs with "positive" and "negative" effects on LSEC morphology. The reports on ethanol/cocaine/nicotine showed uniformly adverse effects on fenestrations, while some of the

prescription drugs (such as metformin, sildenafil, or simvastatin) increased porosity and fenestration frequency. The second section discusses the relationship between hormones, especially vasoactive agents, and LSEC. We observed a correlation between vasoconstriction/vasodilation and fenestration diameter, decrease/increase, respectively, in the literature. In the third section, we summarised cytoskeleton disruption agents and their effects, mainly increasing the number of fenestrations. Also, chemically induced disease models are discussed as well as all various other agents influencing fenestrations. The last part of the review contains four different hypotheses of fenestration regulation based on the existing literature. Numerous cellular mechanisms which tune LSEC porosity are described, such as signalling via NO/ROS/Ca^{2+} or the involvement of the actin and spectrin cytoskeleton components.

Conclusions: We believe that this review can enable researchers and physicians to estimate the effects of new therapeutics based on the proposed mechanisms and help better understand the influence of existing drugs on LSEC.

Paper II

From fixed-dried to wet-fixed to live – comparative super-resolution microscopy of liver sinusoidal endothelial cell fenestrations

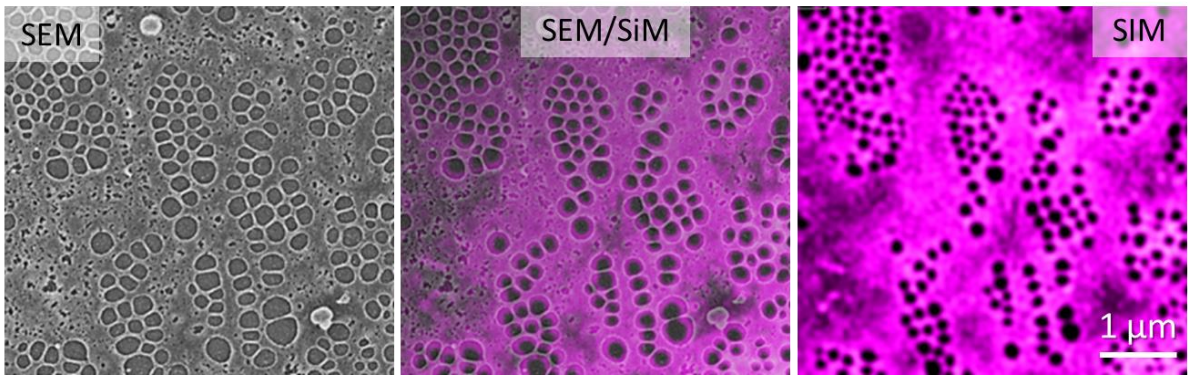

Correlative SIM/SEM of fenestrated area of LSEC

Objectives: After over 50 years of studies on LSEC and fenestrations, the field still suffers from large discrepancies reported in the literature when different imaging techniques are applied. The data reviewed in **Paper I** showed major differences in the reported sizes and numbers of fenestrations measured using different types of microscopies. This article's aim is to show where these discrepancies originate from, by combining multiple microscopy approaches in a correlative manner.

Methods: LSEC were measured using four types of super-resolution microscopies – atomic force microscopy (AFM), structured illumination microscopy (SIM), stimulated-emission depletion microscopy (STED) and scanning electron microscopy (SEM). Each sample was imaged by two of the chosen techniques – SIM/SEM, STED/SEM, AFM/SEM, AFM/STED and fenestration diameters were analysed and compared. Force spectroscopy was applied to study differences between changes in the cell elasticity after fixation with formaldehyde (FA) and glutaraldehyde (GA) in comparison with live cells.

Results: We observed ~30% dilation of fenestration diameter after dehydration during sample processing for SEM. This result can be used as a scaling factor for data comparison between different studies. The difference in fenestration size between wet-fixed cells measured by a label-free technique – AFM, and STED was about 10% and is mostly insignificant when comparing data from different studies. Changes in mechanical properties of the cells after fixation showed that GA-, but not FA-, fixation stiffens the cell enough to reduce the artefacts of AFM force imaging. The combination of non-super resolution fluorescent microscopy and

AFM shows possibilities for post-labelling to combine chemical information with the observation of fenestration dynamics.

Conclusions: The measurements of fenestrations can be obtained from the independent use of all presented techniques; however, their combination provides additional information from a correlative perspective. The difference in fenestration parameters observed in the past studies can be explained and avoided in future studies when differences in the cell preparation and imaging techniques are considered.

Paper III

Quantitative analysis methods for studying fenestrations in liver sinusoidal endothelial cells. A comparative study

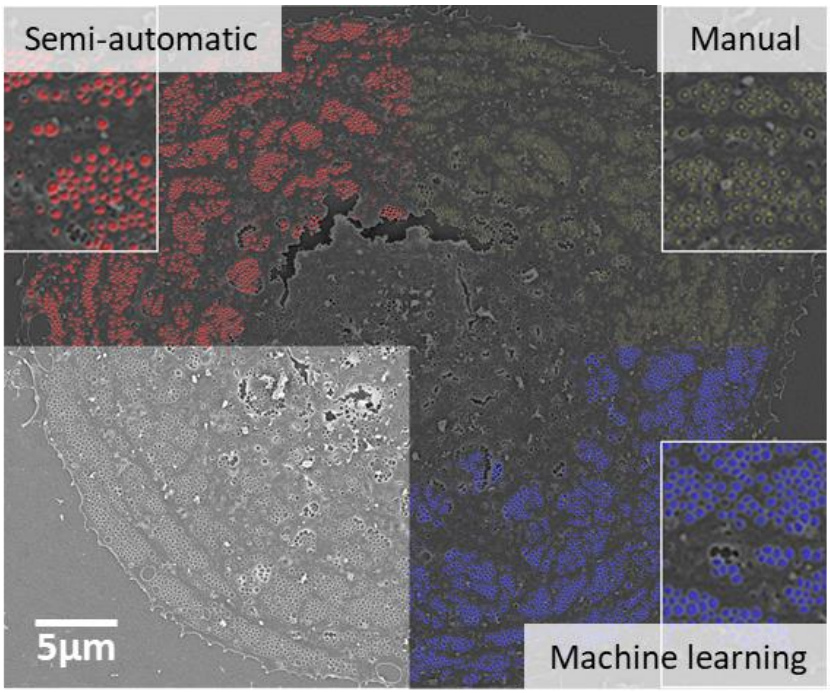

Representation of the SEM image analysis

Objectives: Both the size and number of fenestrations are crucial for maintaining the filtration of macromolecules between the bloodstream and the liver. The quantitative data about fenestration parameters can be obtained in several ways but to date, there is no standardized method. In this paper, we compare three different image analysis approaches (manual, semi-automatic and automatic) by using them to analyse images from three different types of microscopies (atomic force microscopy (AFM), structured illumination microscopy (SIM) and scanning electron microscopy (SEM)). Moreover, we studied user bias in image analysis by comparing data obtained by five independent users.

Methods: We compare 3 different image analysis methods – fully manual, semi-automatic based on the intensity threshold and automatic using machine learning software. High and low magnification AFM, SIM and SEM images were quantitatively analysed using three selected methods. Five different users were given identical data sets and asked to use all three analysis tools to study user bias.

Results: All analysis methods showed some advantages and disadvantages which vary among the different types of microscopies, mostly due to image artefacts. The manual method proved

to be the most precise for counting the number of fenestrations, while semi-automatic methods gave the best precision for diameter measurements and the least user bias. The automatic method is the most efficient, however, it requires high-quality images.

Conclusions: All three investigated quantitative methods can be applied to the analyses of fenestrations. The method selection should be based on factors such as the available imaging platform, the achievable image quality and the size of the image dataset.

Paper IV

Effect of caffeine and other xanthines on liver sinusoidal endothelial cell ultrastructure

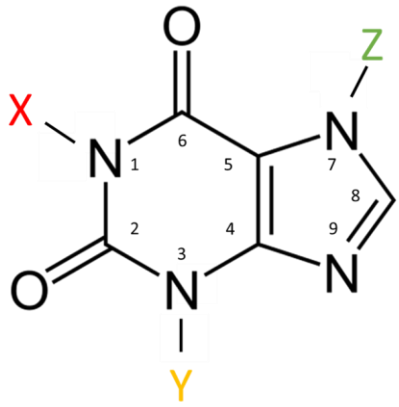

	X	Y	Z
Caffeine	CH_3	CH_3	CH3
Theobromine	H	CH_3	CH_3
Theophylline	CH_3	CH_3	H
Paraxanthine	CH_3	H	CH_3

Chemical structure of xanthines

Objectives: Xanthines, such as caffeine and theobromine, are among the most widely consumed stimulants in the world. They can be found in coffee, tea, and chocolate as well as in drug formulations for asthma and painkillers. Many health benefits of xanthines have been reported, however little is known about their effects on the liver.

Methods: Cryopreserved rat LSEC were treated with low - 8-20 µg/ml, and high - 150 µg/ml, doses of caffeine, theobromine, theophylline, paraxanthine and sildenafil (a drug known to have a possible similar mechanism of action). Cell morphology was examined using SEM and SIM and viability was assessed through the FSA endocytosis assay.

Results: No signs of toxicity were observed for all treatment groups. High doses of caffeine and theophylline showed significant increases in the number of fenestrations but due to the decreased fenestration diameter, theophylline did not affect porosity. Both high and low doses of theobromine also increased fenestration number but not porosity due to changes in the fenestration size. Sildenafil did not affect the number of fenestrations and only high doses (600 ng/ml) significantly decreased fenestration diameter. Analysis of individual animals presented significant differences between rats. In general, high doses of xanthines show larger differences between the bio replicates.

Conclusions: Low dose of theobromine appears as a possible treatment opportunity for, for example, age-related decreases in LSEC porosity. High doses of caffeine and theophylline

could possibly be used to improve LSEC morphology, however, a targeted drug delivery system would be needed to avoid systemic toxicity or side effects.

5 Methodological considerations

5.1 Systematic vs non-systematic review

Paper I is a purposive (non-systematic) review article that focuses on liver fenestrations. The main risk factor for the non-systematic approach is the potential lack of a balanced perspective [198]. Systematic reviews have strictly designed inclusion criteria and articles are selected based on search engines in the available databases, making the results reproducible. This approach allows for quantitative meta-analysis but also paints a precise image of the state of knowledge about a certain research question. On the other hand, a non-systematic approach leaves authors greater inclusion flexibility and possibilities to address the problem from a wider perspective. This freedom can lead to a risk of purposeful or unwanted/ exclusion of some studies and shift the conclusions. Initially, we decided to follow the systematic approach as it is generally considered more valuable and impactful but, as explained below, we ultimately resorted to a non-systematic approach.

In **Paper I,** we decided to sum up all the studies where various agents were tested on LSEC. The main inclusion criterium was reported quantitative data about porosity or fenestration size or fenestration number. The preliminary results from the optimization of the systematic review process led us to many articles that refer to studies in non-indexed volumes. We discovered this is due to the research history within the research community studying the liver sinusoid. In the years 1977-2001, a great amount of data was published in the proceedings of the most important conference in the field – The International Symposium on Cells of the Hepatic Sinusoid. These biannual meetings were concluded with the release of a book by the Kupffer Cell Foundation containing research articles from the participants. Even though these reports did not go under the standard peer-review process, the amount and quality of the data within them influenced our decision to include them and therefore proceed in a non-systematic way. Moreover, the Kupffer Cell Foundation books were released in a very small number of copies and are not available online, so the data is practically inaccessible for a regular reader. By including those findings in **Paper I**, which is published in a gold open access standard, we provided extra insight into those volumes to all readers. Also, the non-systematic approach and inclusion of a broader spectrum of articles allowed us to add a whole section about the structure and regulation of fenestration based on both LSEC studies and more general mechanistic information from reports on signalling pathways in other vascular endothelium.

5.2 Cell isolation and culture

Animal models

The use of animals in research is a regularly discussed issue in both the scientific community and by the public. The ethical dilemma needs to be addressed but by the same token, there is still no alternative for some use of animal models. A good example is preclinical studies in drug development – animals fill the missing gaps between testing the compound on cell lines and human trials. In the context of liver research, the main focus is the toxicity of studied compounds as almost 75% of all post-market drug withdrawals in the United States from 1975 to 2007 were due to liver and/or cardiovascular toxicity [142]. We can assume that those numbers would be even higher if no animal tests were conducted in the preclinical phase.

The definitions of a "research animal" and "procedure" differ between the countries which hinders the comparison between the reports about the use of animals in research. Nevertheless, the total number of animals used for scientific purposes was estimated to be almost 200 million worldwide (data for 2015) [199]. Authors of this report estimated that around 1/3 of all animals are used by China, Japan, and the USA - 20 million, 15 million and 14 million, respectively. The estimation of the number of used animals was not possible due to reporting exclusion/inclusion criteria in different countries – for example, US reports do not include rodents or birds which constitute around 93% of research animals reported in Europe [199]. The EU reported the use of 10.6 million animals in 2018 (Norway was included for the first time in that year in the statistics) [200] with over 50% being mice. Norway alone declared 2.3 million research animals in 2020: 2.2 million fish, 50 222 mice and 3355 rats [201].

In liver research, many different species are in use nowadays. For basic research and early-stage drug development, rodent models are mainly used with mice and rats being the most popular and practical choices. Mice are usually an animal of choice for studying ageing and age-related diseases as the mouse lifespan of about 2-3 years, and genetical similarity to humans of over 90% [202]. The studies on LSEC were conducted on many various species, including popular lab animals such as mice, rats and rabbits, but also baboons, bats, cats, chickens, goats, guinea pigs, pigs, sheep, and trout have been used [4][203][204]. In the history of LSEC research, many species were used just to show that fenestrated morphology is prevalent in all vertebrate species examined. The selection of the animal model depends on many factors related to a particular research question.

Discussion

This project was based on primary LSEC isolated from mice and rats. Rodent models were the only available sources of cells at the time that this thesis work was carried out at UiT the Arctic University of Norway. Nevertheless, the thoroughly optimized protocols for mouse and rat liver perfusion and cell isolation would make rodents the model of choice. In **Paper IV**, we decided to use the cryopreserved rat LSEC isolated at our collaborator lab – the ANZAC Research Institute in Sydney, Australia. The freezing protocol developed by Mönkemöller et al. [205] allows long term storage and transportation of LSEC and the cells can be revived without loss of fenestrated morphology or endocytic capacity. The possibility to ship the cells was crucial for the project due to the prolonged closure of the Unit of Comparative Medicine at UiT (AKM, *Norwegian: Avdeling for komparativ medisin).* It is also a very practical solution as cells from the same animal can be used for several experiments that could not be performed on the same day. Moreover, more efficient use of isolated cells results in a lower number of animals required for the project and is in line with the 3R rule for humane experimental technique (3R – replacement, reduction, and refinement). The decision to use mouse LSEC in **Paper II** was dictated by the previous preliminary results using mouse LSEC. This article was possible thanks to a collaboration between multiple research institutions and cell isolation from only mice was possible at all places. **Paper II** is method development-oriented, so the choice of animal model has only minor, if any, influence on the results. Similarly, **Paper III** focuses on image analysis for different kinds of microscopy, so the datasets were obtained from samples of both mouse and rat LSEC.

In vivo vs *in vitro*

The *in vitro* and *in vivo* approaches are often considered competitive, while actually, they provide complimentary information [206]. *In vivo*, Latin for "within the living", refers to the experiments performed on the whole living organism. In drug development and liver research, it refers mostly to the animal treated with a selected dose of the studied agent or in some cases, to *ex vivo* perfusion of the liver with a selected concentration of the agent. For fenestration research, the term *in vivo* is also commonly used to describe LSEC observed in tissue in comparison to the isolated cells (Figure 2). Due to their nanoscale size, fenestrations have never been shown inside the living organism which explains the not fully correct use of the term *in vivo* within the field of LSEC research. In cell biology, the term *in vitro*, Latin for "in/on the glass", indicates experiments performed on samples outside of their normal biological context. In LSEC studies, it refers to the cells after isolation.

Drug screening is a particular field where the combination of experiments performed on cells and the whole organisms is crucial. In the preclinical phase of the drug development, all *in vivo* studies must be preceded by testing the compounds on the cellular level. That is a requirement for most animal research committees to reduce the testing on animals. Single-cell isolation allows preliminary testing of many drugs in a time- and dose-dependent manner which with the *in vivo* approach would lead to the sacrifice of dozens of animals. Moreover, *in vitro* experiments provide information about drug influence at the cellular level which helps with both the assessment of desired therapeutic effect and the prediction of possible side effects. The target determination is usually easier to demonstrate on the cell of interest while other negative effects require testing on many different cell types. For example, the guidelines for preclinical testing of anticancer drugs suggest *in vitro* studies on various cell lines [207]. Notably, those recommendations do not emphasize any extensive studies on liver cells even though hepatotoxicity is the main cause of the withdrawal of drugs in clinical trials. Additional *in vitro* tests on liver cells and in future in bio-reactors with multiple hepatic cells can benefit drug development. Moreover, the co-culture approach provides a more physiological testing environment that can help to close the gap between *in vitro* and *in vivo* study designs [208], [209] [210].

Primary cells vs cell line

LSEC lose their characteristic fenestrated morphology and other specific cell markers within a few days in cell culture [182][211]. Therefore, all *in vitro* experiments require freshly isolated primary cells. The most popular animal models for studying LSEC are rodents – mice and rats, but there have been studies on many other species [4]. Human LSEC have also been characterised in detail from both adults [212] and foetal sources [213].

Cell lines are the usual alternative to primary cells for the *in vitro* studies, however, establishing an LSEC cell line has proven to be challenging. There were several attempts to immortalize human and mouse LSEC with varying success rates [214][46][215][216][217] [218][219] (reviewed in [220]). Most cell lines showed some limited uptake of FSA and/or LDL which confirms the preservation of limited receptor-mediated endocytosis. Some expressed other LSEC-like features such as CD31, CD34 and von Willebrand factor (VWF) or showed a response to vascular endothelial growth factor (VEGF). Two reports [46][216] presented fenestration-like structures and one study showed an endothelioma cell line with

inducible fenestrations [219] but with parameters far from the primary cells. Fully functional fenestrations in a cell line remain the "holy grail" of the LSEC field.

This project focused on fenestrations and LSEC drug response, which could not be studied on cell lines as none of them have well enough preserved characteristic LSEC morphology. The reasoning was supported by our own previous experience with some LSEC cell lines. Therefore, each experiment was preceded with primary cell isolation and only fresh or cryopreserved LSEC were used.

LSEC viability and endocytosis

The assessment of viability is crucial in the studies of drug response to separate the direct effect of the agent from the secondary effect resulting from cell toxicity. For LSEC, their endocytic capacity can be used as a parameter to measure cell functional viability. Healthy LSEC efficiently take up FSA by well-described clathrin-mediated endocytosis [72] and radiolabelled FSA can be used in a quantitative assay to measure both the cell-associated and degraded fractions [221][58][222]. Degradation of the ligand can be affected independently from receptor-mediated uptake, for example, if tubulin is disrupted and transportation to lysosomes is affected or if there are other endocytosed compounds causing "traffic jams" within the cell. Reduction in FSA uptake is associated with ageing [74] and hepatotoxic effects of drugs [75] but also with dedifferentiation in prolonged cell culture of LSEC [211].

In **Paper IV,** the measurement of FSA uptake has a dual purpose. Firstly, to determine the preservation of endocytic capacity in cryopreserved LSEC and secondly, to assess the cell viability after treatment with xanthines (caffeine, theobromine, theophylline, paraxanthine) and sildenafil. The untreated control groups showed high FSA uptake and degradation that match well with the results of freshly isolated cells. The degradation rate of about 40-50% for 2h experiment is considered typical for rat LSEC. The number of the cells revived after cryopreservation varies between the isolations/animals which affect the absolute values of endocytosis (measured as % of the ligand removed from the supernatant). Therefore, the results are presented as normalized to the control so all experiments can be presented and analysed together. Treatments did not affect the cell-associated fraction and only caffeine showed about 20% decrease in the degraded fraction, which perhaps indicates a light toxic effect. From our experience with other toxic compounds, we know that the degraded fraction is usually the first

affected, so the used caffeine concentration of 150 µg/ml is perhaps on the edge of the toxic dose.

LSEC (structural) viability can also be assessed from the morphological features using microscopy techniques. However, this method allows only to distinguish cell necrosis and late apoptosis that have clear morphological features. To study more subtle and gradual changes, that are important in drug screening, different functional viability assays are necessary.

5.3 LSEC imaging

LSEC are challenging samples in many ways and good imaging protocols are crucial for visualization of fenestrations. There are several factors that need to be considered for successful LSEC imaging such as resolution – fenestrations are nanometre-size; sample preparation – from the surface coating to different fixation and staining methods; and the selection of the imaging technique or image analysis method [223]. In this project, we tried to optimize several types of microscopies in a correlative manner and discuss the achievable resolution, as well as analyse differences between commonly used fixatives (**Paper II**). We also evaluated different methods of image analysis and proposed new ones to improve their efficiency for different types of imaging techniques (**Paper III**).

Resolution

The resolution is a key factor in LSEC imaging. The diameter of fenestrations varies from about 50 nm to 350 nm but holes above that size are often also observed *in vitro* and called gaps. This means that to observe all fenestrations, a technique that can resolve objects as small as 50 nm was necessary. The ability to distinguish two objects as separate is called resolution and is described as the minimum resolvable distance between those two points (Figure 11). There are several ways to determine the resolution limits of microscopy techniques and the achievable resolution is a combination of many factors [224]. Electron microscopy can resolve objects even below 1 nm so it does not need to be considered for LSEC imaging in this section, but optical techniques have a resolution within the fenestration size range and so here only optical diffraction limits will be discussed.

The resolution is a key factor in LSEC imaging. The diameter of fenestrations varies from about 50 nm to 350 nm but holes above that size are often also observed *in vitro* and called

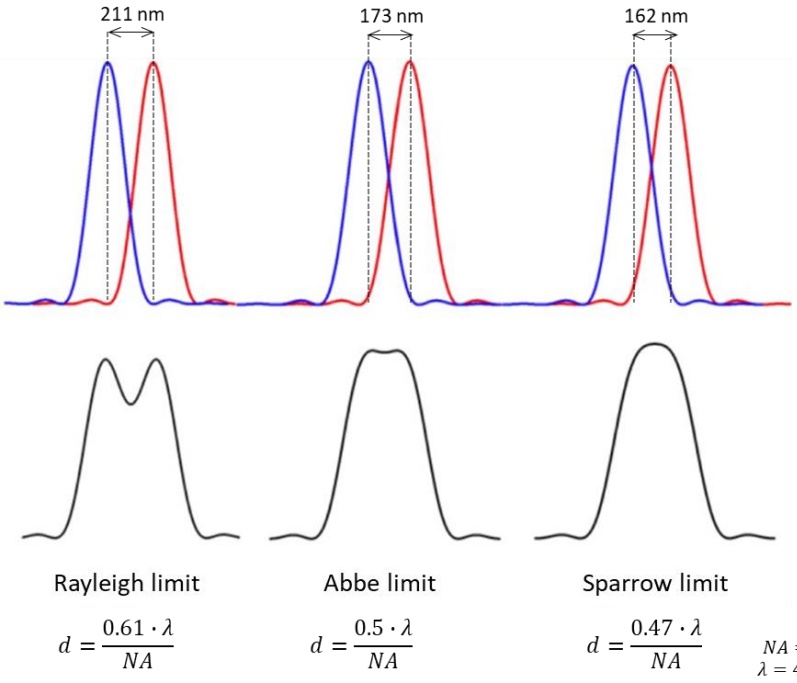

Figure 11 The representation of different resolution limits. Reproduced from [259]

gaps. This means that to observe all fenestrations, a technique that can resolve objects as small as 50 nm was necessary. The ability to distinguish two objects as separate is called resolution and is described as the minimum resolvable distance between those two points (Figure 11). There are several ways to determine the resolution limits of microscopy techniques and the achievable resolution is a combination of many factors [224]. Electron microscopy can resolve objects even below 1 nm so it doesn't need to be considered for LSEC imaging in this section, but optical techniques have a resolution within the fenestration size range and so here only optical diffraction limits will be discussed.

A full understanding of resolution limits requires insight into light and matter interaction. In fluorescent microscopy, each individual fluorophore molecule can be treated as a single point object. Each microscopy setup has a distinct diffraction pattern from a point source called the point spread function (PSF). The observed image is a combination of the actual object and the PSF that is responsible for "blurring" limiting the resolution. There are different ways to access the resolution based on criteria proposed by Rayleigh, Abbe and Sparrow (Figure 11). The first one defines objects as separate if the diffraction central maximum of one object is no closer than the first diffraction minimum of the other object. The second criterium considers two objects as resolved if the distance between them is not smaller than half of the wavelength of the imaging light. The last one defines objects as separate if the intensity in the midpoint between the peaks shows a minimum [225].

The fourth criterium that must be additionally considered is related to the sampling rate. The Nyquist frequency is usually defined for signal processing but for microscopy, it can be related to the labelling density that can influence the resolution. To observe an object of a certain size we have to sample it in intervals of no more than half of the object size. In a practical setup, it means that the pixel size must be at least half of the object size and the pixel size should be in accordance with the resolution. For optical techniques, it is realised by the adjustment of the digital pixel size and for AFM in QI mode by changing the spatial density of the acquired force curves that are calculated into the final image. Often in post-processing, the original pixels are split for more accurate image analysis, especially if automatic software is used.

All these technical aspects had a great influence on the data analysis in **Paper II** and **Paper III**. Both SIM and STED microscopy are getting more popular as an alternative to EM, but their resolution is just on the edge of the small fenestration detection. After collecting data for review **Paper I** and for some of our previous studies [29], we discovered major differences between the reported fenestration size distributions for various kinds of microscopy. The correlative approach allowed us to observe and measure LSEC fenestrations with SIM and STED while using EM as a "ground truth" for the detection of fenestration. Therefore, we knew that we were measuring only the fenestrations not any fenestration-resembling objects or imaging artefacts. SEM images were also used as a scale reference, independently from the microscope calibration. Interestingly, we were able to detect holes as small as 80 nm which is below the theoretical SIM resolution. There are several factors that might contribute to this. Firstly, the final SIM image is reconstructed in a post-acquisition process that can possibly make some fenestrations appear smaller. Secondly, fenestrations are actually negative objects with no signal while the surrounding cell membrane is densely stained. The strong fluorescence can improve the signal-to-noise ratio and have positive effects on image reconstruction and resolution. Finally, the image analysis method is sensitive to the edge detection of fenestrations which in fluorescent microscopy images is blurred due to the PSF.

Selection of the imaging technique

Ideally, the imaging technique should be chosen based on the optimal performance for each type of experiment, however, it is usually dictated by the local availability of the microscopes. In **Paper II** we took advantage of the access to many types of microscopy modalities to provide a comparison between them. Our observation can serve both as a

reference to compare the existing results obtained using different imaging techniques, as well as provide guidance for selecting the right methods for the research question of interest.

When studying the mechanisms behind the fenestration regulation, it is crucial to precisely determine the changes in the size and number of fenestrations. The choice of imaging technique can influence the observed number of fenestrations due to the resolution and three-dimensional structure of LSEC. For example, SIM fenestrations below 80 nm cannot be resolved, apparently lowering the overall number. Moreover, some sieve plates can be placed close to the nucleus and disappear in the z-projection where images from different focal depths are summed up. This means that SIM is not an optimal technique for the precise analysis of fenestration number, especially if a decrease in size is predicted. The resolution issue can be reduced by using for example STED or dSTORM but some fenestrations, especially in perinuclear regions, or within overlapping cells, may remain unresolved. The fenestration number can be measured more precisely using AFM and EM thanks to the label-free nature of those techniques. AFM benefits from easy sample preparation and imaging in wet conditions but obtaining high-resolution images of the whole cells is time-consuming. The acquisition of a single image with a pixel size of 40 nm can take over 30 min which makes it highly impractical for a large number of samples. SEM remains the most time-efficient and, thanks to excellent resolution, the most precise technique for the determination of fenestration number. On the other hand, the sample preparation for EM requires complete dehydration which raises the question of possible deformation of fenestration shape/size as well as of new fenestration formation as an artefact. In **Paper II** we observed only a few fenestration-like structures that were identified as artefacts caused by sample drying, but their number was insignificant in comparison to the thousands of fenestrations measured. We were able to detect those artefacts by combining AFM and SEM correlative imaging. Those observations also agree with the physical properties of the cell membrane. The fusion of lipid bilayers to form fenestration-like structures requires additional energy [226].

Hunting the “true size” of fenestrations

The measurement of the fenestration size proved to be more challenging than the determination of the fenestration number. The range of average fenestration diameters in control/untreated LSEC reported in many different studies varies from about 75 nm to even over 250 nm [29]. There are some clear trends pointing out differences between imaging techniques and between *in vitro*/cell and *in vivo*/tissue data (Supplementary table in [29]).

Paper II provides some clarity by multimodal measurements of the exact same cells/samples and explains the differences in fenestration size observed between the techniques.

In physiological conditions, the fenestration diameter regulates the sieving properties of the liver. By using labelled chylomicron particles, it was possible to indirectly assess the fenestration size. Back in 1982, de Zanger and Wisse [227] orally administered rats with corn oil and measured the fraction of the chylomicrons in the plasma and in the space of Disse. Their data clearly confirmed that the size of particles filtered out of the blood (20-450 nm) matched the measured fenestration size (40-400 nm, TEM *in vivo*). The presented TEM images of liver tissue showed very good preservation and the mean fenestration diameter of 103 nm with a range of 30-250 nm. This result corresponds well with the other *in vivo* results. In general, the diameters measured *in vivo* are smaller than those measured *in vitro*. Steffan et al. [228] showed about 30 nm difference in fenestration size between the *in vitro* and *in vivo* samples which corresponds well with the general trends reported in [29]. There are several possible factors that contribute to that difference. EM remains the only reported technique for imaging fenestrations in tissue, whether in the tissue blocks or sections. That may soon change as recent developments in chip-based super-resolution microscopy enable the use of dSTORM for the imaging of tissue sections [229].

The dehydration step in the sample preparation for EM influences tissue and cells in a different way. Tissue blocks shrink nearly uniformly in all directions which would influence cell shapes in the whole 3D structure [230]. Compared to other microvascular endothelium, LSEC *in vivo* are not directly attached to any substrate or other cells so the shrinkage of the cell body would result in folding that decreases the observed fenestration size. In *in vitro* conditions, LSEC are seeded on a flat substrate. Dehydration causes a reduction in the cell body volume but attachment to the surface does not allow to uniformly shrink the whole cell. Therefore, fenestrations appear dilated as the cell membrane stretches to compensate for the volume loss. We observed that effect clearly in **Paper II** when samples were first measured in wet conditions using AFM or SIM/STED and then dehydrated and visualised by SEM. Fenestration size increases about 30% in that process. The EM data from previous reports obtained for both *in vitro* and *in vivo* conditions support the hypothesis that dehydration is the main cause of the observed differences.

The dehydration-related fenestration dilation may have implications for drug screening EM results. The exact structure of fenestration is not fully known, but the existing data clearly

show that each hole is surrounded by an actin cytoskeleton [32]. We believe that the fine-tuning of the fenestration size is facilitated by some protein systems that include actin-binding proteins, such as spectrin [43] or myosin [4] and membrane anchoring proteins among the others. Moreover, the fusion of the lipid bilayer and maintenance of the opening is an energy-consuming process [226] so there must be some rapidly acting molecular system to open and close fenestrations. We showed previously that some agents such as iodoacetic acid can cause "blinking" of the fenestrations within seconds [43]. The dehydration-related dilation may affect the connection between actin and cell membrane preventing observation of full changes in fenestration size that are unrelated to the actin skeleton remodelling. These preliminary observations need to be further checked to confirm the effect of dehydration and previous results of the effects of some agents on fenestration diameter obtained using EM should be re-evaluated. It is especially important to be able to measure even small changes as any differences in fenestration diameter distribution can affect the filtration within the liver.

Live and fixed cells

Imaging live and fixed cells has advantages and disadvantages that need to be considered. For drug screening where large quantities of samples are required to study both dose- and time-dependency, fixation is a necessity to achieve enough efficiency. Live cell experimental throughput is very low and proper comparison between experiments is especially challenging for primary LSEC as their condition changes rapidly within the first 24 h after isolation. On the other hand, direct observation of the drug effect in real-time can give an extra insight into the mechanism of action. Ideally, a combination of live and fixed cell imaging should be applied to fully understand the effect of the studied agents.

To date, successful live LSEC imaging was reported using AFM [29][50] STED [33] and SIM [231] microscopy. AFM, as a label-free technique, minimizes the interference with the cells and avoids phototoxicity. Fluorescence-based microscopies require staining which can interfere with the LSEC dynamics and/or lead to toxic effects from the high laser intensity. Indeed, di Martino et al. [33] used STED to showed no morphological changes in time after staining with CellTraker for about 90 minutes, compared to the AFM data where even untreated cells showed certain dynamics. The addition of cytochalasin D after staining led to the creation of fenestration like structures, however their size and arrangement suggested they were gaps resulting from toxicity rather than de novo formed sieve plates. Svistounov et al. [48] demonstrated a strong relationship between cell membrane composition and fenestrations

which strongly suggest that dyes that interfere with the cell membrane can influence LSEC. Our preliminary data in this matter confirmed the lack of fenestration dynamics and response to cytochalasin after membrane staining.

Image analysis

The quantitative analysis of LSEC images is crucial for drug screening as it allows precise measurement of changes in fenestration parameters. There are several different approaches to obtain numerical values from the images, from manual counting and measurement to fully automatic machine learning. The overview of the existing reports on LSEC fenestrations from **Paper I** showed major differences in the analysis methods and their possible influence on the observed drug effects. Together with different imaging techniques, it makes comparing between the separate studies a challenge. In **Paper III**, we propose three different analysis methods and test them on images obtained with three commonly used types of microscopy – AFM, SIM and SEM. This article can act as both a guideline for future quantitative analysis of LSEC, as well as help with a comparison between the existing data.

In many reports, the description of the exact measurement methods for fenestration was often omitted, especially if it was performed manually. The lack of standardization in both description of the fenestration parameters and exact protocols to extract these quantitative data makes the comparison between the studies cumbersome. The most commonly used parameters are fenestration diameter, fenestration frequency (number of fenestrations per cell area) and porosity (percentage of the cell area covered by fenestrations), but some reports present data as a number of fenestrations per image or even “total fenestral diameter” [232]. In **Paper III**, we propose to additionally analyse the shape descriptors of fenestrations as the pores do not always appear perfectly circular but rather have an elliptical shape. Therefore, minimal, and maximal diameters can be described as well as their ratio called roundness and be used as an additional parameter for comparison between imaging techniques or drug treatments. We used these additional shape descriptors in **Paper II** to emphasize the differences observed between wet-fixed and fixed-dried cells.

There are several published methods for the analysis of LSEC images, but most concentrate on one microscopy technique and one image analysis method. Cogger and colleagues included the manual measurement methods in their standardized protocol for LSEC preparation using SEM [186]. For fluorescence images, there are two proposed methods: a

semi-automatic method based on contour detection [33] and an adaptive threshold image segmentation [233]. For AFM images, a manual approach for both fenestration size measurement and number quantification was described by Zapotoczny et al. [234]. **Paper III** is our attempt to propose more standard image analysis protocols with precise descriptions to enable users to apply them to any datasets. We also compare the application of the proposed methods to three types of microscopy images and finally study the user bias. The selected methods are based on their low entrance barrier, user-friendliness, no extra computing skills requirement and availability of open-access software. The manual approach is already widely used, but here we optimize the protocol by adding the measurement of both minimal and maximal diameters. This way the method becomes less biased to the choice of the user, especially for less circular, elongated holes. Double measurement also provides the additional shape describing parameters for comparison. The semi-automatic way is based on the intensity thresholding and allows great improvement of the efficiency over the manual approach, however at the cost of accuracy in the detection of fenestrations. We showed that especially for SEM images, the threshold method can underestimate the number of detected holes. On the other hand, this approach showed the best accuracy in the size measurements and the least user bias. The fully automatic approach is designed for the best time efficiency but at the cost of lower accuracy and sensitivity to artefacts. We proposed the use of open access machine learning software Ilastik [196], but similar results should be achievable using other trainable segmentation algorithms.

Paper III provides optimized image analysis protocols that help the potential user to choose the most suitable methods for each experiment. In **Paper II**, we applied the semi-automatic and automatic methods from **Paper III** to analyse the differences between fenestrations measured with various types of microscopy in a correlative manner. The automatization of the analysis allowed us to analyse thousands of fenestrations in each group. To improve the overall accuracy, we optimized the measurement by adjusting the image analysis method to each microscopy pair. In **Paper IV**, we also used a combination of two methods that we showed previously to be the most accurate for each parameter – manual for counting fenestrations and semi-automatic for diameter measurement. Those results show that the application of the right image analysis method is crucial to obtain as much information from the datasets as possible. The development in imaging techniques must be matched with the updates in image analysis to fully use their potential in for example drug screening studies.

Moreover, the optimization of the image analysis allows the adjustment to the lower quality datasets from less advanced or older microscopes.

To better understand the changes in the fenestration diameter distribution in **Paper IV**, we proposed a size-dependent classification of holes into small (<100 nm), medium (100-200 nm) and large (>200 nm). De Zanger and Wisse [227] showed that the chylomicron filtration size-based selectivity depends on the fenestration size. High, and low-density lipoproteins (HDL, LDL) have a diameter below 100 nm while cholesterol-rich chylomicron remnants are usually bigger. The detailed analysis of changes in the whole fenestration size distribution allows us to better predict the physiologically relevant changes in filtration than a simple comparison of average sizes would. For example, an increase in the number of small and large fenestrations and a decrease in medium-sized ones may not affect the average value significantly but the wider diameter distribution would have an effect on the filtration selectivity. We proposed in **Paper IV** the use of Gaussian fit into the data for better assessment of the distribution, next to the detailed analysis of the small/medium/large fractions. The centre of the distribution corresponds to the most commonly occurring size of fenestration and reduces the influence of the outliers. In **Paper III** we showed that especially SEM images of LSEC analysed with the semi-automatic way can detect some pits in the cell membrane as fenestrations. These “false” detected objects usually also have a normal distribution with the centre around 100 nm and can be separated from the fenestration using two separate Gaussian distribution fits. Preliminary data for **Paper IV** suggested that there may be a shift of fenestration size towards smaller diameters. Therefore, to avoid that problem we manually removed the false positive objects after segmentation during image analysis. This adjustment reduced the time efficiency of the method but increased the fenestration detection accuracy.

6 Drug screening

The study of drug effects on LSEC can have a dual purpose. Firstly, it allows for testing the influence of the possible future medicines *in vitro* as a part of the preclinical drug development process. Secondly, agents with known mechanisms of action can be used to better understand the molecular regulatory mechanisms in LSEC. This project is a combination of both approaches. In **Paper I**, we review the existing knowledge about the effects of various drugs on LSEC fenestrations and based on the reported methods we propose the optimized screening protocols in **Paper II** and **Paper III**. Later in **Paper IV**, we apply the improved analysis methods to study the influence of the xanthines on LSEC in vitro. In the second part

of **Paper I**, we discuss the cellular mechanism of action of drugs in the context of fenestration structure and LSEC regulatory systems.

The costs of bringing a drug to the market can be counted in hundreds of millions of dollars, with the main expense being clinical phase I to III trials [235][236]. Only about one out of ten drugs tested in phase I get to market [237]. These statistics show the area for improvement in pre-clinical drug screening. Both animal testing and *in vitro* models dramatically reduce the number of potentially successful compounds. Nevertheless, 90% get through the entire approval process just to meet rejection later, mostly due to unpredicted hepatotoxicity [142]. The improved preclinical models for testing drugs on livers and liver cells may improve the success rate in drug development. The main focus of this project is on LSEC. However, the developed methods can also be applied to multicellular co-culture models. The organ on a chip technology [208], various kinds of bioreactors [209] or in vitro organoids [210] are promising platforms for future drug screening.

The direction of the research is nowadays aimed toward a “bottom-up” approach instead of the historical “top-down”. New agents are designed to fix certain molecular problems and are even designed *in silico* to precisely target certain receptors or genetic sequences [238]. This way, in the early stages, tens of thousands of molecules are designed as possible therapeutics which can then be tested at the cellular level. At this stage usually only the targeted effect is examined, with only a minor evaluation of possible side effects in other cells/organs/tissue. Hepatotoxicity is the main concern in drug development, however, in many cases the certain levels are acceptable until later phases and the focus is directed more towards the development of protective agents or possible direct-acting analogues [139]. The *in vitro* drug screening on liver cells enables early detection of the hepatotoxic effects and helps to point out the exact molecular mechanisms that can be counteracted.

6.1 LSEC and xanthines

The side effects of some therapeutics are not necessary only negative. Some unexpected side effects can be used in therapies for unrelated conditions. An interesting example is sildenafil - the commercial name Viagra - which was developed to treat hypertension by dilating blood vessels in the heart. In phase I of the clinical trials researchers discovered that sildenafil also can be used for the treatment of erectile disfunction in men [239]. Later, it was also shown to improve liver regeneration [240] and was even used as a part of the NAFLD treatment [241].

Hunt et al. [143] reported sildenafil increases LSEC porosity in both young and old mice and induces fenestration dilation in old mice. Sildenafil causes elevated cGMP levels via selective inhibition of phosphodiesterase type 5 (PDE5) and the ATP-binding cassette C5 (ABCC5) that are responsible for cGMP degradation and efflux, respectively [242]. A similar but less specific mechanism of action was reported for xanthines [243] which are the main focus of **Paper IV.**

Xanthines can be found in food and beverages – caffeine in coffee and tea, theobromine in chocolate, theophylline is in use as an asthma medicine and paraxanthine is the main caffeine metabolite that reaches higher plasma concentrations than any other xanthine [244]. The long history of consumption of xanthines and approval for medical use has major implications for possible future applications. In **Paper IV**, we studied xanthines in two concentrations – 8/20 µg/ml which is a physiologically achievable plasma level after consumption of regular food/drinks/medicines containing xanthines, and 150 µg/ml which would be toxic as a plasma concentration but achievable locally if used in a targeted drug delivery system (such as liposomes or nanoparticles). Caffeine is metabolized by hepatocytes with the CYP1A2 enzyme to theobromine, theophylline and paraxanthine [245]. In rodents, all three metabolites are present in the same ratio [246][247], while in humans, about 80% of caffeine is metabolised to paraxanthine [243][248]. The differences in the metabolism and clearance rate can lead to higher plasma concentrations of the metabolites than the original compound. Moreover, caffeine and its metabolites are pharmacologically active and may simultaneously contribute to the overall effects if acting through the same molecular mechanisms [247].

The **Paper IV** results showed increases in fenestration frequency after treatment with high doses of xanthines but mostly without significant changes in porosity due to compensation by a decrease in fenestration size. In lower concentrations, only theobromine caused increases in fenestration frequency. The detailed analysis of the changes in fenestration size distribution showed a general trend of the increase in holes below 100 nm and a decrease in holes above 200 nm. This result may have a physiological implication in the reduction of the filtration of chylomicron remnants larger than 200 nm. On the other hand, increased fenestration frequency after therapeutic treatments could improve the filtration of molecules present in plasma. To fully understand the influence of fenestration number and size on liver filtration, detailed analysis and computer modelling are needed. Nevertheless, the improvement in the fenestration frequency is a promising result for the use as a treatment against conditions causing reduction of fenestrations, such as ageing.

In humans, caffeine metabolism rates vary between individuals, which manifests as different sensitivities to coffee/caffeine [245]. The main cause of this variation was identified in the activity level of the CYP1A2 enzyme, which is responsible for caffeine metabolism [249]. The use of cells from 3 rats allowed us to study the individual animal differences. We observed high variations in the response to the treatments between the animals, especially with the higher concentrations of xanthines. It is not known if LSECs can metabolise caffeine, but according to Bhandari et al. [70], LSEC do not express CYP1A2, and so the observed differences may have other causes. The cells in this study were isolated from male Sprague Dawley (SD) rats, which are an outbred rat stock. The study of whole genotypes of SD rats showed large differences between animals, even from the same breeding facility [250]. The exact molecular mechanism of action of xanthines on LSEC is not known. Hunt et al. [143] showed that sildenafil changes intracellular cGMP and proposed the involvement of NO/cGMP pathway. Xanthines can also influence cGMP levels by non-selective inhibition of PDEs responsible degradation of cGMP (sildenafil is a selective inhibitor of PDE5 [251]). Detailed measurements of the intracellular cGMP will be required to confirm this mechanism. A better understanding of fenestration structure and regulation may also help to delineate the exact mechanism of action of xanthines.

6.2 Structure and regulation of fenestrations

To date, the exact molecular structure and regulatory mechanisms of fenestrations in LSEC remain unknown. This lack of knowledge significantly hinders the development of new therapeutics targeting fenestrations. For many existing drugs with confirmed positive effects on LSEC, we cannot explain the exact molecular mechanism of action. In the second part of **Paper I**, we attempted to combine the existing data on fenestration affecting agents with the hypotheses proposed in previous reports. It allowed the formulation of four independent but overlapping mechanisms: (I) actin (de)polymerization regulates the number of fenestrations, (II) calcium ions regulate the diameter of fenestrations, (III) regulation of fenestrations depends on lipid rafts, (IV) spectrin is involved in the open versus closed state of fenestration.

The overview of the existing knowledge about LSEC fenestration from **Paper I** allows for a better focus on future research into filling the gaps between those hypotheses. It also presents the overlapping mechanisms that can be explained from various angles. For example, points (I) and (II) focus on the actin cytoskeleton and calcium ions which both can be connected via myosin. Phosphorylation of myosin light chains (MLC) can occur through calcium-

dependent activation of calmodulin. The contraction and relaxation of the actin-myosin system seem to affect the size and/or number of fenestrations. On the other hand, the actin-binding protein – spectrin, was shown to facilitate opened/closed state of fenestrations (IV). Spectrin, together with other proteins, creates complexes involved in the maintenance and shaping of the cell plasma membrane. The connection between actin and membrane is supported by anchoring proteins which can be highly affected by local membrane composition changes, such as in lipid rafts (III). The connections between the hypothesis (I) – (IV) show that we are closer than ever to fully solving the fenestration structure puzzle.

The study of mechanisms involved in the regulation of fenestration is even more challenging than finding the structure. Many already proposed signalling pathways can influence the cell in different ways, making it challenging to distinguish between direct and indirect effects. Nevertheless, in **Paper I** we tried to sum up the pathways with reported influences on fenestrations, in combination with other pathways described in endothelial cells. The two main signalling pathways influencing fenestration with a high certainty are acting via Rho/ROCK and NO/cGMP [137][131]. Both can influence actin polymerisation through acting binding proteins (such as profilin, cofilin, and gelsolin) and regulate fenestration via phosphorylation of MLC. Regulation of LSEC via NO is especially interesting due to the lack of smooth muscle cells in liver sinusoids. In regular micro vessels, vasoconstriction and vasodilation are facilitated by cGMP in smooth muscle cells that respond to the NO released by endothelial cells. In sinusoids, it seems like a similar mechanism exists in LSEC in connection with VEGF signalling.

Conclusions

The development of new imaging techniques and image analysis methods has huge implications for preclinical research. The focus of this project is the optimization and implementation of novel approaches for drug screening on LSEC.

By studying all the reported agents that can influence fenestrations, we proposed the possible hypothesis describing fenestration structure and regulatory mechanisms. A better understanding of LSEC regulation will not only help to develop new therapeutics but also explain the mechanisms behind the effects of already known drugs. **Paper I** gathered the information that may be beneficial for researchers working within the liver field, as well as for physicians. Moreover, the analysis of the already used methods in drug screening showed possible ways for the implementation of novel microscopy techniques.

The application of the automated image analysis methods developed in **Paper III** allows the evaluation of hundreds or thousands of images by greatly improving time efficiency. Moreover, the accuracy can be optimized for each parameter and imaging technique by a selection of the optimal image analysis method. All the new proposed protocols are based on user-friendly open-source software showing that advanced image analysis can be performed by anyone regardless of their programming and computer skills.

Studying LSEC with correlative microscopy approaches helps to better understand the observed differences between imaging techniques. In **Paper II**, the combination of label-free (SEM, AFM) and label-dependent (SIM, STED) microscopies allow the determination of the influence of sample preparation steps such as wet and dry fixation on the measurement of fenestrations. We concluded that the previously observed enlargement of diameters in SEM results from sample dehydration. Also, the presented data showed the influence of different fixatives on cell stiffness which can affect the measurement of fenestrations imaged with AFM.

Xanthines, present in many foods and beverages, have a positive effect on LSEC porosity profile *in vitro*. The results of **Paper IV** show that a high concentration (150µg/ml) of caffeine, theobromine, theophylline and paraxanthine increases the fenestration number. The same effect was observed also in the low concentration of theobromine (8µg/ml). If reproducible *in vivo*, these findings may help with the development of re-fenestrating therapies for conditions that lead to decreased LSEC porosity, such as ageing.

Based on the analysis done in **Paper I**, there are several possible routes for future research on finding new therapeutics for refenestration. Some existing drugs enhanced LSEC fenestration *in vitro* in both young and old mice, so further studies are needed to find the right treatment dose that would be of benefit for LSEC [238]. Xanthines have positive effects on LSEC *in vitro,* however the high concentration needed for this effect would have a toxic effect at the systemic level. Targeted drug delivery vectors such as nanoparticles or liposomes may help to directly target LSEC with the required high dose of xanthines. This approach would be especially interesting for treatment of conditions that lead to the reduction or disappearance of fenestrations.

The drug screening in this project was restricted to a single substance at a time, but polypharmacy - regular daily consumption of 4 or more medicines, is a growing problem in our ageing population. The side effects of the drug-cocktail may have to be reconsidered, especially against the increasing background problem of non-alcoholic fatty liver disease. Liver toxicity is the most common of severe side effects leading to drug withdrawals so testing drug combinations on liver cells *in* vitro may help to develop better treatment strategies. The genetic difference between the individuals may also lead to different response to some drugs (such as to caffeine), mostly due to differences in the liver enzyme system activity. An interesting futuristic idea would be to study the cells from individual patients, for example from liver biopsies, for adjustment of the "drug cocktail" to reduce the negative effect on the liver.

From the methods perspective, the development of new super-resolution microscopies and better fluorophores may enable more efficient imaging of LSEC. To date, AFM remains the only technique applicable for live LSEC imaging but the recent advances in optical nanoscopes should soon facilitate the observation of live LSEC. The reduction of the phototoxic effect of light, either by reduction of intensity or exposure time should play a crucial role. Another key factor is the development of new fluorophores that have a minimal effect on the cell and that do not lead to the production of ROS while interacting with photons. The correlative approach that combines label-free techniques such as AFM with super resolution optical microscopy will play a major role in studying dye-cell effects. In **Paper II** we showed the possibilities of used this kind of AFM/STED setup as a single machine on fixed LSEC.

The main aim of **Paper III** was to propose user friendly methods for LSEC image analysis, however there are also other approaches that should be considered in the future. Especially promising for image analysis purpose may be deep learning – a method based on multiple layers of artificial neural network [252]. This approach enables efficient training on large datasets of images and possibly would further improve fenestration analysis. The challenge in application of this methods is the need for

advanced programming skills as the field of machine learning is growing faster than the adjustments of user-friendly interfaces.

Bibliography:

[1] I. M. Arias, W. Jakoby, H. Popper, D. Schacher, and D. Shafritz, Eds., *The liver biology and pathobiology*, Second edi. Raven Press, 1988.

[2] K. Stine and T. Brown, "Hepatic toxicity," in *Principles of toxicology*, Taylor & Francis, 2006.

[3] I. Martinez *et al.*, "The influence of oxygen tension on the structure and function of isolated liver sinusoidal endothelial cells," *Comp. Hepatol.*, vol. 7, pp. 1–11, 2008, doi: 10.1186/1476-5926-7-4.

[4] F. Braet and E. Wisse, "Structural and functional aspects of liver sinusoidal endothelial cell fenestrae: a review," *Comp. Hepatol.*, vol. 1, p. 1, 2002, doi: 10.1186/1476-5926-1-1.

[5] K. Wake and T. Sato, "'The Sinusoid' in the Liver: Lessons Learned from the Original Definition by Charles Sedgwick Minot (1900)," *Anat. Rec.*, vol. 298, no. 12, pp. 2071–2080, 2015, doi: 10.1002/ar.23263.

[6] A. Blouin, R. P. Bolender, and E. R. Weibel, "Distribution of organelles and membranes between hepatocytes and nonhepatocytes in the rat liver parenchyma. A stereological study," *J. Cell Biol.*, vol. 72, no. 2, pp. 441–455, 1977, doi: 10.1083/jcb.72.2.441.

[7] H. Komatsu, A. Koo, and P. H. Guth, "Leukocyte flow dynamics in the rat liver microcirculation," *Microvasc. Res.*, vol. 40, no. 1, pp. 1–13, 1990, doi: 10.1016/0026-2862(90)90002-9.

[8] Y. J. Yoon *et al.*, "Three-Dimensional Imaging of Hepatic Sinusoids in Mice Using Synchrotron Radiation Micro-Computed Tomography," *PLoS One*, vol. 8, no. 7, pp. 1–10, 2013, doi: 10.1371/journal.pone.0068600.

[9] T. Horn, P. Christoffersen, and J. H. Henriksen, "Alcoholic liver injury: defenestration in noncirrhotic livers-a scanning electron microscopic study," *Hepatology*, vol. 7, no. 1, pp. 77–82, 1987, doi: 10.1002/hep.1840070117.

[10] J. H. Henriksen and N. A. Lassen, "Pressure profile in liver sinusoids," *Liver*, vol. 8, no. 2, pp. 88–94, 2008, doi: 10.1111/j.1600-0676.1988.tb00973.x.

[11] F. Vidal-Vanaclocha and E. Barberá-Guillem, "Fenestration patterns in endothelial cells of rat liver sinusoids," *J. Ultrastruct. Res. Mol. Struct. Res.*, vol. 90, no. 2, pp. 115–123, 1985, doi: 10.1016/0889-1605(85)90102-8.

[12] G. L. Semenza, "Oxygen sensing, hypoxia-inducible factors, and disease pathophysiology," *Annu. Rev. Pathol. Mech. Dis.*, vol. 9, pp. 47–71, 2014, doi: 10.1146/annurev-pathol-012513-104720.

[13] T. Kietzmann, "Metabolic zonation of the liver: The oxygen gradient revisited," *Redox Biol.*, vol. 11, no. January, pp. 622–630, 2017, doi: 10.1016/j.redox.2017.01.012.

[14] R. Gebhardt, "Metabolic zonation of the liver: Regulation and implications for liver function," *Pharmacol. Ther.*, vol. 53, no. 3, pp. 275–354, 1992, doi: 10.1016/0163-7258(92)90055-5.

References

[15] N. J. Hewitt *et al.*, "Primary hepatocytes: Current understanding of the regulation of metabolic enzymes and transporter proteins, and pharmaceutical practice for the use of hepatocytes in metabolism, enzyme induction, transporter, clearance, and hepatotoxicity studies," *Drug Metab. Rev.*, vol. 39, no. 1, pp. 159–234, 2007, doi: 10.1080/03602530601093489.

[16] D. L. Knook, N. Blansjaar, and E. C. Sleyster, "Isolation and characterization of Kupffer and endothelial cells from the rat liver," *Exp. Cell Res.*, vol. 109, no. 2, pp. 317–329, 1977, doi: 10.1016/0014-4827(77)90011-8.

[17] D. W. Fawcett, "Observations on the cytology and electron microscopy of hepatic cells," *J Natl Cancer Inst*, vol. 15, no. 5, pp. 1475–1503, 1955.

[18] H. Parks, "The hepatic sinusoidal endothelial cell and its histological relationships," *Electron Microsc. Proc. Stock. Conf.*, 1956.

[19] F. Wassermann, "The structure of the wall of the hepatic sinusoids in the electron microscope," *Zeitschrift fur Zellforsch.*, vol. 49, pp. 13–32, 1958.

[20] M. Yamagishi, "Electron Microscope Studies on the Fine Structure of the Sinusoidal Wall and Fat-Storing Cells of Rabbit Livers," *Arch Histol Jpn*, vol. 18, no. 2, pp. 223–261, 1959.

[21] H. S. Bennett, J. H. Luft, and J. C. Hampton, "Morphological classifications of vertebrate blood capillaries," *Am. J. Physiol.*, vol. 196, no. 2, pp. 381–390, 1959, doi: 10.1152/ajplegacy.1959.196.2.381.

[22] E. Wisse, "An electron microscopic study of the fenestrated endothelial lining of rat liver sinusoids," *J. Ultrasructure Res.*, vol. 31, no. 1–2, pp. 125–150, 1970, doi: 10.1016/S0022-5320(70)90150-4.

[23] F. Braet, R. De Zanger, and E. Wisse, "Drying cells for SEM, AFM and TEM by hexamethyldisilazane: a study on hepatic endothelial cells.," *J. Microsc.*, vol. 186, no. Pt 1, pp. 84–87, 1997, doi: 10.1046/j.1365-2818.1997.1940755.x.

[24] F. Braet, R. De Zanger, S. Kämmer, and E. Wisse, "Noncontact versus contact imaging: an atomic force microscopic study on hepatic endothelial cells in vitro," *Int. J. Imaging Syst. Technol.*, vol. 8, no. 2, pp. 162–167, 1997, doi: 10.1002/(SICI)1098-1098(1997)8:2<162::AID-IMA3>3.3.CO;2-W.

[25] F. Braet, R. De Zanger, C. Seynaeve, M. Baekeland, and E. Wisse, "A comparative atomic force microscopy study on living skin fibroblasts and liver endothelial cells," *J. Electron Microsc. (Tokyo).*, vol. 50, no. 4, pp. 283–290, 2001, doi: 10.1093/jmicro/50.4.283.

[26] F. Braet and E. Wisse, "Imaging surface and submembranous structures in living cells with the atomic force microscope: notes and tricks.," *Methods Mol. Biol.*, vol. 242, no. February 2004, pp. 201–216, 2004, doi: 10.1385/1-59259-647-9:201.

[27] F. Braet and E. Wisse, "AFM imaging of fenestrated liver sinusoidal endothelial cells," *Micron*, vol. 43, no. 12, pp. 1252–1258, 2012, doi: 10.1016/j.micron.2012.02.010.

[28] B. Zapotoczny, K. Szafranska, K. Owczarczyk, E. Kus, S. Chlopicki, and M. Szymonski, "AFM Reveals Dynamic Morphology of Fenestrations in Living Liver Sinusoidal Endothelial Cells," *Sci. Rep.*, vol. 7, 2017, doi: 10.1038/s41598-017-08555-0.

[29] B. Zapotoczny *et al.*, "Tracking Fenestrae Dynamics in Live Murine Liver Sinusoidal Endothelial Cells," *Hepatology*, vol. 69, no. 2, pp. 876–888, 2019, doi: 10.1002/hep.30232.

[30] Z. Gatmaitan, L. Varticovski, L. Ling, R. Mikkelsen, A. M. Steffan, and I. M. Arias, “Studies on fenestral contraction in rat liver endothelial cells in culture.,” *Am. J. Pathol.*, vol. 148, no. 6, pp. 2027–2041, 1996.

[31] V. C. Cogger *et al.*, “Three-dimensional structured illumination microscopy of liver sinusoidal endothelial cell fenestrations,” *J. Struct. Biol.*, vol. 171, no. 3, pp. 382–388, 2010, doi: 10.1016/j.jsb.2010.06.001.

[32] V. Mönkemöller, C. Øie, W. Hübner, T. Huser, and P. McCourt, “Multimodal super-resolution optical microscopy visualizes the close connection between membrane and the cytoskeleton in liver sinusoidal endothelial cell fenestrations.,” *Sci. Rep.*, vol. 5, p. 16279, 2015, doi: 10.1038/srep16279.

[33] J. Di Martino *et al.*, “STED microscopy : a simplified method for liver sinusoidal endothelial fenestrae analysis,” *Biol. Cell*, vol. 110, pp. 159–168, 2018, doi: 10.1111/boc.201800016.

[34] A. Butola *et al.*, “Multimodal on-chip nanoscopy and quantitative phase imaging reveals the nanoscale morphology of liver sinusoidal endothelial cells,” *Proc. Natl. Acad. Sci. U. S. A.*, vol. 118, no. 47, 2021, doi: 10.1073/pnas.2115323118.

[35] R. Diekmann *et al.*, “Chip-based wide field-of-view nanoscopy,” *Nat. Photonics*, vol. 11, no. 5, pp. 322–328, 2017, doi: 10.1038/nphoton.2017.55.

[36] E. Wisse, J. H. Van Dierendonck, R. B. De Zanger, R. Fraser, and R. S. McCuskey, “On the role of the liver endothelial filter in the transport of particulate fat (chylomicrons and their remnants) to parenchymal cells and the influence of certain hormones on the endothelial fenestrae.,” *Commun. Liver Cells*, pp. 195–200, 1980.

[37] K. Szafranska *et al.*, “Quantitative analysis methods for studying fenestrations in liver sinusoidal endothelial cells. A comparative study,” *Micron*, p. 103121, 2021, doi: https://doi.org/10.1016/j.micron.2021.103121.

[38] K. E. Wack, M. A. Ross, V. Zegarra, L. R. Sysko, S. C. Watkins, and D. B. Stolz, “Sinusoidal ultrastructure evaluated during the revascularization of regenerating rat liver,” *Hepatology*, vol. 33, no. 2, pp. 363–378, 2001, doi: 10.1053/jhep.2001.21998.

[39] V. C. Cogger and D. G. Le Couteur, “Fenestrations in the Liver Sinusoidal Endothelial Cell,” in *The Liver: Biology and Pathobiology, Fifth Edition*, 2009, pp. 389–406.

[40] F. Braet *et al.*, “New Observations on Cytoskeleton and Fenestrae in Isolated Rat-Liver Sinusoidal Endothelial-Cells,” *J. Gastroenterol. Hepatol.*, vol. 10, pp. S3–S7, 1995, doi: 10.1111/j.1440-1746.1995.tb01792.x.

[41] I. Spector, F. Braet, N. R. Shochet, and M. R. Bubb, “New anti-actin drugs in the study of the organization and function of the actin cytoskeleton,” *Microsc. Res. Tech.*, vol. 47, no. 1, pp. 18–37, 1999, doi: 10.1002/(SICI)1097-0029(19991001)47:1<18::AID-JEMT3>3.0.CO;2-E.

[42] K. Szafranska, L. D. Kruse, C. F. Holte, P. McCourt, and B. Zapotoczny, “The wHole Story About Fenestrations in LSEC,” *Front. Physiol.*, vol. 12, no. September, 2021, doi: 10.3389/fphys.2021.735573.

[43] B. Zapotoczny *et al.*, “Actin-spectrin scaffold supports open fenestrae in liver sinusoidal endothelial cells,” *Traffic*, no. September, pp. 932–942, 2019, doi: 10.1111/tra.12700.

References

[44] R. G. Parton and K. Simons, "The multiple faces of caveolae," *Nat. Rev. Mol. Cell Biol.*, vol. 8, no. 3, pp. 185–194, 2007, doi: 10.1038/nrm2122.

[45] M. Ogi *et al.*, "Distribution and localization of caveolin-1 in sinusoidal cells in rat liver," *Med. Electron Microsc.*, vol. 36, no. 1, pp. 33–40, 2003, doi: 10.1007/s007950300004.

[46] V. C. Cogger *et al.*, "The response of fenestrations, actin, and caveolin-1 to vascular endothelial growth factor in SK Hep1 cells.," *Am. J. Physiol. Gastrointest. Liver Physiol.*, vol. 295, no. 1, pp. G137–G145, 2008, doi: 10.1152/ajpgi.00069.2008.

[47] A. Warren, V. C. Cogger, I. M. Arias, R. S. McCuskey, D. G. LeCouteur, and D. G. Le Couteur, "Liver sinusoidal endothelial fenestrations in caveolin-1 knockout mice.," *Microcirculation*, vol. 17, no. 1, pp. 32–38, 2010, doi: 10.1111/j.1549-8719.2009.00004.x.

[48] D. Svistounov *et al.*, "The Relationship between Fenestrations, Sieve Plates and Rafts in Liver Sinusoidal Endothelial Cells," *PLoS One*, vol. 7, no. 9, pp. 1–9, 2012, doi: 10.1371/journal.pone.0046134.

[49] V. C. Cogger, U. Roessner, A. Warren, R. Fraser, and D. G. Le Couteur, "A Sieve-Raft Hypothesis for the Regulation of Endothelial Fenestrations," *Comput. Struct. Biotechnol. J.*, vol. 8, no. 11, pp. 1–9, 2013, doi: 10.5936/csbj.201308003.

[50] B. Zapotoczny, K. Szafranska, K. Owczarczyk, E. Kus, S. Chlopicki, and M. Szymonski, "Atomic Force Microscopy Reveals the Dynamic Morphology of Fenestrations in Live Liver Sinusoidal Endothelial Cells," *Sci. Rep.*, vol. 7, no. 1, p. 7994, 2017, doi: 10.1038/s41598-017-08555-0.

[51] F. Braet, I. Spector, R. B. de Zanger, and E. Wisse, "Fenestrae-forming center (FFC): a novel structure involved in the formation of liver sinusoidal endothelial cell fenestrae," *Kupffer Cell Found. Cells Hepatic Sinusoid, Vol. 7*, p. 144, 1999.

[52] F. Braet, I. Spector, R. De Zanger, and E. Wisse, "A novel structure involved in the formation of liver endothelial cell fenestrae revealed by using the actin inhibitor misakinolide.," *Proc. Natl. Acad. Sci. U. S. A.*, vol. 95, no. 23, pp. 13635–13640, 1998, doi: 10.1073/pnas.95.23.13635.

[53] E. Wisse *et al.*, "Fixation methods for electron microscopy of human and other liver," *World J. Gastroenterol.*, vol. 16, no. 23, pp. 2851–2866, 2010, doi: 10.3748/wjg.v16.i23.2851.

[54] K. K. Sørensen *et al.*, "The scavenger endothelial cell: a new player in homeostasis and immunity.," *Am. J. Physiol. - Regul. Integr. Comp. Physiol.*, vol. 303, no. 12, pp. R1217-30, 2012, doi: 10.1152/ajpregu.00686.2011.

[55] Y. Kawai, B. Smedsrød, K. Elvevold, and K. Wake, "Uptake of lithium carmine by sinusoidal endothelial and Kupffer cells of the rat liver: New insights into the classical vital staining and the reticulo-endothelial system," *Cell Tissue Res.*, vol. 292, no. 2, pp. 395–410, 1998, doi: 10.1007/s004410051069.

[56] L. Aschoff, "Das reticulo-endotheliale System," in *Ergebnisse der Inneren Medizin und Kinderheilkunde*, 1924.

[57] R. van Furth, Z. A. Cohn, J. G. Hirsch, J. H. Humphrey, W. G. Spector, and H. L. Langevoort, "The mononuclear phagocyte system: a new classification of macrophages, monocytes, and their precursor cells.," *Bull. World Health Organ.*, vol. 46, no. 6, pp. 845–852, 1972.

[58] B. Smedsrod, H. Pertoft, S. Gustafson, and T. C. Laurent, “Scavenger functions of the liver endothelial cell,” *Biochem. J.*, vol. 266, no. 2, pp. 313–327, 1990, doi: 10.1042/bj2660313.

[59] S. Bhandari, A. K. Larsen, P. McCourt, B. Smedsrød, and K. K. Sørensen, “The Scavenger Function of Liver Sinusoidal Endothelial Cells in Health and Disease,” *Front. Physiol.*, vol. 12, pp. 1–23, 2021, doi: 10.3389/fphys.2021.757469.

[60] T. Seternes, K. Sørensen, and B. Smedsrød, “Scavenger endothelial cells of vertebrates: A nonperipheral leukocyte system for high-capacity elimination of waste macromolecules,” *Proc. Natl. Acad. Sci. U. S. A.*, vol. 99, no. 11, pp. 7594–7597, 2002, doi: 10.1073/pnas.102173299.

[61] B. Smedsrød, “Clearance function of scavenger endothelial cells,” *Comp. Hepatol.*, vol. 3, 2004.

[62] E. Wisse, “An ultrastructural characterization of the endothelial cell in the rat liver sinusoid under normal and various experimental conditions, as a contribution to the distinction between endothelial and Kupffer cells,” *J. Ultrasructure Res.*, vol. 38, no. 5–6, pp. 528–562, 1972, doi: 10.1016/0022-5320(72)90089-5.

[63] I. Malovic *et al.*, “The mannose receptor on murine liver sinusoidal endothelial cells is the main denatured collagen clearance receptor,” *Hepatology*, vol. 45, no. 6, pp. 1454–1461, 2007, doi: 10.1002/hep.21639.

[64] C. I. Øie, R. Olsen, B. Smedsrød, and J. Hansen, “Liver sinusoidal endothelial cells are the principal site for elimination of unfractionated heparin from the circulation,” *Am J Physiol Gastrointest Liver Physiol*, pp. 520–528, 2008, doi: 10.1152/ajpgi.00489.2007.

[65] R. Blomhoff, W. Eskild, and T. Berg, “Endocytosis of formaldehyde-treated serum albumin via scavenger pathway in liver endothelial cells,” *Biochem. J.*, vol. 218, no. 1, pp. 81–86, 1984, doi: 10.1042/bj2180081.

[66] Y. B. De Rijke, E. Biessen, C. Vogelezang, and T. Berkel, “Binding characteristics of scavenger receptors on liver endothelial and Kupffer cells for modified low-density lipoproteins,” *Biochem. J.*, vol. 304, pp. 69–73, 1994.

[67] T. Løvdal, E. Andersen, A. Brech, and T. Berg, “Fc receptor mediated endocytosis of small soluble immunoglobulin G immune complexes in Kupffer and endothelial cells from rat liver,” *J. Cell Sci.*, vol. 113, pp. 3255–3266, 2000.

[68] J. Simon-Santamaria *et al.*, “Efficient uptake of blood-borne BK and JC polyomavirus-like particles in endothelial cells of liver sinusoids and renal Vasa recta,” *PLoS One*, vol. 9, no. 11, 2014, doi: 10.1371/journal.pone.0111762.

[69] R. Kjeken, S. A. Mousavi, A. Brech, T. Gjøen, and T. Berg, “Fluid phase endocytosis of [125I]iodixanol in rat liver parenchymal, endothelial and Kupffer cells,” *Cell Tissue Res.*, vol. 304, no. 2, pp. 221–230, 2001, doi: 10.1007/s004410100348.

[70] S. Bhandari *et al.*, “Transcriptome and proteome profiling reveal complementary scavenger and immune features of rat liver sinusoidal endothelial cells and liver macrophages,” *BMC Mol. Cell Biol.*, vol. 21, no. 1, pp. 1–25, 2020, doi: 10.21203/rs.2.24396/v1.

[71] P. A. G. Mccourt, “Characterization of a Hyaluronan Receptor on Rat Sinusoidal Liver Endothelial Cells and Its Functional Relationship to Scavenger Receptors,” *Hepatology*, pp. 1276–1286, 1999.

References

[72] B. Hansen *et al.*, "Stabilin-1 and stabilin-2 are both directed into the early endocytic pathway in hepatic sinusoidal endothelium via interactions with clathrin/AP-2, independent of ligand binding," *Exp. Cell Res.*, vol. 303, no. 1, pp. 160–173, 2005, doi: 10.1016/j.yexcr.2004.09.017.

[73] S. A. Mousavi, M. Sporstøl, C. Fladeby, R. Kjeken, N. Barois, and T. Berg, "Receptor-mediated endocytosis of immune complexes in rat liver sinusoidal endothelial cells is mediated by FcγRIIb2," *Hepatology*, vol. 46, no. 3, pp. 871–884, 2007, doi: 10.1002/hep.21748.

[74] J. Simon-Santamaria *et al.*, "Age-Related Changes in Scavenger Receptor-Mediated Endocytosis in Rat Liver Sinusoidal Endothelial Cells," *J Gerontol A Biol Sci Med Sci*, vol. 65A, no. 9, pp. 951–960, 2010, doi: DOI 10.1093/gerona/glq108.

[75] R. S. McCuskey, "Sinusoidal endothelial cells as an early target for hepatic toxicants," *Clin. Hemorheol. Microcirc.*, vol. 34, no. 1–2, pp. 5–10, 2006.

[76] C. H. C. M. Buys, A. S. H. De Jong, J. M. W. BOuma, and M. Gruber, "Rapid Uptake By Liver Sinusoidal Cells Of Serum Albumin Modified With Retention Of Its Compact Conformation," *Biochim. Biophys. Acta*, vol. 392, pp. 95–100, 1975.

[77] R. Li *et al.*, "Role of liver sinusoidal endothelial cells and stabilins in elimination of oxidized low-density lipoproteins.," *Am. J. Physiol. Gastrointest. Liver Physiol.*, vol. 300, no. 1, pp. G71-81, 2011, doi: 10.1152/ajpgi.00215.2010.

[78] T. H. Mogensen, "Pathogen Recognition and Inflammatory Signaling in Innate Immune Defenses," *Clin. Microbiol. Rev.*, vol. 22, no. 2, pp. 240–273, 2009, doi: 10.1128/CMR.00046-08.

[79] Y. Wang and Y. Liu, "Gut-liver-axis: Barrier function of liver sinusoidal endothelial cell," *J. Gastroenterol. Hepatol.*, vol. 36, no. 10, pp. 2706–2714, 2021, doi: 10.1111/jgh.15512.

[80] A. Uhrig *et al.*, "Development and functional consequences of LPS tolerance in sinusoidal endothelial cells of the liver," *J. Leukoc. Biol.*, vol. 77, pp. 626–633, 2005, doi: 10.1189/jlb.0604332.

[81] A. Roghanian, R. J. Stopforth, L. N. Dahal, and M. S. Cragg, "New revelations from an old receptor: Immunoregulatory functions of the inhibitory Fc gamma receptor, FcγRIIB (CD32B)," *J. Leukoc. Biol.*, vol. 103, no. 6, pp. 1077–1088, 2018, doi: 10.1002/JLB.2MIR0917-354R.

[82] S. Shetty, P. F. Lalor, and D. H. Adams, "Liver sinusoidal endothelial cells — gatekeepers of hepatic immunity," *Nat. Rev. Gastroenterol. Hepatol.*, 2018, doi: 10.1038/s41575-018-0020-y.

[83] S. Huang *et al.*, "LSECs express functional NOD1 receptors : A role for NOD1 in LSEC maturation-induced T cell immunity in vitro," *Mol. Immunol.*, vol. 101, pp. 167–175, 2018, doi: 10.1016/j.molimm.2018.06.002.

[84] P. F. Lalor, P. Shields, and A. J. Grant, "Recruitment of lymphocytes to the human liver," *Immunol. Cell Biol.*, vol. 80, pp. 52–64, 2002.

[85] J. Wong *et al.*, "A minimal role for selectins in the recruitment of leukocytes into the inflamed liver microvasculature," *J. Clin. Invest.*, vol. 99, no. 11, pp. 2782–2790, 1997, doi: 10.1172/JCI119468.

[86] A. Warren, D. G. Le Couteur, R. Fraser, D. G. Bowen, G. W. Mccaughan, and P. Bertolino, "T Lymphocytes Interact With Hepatocytes Through Fenestrations in Murine Liver Sinusoidal Endothelial Cells," *Hepatology*, vol. 44, no. 5, pp. 1182–1190, 2006, doi: 10.1002/hep.21378.

[87] L. P. Ganesan, S. Mohanty, J. Kim, K. R. Clark, J. M. Robinson, and L. Clark, "Rapid and Efficient Clearance of Blood-borne Virus by Liver Sinusoidal Endothelium," *Plos Pathog.*, vol. 7, no. 9, 2011, doi: 10.1371/journal.ppat.1002281.

[88] J. M. Mates *et al.*, "Mouse liver sinusoidal endothelium eliminates HIV-like Particles from Blood at a rate of 100 Million per Minute by a second-Order Kinetic Process," *Front. Immunol.*, vol. 8, 2017, doi: 10.3389/fimmu.2017.00035.

[89] S. Giugliano *et al.*, "Hepatitis C Virus Infection Induces Autocrine Interferon Signaling by Human Liver Endothelial Cells and Release of Exosomes, Which Inhibits Viral Replication," *Gastroenterology*, vol. 148, no. 2, pp. 392-402.e13, 2015, doi: 10.1053/j.gastro.2014.10.040.

[90] A. Saviano and T. F. Baumert, "Unraveling the role of liver sinusoidal endothelial cells in COVID-19 liver injury," *J. Hepatol.*, vol. 75, 2020.

[91] K. K. Sørensen *et al.*, "Liver sinusoidal endothelial cells," *Compr. Physiol.*, vol. 5, no. 4, pp. 1751–1774, 2015, doi: 10.1002/cphy.c140078.

[92] J. Gracia-Sancho, E. Caparrós, A. Fernández-Iglesias, and R. Francés, "Role of liver sinusoidal endothelial cells in liver diseases," *Nat. Rev. Gastroenterol. Hepatol.*, vol. 0123456789, 2021, doi: 10.1038/s41575-020-00411-3.

[93] X.-K. Wang and Z.-G. Peng, "Targeting Liver Sinusoidal Endothelial Cells: An Attractive Therapeutic Strategy to Control Inflammation in Nonalcoholic Fatty Liver Disease," *Front. Pharmacol.*, vol. 12, 2021, doi: 10.3389/fphar.2021.655557.

[94] N. J. Hunt, P. A. G. Mccourt, D. G. Le, V. C. Cogger, D. G. Le Couteur, and V. C. Cogger, "Novel targets for delaying aging : The importance of the liver and advances in drug delivery," *Adv. Drug Deliv. Rev.*, vol. 135, pp. 39–49, 2018, doi: 10.1016/j.addr.2018.09.006.

[95] D. G. Le Couteur *et al.*, "Pseudocapillarization and associated energy limitation in the aged rat liver," *Hepatology*, vol. 33, no. 3, pp. 537–543, 2001, doi: 10.1053/jhep.2001.22754.

[96] D. G. Le Couteur *et al.*, "Old age and the hepatic sinusoid," *Anat. Rec.*, vol. 291, no. 6, pp. 672–683, 2008, doi: 10.1002/ar.20661.

[97] D. G. Le Couteur, R. Fraser, S. Hilmer, L. P. Rivory, and A. J. McLean, "The hepatic sinusoid in aging and cirrhosis: Effects on hepatic substrate disposition and drug clearance," *Clin. Pharmacokinet.*, vol. 44, no. 2, pp. 187–200, 2005, doi: 10.2165/00003088-200544020-00004.

[98] D. G. Le Couteur and A. J. McLean, "The aging liver: Drug clearance and an oxygen diffusion barrier hypothesis," *Clin. Pharmacokinet.*, vol. 34, no. 5, pp. 359–373, 1998, doi: 10.2165/00003088-199834050-00003.

[99] R. Fraser *et al.*, "The liver sieve and atherosclerosis," *Pathology*, vol. 44, no. 3, pp. 181–186, 2012, doi: 10.1097/PAT.0b013e328351bcc8.

[100] R. Fraser, B. R. Dobbs, and G. W. T. Rogers, "Lipoproteins and the liver sieve: The role of the fenestrated sinusoidal endothelium in lipoprotein metabolism, atherosclerosis, and cirrhosis," *Hepatology*, vol. 21, no. 3, pp. 863–874, 1995, doi: 10.1016/0270-9139(95)90542-1.

References

[101] E. Wisse, R. B. de Zanger, K. Charels, P. Van Der Smissen, and R. S. McCuskey, "The liver sieve: Considerations concerning the structure and function of endothelial fenestrae, the sinusoidal wall and the space of Disse," *Hepatology*, vol. 5, no. 4, pp. 683–692, 1985, doi: 10.1002/hep.1840050427.

[102] P. L. Wright, K. F. Smith, W. A. Day, and R. Fraser, "Small Liver Fenestrae May Explain the Susceptibility of Rabbits to Atherosclerosis," *Arteriosclerosis*, vol. 3, no. 4, 1983.

[103] R. Fraser, V. R. Heslop, F. E. M. Murray, and W. A. Day, "Ultrastructural studies of the portal transport of fat in chickens," *Br. J. Exp. Pathol.*, vol. 67, no. 6, pp. 783–791, 1986.

[104] M. Naito and E. Wisse, "Filtration effect of endothelial fenestrations on chylomicron transport in neonatal rat liver sinusoids," *Cell Tissue Res.*, vol. 190, no. 3, pp. 371–382, 1978, doi: 10.1007/BF00219553.

[105] G. W. T. Rogers, B. R. Dobbs, and R. Fraser, "Decreased hepatic uptake of cholesterol and retinol in the dimethylnitrosamine rat model of cirrhosis," *Liver*, vol. 12, no. 5, pp. 326–329, 1992, doi: 10.1111/j.1600-0676.1992.tb00581.x.

[106] L. D. Deleve, "Liver sinusoidal endothelial cells in hepatic fibrosis," *Hepatology*, vol. 61, no. 5, pp. 1740–1746, 2015, doi: 10.1002/hep.27376.

[107] N. Nieto, "Oxidative-stress and IL-6 mediate the fibrogenic effects of rodent Kupffer cells on stellate cells," *Hepatology*, vol. 44, no. 6, pp. 1487–1501, 2006, doi: 10.1002/hep.21427.

[108] J. Gracia-Sancho, E. Caparrós, A. Fernández-Iglesias, and R. Francés, "Role of liver sinusoidal endothelial cells in liver diseases," *Nat. Rev. Gastroenterol. Hepatol.*, vol. 18, no. 6, pp. 411–431, 2021, doi: 10.1038/s41575-020-00411-3.

[109] G. Bedogni *et al.*, "Incidence and natural course of fatty liver in the general population: The dionysos study," *Hepatology*, vol. 46, no. 5, pp. 1387–1391, 2007, doi: 10.1002/hep.21827.

[110] E. Hashimoto, M. Taniai, and K. Tokushige, "Characteristics and diagnosis of NAFLD/NASH," *J. Gastroenterol. Hepatol.*, vol. 28, no. S4, pp. 64–70, 2013, doi: 10.1111/jgh.12271.

[111] E. Maslak, A. Gregorius, and S. Chlopicki, "Liver sinusoidal endothelial cells (LSECs) function and NAFLD; NO-based therapy targeted to the liver," *Pharmacol. Reports*, vol. 67, no. 4, pp. 689–694, 2015, doi: 10.1016/j.pharep.2015.04.010.

[112] P. Verhaegh *et al.*, "Electron microscopic observations in perfusion-fixed human non-alcoholic fatty liver disease biopsies," *Pathology*, vol. 53, no. 2, pp. 220–228, 2021, doi: 10.1016/j.pathol.2020.07.018.

[113] E. Kus *et al.*, "LSEC Fenestrae Are Preserved despite Pro-inflammatory Phenotype of Liver Sinusoidal Endothelial Cells in Mice on High Fat Diet," *Front. Physiol.*, vol. 10, 2019, doi: 10.3389/fphys.2019.00006.

[114] E. Wisse *et al.*, "Fat causes necrosis and inflammation in parenchymal cells in human steatotic liver," *Histochem. Cell Biol.*, vol. 157, no. 1, pp. 27–38, 2022, doi: 10.1007/s00418-021-02030-8.

[115] S. Francque *et al.*, "Increased intrahepatic resistance in severe steatosis: endothelial dysfunction, vasoconstrictor overproduction and altered microvascular architecture.," *Lab. Invest.*, vol. 92, no. 10, pp. 1428–39, 2012, doi: 10.1038/labinvest.2012.103.

[116] A. Warren, P. Bertolino, V. C. Cogger, A. J. McLean, R. Fraser, and D. G. Le Couteur, "Hepatic pseudocapillarization in aged mice," *Exp. Gerontol.*, vol. 40, no. 10, pp. 807–812, 2005, doi: 10.1016/j.exger.2005.06.012.

[117] S. J. Mitchell *et al.*, "Age-Related Pseudocapillarization of the Liver Sinusoidal Endothelium Impairs the Hepatic Clearance of Acetaminophen in Rats," *J Gerontol A Biol Sci Med Sci*, vol. 66A, no. 4, pp. 400–408, 2011, doi: 10.1093/gerona/glq221.

[118] V. C. Cogger, A. Warren, R. Fraser, M. Ngu, A. J. McLean, and D. G. Le Couteur, "Hepatic sinusoidal pseudocapillarization with aging in the non-human primate," *Exp. Gerontol.*, vol. 38, no. 10, pp. 1101–1107, 2003, doi: 10.1016/j.exger.2003.07.002.

[119] A. J. Mclean, V. C. Cogger, G. C. Chong, A. Warren, and A. M. A. Markus, "Age-related pseudocapillarization of the human liver," *J. Pathol.*, vol. 200, pp. 112–117, 2003, doi: 10.1002/path.1328.

[120] D. G. Le Couteur, R. Fraser, V. C. Cogger, and A. J. McLean, "Hepatic pseudocapillarisation and atherosclerosis in ageing," *Lancet*, vol. 359, no. 9317, pp. 1612–1615, 2002, doi: 10.1016/S0140-6736(02)08524-0.

[121] T. Nagai *et al.*, "Actin filaments around endothelial fenestrae in rat hepatic sinusoidal endothelial cells," *Med. Electron Microsc.*, vol. 37, no. 4, pp. 252–255, 2004, doi: 10.1007/s00795-004-0262-3.

[122] T. Svitkina, "The actin cytoskeleton and actin-based motility," *Cold Spring Harb. Perspect. Biol.*, vol. 10, no. 1, pp. 1–21, 2018, doi: 10.1101/cshperspect.a018267.

[123] F. Braet, L. Soon, K. Vekemans, P. Thordarson, and I. Spector, "Actin-Binding Drugs: An Elegant Tool to Dissect Subcellular Processes in Endothelial and Cancer Cells," in *Actin-Binding Proteins and Disease*, 2008, pp. 37–49.

[124] M. R. Bubb, A. M. J. Senderowicz, E. A. Sausville, K. L. K. Duncan, and E. D. Korn, "Jasplakinolide, a cytotoxic natural product, induces actin polymerization and competitively inhibits the binding of phalloidin to F-actin," *J. Biol. Chem.*, vol. 269, no. 21, pp. 14869–14871, 1994.

[125] N. Simionescu, F. Lupu, and M. Simionescu, "Rings of membrane sterols surround the openings of vesicles and fenestrae, in capillary endothelium," *J. Cell Biol.*, vol. 97, pp. 1592–1600, 1983, doi: 10.1083/jcb.97.5.1592.

[126] M. Simionescu, N. Simionescu, and G. E. Palade, "Preferential distribution of anionic sites on the basement membrane and the abluminal aspect of the endothelium in fenestrated capillaries," *J. Cell Biol.*, vol. 95, no. 2, pp. 425–434, 1982, doi: 10.1083/jcb.95.2.425.

[127] Y. Liu *et al.*, "Animal models of chronic liver diseases," *Am. J. Physiol. - Gastrointest. Liver Physiol.*, vol. 304, no. 5, 2013, doi: 10.1152/ajpgi.00199.2012.

[128] B. Delire, P. Stärkel, and I. Leclercq, "Animal models for fibrotic liver diseases: What we have, what we need, and what is under development," *J. Clin. Transl. Hepatol.*, vol. 3, no. 1, pp. 53–66, 2015, doi: 10.14218/JCTH.2014.00035.

[129] R. Fraser, G. W. T. Rogers, L. M. Bowler, W. A. Day, and B. R. Dobbs, "Defenestration and vitamin a status in a rat model of cirrhosis," *Kupffer Cell Found. Cells Hepatic Sinusoid, Vol. 3*, p. 195, 1991.

References

[130] B. Tamba-Lebbie, G. W. T. Rogers, B. R. Dobbs, and R. Fraser, “Defenestration of the hepatic sinusoidal endothelium in the dimethylnitrosamine fed rat: is this process reversible?,” *Kupffer Cell Found. Cells Hepatic Sinusoid, Vol. 4*, p. 179, 1993.

[131] G. Xie *et al.*, “Role of differentiation of liver sinusoidal endothelial cells in progression and regression of hepatic fibrosis in rats,” *Gastroenterology*, vol. 142, no. 4, pp. 918-927.e6, 2012, doi: 10.1053/j.gastro.2011.12.017.

[132] L. D. Deleve, X. Wang, J. Tsai, G. Kanel, S. Strasberg, and Z. A. Tokes, “Sinusoidal obstruction syndrome (veno-occlusive disease) in the rat is prevented by matrix metalloproteinase inhibition,” *Gastroenterology*, vol. 125, no. 3, pp. 882–890, 2003, doi: 10.1016/S0016-5085(03)01056-4.

[133] L. D. DeLeve *et al.*, “Characterization of a reproducible rat model of hepatic veno-occlusive disease,” *Hepatology*, vol. 29, no. 6, pp. 1779–1791, 1999, doi: 10.1002/hep.510290615.

[134] Y. Ito *et al.*, “Mechanisms and pathophysiological implications of sinusoidal endothelial cell gap formation following treatment with galactosamine/endotoxin in mice,” *Am. J. Physiol. - Gastrointest. Liver Physiol.*, vol. 291, no. 2, pp. 211–218, 2006, doi: 10.1152/ajpgi.00312.2005.

[135] R. Cheluvappa, H. A. Jamieson, S. N. Hilmer, M. Muller, and D. G. Le Couteur, “The effect of Pseudomonas aeruginosa virulence factor, pyocyanin, on the liver sinusoidal endothelial cell,” *J. Gastroenterol. Hepatol.*, vol. 22, no. 8, pp. 1350–1351, 2007, doi: 10.1111/j.1440-1746.2007.05016.x.

[136] H. Yokomori *et al.*, “Rho modulates hepatic sinusoidal endothelial fenestrae via regulation of the actin cytoskeleton in rat endothelial cells,” *Lab. Investig.*, vol. 84, no. 7, pp. 857–864, 2004, doi: DOI 10.1038/labinvest.3700114.

[137] L. Venkatraman and L. Tucker-Kellogg, “The CD47-binding peptide of thrombospondin-1 induces defenestration of liver sinusoidal endothelial cells,” *Liver Int.*, vol. 33, no. 9, pp. 1386–1397, 2013.

[138] R. B. de Zanger, F. Braet, M. R. ArnezCamacho, and E. Wisse, “Prolongation of hepatic endothelial cell cultures by phorbol myristate acetate,” *Kupffer Cell Found. Cells Hepatic Sinusoid, Vol. 6*, p. 97, 1997.

[139] F. Ballet, “Hepatotoxicity in drug development: Detection, significance antf solutions,” *J. Hepatol.*, vol. 26, pp. 26–36, 1997, doi: 10.1016/s0168-8278(97)80494-1.

[140] L. A. Vernetti, A. Vogt, A. Gough, and D. L. Taylor, “Evolution of Experimental Models of the Liver to Predict Human Drug Hepatotoxicity and Efficacy,” *Clin. Liver Dis.*, vol. 21, no. 1, pp. 197–214, 2017, doi: 10.1016/j.cld.2016.08.013.

[141] L. V. Sacks, H. H. Shamsuddin, Y. I. Yasinskaya, K. Bouri, M. L. Lanthier, and R. E. Sherman, “Scientific and regulatory reasons for delay and denial of FDA approval of initial applications for new drugs, 2000-2012,” *JAMA - J. Am. Med. Assoc.*, vol. 311, no. 4, pp. 378–384, 2014, doi: 10.1001/jama.2013.282542.

[142] J. L. Stevens and T. K. Baker, “The future of drug safety testing: expanding the view and narrowing the focus,” *Drug Discov. Today*, vol. 14, no. 3–4, pp. 162–167, 2009, doi: 10.1016/j.drudis.2008.11.009.

[143] N. J. Hunt *et al.*, “Manipulating fenestrations in young and old liver sinusoidal endothelial cells,” *Am. J. Physiol. - Gastrointest. Liver Physiol.*, vol. 316, no. 1, pp. G144–G154, 2019, doi: 10.1152/ajpgi.00179.2018.

[144] D. Hide *et al.*, “Ischemia/reperfusion injury in the aged liver: The importance of the sinusoidal endothelium in developing therapeutic strategies for the elderly,” *Journals Gerontol. - Ser. A Biol. Sci. Med. Sci.*, vol. 75, no. 2, pp. 268–277, 2020, doi: 10.1093/gerona/glz012.

[145] E. Wisse *et al.*, “Structure and function of sinusoidal lining cells in the liver.,” *Toxicol. Pathol.*, vol. 24, no. 1, pp. 100–111, 1996, doi: 10.1177/019262339602400114.

[146] R. S. McCuskey *et al.*, “Effects of ethanol and cocaine alone or in combination on the hepatic sinusoids of mice and rats,” *Kupffer Cell Found. Cells Hepatic Sinusoid, Vol. 4*, p. 376, 1993.

[147] R. Fraser, S. A. Clark, W. A. Day, and F. E. Murray, “Nicotine decreases the porosity of the rat liver sieve: a possible mechanism for hypercholesterolaemia.,” *Br. J. Exp. Pathol.*, vol. 69, no. 3, pp. 345–50, 1988.

[148] K. Furrer *et al.*, “Serotonin reverts age-related capillarization and failure of regeneration in the liver through a VEGF-dependent pathway,” *Proc. Natl. Acad. Sci. U. S. A.*, vol. 108, no. 7, pp. 2945–2950, 2011, doi: 10.1073/pnas.1012531108.

[149] M. Lesurtel *et al.*, “Platelet-derived serotonin mediates liver regeneration,” *Science (80-.).*, vol. 312, no. 104, pp. 104–107, 2006, doi: 10.1126/science.1123842.

[150] E. Abbe, “On the conditions of orthoscopic and pseudoscopic effects in the binocular microscope,” *J. R. Microsc. Soc.*, vol. 1, no. 1, 1881.

[151] N. Hilal, W. R. Bowen, L. Alkhatib, and O. Ogunbiyi, “A review of atomic force microscopy applied to cell interactions with membranes,” *Chem. Eng. Res. Des.*, vol. 84, no. A4, pp. 282–292, 2006, doi: 10.1205/cherd05053.

[152] A. Eifert and C. Kranz, “Hyphenating Atomic Force Microscopy,” *Anal. Chem.*, vol. 86, pp. 5190–5200, 2014.

[153] G. Binning, C. F. Quate, and C. Gerber, “Atomic Force Microscope,” *Phys. Rev. Lett.*, vol. 56, no. 9, 1986, doi: 10.1201/9781420075250.

[154] G. Binning, H. Rohrer, C. Gerber, and E. Weibel, “Surface studies by scanning tunneling microscopy,” *Phys. Rev. Lett.*, vol. 49, no. 1, pp. 57–61, 1982, doi: 10.1103/PhysRevLett.49.57.

[155] B. Zapotoczny, K. Owczarczyk, K. Szafranska, E. Kus, S. Chlopicki, and M. Szymonski, “Morphology and force probing of primary murine liver sinusoidal endothelial cells,” *J. Mol. Recognit.*, no. e2610, pp. 1–8, 2017, doi: 10.1002/jmr.2610.

[156] F. Braet, C. Rotsch, E. Wisse, and M. Radmacher, “Comparison of fixed and living liver endothelial cells by atomic force microscopy,” *Appl. Phys. A Mater. Sci. Process.*, vol. 66, no. SUPPL. 1, pp. 575–578, 1998, doi: 10.1007/s003390051204.

[157] F. Braet *et al.*, “Contribution of high-resolution correlative imaging techniques in the study of the liver sieve in three-dimensions,” *Microsc. Res. Tech.*, vol. 70, no. 3, pp. 230–242, 2007, doi: 10.1002/jemt.20408.

References

[158] B. Zapotoczny, F. Braet, E. Wisse, M. Lekka, and M. Szymonski, "Biophysical nanocharacterization of liver sinusoidal endothelial cells through atomic force microscopy," *Biophys. Rev.*, vol. 12, no. 3, pp. 625–636, 2020, doi: 10.1007/s12551-020-00699-0.

[159] M. Szymonski, M. Targosz-Korecka, and K. E. Malek-Zietek, "Nano-mechanical model of endothelial dysfunction for AFM-based diagnostics at the cellular level," *Pharmacol. Reports*, vol. 67, no. 4, pp. 728–735, 2015, doi: 10.1016/j.pharep.2015.05.003.

[160] J. Fels, P. Jeggle, K. Kusche-Vihrog, and H. Oberleithner, "Cortical actin nanodynamics determines nitric oxide release in vascular endothelium," *PLoS One*, vol. 7, no. 7, 2012, doi: 10.1371/journal.pone.0041520.

[161] X. Shu *et al.*, "Mechanotransduction of liver sinusoidal endothelial cells under varied mechanical stimuli," *Acta Mech. Sin. Xuebao*, vol. 37, pp. 201–217, 2021, doi: 10.1007/s10409-021-01057-3.

[162] M. Targosz-Korecka, G. Daniel Brzezinka, J. Danilkiewicz, Z. Rajfur, and M. Szymonski, "Glutaraldehyde fixation preserves the trend of elasticity alterations for endothelial cells exposed to TNF-α," *Cytoskeleton*, vol. 72, no. 3, pp. 124–130, 2015, doi: 10.1002/cm.21217.

[163] H. Hertz, "Ueber die Berührung fester elastischer Körper," *J. fur die Reine und Angew. Math.*, vol. 1882, no. 92, pp. 156–171, 1882, doi: 10.1515/crll.1882.92.156.

[164] M. Lekka, P. Laidler, D. Gil, J. Lekki, Z. Stachura, and a Z. Hrynkiewicz, "Elasticity of normal and cancerous human bladder cells studied by scanning force microscopy.," *Eur. Biophys. J.*, vol. 28, no. 4, pp. 312–316, 1999, doi: 10.1007/s002490050213.

[165] S. Mueller and L. Sandrin, "Liver stiffness: a novel parameter for the diagnosis of liver disease," *Hepatic Med. Evid. Res.*, pp. 3–9, 2010, doi: 10.1007/978-3-030-40542-7_1.

[166] M. Rusaczonek, B. Zapotoczny, M. Szymonski, and J. Konior, "Application of a layered model for determination of the elasticity of biological systems," *Micron*, vol. 124, no. June, p. 102705, 2019, doi: 10.1016/j.micron.2019.102705.

[167] R. Heintzmann and C. Cremer, "Laterally modulated excitation microscopy: improvement of resolution by using a diffraction grating," *Proc. SPIE*, vol. 3568, p. 185, 1999.

[168] M. G. L. Gustafsson *et al.*, "Three-dimensional resolution doubling in wide-field fluorescence microscopy by structured illumination," *Biophys. J.*, vol. 94, no. 12, pp. 4957–4970, 2008, doi: 10.1529/biophysj.107.120345.

[169] N. Bonnet and P. Vautrot, "Image analysis: Is the fourier transform becoming obsolete?," *Microsc. Microanal. Microstruct.*, vol. 8, no. 1, pp. 59–75, 1997, doi: 10.1051/mmm:1997106.

[170] M. V. Sednev, V. N. Belov, and S. W. Hell, "Fluorescent dyes with large Stokes shifts for super-resolution optical microscopy of biological objects: A review," *Methods Appl. Fluoresc.*, vol. 3, no. 4, 2015, doi: 10.1088/2050-6120/3/4/042004.

[171] G. T. Dempsey, J. C. Vaughan, K. H. Chen, M. Bates, and X. Zhuang, "Evaluation of fluorophores for optimal performance in localization-based super-resolution imaging," *Nat. Methods*, vol. 8, no. 12, pp. 1027–1040, 2011, doi: 10.1038/nmeth.1768.

[172] L. Shao, P. Kner, E. H. Rego, and M. G. L. Gustafsson, "Super-resolution 3D microscopy of live whole cells using structured illumination.," *Nat. Methods*, vol. 8, no. 12, pp. 1044–1046, 2011, doi: 10.1038/nmeth.1734.

[173] A. Curd, A. Cleasby, K. Makowska, A. York, H. Shroff, and M. Peckham, “Construction of an instant structured illumination microscope,” *Methods*, vol. 88, pp. 37–47, 2015, doi: 10.1016/j.ymeth.2015.07.012.

[174] M. G. L. Gustafsson, “Nonlinear structured-illumination microscopy: Wide-field fluorescence imaging with theoretically unlimited resolution,” *Proc. Natl. Acad. Sci. U. S. A.*, vol. 102, no. 37, pp. 13081–13086, 2005, doi: 10.1073/pnas.0406877102.

[175] D. Li *et al.*, “Extended-resolution structured illumination imaging of endocytic and cytoskeletal dynamics,” *Science (80-.).*, vol. 349, no. 6251, pp. 1–26, 2015, doi: 10.1126/science.aab3500.

[176] E. H. Rego *et al.*, “Nonlinear structured-illumination microscopy with a photoswitchable protein reveals cellular structures at 50-nm resolution,” *Proc. Natl. Acad. Sci. U. S. A.*, vol. 109, no. 3, 2012, doi: 10.1073/pnas.1107547108.

[177] S. W. Hell and J. Wichmann, “Breaking the diffraction resolution limit by stimulated emission: stimulated-emission-depletion fluorescence microscopy,” *Opt. Lett.*, vol. 19, no. 11, p. 780, 1994, doi: 10.1364/ol.19.000780.

[178] T. A. Klar and S. W. Hell, “Subdiffraction resolution in far-field fluorescence microscopy,” *Opt. Lett.*, vol. 24, no. 14, p. 954, 1999, doi: 10.1364/ol.24.000954.

[179] M. J. Sarmento *et al.*, “Exploiting the tunability of stimulated emission depletion microscopy for super-resolution imaging of nuclear structures,” *Nat. Commun.*, vol. 9, no. 1, pp. 1–11, 2018, doi: 10.1038/s41467-018-05963-2.

[180] K. L. Tosheva, Y. Yuan, P. Matos Pereira, S. n. Culley, and R. Henriques, “Between life and death: Strategies to reduce phototoxicity in super-resolution microscopy,” *J. Phys. D. Appl. Phys.*, vol. 53, no. 16, 2020, doi: 10.1088/1361-6463/ab6b95.

[181] C. Eggeling *et al.*, “Direct observation of the nanoscale dynamics of membrane lipids in a living cell,” *Nature*, vol. 457, no. 7233, pp. 1159–1162, 2009, doi: 10.1038/nature07596.

[182] J. Di Martino *et al.*, “Actin Depolymerization in Dedifferentiated Liver Sinusoidal Endothelial Cells Promotes Fenestrae Re-Formation,” *Hepatol. Commun.*, vol. 3, no. 2, pp. 213–219, 2019, doi: 10.1002/hep4.1301.

[183] E. Ruska, “Die elektronenmikroskopische Abbildung elektronenbestrahlterOberflächen,” *Z Phys*, vol. 83, 1933.

[184] M. Knoll, “Aufladepotentiel und Sekundäremission elektronenbestrahlterKörper,” *Z tech Phys*, vol. 16, 1935.

[185] D. McMullan, “Scanning Electron Microscopy 1928 – 1965 *,” *Scanning*, vol. 17, pp. 175–185, 1995.

[186] V. C. Cogger, J. N. O’Reilly, A. Warren, and D. G. Le Couteur, “A Standardized Method for the Analysis of Liver Sinusoidal Endothelial Cells and Their Fenestrations by Scanning Electron Microscopy,” *J. Vis. Exp.*, no. 98, pp. 1–9, 2015, doi: 10.3791/52698.

[187] M. Cosentino, C. Canale, P. Bianchini, and A. Diaspro, “AFM-STED correlative nanoscopy reveals a dark side in fluorescence microscopy imaging,” *Sci. Adv.*, vol. 5, no. 6, pp. 1–8, 2019, doi: 10.1126/sciadv.aav8062.

References

[188] Ø. I. Helle, C. I. Øie, P. McCourt, and B. S. Ahluwalia, "Chip-based optical microscopy for imaging membrane sieve plates of liver scavenger cells," *Proc. SPIE*, vol. 9554, 2015, doi: 10.1117/12.2187277.

[189] Ø. I. Helle, D. A. Coucheron, J. C. Tinguely, C. I. Øie, and B. S. Ahluwalia, "Nanoscopy on-a-chip : super-resolution imaging on the millimeter scale," *Optix Express*, vol. 27, no. 5, pp. 6700–6710, 2019.

[190] J. C. Tinguely *et al.*, "Photonic-chip assisted correlative light and electron microscopy," *Commun. Biol.*, vol. 3, no. 1, 2020, doi: 10.1038/s42003-020-01473-4.

[191] V. Zazzu and M. Brigida, *Mathematical Models in Biology*. 2015.

[192] C. Wählby, "Mathematical Models in Biology," *Math. Model. Biol.*, pp. 1–16, 2015, doi: 10.1007/978-3-319-23497-7.

[193] J. Schindelin *et al.*, "Fiji: an open-source platform for biological-image analysis," *Nat. Methods*, vol. 9, pp. 676–682, 2012.

[194] T. R. Jones *et al.*, "Scoring diverse cellular morphologies in image-based screens with iterative feedback and machine learning," *Proc. Natl. Acad. Sci. U. S. A.*, vol. 106, no. 6, pp. 1826–1831, 2009, doi: 10.1073/pnas.0808843106.

[195] I. Arganda-Carreras *et al.*, "Trainable Weka Segmentation: A machine learning tool for microscopy pixel classification," *Bioinformatics*, vol. 33, no. 15, pp. 2424–2426, 2017, doi: 10.1093/bioinformatics/btx180.

[196] S. Berg *et al.*, "Ilastik: Interactive Machine Learning for (Bio)Image Analysis," *Nat. Methods*, vol. 16, no. 12, pp. 1226–1232, 2019, doi: 10.1038/s41592-019-0582-9.

[197] A. E. Carpenter *et al.*, "CellProfiler: Image analysis software for identifying and quantifying cell phenotypes," *Genome Biol.*, vol. 7, no. 10, 2006, doi: 10.1186/gb-2006-7-10-r100.

[198] D. A. Cook, "Systematic and Nonsystematic Reviews: Choosing an Approach," *Healthc. Simul. Res.*, pp. 55–60, 2019, doi: 10.1007/978-3-030-26837-4_8.

[199] K. Taylor and L. R. Alvarez, "An Estimate of the Number of Animals Used for Scientific Purposes Worldwide in 2015," *Altern. Lab. Anim.*, vol. 47, no. 5–6, pp. 196–213, 2019, doi: 10.1177/0261192919899853.

[200] European Commission, "Summary Report on the statistics on the use of animals for scientific purposes in the Member States of the European Union and Norway in 2018," 2021.

[201] Mattilsynet, "Bruk av dyr i forsøk I 2020 Antallet forsøksdyr er innrapporterte tall fra forskere og forsøksdyrvirksomheter.," 2021.

[202] Mouse Genome Sequencing Consortium, "Initial sequencing and comparative analysis of the mouse genome," *Nature*, vol. 420, no. 6915, pp. 520–562, 2002, doi: 10.1038/nature01262.

[203] R. Fraser, W. A. Day, and N. S. Fernando, "Atheroclerosis and the liver sieve," *Kupffer Cell Found. Cells Hepatic Sinusoid, Vol. 1*, pp. 317–322, 1986.

[204] M. Ohata, Y. Tanuma, and T. Ito, “A transmission electron microscopic study on sinusoidal cells of guinea pig liver, with special reference to the occurrence of a canalicular system and ‘pored domes’ in the endothelium.,” *Arch. Histol. Jpn.*, vol. 47, no. 4, pp. 359–76, 1984, doi: 10.1679/aohc.47.359.

[205] V. Mönkemöller *et al.*, “Primary rat LSECs preserve their characteristic phenotype after cryopreservation,” *Sci. Rep.*, vol. 8, no. 1, pp. 1–10, 2018, doi: 10.1038/s41598-018-32103-z.

[206] A. Khan, K. Waqar, A. Shafique, R. Irfan, and A. Gul, “In vitro and in vivo animal models: The engineering towards understanding human diseases and therapeutic interventions,” in *Omics Technologies and Bio-engineering: Towards Improving Quality of Life*, vol. 1, Elsevier Inc., 2018, pp. 431–448.

[207] K. J. Harrington *et al.*, “Guidelines for preclinical and early phase clinical assessment of novel radiosensitisers,” *Br. J. Cancer*, vol. 105, no. 5, pp. 628–639, 2011, doi: 10.1038/bjc.2011.240.

[208] Y. Du, N. Li, and M. Long, “Liver sinusoid on a chip,” *Methods Cell Biol.*, vol. 146, pp. 105–134, 2018, doi: 10.1016/bs.mcb.2018.06.002.

[209] G. H. Underhill and S. R. Khetani, “Bioengineered Liver Models for Drug Testing and Cell Differentiation Studies,” *Cmgh*, vol. 5, no. 3, pp. 426-439.e1, 2018, doi: 10.1016/j.jcmgh.2017.11.012.

[210] L. A. Van Grunsven, “3D in vitro models of liver fibrosis,” *Adv. Drug Deliv. Rev. journa*, vol. 121, pp. 133–146, 2017, doi: 10.1016/j.addr.2017.07.004.

[211] K. Elvevold, G. Ivar, A. Revhaug, and K. Bertheussen, “Long-term preservation of high endocytic activity in primary cultures of pig liver sinusoidal endothelial cells,” *Eur. J. Cell Biol.*, vol. 84, pp. 749–764, 2005, doi: 10.1016/j.ejcb.2005.05.003.

[212] E. Wisse, F. Jacobs, B. Topal, P. Frederik, and B. De Geest, “The size of endothelial fenestrae in human liver sinusoids: implications for hepatocyte-directed gene transfer,” *Gene Ther.*, vol. 15, no. 17, pp. 1193–1199, 2008, doi: 10.1038/gt.2008.60.

[213] A. Couvelard, J. Y. Scoazec, M. C. Dauge, A. F. Bringuier, F. Potet, and G. Feldmann, “Structural and functional differentiation of sinusoidal endothelial cells during liver organogenesis in humans,” *Blood*, vol. 87, no. 11, pp. 4568–4580, 1996, doi: 10.1182/blood.v87.11.4568.bloodjournal87114568.

[214] R. Parent *et al.*, “An immortalized human liver endothelial sinusoidal cell line for the study of the pathobiology of the liver endothelium,” *Biochem. Biophys. Res. Commun.*, vol. 450, no. 1, pp. 7–12, 2014, doi: 10.1016/j.bbrc.2014.05.038.

[215] T. Matsumura *et al.*, “Establishment of an Immortalized Human-Liver Endothelial Cell Line with SV40T AND hTERT,” *Transplantation*, vol. 77, no. 9, pp. 1357–1365, 2004, doi: 10.1097/01.TP.0000124286.82961.7E.

[216] X. Zhao *et al.*, “Spontaneous immortalization of mouse liver sinusoidal endothelial cells,” *Int. J. Mol. Med.*, vol. 35, no. 3, pp. 617–624, 2015, doi: 10.3892/ijmm.2015.2067.

[217] R. C. Huebert *et al.*, “Immortalized Liver Endothelial Cells: A Cell Culture Model for Studies of Motility and Angiogenesis,” *Lab Invest*, vol. 90, no. 12, 2010, doi: 10.1038/labinvest.2010.132.

References

[218] Y. Maru, S. K. Hanks, and M. Shibuya, “The tubulogenic activity associated with an activated form of Flt-1 kinase is dependent on focal adhesion kinase,” *Biochim. Biophys. Acta - Mol. Cell Res.*, vol. 1540, no. 2, pp. 147–153, 2001, doi: 10.1016/S0167-4889(01)00127-6.

[219] M. Ju, S. Ioannidou, and P. Munro, “A Na,K-ATPase–Fodrin–Actin Membrane Cytoskeleton Complex is Required for Endothelial Fenestra Biogenesis,” *cells*, vol. 9, no. 1387, 2020, doi: 10.3390/cells9061387.

[220] J. Poisson *et al.*, “Liver sinusoidal endothelial cells: Physiology and role in liver diseases,” *J. Hepatol.*, vol. 66, no. 1, pp. 212–227, 2017, doi: 10.1016/j.jhep.2016.07.009.

[221] B. Smedsrød, J. Melkko, N. Araki, H. Sano, and S. Horiuchi, “Advanced glycation end products are eliminated by scavenger-receptor- mediated endocytosis in hepatic sinusoidal Kupffer and endothelial cells,” *Biochem. J.*, vol. 322, pp. 567–573, 1997.

[222] H. S. Wileys and D. D. Cunningham, “The endocytotic rate constant. A cellular parameter for quantitating receptor-mediated endocytosis.,” *J. Biol. Chem.*, vol. 257, no. 8, pp. 4222–4229, 1982, doi: 10.1016/S0021-9258(18)34709-4.

[223] C. I. Øie *et al.*, “New ways of looking at very small holes - Using optical nanoscopy to visualize liver sinusoidal endothelial cell fenestrations,” *Nanophotonics*, 2018, doi: 10.1515/nanoph-2017-0055.

[224] J. Demmerle, E. Wegel, L. Schermelleh, and I. M. Dobbie, “Assessing resolution in super-resolution imaging,” *Methods*, vol. 88, no. 2015, pp. 3–10, 2015, doi: 10.1016/j.ymeth.2015.07.001.

[225] C. M. Sparrow, “on Spectroscopic Resolving Power,” *Astrophys. J.*, vol. 44, 1916, doi: 10.1086/142271.

[226] Z. Zheng, S. Lü, and M. Long, “Simulation and prediction of membrane fusion dynamics,” *Theor. Appl. Mech. Lett.*, p. 100321, 2022, doi: 10.1016/j.taml.2022.100321.

[227] R. B. de Zanger and E. Wisse, “The filtration effect of rat fenestrated sinusoidal endothelium on the passage of remnant chylomicrons to the space of disse,” *sinusoidal liver cells*, 1982.

[228] A. Steffan, J. Gendrault, and A. Kirn, “Increase in the number of fenestrae in mouse endothelial liver cells by altering the cytoskeleton with cytochalasin B,” *Hepatology*, vol. 7, no. 6, pp. 1230–1238, 1987, doi: 10.1002/hep.1840070610.

[229] L. E. Villegas-Hernández, M. Nystad, F. Ströhl, P. Basnet, G. Acharya, and B. S. Ahluwalia, “Visualizing ultrastructural details of placental tissue with super-resolution structured illumination microscopy,” *Placenta*, vol. 97, pp. 42–45, 2020, doi: 10.1016/j.placenta.2020.06.007.

[230] J. Bastacky, T. L. Hayes, and R. P. Gelinas, “Quantitation of shrinkage during preparation for scanning electron microscopy: Human lung,” *Scanning*, vol. 7, no. 3, pp. 134–140, 1985, doi: 10.1002/sca.4950070306.

[231] V. Mönkemöller, “Optical Super-Resolution Microscopy of the Structure and Dynamics of Cellular Nanopores,” Dissertation an der Fakultät für Physik der Universität Bielefeld Bielefeld, 2016.

[232] X. Luo *et al.*, “Caveolin 1-related autophagy initiated by aldosterone-induced oxidation promotes liver sinusoidal endothelial cells defenestration,” *Redox Biol.*, vol. 13, pp. 508–521, 2017, doi: 10.1016/j.redox.2017.07.011.

[233] C. Kong *et al.*, “Multiscale and Multimodal Optical Imaging of the Ultrastructure of Human Liver Biopsies,” *Front. Physiol.*, vol. 12, 2021, doi: 10.3389/fphys.2021.637136.

[234] B. Zapotoczny, K. Szafranska, E. Kus, S. Chlopicki, and M. Szymonski, “Quantification of Fenestrations in Liver Sinusoidal Endothelial Cells by Atomic Force Microscopy,” *Micron*, vol. 101, pp. 48–53, 2017, doi: https://doi.org/10.1016/j.micron.2017.06.005.

[235] S. M. Paul *et al.*, “How to improve RD productivity: The pharmaceutical industry’s grand challenge,” *Nat. Rev. Drug Discov.*, vol. 9, no. 3, pp. 203–214, 2010, doi: 10.1038/nrd3078.

[236] V. Prasad and S. Mailankody, “Research and development spending to bring a single cancer drug to market and revenues after approval,” *JAMA Intern. Med.*, vol. 177, no. 11, pp. 1569–1575, 2017, doi: 10.1001/jamainternmed.2017.3601.

[237] David W. Thomas, Justin Burns, John Audette, Adam Carroll, Corey Dow-Hygelund, and Michael Hay, “Clinical Development Success Rates 2006-2015,” 2016.

[238] G. Sager, E. O. Ørvoll, R. A. Lysaa, I. Kufareva, R. Abagyan, and A. W. Ravna, “Novel cGMP efflux inhibitors identified by virtual ligand screening (VLS) and confirmed by experimental studies,” *J. Med. Chem.*, vol. 55, no. 7, pp. 3049–3057, 2012, doi: 10.1021/jm2014666.

[239] Food And Drug Administration, “FDA Approves Impotence Pill, Viagra.,” *ScienceDaily*, 1998.

[240] S. Yardimci *et al.*, “Sildenafil accelerates liver regeneration after partial hepatectomy in rats,” *Transplant. Proc.*, vol. 44, no. 6, pp. 1747–1750, 2012, doi: 10.1016/j.transproceed.2012.04.003.

[241] A. Bruckbauer *et al.*, “A Combination of Leucine, Metformin, and Sildenafil Treats Nonalcoholic Fatty Liver Disease and Steatohepatitis in Mice,” *Int. J. Hepatol.*, vol. 2016, no. January, 2016, doi: 10.1155/2016/9185987.

[242] L. Aronsen, E. Orvoll, R. Lysaa, A. W. Ravna, and G. Sager, “Modulation of high affinity ATP-dependent cyclic nucleotide transporters by specific and non-specific cyclic nucleotide phosphodiesterase inhibitors,” *Eur. J. Pharmacol.*, vol. 745, pp. 249–253, 2014, doi: 10.1016/j.ejphar.2014.10.051.

[243] M. J. Arnaud, “Pharmacokinetics and metabolism of natural methylxanthines in animal and man,” in *Handbook of Experimental Pharmacology*, vol. 200, 2011, pp. 471–478.

[244] Committee on military nutrition research, *Caffeine for the Sustainment of Mental Task Performance: Formulations for Military Operations*. National Academy Press, 2001.

[245] A. Nehlig, “Interindividual differences in caffeine metabolism and factors driving caffeine consumption,” *Pharmacol. Rev.*, vol. 70, no. 2, pp. 384–411, 2018, doi: 10.1124/pr.117.014407.

[246] M. Arnaud, “Comparative metabolic disposition of [1-Me14C] caffeine in rats , mice , and Chinese hamsters,” *Drug Metab. Dispos.*, vol. 13, no. 4, 1985.

References

[247] M. Orrú *et al.*, "Psychostimulant pharmacological profile of paraxanthine, the main metabolite of caffeine in humans," *Neuropharmacology*, vol. 67, pp. 476–484, 2013, doi: 10.1016/j.neuropharm.2012.11.029.

[248] J. Sawynok and T. Yaksh, "Caffeine as an analgesic adjuvant: a review of pharmacology and mechanisms of action," *Pharmacol Rev*, vol. 45, no. 1, 1993.

[249] B. B. Rasmussen, T. H. Brix, K. O. Kyvik, and K. Brøsen, "The interindividual differences in the 3-demthylation of caffeine alias CYP1A2 is determined by both genetic and environmental factors," *Pharmacogenetics*, vol. 12, no. 6, pp. 473–478, 2002, doi: 10.1097/00008571-200208000-00008.

[250] A. F. Gileta *et al.*, "Genetic characterization of outbred Sprague Dawley rats and utility for genome-wide association studies," *bioRxiv*, pp. 0–61, 2018, doi: 10.1101/412924.

[251] J. D. Corbin, S. H. Francis, and D. J. Webb, "Phosphodiesterase type 5 as a pharmacologic target in erectile dysfunction," *Urology*, vol. 60, no. 2 SUPPL. 2, pp. 4–11, 2002, doi: 10.1016/S0090-4295(02)01686-2.

[252] Y. Lecun, Y. Bengio, and G. Hinton, "Deep learning," *Nature*, vol. 521, no. 7553, pp. 436–444, 2015, doi: 10.1038/nature14539.

[253] U. Frevert *et al.*, "Intravital observation of plasmodium berghei sporozoite infection of the liver," *PLoS Biol.*, vol. 3, no. 6, pp. 1034–1046, 2005, doi: 10.1371/journal.pbio.0030192.

[254] N. Kawasegi *et al.*, "Nanomachining of silicon surface using atomic force microscope with diamond tip," *J. Manuf. Sci. Eng. Trans. ASME*, vol. 128, no. 3, pp. 723–729, 2006, doi: 10.1115/1.2163364.

[255] M. Kopycinska-Müller, R. H. Geiss, and D. C. Hurley, "Contact mechanics and tip shape in AFM-based nanomechanical measurements," *Ultramicroscopy*, vol. 106, no. 6, pp. 466–474, 2006, doi: 10.1016/j.ultramic.2005.12.006.

[256] M. G. L. Gustafsson, "Surpassing the lateral resolution limit by a factor of two using structured illumination microscopy," *J. Microsc.*, vol. 198, no. 2, pp. 82–87, 2000, doi: 10.1046/j.1365-2818.2000.00710.x.

[257] Zeiss, "GeminiSEM 360 Your Field Emission SEM for Informative Imaging and Fast Understanding in Core Facilities."

[258] Wikimedia Commons, "Electron-matter interaction volume and various types of signal generated," 2020. .

[259] A. Diaspro and P. Bianchini, "Optical nanoscopy," *Riv. del Nuovo Cim.*, vol. 43, no. 8, pp. 385–455, 2020, doi: 10.1007/s40766-020-00008-1.

Paper I

The wHole Story About Fenestrations in LSEC

Szafranska K., Kruse L.D., Holte C.F., McCourt P., Zapotoczny B.

Frontiers in Physiology
2021, vol.12, article 735573
https://doi.org/10.3389/fphys.2021.735573

frontiers in Physiology

REVIEW
published: 13 September 2021
doi: 10.3389/fphys.2021.735573

The wHole Story About Fenestrations in LSEC

Karolina Szafranska[1†], Larissa D. Kruse[1†], Christopher Florian Holte[1†], Peter McCourt[1] and Bartlomiej Zapotoczny[1,2]*

[1] Vascular Biology Research Group, Department of Medical Biology, University of Tromsø – The Arctic University of Norway, Tromsø, Norway, [2] Department of Biophysical Microstructures, Institute of Nuclear Physics, Polish Academy of Sciences, Kraków, Poland

The porosity of liver sinusoidal endothelial cells (LSEC) ensures bidirectional passive transport of lipoproteins, drugs and solutes between the liver capillaries and the liver parenchyma. This porosity is realized via fenestrations – transcellular pores with diameters in the range of 50–300 nm – typically grouped together in sieve plates. Aging and several liver disorders severely reduce LSEC porosity, decreasing their filtration properties. Over the years, a variety of drugs, stimulants, and toxins have been investigated in the context of altered diameter or frequency of fenestrations. In fact, any change in the porosity, connected with the change in number and/or size of fenestrations is reflected in the overall liver-vascular system crosstalk. Recently, several commonly used medicines have been proposed to have a beneficial effect on LSEC re-fenestration in aging. These findings may be important for the aging populations of the world. In this review we collate the literature on medicines, recreational drugs, hormones and laboratory tools (including toxins) where the effect LSEC morphology was quantitatively analyzed. Moreover, different experimental models of liver pathology are discussed in the context of fenestrations. The second part of this review covers the cellular mechanisms of action to enable physicians and researchers to predict the effect of newly developed drugs on LSEC porosity. To achieve this, we discuss four existing hypotheses of regulation of fenestrations. Finally, we provide a summary of the cellular mechanisms which are demonstrated to tune the porosity of LSEC.

Keywords: fenestration, fenestra, nanopores, LSEC, liver sinusoidal endothelial cells, porosity, liver disease, drug response

OPEN ACCESS

Edited by:
Leo A. van Grunsven, Vrije Universiteit Brussel, Belgium

Reviewed by:
Savneet Kaur, The Institute of Liver and Biliary Sciences (ILBS), India
Edward N. Harris, University of Nebraska System, United States

***Correspondence:**
Peter McCourt
peter.mccourt@uit.no

†These authors have contributed equally to this work and share first authorship

Specialty section:
This article was submitted to Gastrointestinal Sciences, a section of the journal Frontiers in Physiology

Received: *02 July 2021*
Accepted: *16 August 2021*
Published: *13 September 2021*

Citation:
Szafranska K, Kruse LD, Holte CF, McCourt P and Zapotoczny B (2021) The wHole Story About Fenestrations in LSEC. Front. Physiol. 12:735573. doi: 10.3389/fphys.2021.735573

INTRODUCTION

Within the human body, the main blood-organ barrier is made up of a single layer of thin endothelial cells. In the liver, the microcirculation has a unique morphology that facilitates bi-directional exchange of substrates between hepatocytes and blood in the liver sinusoids (Cogger and Le Couteur, 2009; Fraser et al., 2012). Liver sinusoidal endothelial cells (LSEC) are very thin and perforated with transcellular pores (50–300 nm in diameter) that are also termed as fenestrae or fenestrations (**Figure 1**). These structures were first correctly identified as such with transmission electron microscopy (TEM) by Yamagishi (1959) and described in detail by Wisse (1970). Between 2 and 20% of the LSEC surface is covered by fenestrations which are either scattered individually across the surface or clustered into groups called sieve plates. As there are no diaphragms or

underlying basement membrane, fenestrations make LSEC a highly efficient ultrafiltration system. LSEC thus retain blood cells inside the vessel lumen, whereas small molecules, such as drugs, proteins, lipoproteins, and small viruses can pass this endothelial barrier via fenestrations to reach the surrounding hepatocytes, and vice versa (Fraser et al., 1995a). Fenestrations are therefore a vital structure in liver physiology, providing the primary communication conduit between the liver and the rest of the body, via the circulation. LSEC fenestrations, and the effects of various agents upon them, have been studied extensively with electron microscopy. During the last decade new techniques have been developed and became available to investigate fenestrations in cultured LSEC. Super-resolution optical microscopy provided first detailed information about the composition of fenestration (Cogger et al., 2010, 2013; Mönkemöller et al., 2015; Zapotoczny et al., 2019a) while atomic force microscopy (AFM) provided first information about the dynamics of fenestrations *in vitro* (Zapotoczny et al., 2019b, 2020). Such tools will accelerate the development of therapies that can reverse the loss of fenestrations seen in aging and liver fibrosis (DeLeve, 2015; Hunt et al., 2019).

Fenestration loss during aging manifests as changes in the liver microcirculation, in particular within LSEC, which is a likely cause of dyslipidemia (Le Couteur et al., 2002) and insulin resistance in old age (Mohamad et al., 2016). At the morphological level, LSEC in old age have markedly reduced porosity (percent of the cell surface area covered in fenestrations) by about 50% – in other words, old LSEC become "defenestrated" (**Figure 2**). This defenestration results in hampered bi-directional traffic of substrates between the blood and the hepatocytes. Biomolecules such as lipoproteins, or hormones, or drugs (such as statins or insulin) pass less easily through aged LSEC to reach the hepatocytes to be processed and/or exert their effects. For example, older rats showed a significant reduction in the hepatic volume of insulin distribution (Mohamad et al., 2016), showing that fenestrations facilitate insulin transfer to hepatocytes. Another example is the transfer of lipoproteins across LSEC, which was almost totally abolished in livers from old animals, providing a novel mechanism for age-related dyslipidemia and postprandial hyperlipidemia (Hilmer et al., 2005) and is now accepted as a significant factor in age-related hyperlipidemia (Liu et al., 2015). The same applies in the reverse direction across LSEC – biomolecules produced by the hepatocytes need to pass through fenestrations for release into the plasma, and defenestration hinders this process. Age-related LSEC defenestration is also accompanied by altered expression of many vascular proteins including von Willebrand factor, ICAM-1, laminin, caveolin-1 and various collagens (Le Couteur et al., 2008). However, these changes occur without any age-related pathology of hepatocytes or activation of stellate cells (Warren et al., 2011). The sum of all these processes results in a state whereby liver sinusoidal vessels become more like continuous capillaries, but without the other manifestations seen in diseased livers during "capillarization." Age-related defenestration is therefore also termed "pseudocapillarization." Cellular senescence is one hallmark of aging (Robbins et al., 2021), and (Grosse et al., 2020) proposed that LSEC become senescent at 10–12 months of age in mice, as evidenced by the increased expression of the senescence marker p16. Senolytic drugs (which selectively kill senescent cells) have been proposed as a potential therapy to alleviate the effects of senescent cell mediated aging and disease (Robbins et al., 2021). However, $p16^{high}$ LSEC are essential for mouse healthspan, as ablation of these cells results in disruption of the hepatic sinusoid and liver fibrosis (Grosse et al., 2020).

Defenestration of LSEC also occurs during chronic liver disease, liver fibrosis and consequently cirrhosis, which are an increasing worldwide problem, and are becoming a major cause of morbidity and death (Asrani et al., 2019). Currently, there is no therapy that can alleviate fibrosis progression or reverse fibrosis (Higashi et al., 2017). Fibrosis is characterized by excessive extracellular matrix production from activated stellate cells. In addition to LSEC defenestration, during chronic liver disease, a basement membrane develops in the Space of Disse, leading to the process of capillarization, and thereby further reducing the free passage of substrates to and from the hepatocytes (Poisson et al., 2017). Defenestration of LSEC occurs earlier than the formation of fibrous septa in liver diseases such as alcoholic liver injury and non-alcoholic fatty liver disease (Horn et al., 1987) which could indicate that LSEC can play an important role during the early stages of fibrosis. Restoration of differentiation to LSEC led to quiescence of hepatic stellate cells and regression of fibrosis in thioacetamide challenged rats (Xie et al., 2012b) potentially suggesting that therapies that revert LSEC from a diseased/defenestrated state to a normal state may also be of benefit for treatment of liver fibrosis (DeLeve, 2015).

As mentioned above, defenestration of the liver sinusoidal endothelium impairs the hepatic clearance of pharmacological agents (Mitchell et al., 2011). As for lipoproteins and insulin, fenestrations are conduits for pharmaceuticals, from the plasma to the hepatocytes. Reduction in LSEC porosity thus reduces the passage of drugs to the cells where they are processed and metabolized. This can result in elevated and potentially toxic concentrations of drugs in the elderly (and patients with liver disease), when administering drug doses appropriate for healthy young people. In addition, polypharmacy is becoming a major issue in the aging population, with over 42% of people over 65 years of age were reported being administrated five or more different medications per day (Midão et al., 2018). The majority of these medications need to cross the liver sinusoidal endothelium to be detoxified, and it is possible that some of the polypharmacy "cocktails" are detrimental for LSEC porosity. Another serious consequence of reduced porosity is that statins are less able to reach the hepatocytes and inhibit cholesterol production. Increased statin doses are then required to achieve therapeutic effects, sometimes resulting in side effects such as muscle pain and rhabdomyolysis, resulting in medication non-compliance in patients.

Given the vital role of LSEC fenestrations (and the bi-directional flow of substrates through them) in physiology and homeostasis, a better understanding of how these structures are regulated will enable us to design novel therapeutic approaches targeting biological changes of aging and liver diseases.

It needs to be highlighted, however, that many reports in the literature "suffer" from developing experimental methodologies.

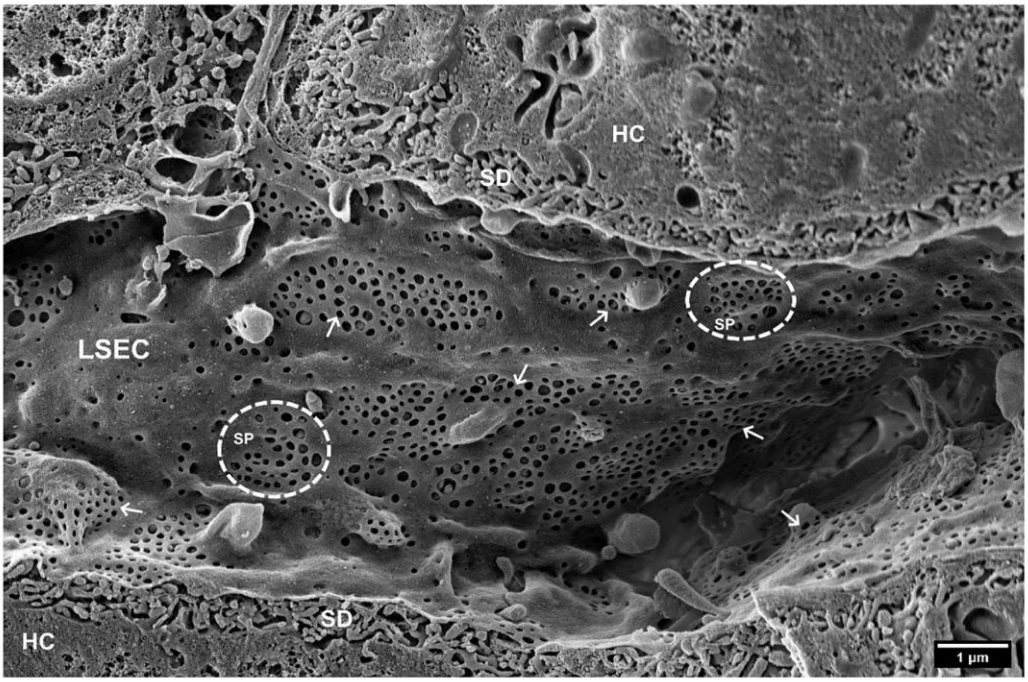

FIGURE 1 | SEM image of hepatic sinusoids of a C57BL6 mouse, approximately 4 months old. Liver Sinusoidal Endothelial Cells (LSECs) are covered in multiple fenestrations (arrows) arranged into sieve plates (SP, dotted line circles) distributed over the whole sinusoid. SD, space of Disse; HC, hepatocytes. (Courtesy of Karen K. Sørensen, UiT, Tromsø, Norway).

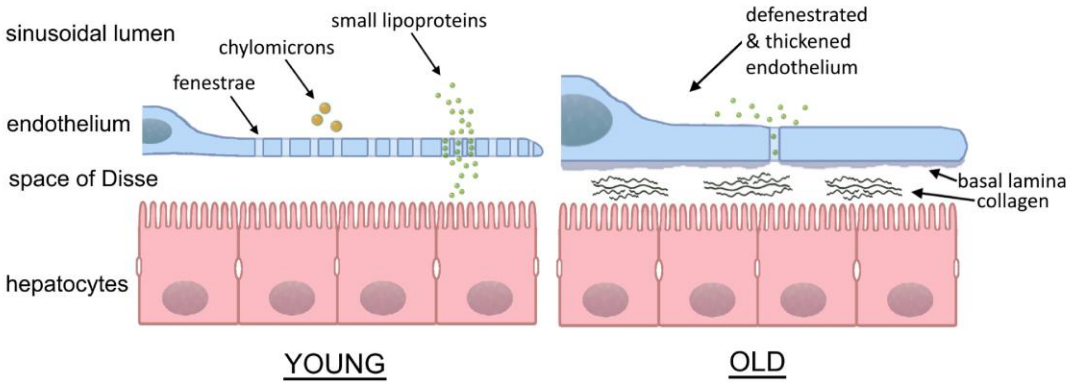

FIGURE 2 | Sinusoidal lumen in young and old liver. With age, the fenestrated morphology of the sinusoids is lost in the process of "pseudocapillarization." Additionally, the endothelium thickens and collagen deposits can be found within the space of Disse. The result is the inhibition of transfer between the blood and hepatocytes. (Courtesy of Eike Struck, UiT, Tromsø, Norway and David Le Couteur, ANZAC Research Institute, Sydney, Australia).

Errors during liver perfusion, cell isolation methodologies and sample preparations may lead to altered cell phenotypes. Also, it should be noted that studies from pre-super-resolution era where light microscopy was the only technique used for quantification of fenestrations may be imprecise. As reported, fenestrations in LSEC are in the range of 50–300 nm, gathered in sieve plates of several to tens of pores, with limited number of gaps (DeLeve and Maretti-Mira, 2017). These can be visualized only using non-diffraction limited methods such as electron microscopy, optical nanoscopy, or atomic force microscopy. The distribution of fenestration diameter in this range was presented for both LSEC in tissue (*in vivo*) and for isolated cells (*in vitro*). *In vivo* data are limited to fixed and dried material, while data for isolated LSEC covers fixed and dried, wet-fixed, and live cells. Recently, we summarized that the differences in mean fenestration diameter for fixed and dried, wet-fixed and live LSECs *in vitro* can be up to 30% (Supplementary Table 1 in Zapotoczny et al., 2019b). The differences between *in vivo* and *in vitro* data can be even larger *ibid*., (Wisse et al., 2010). The comparison between the groups in a single report provides information about the alterations as the same microscopy method is applied. The methodological details enabling avoiding errors in imaging and data analysis

were described: SEM (Wisse et al., 2010; Cogger et al., 2015; Szafranska et al., 2021), AFM (Zapotoczny et al., 2017a, 2020; Szafranska et al., 2021), SIM (Kong et al., 2021; Szafranska et al., 2021). Moreover, the comparative measurements using different microscopies were reported in the past showing good correlation between the methods. However, the comparative analysis of newly developed techniques applied recently for LSECs, such as SIM, STED, and AFM, is lacking. Each method has its advantages and limitations. To enable easy tracking of the model (*in vivo*/*in vitro* and microscopy technique) we provide the relevant information in the presented tables.

The purpose of this review is to: (i) provide a medical and cell biology "tool-kit," for researchers and clinicians to design potential LSEC refenestration strategies and (ii) summarize the existing knowledge around fenestration biology which can help to find new ways to reveal how fenestrations actually work. The first part of this review fucuses on the reported influence of drugs on LSEC fenestration number and porosity, while the second part gives a deeper knowledge about fenestration biology and mechanisms behind structure, formation and maintenance of fenestration. This review does not cover a number of other aspects of LSEC biology, but these can be found in in the following excellent reviews about LSEC in: diseases (Gracia-Sancho et al., 2021; Wang and Peng, 2021), hepatic fibrosis (DeLeve, 2015), mechanotransduction (Shu et al., 2021), inflammation and cancer (Wilkinson et al., 2020; Yang and Zhang, 2021), receptor expression (Pandey et al., 2020), immunological functions (Shetty et al., 2018), aging (Hunt et al., 2019), scavenging (Sørensen et al., 2012), and overall biology of LSECs (Sørensen et al., 2015).

LSEC AND DRUG INTERACTIONS

Recreational and Medicinal Drugs, and Their Effects on LSEC Porosity

The human race already uses an extensive array of drugs for medical and recreational purposes. The majority of these compounds are safe, or at least relatively safe for normal human consumption if used appropriately. Reported negative side-effects of these drugs are typically well-documented at the systemic or organ level, but little is known about their direct effects on LSEC fenestration status. Additionally, some drugs with other intended targets may actually have positive side effects on LSEC fenestration, leading to increased LSEC porosity and improving bi-directional exchange of solutes between hepatocytes and plasma. This concept was first tested by Hunt et al. (2019, 2020) who found that a number of drugs for intended use for the treatment of high blood pressure, erectile dysfunction and diabetes improved LSEC porosity in young and old mice. **Table 1** lists the effects of some recreational and medicinal drugs on LSEC fenestrations.

Recreational Drugs

The effects of recreational drugs on LSEC porosity have not been studied extensively (**Table 1**). The few studies performed showed that the recreational drugs nicotine, ethanol, and cocaine reduce LSEC porosity (Fraser et al., 1988; McCuskey et al., 1993), while the psychedelic drug 2,5-Dimethoxy-4-iodoamphetamine (DOI) increases porosity in LSEC in young and old rodents (Cogger et al., 2014; Hunt et al., 2019). The effects on LSEC porosity of other recreational/non-medicinal drugs such as opioids, amphetamines, cannabis, and xanthines (such as caffeine and theobromine) have, to the best of our knowledge, not been studied. This would be an area of great interest, given the extensive use of all of these among the general population. This is exemplified by opioid use (which is also for medicinal purposes) leading to the current "opioid epidemic" in the US arising from the use of prescription oxycodone. Below is a summary of the reported interactions of ethanol, cocaine, DOI, and nicotine with LSEC.

Ethanol Given the wide use and general acceptance of alcohol, and the suggested health benefits from moderate consumption, it was discussed in the LSEC field whether moderate amounts of alcohol could improve LSEC porosity and thereby lipoprotein clearance. Of the studies (*in vitro* and *in vivo*) investigating the effects of ethanol on LSEC, the majority were performed in rats, but mice, baboons and human LSEC were studied as well, with electron and atomic force microscopy methods used as readout. Several studies reported that the fenestration number was reduced, while the average fenestration diameter was increased – this pattern was consistent in all the *in vitro* studies (Mak and Lieber, 1984; Charles et al., 1986; Van Der Smissen et al., 1986; Horn et al., 1987; Tanikawa et al., 1991; McCuskey et al., 1993; Braet et al., 1994, 1995a, 1996c; de Zanger et al., 1997) and with reduced porosity reported in one study (Takashimizu et al., 1999). Takashimizu et al. (1999) described reduction in fenestration diameter in rat during *in vivo* continuous administration of ethanol into the portal vein, and pre-treatment with **BQ123** [an endothelin (ET) receptor antagonist, see **Table 2**] reduced the effect of ethanol. One *in vivo* study reported no changes in in the liver sinusoids in mice after 9 weeks of ethanol feeding (McCuskey et al., 1993) but ethanol in combination with cocaine caused the sinusoids to become thickened and defenestrated. In other *in vivo* chronic ethanol challenge studies (ethanol given to rats in food, or human studies where biopsies were used), one rat study yielded results consistent with the *in vitro* findings (reduced fenestration number, increased diameter, reduced porosity) (Tanikawa et al., 1991) while the other study reported reduced fenestration diameter and number – this was the only study to find that the diameter became smaller after ethanol challenge (Takashimizu et al., 1999). In the human biopsy study, similar results were obtained - chronic alcohol consumption (defined as > 60 g alcohol intake every day for more than 3 years) resulted in fewer fenestrations, diameters of between 50–300 nm and a "visible difference" for porosity between the two groups. A study in baboons showed that the duration of alcohol consumption does not seem to have any impact on fenestrations (diameter in second group (4–24 months alcohol consumption vs. 61–112 months) was larger than control but smaller than first group) (Mak and Lieber, 1984). In summary, ethanol at any dose does not appear to improve LSEC porosity but rather has the opposite effect.

TABLE 1 | Influence of medicinal drugs on LSEC fenestrations.

	Fenestration diameter	Porosity	Fenestration frequency	References	Methods
Recreational drugs					
Ethanol	+/-	-	-	Van Der Smissen et al., 1986; Braet et al., 1995a	SEM, TEM, *in vitro*
				Mak and Lieber, 1984; Charles et al., 1986; de Zanger et al., 1997	SEM, *in vivo*
				Tanikawa et al., 1991; McCuskey et al., 1993	TEM, *in vivo*
				Horn et al., 1987; Takashimizu et al., 1999	SEM, *in vivo*
				Braet et al., 1996c	SEM, AFM, *in vitro*
				Braet et al., 1994	SEM, *in vitro*
Ethanol +cocaine	nd	-	-	McCuskey et al., 1993	TEM, *in vivo*
Cocaine	nd	nd	nd	McCuskey et al., 1993	TEM, *in vivo*
2,5-Dimethoxy-4-iodoamphetamine (DOI)	+	+/-	+/-	Furrer et al., 2011; Cogger et al., 2014	SEM, *in vivo*
				Hunt et al., 2019	SEM *in vitro*
Nicotine	-	- -	-	Fraser et al., 1988	SEM, *in vivo*
Prescription drugs					
Acetaminophen/paracetamol +ethanol	G	nd	nd	McCuskey et al., 2004	SEM, TEM, *in vivo*, *in vitro*
Acetaminophen/paracetamol	G	-	-	Ito et al., 2006b	SEM, *in vivo*
				Walker et al., 1983	SEM, TEM, *in vivo*
				McCuskey et al., 2004; McCuskey, 2006	SEM, TEM, *in vivo*, *in vitro*
Amlodipine	-	+	+	Hunt et al., 2019	SEM, *in vitro*
Bosentan	0	+	+	Hunt et al., 2019	SEM, *in vitro*
Colchicine	nd	nd	0	Braet et al., 1996b	TEM, *in vitro*
Disulfiram	-	nd	+	Bernier et al., 2020	SEM, *in vivo*
Metformin	0	+	+	Hunt et al., 2020	SEM, *in vitro*, *in vivo*
				Alfaras et al., 2017	SEM, *in vivo*
Nicotinamide mononucleotide (NMN)	0	+	+	Hunt et al., 2019	SEM, *in vitro*
				Mao et al., 2019	dSTORM, *in vitro*
Cholesterol	0	0	0	Fraser et al., 1988, 1989	SEM, *in vivo*
Cholesterol +nicotine	-	-	-	Fraser et al., 1988	SEM, *in vivo*
Pantethine + cholesterol	+	+	+	Fraser et al., 1989	SEM, *in vivo*
Prostaglandin E1	+			Oda et al., 1997	SEM, TEM, *in vitro*
Sildenafil	0/+	++	+	Hunt et al., 2019	SEM, *in vitro*
				Mao et al., 2019	dSTORM, *in vitro*
Simvastatin	+	+	+	Hide et al., 2020	SEM, TEM, *in vivo*, SEM, *in vitro*
				Venkatraman and Tucker-Kellogg, 2013; Hunt et al., 2019	SEM, *in vitro*
Taxol	nd	nd	0	Braet et al., 1996b	TEM, *in vitro*
TNF-related apoptosis-inducing ligand (TRAIL)	+/0	+/0	+/0	Hunt et al., 2019	SEM, *in vitro*

"0," no change; G, gaps; increase: "+," <50%; "++," 50–100%; "+++," >100%; decrease: "-," <50%; "- -," >50%; "- - -," defenestration; "nd," no data.

Cocaine is a widely used recreational drug with vasoconstricting properties (Kim and Park, 2019), often consumed in combination with alcohol. In a study from McCuskey et al. (1993), mice challenged with cocaine alone developed basement membrane deposition in the space of Disse, some hepatocellular necrosis and slightly reduced centrilobular sinusoid blood flow after 5 weeks, worsening up to 9 weeks of challenge. In combination with ethanol these changes were significantly exacerbated, in addition the sinusoidal endothelium was thickened and defenestrated. Interestingly rats were more resistant to these challenges, only developing some of these changes at the end of the 15-week treatment regime. The

TABLE 2 | Influence of hormones and other agents acting on LSEC fenestrations.

	Fenestration diameter	Porosity	Fenestration frequency	References	Methods
Vasoactive stimuli					
Vasodilators					
Acetylcholine	+	nd	nd	Tsukada et al., 1986; Oda et al., 1990	SEM, *in vivo*, *in vitro*
Bethanechol	+	nd	nd	Oda et al., 1990	SEM, *in vivo*
Isoproterenol	+	nd	nd	Oda et al., 1990	SEM, *in vivo*, *in vitro*
Vasoactive intestinal peptide (VIP)	+	nd	nd	Oda et al., 1990	SEM, *in vivo*
BQ-123	++	nd	-	Watanabe et al., 2007	SEM, TEM, *in vivo*
Vasoconstrictors					
Endothelin (ET)	-	-	nd	Oda et al., 1997; Kamegaya et al., 2002	SEM, *in vitro*
Neuropeptide Y	-	nd	nd	Oda et al., 1990	SEM, *in vivo*
Norepinephrine/ noradrenaline	-	nd	nd	Tsukada et al., 1986; Oda et al., 1990	SEM, *in vivo*, *in vitro*
				Wisse et al., 1980	TEM, SEM, *in vivo*
Serotonin	-	nd	nd	Wisse et al., 1980; Braet et al., 1995a	SEM, TEM, *in vivo*
				Tanikawa et al., 1991	TEM, *in vivo*
				Braet et al., 1996c	SEM, AFM, *in vitro*
				Kalle et al., 1997	AFM, *in vitro*
Pilocarpin	-	nd	nd	Wisse et al., 1980	TEM, SEM, *in vivo*
Adrenaline/ epinephrine	-	nd	nd	Wisse et al., 1980	TEM, SEM, *in vivo*
Signaling/Maintenance					
Vascular endohelial growth factor (VEGF)	+	+++	++	Funyu et al., 2001; Yokomori et al., 2003	SEM, *in vitro*
				Carpenter et al., 2005	SEM, TEM, *in vivo*
				Xie et al., 2012b	SEM, *in vivo*, *in vitro*
Bone morphogenetic protein (BMP)	Strain specific	Strain specific	Strain specific	Desroches-Castan et al., 2019a,b	(a) SEM, *in vivo*, *in vitro* (b) SEM, *in vitro*
Platelet derived growth factor (PDGF-B) signaling	nd	-	nd	Raines et al., 2011	TEM, *in vivo*
Liver X receptor (LXR)	NA	NA	NA	Xing et al., 2016	SEM, TEM, *in vivo*
Hedgehog (Hh) signaling	nd	-	nd	Xie et al., 2012a	SEM, *in vitro*
Plasmalemma vesicle associated protein (PLVAP)	+/-	+/-	+/-	Herrnberger et al., 2014	SEM, TEM, *in vivo*
				Auvinen et al., 2019	SEM, *in vivo*

"0," no change; G, gaps; "nd," no data; "NA," not applicable. increase: "+," <50%; "++," 50–100%; "+++," >100%; decrease: "-," <50%; "--," >50%; "---," defenestration.

mechanism(s) by which cocaine and cocaine/ethanol challenge elicit these changes remains to be elucidated, but in any case the combined abuse of these drugs raises particular concerns with regards to liver function.

Nicotine is the primary stimulant found in tobacco products and is also a known vasoconstrictor (Benowitz and Burbank, 2016). Rats fed nicotine (dose equivalent to 50–100 cigarettes per day in humans for 6 weeks) had LSEC porosity 40% of that of controls, primarily as a function of reduced average fenestration diameter and not of reduced fenestration number. The nicotine treated animals also had near 50% higher serum cholesterol than controls, probably as a consequence of reduced LSEC porosity and thereby filtration of low-density lipoprotein (LDL) out from the plasma of these animals (Fraser et al., 1988). Nicotine and cholesterol fed animals had similar porosity and diameter to nicotine-fed only animals. Together with results from cholesterol-only fed animals (no visible changes), it suggests that nicotine (but not cholesterol) has an effect on fenestrations (Fraser et al., 1988). Other studies have shown that oral nicotine induces an atherogenic lipoprotein profile (Cluette-Brown et al., 1986) (including increased plasma LDL) and impairs plasma LDL clearance (Hojnacki et al., 1986). The mechanism of action

of nicotine in the LSEC context remains to be elucidated but given the continued consumption of nicotine by humans in various forms (e.g., tobacco products, e-cigarettes, and nicotine supplements) this field warrants further study.

2,5-Dimethoxy-4-iodoamphetamine (DOI) is a substituted amphetamine but is not a stimulant. It is a potent 5-HT_{2A} serotonin receptor agonist and is used recreationally as a hallucinogenic drug (Lapoint et al., 2013). DOI induces cutaneous vascular constriction in rabbits and rats, and this is the suggested cause of hyperthermia resulting from serotonin receptor stimulation (Blessing and Seaman, 2003). DOI has reported beneficial effects on survival, liver regeneration and LSEC morphology after partial hepatectomy (Tian et al., 2011). Furrer et al. (2011) showed that *in vivo* DOI challenge increased porosity in old but not young LSEC, and pre-treatment of old mice with DOI prior to partial hepatectomy resulted in LSEC with improved porosity (Furrer et al., 2011). However, the finding that DOI improved porosity in aged LSEC is at odds with the *in vivo* study of Cogger et al. (2014) who found that DOI improved LSEC porosity in young but not old animals. Both studies used SEM of tissue blocks to quantify fenestrations. Further complicating the DOI story, SEM *in vitro* studies by Hunt et al. (2019) on cultured LSEC from young and old mice revealed that DOI challenge increased porosity in old but not young LSEC, and this increase was most likely a function of increase in both fenestration diameter and frequency. LSEC respond to ligands for the 5-HT2 receptor, as they were reported to being inhibited by ketanserin (a selective 5-HT2 receptor antagonist) (Gatmaitan et al., 1996). The role of 5-HT2A and 2B receptors was proposed as being involved in liver regeneration after liver partial hepatectomy (Lesurtel et al., 2006). Similarly, the presence of the 5HT2 receptor was later highlighted (Braet and Wisse, 2002; Braet, 2004). However, newly reported data showed that known 5-HT receptor mRNAs were absent or at very low levels in mouse, rat and human LSEC (Bhandari et al., 2020). It would thus be of interest to resolve the question of DOI mediated effects, the downstream mechanisms, and whether there is/are age-related responses to DOI.

Medicinal Drugs

Pharmaceutical treatment and prevention of diseases is constantly evolving, with an increasing number of novel medicines entering the market every year. It was reported that the EU retail pharmaceutical bill was around EUR 190 billion in 2018 (OECD/European Union, 2020). Hepatic clearance and metabolism are the basic routes of removing drugs from the system. With decreased porosity prolonged circulation of drugs increases their side effects. Nitric oxide (NO)-based drug therapy was shown to have beneficial effects on the liver (Maslak et al., 2015) and detailed studies on isolated cells confirm the positive role of NO on fenestrated morphology in LSEC (Xie et al., 2012b). Medicinal drugs with other intended targets may also affect LSEC. A recent comparative study revealed the different drug effects on fenestrations in LSEC in an age-related manner (Hunt et al., 2019). Here we summarize the effects of various medicines where fenestration number and size were reported.

Amlodipine is a calcium channel blocker used to treat hypertension by dilating blood vessels to reduce blood pressure. Amlodipine is also reported to increase endothelial NO (Xu et al., 2002; Mason et al., 2014). Hunt et al. (2019) reported that amlodipine increased the porosity in cultured LSEC from both young and old animals and proposed that this increase was more likely mediated by NO production than by calcium transport blockage. This safe and commonly used blood pressure medicine may thus also represent a pharmacological means to counteract age-related defenestration.

Bosentan is a competitive antagonist of endothelin -A and -B receptors, and is used to treat moderate pulmonary hypertension, exerting its vasodilative effect via ET-A receptors (Bacon et al., 1996). Endothelin-1 (ET-1) constricts fenestrations pronouncedly and reduces porosity (Kamegaya et al., 2002), and an ET-B receptor antagonist (BQ788) blocked this effect while an ET-A receptor antagonist (BQ485) partially blocked the ET-1 effect (Kamegaya et al., 2002). The ET-A receptor antagonist **BQ123** increased fenestration diameters, but caused major gaps in sinusoidal cells and fusions of fenestrations within sieve plates (Watanabe et al., 2007). Hunt et al. (2019) demonstrated that lower doses of bosentan increased the porosity of LSEC from old mice, while LSEC from younger mice were non-responsive. Bosentan treatment of LSEC did not elicit an increase in NO production in this study.

Colchicine is used as a therapy for gout and familial Mediterranean fever. It decreases inflammation but its pharmacotherapeutic mechanism of action is not fully understood – its main mechanism of action is tubulin disruption (Leung et al., 2015). Treatment of cultured rat LSEC with 200 μM colchicine did not affect porosity while causing significant loss of microtubules. Interestingly, the microtubules surrounding sieve plates were still present (Braet et al., 1996b). Together with the effect of taxol, which completely disrupts microtubules and prevents cytochalasin-mediated induction of fenestrations, this would suggest that tubulin architecture may have a crucial role in LSEC porosity. **Taxol** (generic name paclitaxel) is a microtubule-stabilizing drug used for the treatment of ovarian, breast, and lung cancer, as well as Kaposi's sarcoma (Weaver, 2014). Braet et al. (1996b) challenged cultured rat LSEC with 10 μM taxol and saw no change in porosity but reported an overabundance of microtubules throughout the cytoplasm, and alongside sieve plates. Moreover, treatment with 10 μM taxol not only did not show a significant change in fenestration number but pretreatment with taxol and two hours later with cytochalasin B, inhibits the effect of the latter, i.e., the increase in fenestration number is reduced in comparison to treatment with cytochalasin B only.

Disulfiram (commercial name Antabuse) is a FDA approved treatment for chronic alcohol addiction. It is an inhibitor of acetaldehyde dehydrogenase and causes the feeling of a hangover immediately upon alcohol consumption (Suh et al., 2006). It is an inhibitor of the transcription factor NF-KB (Schreck et al., 1992) which contributes to its anti-inflammatory properties. In the experimental setting, the consumption of disulfiram was found to normalize body weight in mice. It was also found to increase the frequency of LSEC fenestrations *in vivo*, while decreasing

their average diameter, resulting in no net increase in porosity in mice and rats (Bernier et al., 2020). The mechanism(s) by which disulfiram increases fenestration number remain to be elucidated.

Metformin is a first line treatment for type II diabetes for serum glucose reduction (Maruthur et al., 2016). The mechanism by which this drug exerts this effect remains to be elucidated, but its primary target appears to be hepatocyte mitochondria via inhibition of complex I of the respiratory chain. Inhibition of gluconeogenesis (Owen et al., 2000) results in the activation of the energy sensor AMP-activated protein kinase (AMPK) leading to increased beta-oxidation of fatty acids. Alfaras et al. (2017) tested 1% metformin administered every-other-week or 2-weeks-every-month to mice – these strategies being chosen to avoid metformin induced nephrotoxicity. They found numerous health benefits, particularly with the every-other-week regime, and that the every-other-week approach also increased porosity in LSEC in 2-year-old mice. Metformin (50 μM) increased LSEC porosity *in vitro* in both young and old mice by 25 and 50%, respectively (Hunt et al., 2020). This increase was due to increases in fenestration frequency (20 and 50%, respectively) since the fenestration diameter remained unchanged. *In vivo* studies in mice treated with 0.1% metformin in their diet increased LSEC porosity/fenestration frequency in young and old mice and reduced the age-related loss of porosity in older mice by 50% (Hunt et al., 2020). The mechanism of metformin action in LSEC, with regards to fenestration status, remains to be established.

Nicotinamide mononucleotide (NMN) is a key nicotinamide adenine dinucleotide (NAD+) intermediate. Long-term administration of NMN is reported to mitigate age-related physiological decline in mice (Mills et al., 2016), while short term *in vitro* treatment reverses endothelial dysfunction (Mateuszuk et al., 2020). NMN increased LSEC porosity in young and old mice, via increased fenestration frequency, while the average fenestration diameter was essentially unchanged (Hunt et al., 2019). NMN challenge had no apparent effects on NOS or cGMP levels in LSEC. Analysis of NMN challenged LSEC using direct stochastical optical reconstruction microscopy (dSTORM) revealed that the F-actin within LSEC was more condensed and that the actin rings delineating fenestrations became more pronounced (Mao et al., 2019). The mode of NMN action in LSEC remains to be elucidated – NAD + associates with sirtuins which play a critical role in multiple cellular functions (Imai and Yoshino, 2013) so the study of the role of sirtuins in fenestration biology is therefore warranted.

Pantethine is a derivative of vitamin B5 and has been suggested as a therapy for reducing LDL levels (Rumberger et al., 2011). Fraser et al. (1989) studied the effect of pantethine in cholesterol fed rabbits. The pantethine plus cholesterol fed animals had higher LSEC porosity, fenestration diameter and frequency and lower total cholesterol than the animals fed cholesterol alone. **Cholesterol** feeding had no effect on LSEC porosity. The same result had been found in another study (Fraser et al., 1988). Unfortunately, there was no group fed only pantethine, so it would be interesting to establish if pantethine alone increases LSEC porosity and if this can explain (in part) the reported pantethine-mediated reduction of plasma LDL seen in other studies (Fraser et al., 1989; Rumberger et al., 2011).

Paracetamol (also known as acetaminophen or commercially as APAP, Panadol) is one of the most widely used analgesic medicines. Acute overdoses of paracetamol can cause lethal liver damage, due to the toxic metabolite *N*-acetyl-*p*-benzoquinone imine (NAPQI) (Hodgman and Garrard, 2012). The consensus is that, *in vivo*, paracetamol reduces rodent LSEC porosity both via reduction of fenestration diameter and frequency at "clinical" doses (Walker et al., 1983; McCuskey et al., 2004; McCuskey, 2006; Ito et al., 2006b). The *in vitro* effect of paracetamol on LSEC was reported to be dependent on NAPQI induced depletion of glutathione levels. In C3H mice, acetaminophen is directly toxic to LSEC via P450 activation, while in Swiss Webster mice the toxic effect on LSEC was indirectly driven by hepatocytes (DeLeve et al., 1997). APAP-induced LSEC injury precedes hepatocellular injury, supporting the hypothesis that LSECs are an early and direct target for APAP toxicity. These findings also suggest that reduced sinusoidal perfusion and increased Kupffer cell activity contribute to the development of APAP-induced liver injury (Ito et al., 2003). Although it was presented that large gaps are formed and the porosity is reduced in LSEC *in vivo*, the effects of paracetamol challenge on LSEC porosity *in vitro* have not been reported.

Prostaglandin E1 (synthetic form: alprostadil) is a naturally occurring eicosanoid used as vasodilator for several different medical purposes (Kirtland, 1988). Applications include erectile dysfunction (ED) treatment in men who do not respond to PDE5 inhibitors (Hanchanale and Eardley, 2014) and the opening of ductus arteriosus in neonates requiring heart surgery (Singh and Mikrou, 2018). Prostaglandin E1 exerts its effect via the production of nitric oxide which stimulates soluble guanylyl cyclase to increase production of cyclic GMP (cGMP) and/or by the direct binding of prostaglandin to prostaglandin receptors, activating adenylyl cyclase to convert ATP to cyclic AMP (cAMP). The end result is the same in either pathway - decreased intracellular Ca^{2+} (Namkoong et al., 2005). Oda et al. (1997) showed that prostaglandin E1 significantly increased LSEC fenestration diameter in rat LSEC and also caused partial fusion of some fenestrations within sieve plates. They also reported increased Ca^{2+}-ATPase on fenestral plasma membrane after prostaglandin E1 challenge and postulated that cytoplasmic Ca^{2+} efflux caused relaxation (and thereby dilation) of LSEC fenestrations.

Sildenafil (also known as Viagra) is a vasoactive agent used for the treatment of ED. It is a potent and selective inhibitor of cGMP-specific phosphodiesterase (PDE) type 5, due to its structural similarity to cGMP (Bender and Beavo, 2006). Sildenafil increases cGMP levels by inactivating PDEs that metabolize cGMP to GMP as well as by blocking ABCC5 transport protein responsible for active efflux of cGMP from the cell (Aronsen et al., 2014). cGMP is an intracellular mediator of the NO pathway that can lead to relaxion of the vascular smooth muscle (vasodilation) and thereby increase blood flow (Denninger and Marletta, 1999). Hunt et al. (2019) challenged LSEC from young (3–4 months) and old (18–25 months) mice with sildenafil and found that porosity and fenestration frequency (but not diameter) increased in LSEC from young and old mice. Sildenafil also increased cGMP levels, NO synthesis and levels of

phosphorylated nitric oxide synthase (pNOS). Mao et al. (2019) also challenged LSEC (from young mice) and found that the actin rings (which delineate fenestrations) and actin stress fibers became more pronounced. In contrast to Hunt et al. (2019) and Mao et al. (2019) found that sildenafil increased fenestration diameter on average by 30%. This inconsistency might be due to the methods used – the first study used SEM to score LSEC morphology after dehydration, while the second study used dSTORM on "wet" LSEC samples. Sildenafil (and other PDE and ABC transporters inhibitors) may be an interesting therapeutic option to increase LSEC porosity in the elderly.

Simvastatin is a cholesterol lowering agent. Its cholesterol reducing action is via inhibition of 3-hydroxy-3-methylglutaryl (HMG) coenzyme A reductase, the rate limiting enzyme in cholesterol synthesis. Simvastatin also upregulates NO levels suggesting vascular protective effects beyond cholesterol reduction (de Sotomayor et al., 2005; Rikitake and Liao, 2005). Hide et al. (2020) reported that simvastatin was somewhat protective against warm ischemia reperfusion induced LSEC defenestration in (male Wistar) rats, so simvastatin may be able to provide a protective role in maintenance of porosity. Venkatraman and Tucker-Kellogg (2013) showed that simvastatin can antagonize Rho/ROCK (Rho-associated protein kinase) signaling, protecting from the defenestration resulting from activation of this pathway. Moreover, simvastatin treatment led to increase on both porosity and fenestration frequency in (male Wistar) rats. Interestingly these results in rats were not replicated in mice. Findings of Hunt et al. (2019) in (male C57/BL6) mice showed no significant changes in porosity or fenestration frequency in young or old mice, and only a 20% increase in mean diameter in the aged group. These findings may suggest species dependent difference in the simvastatin mechanism of action.

TRAIL [tumor necrosis factor (TNF)-related apoptosis-inducing ligand] is a protein ligand reported to induce cell death in transformed cells by binding to "death receptors" (Wiley et al., 1995). It is also reported to induce NO production *via* eNOS (Bartolo et al., 2015). Hunt et al. (2019) reported that LSEC challenged with lower doses of TRAIL increased LSEC porosity and fenestration frequency in young but not old mice. The lack of TRAIL response of old mice LSEC could be explained by reduced expression of TRAIL receptors in older mouse LSEC, but the level of TRAIL receptor expression in young vs. old mice remains to be determined.

Hormones and Other Agents Acting on LSEC

LSEC and Vasoactive Agents

Vasoactive signaling molecules commonly act through a receptor induced relaxation in the smooth muscle surrounding the vasculature (Webb, 2003). Signaling is mostly mediated by the NO/cGMP pathway and via intracellular calcium concentrations (Chen et al., 2008). Crucially, whether a stimuli directs toward constriction or relaxation will depend on the tissue specific expression of certain receptors and the presence or absence of inhibition of parallel pathways.

Hepatic sinusoids lack smooth muscle cells but can dilate and contract responding to various vasoactive agents. Moreover, according to the two main studies addressing this issue (Oda et al., 1990; Gatmaitan et al., 1996), LSEC porosity and fenestration diameter seem to correlate with vasodilation or vasoconstriction (**Table 2**). These results suggest that vasodilators and vasoconstrictors have a direct effect upon the fenestrations of LSEC. The lack of super resolution techniques for living cells was one of the main drawbacks at the time of these studies of vasoactive agents' effects on LSEC. It will be therefore beneficial for the field investigate the role of vasoconstriction and dilation in fenestration regulation using live cell imaging techniques, such as AFM, SIM or stimulated emission depletion microscopy (STED).

Vasodilators

Acetylcholine is a vasodilator acting through the cholinergic/muscarinic receptor (Sakai, 1980). In LSEC acetylcholine dilates sinusoids increasing blood flow rate and increasing fenestration diameter (Oda et al., 1990), when administered intravenously. On the other hand, **cholinergic receptor agonists** were also noted to cause narrowing of the sinusoids: **bethanechol, carbachol,** and **pilocarpine** applied topically to the liver caused constriction of the liver microvasculature, but fenestrations were not quantified (Reilly et al., 1982; McCuskey and Reilly, 1993). To further complicate these findings, intravascular admission of pilocarpine decreased while bethanechol increased the fenestration diameter. These differences in the effects can be explained by the expression of certain receptors responding to the same stimuli but having contradictory effects, however, further studies are needed. **Bethanechol** is already used as a therapy for postoperative and postpartum non-obstructive urinary retention, it would therefore be of interest to further study its effects on LSEC porosity (Oda et al., 1990). **Vasoactive intestinal peptide (VIP)** is a class II G-protein coupled receptor ligand (Umetsu et al., 2011). It has multiple physiological effects including vasodilation and increased gut motility during digestion (Iwasaki et al., 2019). VIP was shown to dilate the sinusoids and fenestra, increasing blood flow through the sinusoids which would enhance the uptake of circulating nutrients after a meal (Oda et al., 1990). **Isoprenaline** (also known as isoproterenol) is another vasodilating agent acting as a β-adrenergic receptor agonist. This G-protein is essential for cardiac function (reviewed in Wachter and Gilbert, 2012) and is used to treat bradycardia and (rarely) asthma. The effect on LSEC follows that of other of vasodilating agents increasing in both sinusoidal blood flow and fenestration diameter (Oda et al., 1990).

Vasoconstrictors

Serotonin (also known as 5-HT) is a monoamine neurotransmitter with numerous physiological functions (Berger et al., 2009). Depending on the particular receptors expressed in each vessel wall and surrounding smooth muscle tissue, serotonin can cause vasoconstriction or vasodilation in different vascular beds (Kaumann and Levy, 2006). In the liver, serotonin constricts sinusoids and reduces fenestration size (Wisse et al., 1980; Oda et al., 1990). Gatmaitan et al. (1996)

showed that the effect is mediated by decreasing cAMP and increasing intracellular calcium levels in a matter of seconds. **Endothelin (ET)** is a vasoconstricting peptide that is produced in the endothelium and plays an important role in vascular homeostasis (Kawanabe and Nauli, 2011). In LSEC, it decreases both the number and the size of fenestrations (Kamegaya et al., 2002; Yokomori et al., 2006) and it reduces the blood-flow through the sinusoids (Zhang et al., 1994). Many ET receptor antagonists are used as an efficient treatment for hypertension. ET-A receptor antagonist **(BQ-123)** treatment (but not ET-B receptor antagonists) abolished ET induced defenestration and contraction of fenestrations (Yokomori et al., 2006). Blocking ET-1 activity *in vivo* by BQ-123 led to gap formation shown by SEM and TEM (Watanabe et al., 2007). The α-adrenergic receptor family mediates vasoconstriction and is coupled to guanine nucleotide regulatory proteins (G-proteins) (reviewed in Ruffolo and Hieble, 1994). **α-adrenergic receptor agonists** were found to have different effects on LSEC, **epinephrine** (adrenaline) decreased sinusoidal blood flow and contracted sinusoids and LSEC fenestrations (Oda et al., 1990), while in another study sinusoids were found slightly enlarged, and fenestrations unchanged (Wisse et al., 1980). **Norepinephrine** (noradrenaline) was found to contract sinusoids and fenestrations in both studies (Wisse et al., 1980; Oda et al., 1990). **Neuropeptide Y (NPY)**, another vasoconstrictor generally coupled to G-protein signaling, is involved in various physiological and homeostatic processes (White, 1993) but also inhibits gastrointestinal motility (Holzer et al., 2012). In LSEC, NPY constricts both sinusoid and fenestrations (Oda et al., 1990).

Signaling and Fenestration Maintenance

One of the most challenging aspects of studying LSEC is the dedifferentiation *in vitro* after cell extraction. LSEC lose their characteristic porous morphology after just few days in culture, significantly restricting time for experiments. There have been many attempts to slow down, stop or reverse that process (Bravo et al., 2019; Di Martino et al., 2019) but the main mechanism(s) behind the loss of fenestrations remain unknown.

Vascular Endothelial Growth Factor (VEGF) is a hormone that stimulates acetogenesis and angiogenesis (Apte et al., 2019). In LSEC, VEGF has been shown to increase LSEC porosity *in vitro* (Funyu et al., 2001; Yokomori et al., 2003) as well as to prolong the fenestrated phenotype of cultured LSEC *in vitro* (Xie et al., 2012b). Downregulation of VEGF signaling has been associated with LSEC defenestration, capillarization of sinusoids, and abnormal liver physiology (Carpenter et al., 2005; DeLeve, 2015). DeLeve (2015) showed that VEGF promotes fenestration formation/maintenance *via* NO-dependent and NO-independent pathways. Moreover, VEGF can induce fenestration like structures in other microvasculature, e.g., rat cremaster capillary (Roberts and Palade, 1995).

Bone Morphogenetic Protein 9 (BMP9, also known as GDF2) is a circulating endothelial quiescence factor (David et al., 2008). In LSEC it has been indicated as necessary for fenestration maintenance and treating cells with BMP9 prolonged fenestrated phenotype in cultured LSEC (Desroches-Castan et al., 2019a). BMP9 knockouts in 129/Ola mice showed very low fenestration frequency compared to WT, without changes to diameters (Desroches-Castan et al., 2019a). However, a follow up study using C57/Black mice did not confirm these results (Desroches-Castan et al., 2019b).

Platelet derived growth factor B (PDGF) is a member of the PDGF family of major mitogens for many cell types (Fredriksson et al., 2004). Hepatic vascular permeability was highly increased in PDGF-B retention deficient mice, with a three-fold increase in FITC-dextran absorption and a more fenestrated phenotype (Raines et al., 2011). PDGF-B signaling is involved in pericyte recruitment and function, and stellate cell activation (Raines et al., 2011).

Liver X receptor (LXR) is a nuclear receptor expressed in a number of tissues, but with highest expression in the liver (Willy et al., 1995). Oxysterols are natural ligands of LXR and LXR deletion exacerbates CCl_4 induced capillarization and basement membrane deposition (Xing et al., 2016). LXR also acts antagonistically on Hedgehog signaling (Hh) (Kim et al., 2009), while LSEC produce and respond to Hh ligands and use Hh signaling to regulate complex phenotypic changes that occur during capillarization. Moreover, inhibition of Hh using **cyclopamine** induced fenestration *in vitro* (Xie et al., 2012a).

Plasmalemma vesicle-associated protein (PLVAP) is associated with angiogenesis and vascular permeability, with less expression in barrier endothelium, and its expression is stimulated by VEGF (Bosma et al., 2018). PLVAP was found to be associated with a normally fenestrated phenotype, while PLVAP deficient mice present extremely low porosity and accumulation of collagen in the space of Disse (Herrnberger et al., 2014). Auvinen et al. (2019) found that there was no difference in number of fenestrations in PLVAP–/– mice, though their data shows greater variability in the knockouts. Both studies used SEM of tissue blocks for quantitative analysis of fenestrations. The difference may relate to the methods used to attain the knockouts raising the question of either knockouts being too broad/non-specific or insufficient. PLVAP mutations are associated with loss of fenestration diaphragms in other tissues (such as small intestine) (Elkadri et al., 2015).

Lab Tools and Experimental Models

Experimental Animal Models for the Study of LSEC Fenestrations

Liver sinusoidal endothelial cells are the first line of defense in the liver and alterations in LSEC play a crucial role in the development of many liver diseases such as fibrosis, cirrhosis, or cancer (Gracia-Sancho et al., 2021) as well as in the age-related conditions (Hunt et al., 2018). To better understand this role, many animal models have been used. Challenge with certain drugs can mimic the development of these diseases and reduce the time and/or costs compared to waiting for them to spontaneously occur in animals (**Table 3**). Although the exact mechanism of action of many of these drugs is not known, the outcome is similar enough to study and propose possible treatments.

Cirrhosis is a pathological liver state characterized by abnormalities in hepatic architecture such as loss of fenestrations

TABLE 3 | Experimental models and lab tools affecting LSEC fenestrations.

	Fenestration diameter	Porosity	Fenestration frequency	References	Methods
Cytoskeleton disruptors					
Cytochalasin B	0/+	+++	+++	Braet et al., 1996a,b,c	a/b AFM, SEM, *in vitro* c SEM, TEM, *in vitro*
				Steffan et al., 1987	SEM, TEM, *in vitro* SEM, *in vivo*
				Braet et al., 1995a	TEM, *in vitro*
				Zapotoczny et al., 2017b, 2019b	AFM, *in vitro* live
				Spector et al., 1999	FL, SEM, TEM, *in vitro*
				Oda et al., 1993	SEM, TEM, *in vitro*
				Van Der Smissen et al., 1986	TEM, *in vitro*, *in vivo*
				Steffan et al., 1986	SEM, *in vivo*
				Kalle et al., 1997	AFM, *in vitro*
Cytochalasin D	0/-	+	+	Svistounov et al., 2012; Hunt et al., 2019	SEM, *in vitro*
Dihydrohalichondramide	-	nd	++	Braet et al., 2002	SEM, *in vitro*
Halihondramide	-	nd	++	Braet et al., 2002	SEM, *in vitro*
Jasplakinolide	-	nd	+	Zapotoczny et al., 2019b	AFM, *in vitro* live
				Braet et al., 1998	SEM, TEM, *in vitro*
				Spector et al., 1999	FL, *in vitro*
Latrunculin A	0	nd	++	Braet et al., 1996a	SEM, TEM, *in vitro*
				Spector et al., 1999	FL, *in vitro*
				Braet et al., 1997	SEM, *in vitro*
Misakinolide	-	nd	++	Braet et al., 1998, 1999; Spector et al., 1999	SEM, TEM, *in vitro*
Swinholide A	- -	nd	+++	Braet et al., 1998, 1999; Spector et al., 1999	SEM, TEM, *in vitro*
Disease models					
Dimethyl nitrosamine (DMN)	-	- -	nd	Fraser et al., 1991, 1995b; Rogers et al., 1992; Tamba-Lebbie et al., 1993	SEM, *in vivo*
Endotoxin/LPS	-/G	- -/0	-		SEM, *in vivo*
				Dobbs et al., 1994; Fraser et al., 1995b	
					SEM, TEM, *in vivo*
				Frenzel et al., 1977; Ito et al., 2006a	
				Sasaoki et al., 1995	SEM, *in vitro*
Galactosamine + endotoxin	G	nd	-	Ito et al., 2006a	SEM, TEM, *in vivo*
Galactosamine + endotoxin + matrix metaloproteinase	0	nd	0	Ito et al., 2006a	SEM, TEM, *in vivo*
Monocrotaline	G	nd	- -	DeLeve et al., 1999	SEM, TEM, *in vivo*
				DeLeve et al., 2003a,b	SEM, *in vivo*
Monocrotaline + V-PYRRO/NO	0	0	nd	DeLeve et al., 2003b	SEM, *in vivo*
Poloxamer 407	nd	nd	- -	Cogger et al., 2006	SEM, TEM, *in vitro*, *in vivo*
Pyocyanin	nd	- -	nd	Cheluvappa et al., 2007	SEM, *in vitro*
Thioacetamide (TAA)	-	- -	nd	Mori et al., 1993a,b	SEM, TEM, *in vivo*
				Xie et al., 2012b	SEM, *in vivo*
Other					
Superoxide anion (SOA) and nitric oxide NO	G	nd	-	Deaciuc et al., 1999	SEM, TEM, *in vivo*
7 keto cholesterol (7KC)	+	+	+	Svistounov et al., 2012; Hunt et al., 2019	SEM, *in vitro*
Antimycin A	nd	-	- - -	Zapotoczny et al., 2017b	AFM, *in vitro* live
				Braet et al., 2003	SEM, TEM, *in vitro*
Arsenic	nd	- -	nd	Straub et al., 2008	SEM, TEM, *in vitro*, *in vivo*
C3 transferase	+	+	nd	Yokomori et al., 2004	SEM, TEM, *in vitro*

(Continued)

TABLE 3 | (Continued)

	Fenestration diameter	Porosity	Fenestration frequency	References	Methods
Calcium ionophore	-	nd	0	Zapotoczny et al., 2019a	AFM, *in vitro*
				Oda et al., 1993	SEM, TEM, *in vivo*
Calmodulin agonist w7	+	nd	nd	Oda et al., 1993	SEM, TEM, *in vitro*
Cyclopamine	nd	+	nd	Xie et al., 2012a	SEM, *in vitro*
Diamide	nd	nd	- - -	Zapotoczny et al., 2019a	AFM, *in vitro* live
Hydrogen peroxide	+/G	- -/+	-	Cogger et al., 2001	SEM, TEM, *in vivo*
				Straub et al., 2008	SEM, TEM, *in vitro*, *in vivo*
Iodoacetic acid	nd	nd	+	Zapotoczny et al., 2019a	AFM, *in vitro* live
Lysophosphatic acid (LPA)	-	nd	- -	Yokomori et al., 2004	SEM, TEM, *in vitro*
Phorbol myristate acetate (PMA)	0	nd	-	de Zanger et al., 1997	SEM, *in vitro*
S-nitroso-*N*-acetyl penicillamine (SNAP)	G	nd	0	Deaciuc et al., 1999	SEM, TEM, *in vivo*
Staurosporine	0	nd	-	de Zanger et al., 1997	SEM, *in vitro*
Tert-butyl hydroperoxide	G	+	0	Cogger et al., 2004	SEM, TEM, *in vitro*, *in vivo*
Triton x100	0	- -	nd	Svistounov et al., 2012	SEM, *in vitro*
Trombospondin 1	nd	- -	- -	Venkatraman and Tucker-Kellogg, 2013	SEM, *in vitro*

"0," no change; G, gaps; nd, no data; increase: "+," <50%; "++," 50–100%; "+++," >100%; decrease: "-," <50%; "- -," >50%; "- - -," defenestration.

(defenestration) and the build-up of basement membrane formed from collagen deposition in the space of Disse. Interestingly, the first stages of capillarization and defenestration was reported to be reversible prior to the deposition of collagen and formation of a basement membrane which indicates progression from fibrosis to cirrhosis (Xie et al., 2012b). Drugs such as **dimethyl nitrosamine (DMN)** or **thioacetamide (TAA**) are used to induce cirrhotic morphology in LSEC in animal models. Chronic admission of DMN (Fraser et al., 1991; Tamba-Lebbie et al., 1993) and TAA (Mori et al., 1993b; Xie et al., 2012b) was shown to lead to the loss of fenestrations, however the precise mechanism(s) behind this remains unknown. It was suggested that soluble guanine cyclase (sGC) is a crucial element of signaling necessary to maintain fenestrated LSEC morphology. sGC activation normalizes LSEC phenotype and completely prevents progression of fibrosis despite ongoing TAA exposure, so the limiting defect responsible for capillarization in this model of cirrhosis was in the NO/sGC/cGMP pathway (Xie et al., 2012b). Defenestration is an important step not only in cirrhosis and fibrosis but also with aging and its development and has an impact on the whole organism. Lack of filtration of chylomicrons and chylomicron remnants leads to hyperlipidemia (Rogers et al., 1992). Cogger et al. (2006) showed that **poloxamer 407**, a synthetic surfactant causes dramatic defenestration and massive hyperlipidemia. This finding suggests a direct role of LSEC porosity in the lipid clearance in the liver.

Monocrotaline has been used to a model hepatic veno-occlusive disease (DeLeve et al., 1999) and sinusoidal obstruction syndrome (SOS) (DeLeve et al., 2003a,b). Toxic effects were observed only in LSEC but not in hepatocytes nor in other parts of the endothelium. LSEC metabolize monocrotaline by conjugation to glutathione and detoxify to pyrrolic metabolite. It is believed to be a stable reproducible model resulting in a decreased number of fenestrations, gap formation and discontinuous sinusoid occurrence (DeLeve et al., 1999). It is an important reminder that LSEC also can metabolize drugs and it is not only the hepatocytes that have this function in the liver.

Galactosamine, together with **endotoxin** or **TNF**, causes gap formation in the sinusoids and can be used to study the neutrophil extravasation in the acute inflammatory tissue injury (Ito et al., 2006a). It was shown that inhibition of **matrix metalloproteinases**, which are involved in gap formation, reduces the neutrophil accumulation in the sinusoids. **Bacterial endotoxin** alone plays a role in the pathogenesis of cirrhosis, decreasing both number and diameter of fenestrations (Dobbs et al., 1994). Other bacterial toxins, such as **pyocyanin** or **LPS**, are used in studies of post-transplantation complications such as sepsis or ischemia-reperfusion injury. **Pyocyanin** treatment decreases porosity by its effects on the frequency of fenestrations and can be prevented by addition of catalase. This result suggests that the mechanism involves hydrogen peroxide–induced oxidative stress (Cheluvappa et al., 2007).

Another bacterial toxin, ***Clostridium botulinum* C3-like transferase (C3-transferase**), together with **lysophosphatic acid (LPA)** was tested in a study from 2004. C3-transferase is a rho inhibitor, while LPA is a rho stimulator. Rho was found to be an important regulator of the actin cytoskeleton and was therefore tested for its influence on fenestration and LSEC in general. The *in vitro* experiments on rat LSEC showed dilation and fusion of fenestrations after treatment with C3-transferase, while contraction occurred when the cells were treated with LPA. Additionally LPA caused an increase in F-actin stress fiber and actin microfilaments, while C3-transferase treatment showed the opposite (Yokomori et al., 2004).

Several models of experimental liver injury show similar morphological alterations, including gaps and ruptured sinusoids. Deaciuc et al. (1999) showed that these early changes can be mediated by the free radical species. The *in vitro* treatment

of rat LSEC with **superoxide anion** or **nitric oxide** resemble the observations from *in vivo* experiments with various hepatotoxins. Treatment with **hydrogen peroxide** also increased fenestration diameter and decreased fenestration number (Cogger et al., 2001). High porosity values can be misleading in the studies where gap formation is observed so measurement of all three morphology parameters should be considered. Straub et al. (2008) presented that effect of low doses of **arsenic**, mimicking water contamination levels, also act through reactive oxygen species (ROS) generated by NADPH oxidase (NOX). This mechanism was confirmed by the protective (against arsenite) results from NOX deficient mice and use of NOX inhibitors.

Cytoskeleton Disruptors

Numerous agents acting on the actin cytoskeleton have significant effects on fenestration (**Table 3**). Two main groups include marine sponge- and mushroom-derived toxins. Relatively well-known mechanisms of action of these toxins allowed the study of the link between actin cytoskeleton and fenestrae. An extensive chapter from Braet et al. (2008), provides an overview on the *in vitro* effects of actin binding agents such as **cytochalasin B, latrunculin A, jasplakinolide A, swinholide A, misakinolide A, halichondramide, and dihydrohalichondramide**. Despite different mechanisms of promoting/inhibiting actin polymerization or fiber stabilization, all drugs result in an increase of fenestration number. The most surprising finding is the effects of jasplakinolide which promotes polymerization and stabilization of actin in other cells, but in LSEC no such effect was shown. Instead, the loss of fibers and accumulation of actin in single spots occurs within minutes of jasplakinolide treatment (Spector et al., 1999). These structures, described as 'actin dots,' are not fully understood, but they resemble recently described actin asters which may be connected with lipid raft reorganization (Fritzsche et al., 2017). There is an ongoing discussion about the specificity of those agents for actin. For example, cytochalasin B (but not D) was shown to influence transport of glucose across cell membranes and its overall effect can be influenced by changes in glycolysis and metabolism (Kapoor et al., 2016). **Iodoacetic acid** acts on both actin and spectrin and was shown to decrease stress filament formation. Moreover, it caused an increase in porosity and rapid opening and closing of fenestrations (Zapotoczny et al., 2019a). Nevertheless, agents acting on the actin cytoskeleton remain the most important tools for studying fenestration structure and dynamics.

Other Agents Affecting Fenestrations

Svistounov et al. (2012) emphasized the importance of lipid membrane stability and lipid rafts on LSEC morphology. Surfactants such as **Triton X100** or **poloxamer** showed destabilization of the cell membrane and promotion of lipid raft formation which resulted in a decrease or even complete ablation of fenestrations. Moreover, the reduction of lipid raft formation by **7 keto-cholesterol (7KC)** increased the number of fenestrations showing the connection between fenestration structure, actin and cell membrane (Hunt et al., 2019).

Thrombospondin 1 (TSP) is a matrix glycoprotein with pro-fibrotic effects. In a study from 2013 (Venkatraman and Tucker-Kellogg, 2013) it was shown to cause dose-dependent defenestration in LSECs at 100 ng/mL. The authors additionally showed that the CD47-binding fragment of TSP1, p4N1 – which has anti-angiogenic effects in endothelial cells, also induces defenestration in LSECs.

The influence of **phorbol myristate acetate (PMA)**, a protein-kinase-C (PKC) activator and **staurosporine**, a PKC inhibitor, on LSEC have been examined by de Zanger et al. (1997). The *in vitro* treatment of rat cells for 2–7 days resulted in a decrease in porosity, due to the decrease in fenestration number without any observable change in fenestration diameter, when treated with PMA. However, despite the decrease in porosity, PMA improves LSEC cultures in terms of viability and purit, and fenestrated morphology was maintained after 7 days (de Zanger et al., 1997). Treatment with staurosporine or PMA and staurosporine showed enlarged fenestrations, gap formation and a decrease in porosity. The authors concluded that PMA acts on LSEC through PKC based on the staurosporine treatment neutralizing the PMA treatment effects.

Deaciuc et al. (1999) tested rat livers challenged with superoxide anion [**S-nitroso-*N*-acetyl penicillamine (SNAP)**] and nitric oxide [xanthine oxidase plus hypoxanthine (XO + HX)] generating substances. They theorized that early morphological LSEC alterations associated with liver injury are influenced by free radical species. When they perfused the rat livers with SNAP, they found a suppression of hyaluronan uptake (a test of LSEC endocytosis capacity) and the formation/creation of large gaps in LSEC morphology, sometimes instead of sieve plates, and sometimes together with fenestrations present in sieve plates.

MECHANISMS

As discussed above, a variety of agents have been tested so far showing their effect on fenestrae. Some of the agents changed the number of fenestrations, while others alter their diameters or distribution (gathered in sieve plates or individual fenestrations), including the formation of gaps. However, the clear understanding of why individual drugs have their effects on LSEC is still lacking. The main reason is that many drugs have cross-effects at the cellular level, affecting more than one cellular mechanism/pathway, including the rearrangement of cytoskeleton. Therefore, it is challenging to predict how a drug will work on LSEC fenestrations.

A thorough analysis of the effects of a variety of agents changing porosity, fenestration frequency, and fenestration diameters (including gap formation) resulted in four different hypotheses. These independent but overlapping ideas describe the possible mechanisms behind fenestration structure and dynamics.

(I) *Actin (de)polymerization regulates the number of fenestrations* (Braet et al., 1996b; Spector et al., 1999; Braet and Wisse, 2002; Mönkemöller et al., 2015). The hypothesis was discussed in Braet et al. (1995a), Braet et al. (1996b) and has been developed over the years. It was presented that the cytoskeleton plays a crucial role in the porosity

of LSEC. Fenestrae-associated cytoskeleton rings (FACR) surround each fenestration and sieve plate-associated cytoskeleton surround sieve plates (Braet et al., 1995b). The application of actin (de)polymerization targeting drugs revealed the direct connection between actin cytoskeleton and fenestration number in LSEC (Spector et al., 1999; Carpenter et al., 2005). However, the disruption of actin does not destroy fenestration structure, which indicated the complex structure of FACR. Later it was reported that actin filaments surround each fenestration within a sieve plate (Mönkemöller et al., 2015).

(II) *Calcium ions regulate the diameter of fenestrations*. This second hypothesis was summed up in 2002 (Braet and Wisse, 2002). It is mainly based on the research of Oda and Yokomori presenting the role of calcium/calmodulin/actomyosin in the contractility of fenestration diameters (Oda et al., 1990; Yokomori et al., 2004). The regulation of myosin light chain (MLC) phosphorylation occurs via calcium-calmodulin signaling. Further it was suggested that MLC kinase and phosphatase may exert different effects on cell morphology (Yokomori et al., 2004).

(III) *Regulation of fenestrations depends on lipid rafts*. The sieve-raft hypothesis assumes that fenestrations are formed in the flat areas of the cell periphery, in between lipid rafts, where the cell membrane is more flexible and more prone to shape changes (Svistounov et al., 2012). Also, other ways in which lipid rafts can be connected with fenestration were proposed, such as influence on signal transduction or indirect regulation of some signaling pathways.

(IV) *Spectrin is involved in the open versus closed state of fenestration*. The hypothesis decouples the direct actin regulation from the number of fenestrations. Instead, the interplay between the membrane scaffold and actin cytoskeleton is responsible for the opening of the fenestration within the actin ring (Zapotoczny et al., 2019a).

All the above hypotheses do not exclude each other and only emphasize how complicated the mechanisms regulating the number, shape, and size of fenestrations can be. In the following subsections we will focus on the physiological regulation of number and size of fenestrations, apart from the direct (often toxic) effect of actin disturbing drugs (described above). The analysis of different agents acting on LSEC fenestrations leads to the conclusion that the phosphorylation of myosin light chain (MLC) is the core of various pathways regulating actin (de)polymerization. Calcium dependent and independent activation (phosphorylation) of MLC and release of actin binding proteins (such as tropomodulin, tropomyosin, caldesmon) leads to contraction of fenestrations and decrease in the number of fenestrations, while MLC dephosphorylation leads to the relaxation of MLC and promotes more fenestrated morphology of LSEC. The local balances regulating the levels of calcium, ROS, or NO in different parts of the cell ensure active control over the dynamics of fenestrated LSEC. The regulation covers the (de)activation of membrane proteins which may affect actin association to the membrane. Finally, the oxidative state of membrane cytoskeleton and lipid rafts distribution are additionally (passively or actively) involved in this regulation.

Cytoskeleton

SEM and TEM allowed visualization of the fenestrae-associated cytoskeleton rings (FACR) in LSEC (Braet et al., 1996b). Preparations of "ghost" cells, after removing cell membrane with detergent, revealed a network of filaments associated with sieve plates surrounded by thicker filaments. Precise identification was not possible, but the high resolution of those techniques allowed diameter measurements suggesting a mesh of actin fibers surrounded by microtubules. The gap in the chemical information has been filled with super resolution fluorescence microscopy. Mönkemöller et al. (2015) showed the first direct correlation between the localization of cell membrane and actin around fenestration, using SIM. Recently, FACR structures could be also visualized in high resolution using AFM and dSTORM (Zapotoczny et al., 2017b, 2019a). It was also presented that the complete actin ring is necessary to form an open pore within a FACR (Zapotoczny et al., 2019a).

Cytoskeleton remodeling that influences the number of fenestrations was demonstrated for live LSEC. During the first hours after isolation LSEC spread on the substrate, opening and closing individual fenestrations and whole sieve plates. It indicated that fenestrations are not preserved from the *in vivo* to the *in vitro* state and their formation and closing is dynamic as previously suggested (Braet and Wisse, 2012). With time, the dynamics of fenestrations was shown to be slower (Zapotoczny et al., 2020). Still, fenestrations in isolated LSEC were shown to freely migrate several micrometers, and changing their diameter up to 200% during their $\sim$ 20 min lifespan.

Interesting labyrinth like structures have been observed *in vitro* in the proximity of the perinuclear area of LSEC (Braet et al., 2009). Some fenestrations form three dimensional multi-folded tunnels that are not always passing through the cell which contradicts the sieving role of LSEC. One possible explanation could be that these structures are caused by the cell isolation process because they have not been observed *in vivo* (in tissue samples). After digestion of the liver with Liberase/collagenase cells are detached from each other, perhaps disrupting parts of their cytoskeleton in a way that can be beyond repair after reattachment *in vitro*. Another explanation assumes that microfilament-disruption induces translocation of pre-existing three-dimensional organized fenestrae forming centers (FFCs) from the perinuclear area toward the peripheral cytoplasm (Braet et al., 1998, 2007). Recently, the formation of FFC was shown in live LSEC. It was confirmed that FFC are involved in the rapid increase in fenestration number, both in control and drug treated LSEC.

The importance of the actin cytoskeleton and the structure of FACR was confirmed by the dramatic effects of any agent directly affecting actin. Actin disruptors (see **Table 3** and **Figure 3**) were shown to rapidly induce the formation of new fenestrations (up to 300% porosity increase in 30 min by cytochalasin B) despite different mechanisms of actin depolymerization (Steffan et al., 1987; Zapotoczny et al., 2017b).

Other drugs that indirectly cause actin depolymerization, such as iodoacetic acid, metformin or sildenafil, also resulted in the increase in fenestration number (Hunt et al., 2019; Zapotoczny et al., 2019a). Altogether, agents acting on actin cytoskeleton remain the most important tools in studying fenestration structure and dynamics.

Understanding the mode of action of actin disturbing agents may help us reveal fenestration structure. Actin fibers are regulated by a set of proteins such as profilin, gelsolin, or cofilin that create the dynamic, out-of-equilibrium state. Every actin-binding protein, regardless of the location of its actin-binding site, influences the adenine nucleotide exchange rate of actin and the ratio of G (monomer/globular) and F (polymerized/filamentous) actin (**Figure 3**). Control over that process is maintained by many signaling pathways allowing LSEC to adjust the morphology according to internal and external stimuli. Actin disrupting agents act similarly to those controlling proteins. However, they lack control or feedback loop systems therefore result in rapid and dramatic changes. The importance of the controlled signaling is especially visible in prolonged *in vitro* LSEC culture where changes in cytoskeleton, such as stress fiber formation and fenestration disappearance, occur (Yokomori et al., 2004). However, the direct relationship between the actin polymerization into the thick stress fibers and the decrease in the number of fenestrations needs to be evaluated.

In fact, actin is the only demonstrated protein that was validated to have a direct impact on the number of fenestrations. Therefore, we discuss the various signaling pathways leading to actin and actin related proteins and the ways to affect them to observe the desired effect on fenestrations in the next section.

MLC Phosphorylation – The Core of the Fenestration's Regulation

Myosins convert ATP to create a mechanical force on actin. Created tension in actomyosin cytoskeleton is necessary for number of cellular processes, including cell motility, cytokinesis and intracellular trafficking (Brito and Sousa, 2020). The myosins contain a neck region allowing to bind myosin light chain (MLC) domains, which are regulated by the phosphorylation and dephosphorylation via MLCK and MLCP respectively. In its phosphorylated/active form, MLC results in activation of ATP dependent myosin heavy chain binding to f-actin, which creates an active contractile force. With 30 classes of molecular motors in myosin superfamily regulating variety of cellular processes (Brito and Sousa, 2020) several reports have been dedicated to the role of MLC in the regulation of fenestration diameters. In the following subsections we focused on the cellular machinery involved in the regulation of MLC phosphorylation via calcium, NO, and ROS pathways.

Lipid Rafts

The existence and role of lipid rafts has caused divisions in the scientific community in recent years and during The Keystone Symposium on Lipid Rafts and Cell Function (2006) the following definition was adopted: "Membrane rafts are small (10–200 nm), heterogeneous, highly dynamic, sterol- and sphingolipid-enriched domains that compartmentalize cellular processes. Small rafts can sometimes be stabilized to form larger platforms through protein-protein and protein–lipid interactions." The role of lipid rafts in fenestrations structure and dynamics was studied only recently (Svistounov et al., 2012) and then the hypothesis of sieve-raft regulation of fenestrations was proposed by Cogger et al. (2013). Visualization with SIM revealed that rafts are not present inside sieve plates but rather surround them in an inverse distribution (Svistounov et al., 2012). Fenestrations are formed in the flat, non-raft lipid-disordered regions and are prone to changes in raft organization. 7 keto cholesterol (7KC) increases lipid ordered, non-raft regions and thus promotes fenestration formation while detergent Triton X-100 increases the relative area of raft rich regions and decreases fenestration number (Svistounov et al., 2012; Hunt et al., 2018) (causing complete defenestration at high Triton X-100 concentrations). High doses of 7KC caused gap formation and retraction of cell membrane, which can be explained by deficits in cell membranes after depletion of rafts. Another detergent, poloxamer 407, was also reported to elicit massive defenestration of LSEC (Cogger et al., 2006). Interestingly, pre-treatment with Triton X-100 (increases rafts) abrogated the effect of cytochalasin D and no increase in porosity was observed (Svistounov et al., 2012). This result elucidates the tight connection between rafts and actin cytoskeleton in fenestration structure and/or dynamics. However, it was reported that the lipid rafts in biological membranes induced by detergents may not fully resemble the normal functional rafts (Heerklotz, 2002).

Rafts are enriched in sphingolipids and cholesterol which engenders membrane stability and provides a platform for many membrane proteins that may contribute to their connection to the actin cytoskeleton (Viola and Gupta, 2007). The anchoring of actin to the lipid rafts was suggested to be realized through the FERM domain of ERM proteins and talin (Chichili and Rodgers, 2009), as well as adducin (Yang et al., 2018) and spectrin (Ciana et al., 2011). Functional rafts may not be steady-state phenomena; they might form, grow, cluster or break up, shrink, and vanish according to functional requirements, regulated by rather subtle changes in the activity (disordering or ordering) of membrane compounds (Heerklotz, 2002). These properties might be connected with the dynamic nature of fenestrations and LSEC's ability to rapidly respond via morphology changes. The amount of lipid rafts may also have an indirect effect on fenestrations, through interactions independent of actin. It has been reported that ABC transporters, which decrease intracellular cGMP levels by its efflux, work less efficiently out of raft regions (Klappe et al., 2009). cGMP is an important signaling molecule that acts on fenestrations through PKG, decreasing intracellular calcium and promoting relaxation, both of which are connected with growing fenestration number. Lipid rafts may also affect many signal transduction pathways in the cell by serving as platforms to bring receptors into proximity with activating kinases, scaffolding proteins, and adaptor molecules that are constituent residents of lipid rafts (Rauch and Fackler, 2007).

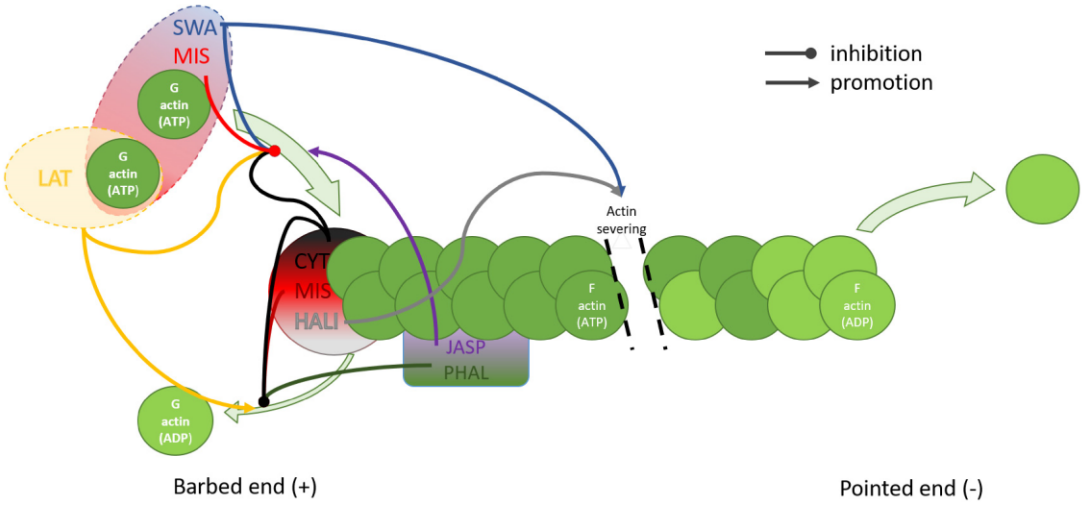

FIGURE 3 | Schematic representation of the effects of actin disrupting drugs on actin filaments. Depolymerization of the barbed end of the actin filament is inhibited by CYT, MIS, and HALI which cap the barbed end, and by PHAL and JASP which attach from the side, additionally stabilizing the fiber. Latrunculin promotes depolymerization by specific sequestration of monomeric actin. Polymerization is stimulated by JASP which also binds competitively to PHAL. Barbed end polymerization is inhibited by CYT, LAT, SWA, and MIS. Both MIS and SWA bind two actin monomers, however only MIS caps the barbed end. HALI and SWA stimulate severing of the actin filament. CYT, cytochalasin; HALI, halihondramide; JASP, jasplakinolide; LAT, latrunculin; MIS, misakinolide; PHAL, phalloidin; SWA, swinholide.

Spectrin

It was reported that only completely closed FACR structures contained fenestrations in the open state (Zapotoczny et al., 2019a). It was proposed that spectrin arranges actin to form a ring-like structure. Although the actin cytoskeleton is important part of fenestration structure, the membrane scaffold has a role in the regulation of opening of fenestration within FACR. In the spectrin-actin hypothesis, fenestrations can be opened if the cell height does not exceed 300–400 nm, which is double the length of the spectrin unit (Zapotoczny et al., 2019a). The proposed mechanism is based on the observation of both open and closed fenestrations within actin rings in live LSEC *in vitro*. The switch between the open and closed state was pharmacologically induced. The actin-spectrin complexes are strong enough to allow migration of the individual fenestrations across the cell membrane. Moreover, it can explain, why actin depolymerizing agents induce new fenestrations: spectrin can arrange short actin fibers to form ring like structures, and decreased cell height allows spectrin units to bind, forming new FACRs. In 2020, the role of actin/fodrin (non-erythroidal spectrin) was reported to be required in fenestration biogenesis in the endothelioma cell line bEND5, in which fenestrations can be induced pharmacologically (Ju et al., 2020). Authors showed a close association between beta actin and spectrin. Moreover, they reported that knockout of alpha spectrin resulted in 10-fold decrease in the number of fenestrations. Nevertheless, despite the increasing interest in this membrane cytoskeletal protein the knowledge of membrane skeleton regulation in endothelial cells is poorly understood.

Regulation *via* Ca^{2+}

The role of calcium in the regulation of fenestration diameters was discussed by Braet and Wisse (2002). The serotonin induced influx of calcium was described to cause calcium-calmodulin dependent phosphorylation of MLCK decreasing the size of fenestrae, denoted as contraction. The reverse effect remained as speculation. Later, Yokomori et al. (2004) summarized that calcium influx affected not only MLCK, but also Rho activity. Thus, calcium can affect both MLCK and ROCK dependent phosphorylation of MLC. The authors presented results of LPA and C3 transferase, causing fenestration closing and dilating respectively, indicating that they act through MLC phosphorylation. In the **Figure 4** we extended the possible regulation of MLC phosphorylation, based on the current state of knowledge. MLC is activated by the calcium mediated phosphorylation via myosin light chain kinase (MLCK) (Rigor et al., 2013). The activity of MLCK is increased by Ca^{2+}-calmodulin binding and by phosphorylation by protein kinase C (PKC). PKC can also further promote MLC phosphorylation by inhibition of MLCP, however, this pathway was not confirmed in endothelium (Somlyo and Somlyo, 2000). The activation of MLCK can be hampered by the cAMP dependent kinase – protein kinase A (PKA). PKA binds to the similar region of MLCK to the Ca^{2+}-calmodulin complex binding domain, hampering calcium dependent MLC phosphorylation. However, the activation of MLC is not sufficient to create a contractile force of the actomyosin complex. The actin binding proteins ensure additional control. Actin is stabilized by e.g., tropomyosin, tropomodulin, caldesmon, or calpain. The release of these proteins from actin is controlled in a calcium-concentration-dependent manner, allowing myosin to reach actin (Hepler, 2016). Moreover, the activation of actin polymerization processes, e.g., by gelsolin, profilin or cofilin is also calcium dependent and results in an increase in actin polymerization. The calcium level, regulated by calcium membrane channels and pumps or

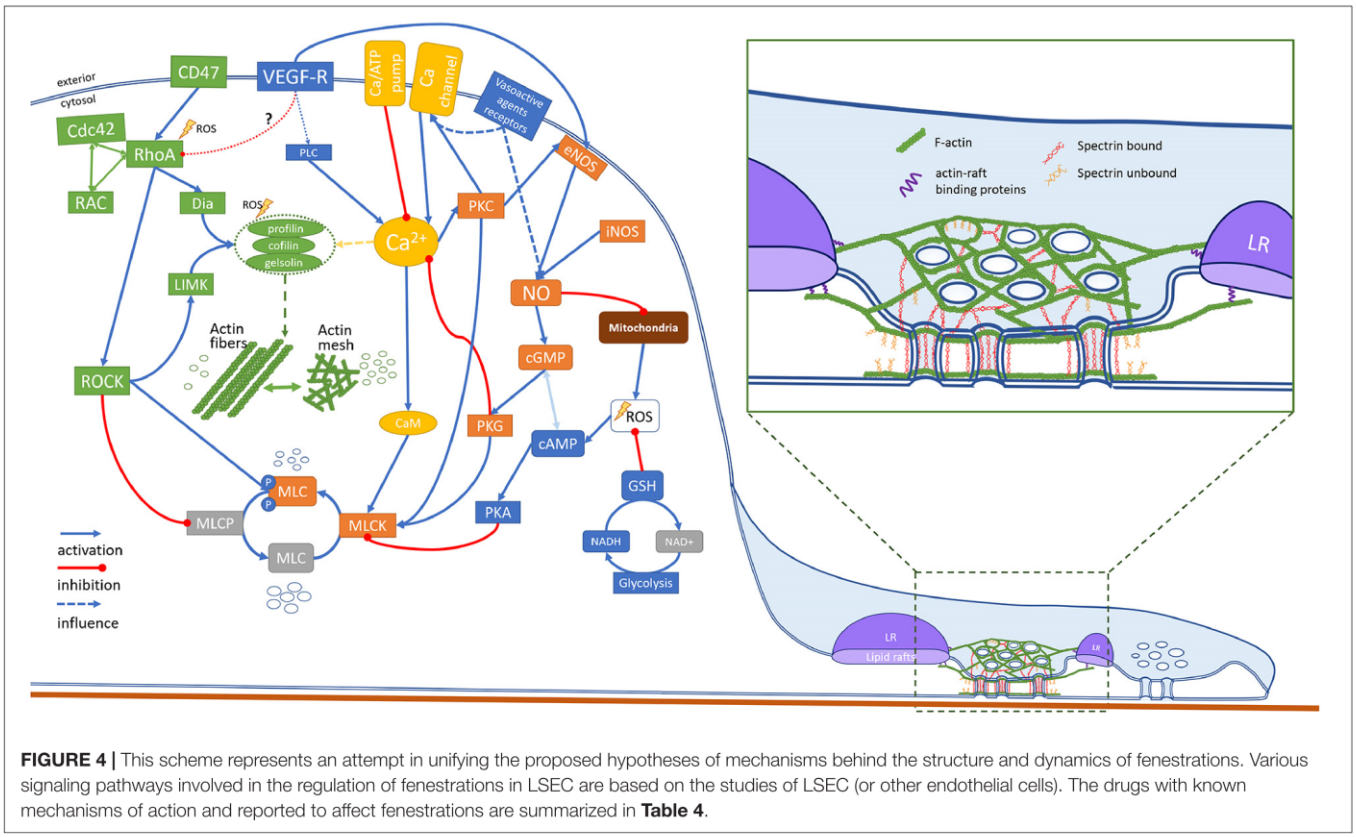

FIGURE 4 | This scheme represents an attempt in unifying the proposed hypotheses of mechanisms behind the structure and dynamics of fenestrations. Various signaling pathways involved in the regulation of fenestrations in LSEC are based on the studies of LSEC (or other endothelial cells). The drugs with known mechanisms of action and reported to affect fenestrations are summarized in **Table 4**.

by endoplasmic reticulum release, causes a cascade of cellular mechanisms driving local changes in the cytoskeleton. These changes vary in different cells and the details of these processes is beyond the scope of this review. The contraction of actomyosin is permanent. It means that it must be actively undone to ensure actomyosin relaxation. The balance of (de)phosphorylation of MLC is maintained by MLC phosphatase (MLCP). The enzyme activity is independent of the calcium plasma concentration (Álvarez-Santos et al., 2020). In addition to the role in the dephosphorylation of MLC, it exhibits phosphatase activity toward other proteins, such as ankyrin, adducin, Tau, merlin, calcineurin-A, interleukin-16, Rb, moezin, and ezrin (Kiss et al., 2019). Inhibition of MLCP (MYPT1 complex) by activation of the RhoA/ROCK pathway, results in indirect increase in the level of phosphorylated MLC and an increase in/of the contractile forces. PKA, PKG, and PKC also cause phosphorylation of MLCP. However, a recent study showed that in contrast to the RhoA/ROCK pathway, PKG- induced phosphorylation has no effect on MLCP activity (MacDonald and Walsh, 2018). It needs to be emphasized that the phosphorylation of MLC is connected to the formation of fibrous actin (via activation of actin nucleation proteins – e.g., gelsolin, profilin, cofilin, as mentioned) and vice versa. It was suggested that actin polymerization is necessary for force development (Mehta and Gunst, 1999). Therefore, the actin relaxation/contraction state is to some extent connected with the (de)polymerization of actin. The effects of certain drugs on fenestrations may be a sum of both.

Regulation *via* NO

Nitric oxide is one of the most important signaling molecules in endothelial cells and plays a crucial role in the maintenance of fenestrations in LSEC (DeLeve, 2015). NO stimulates sGC synthase and thus increases the cGMP level which then starts a cascade of signaling. cGMP stimulates the efflux of intracellular calcium into endoplasmic reticulum storage which reduces activation of MLCK through calmodulin. There are also suggestions that cGMP in microvascular endothelium can act through PKG to activate MLCP leading to further dephosphorylation of MLC (Rigor et al., 2013), but this mechanism was shown only in vascular smooth muscle cells. As described above, we propose that inactivation of MLCK together with a decrease in Ca^{2+} leads to actin relaxation, which results in the increase in fenestration diameter and/or number. There is also evidence of crosstalk between cGMP and cAMP levels which could further affect the MLC phosphorylation state (Chong et al., 2005). The exact mechanisms of action of NO on LSEC fenestration have not been described yet, however the cGMP/Ca pathway has been shown to be a part of VEGF induced NO production (Xie et al., 2012b; DeLeve, 2015). Two main sources of intracellular NO are synthases eNOS (activated among others by VEGF, endothelin, or estrogen) and iNOS (activated by cytokines during liver injuries). Both are responsible for LSEC phenotype maintenance as well as cell response to pathophysiological conditions (DeLeve et al., 2003b). The results of treatment with PMA — which activates PKC and can lead to increased NO production by eNOS — show a positive

TABLE 4 | Agents with known mechanism of action and their effects on LSEC fenestrations.

Inhibitor	Target	Effect	References
C3 transferase	RhoA	FN ↑, D ↑	Yokomori et al., 2004
Simvastatin	CD47	FN ↑, D ↑	Hunt et al., 2019
Y27635	ROCK	FN ↑	Venkatraman and Tucker-Kellogg, 2013
W7	Calmodulin	D ↑	Oda et al., 1993
7 keto cholesterol	Lipid rafts	FN ↑, D ↑	Svistounov et al., 2012
Amlodipine	Ca channel	FN ↑	Hunt et al., 2019
Promotor/activator	**Target**	**Effect**	**References**
LPA	RhoA	D↓	Yokomori et al., 2004
Sildenafil Amlodipine TRAIL	cGMP	FN↑	Hunt et al., 2019
Phorbol myristate	PKC	FN↓	de Zanger et al., 1997
Thrombospondin	CD47	Defenestration	Venkatraman and Tucker-Kellogg, 2013
Simvastatin	NO	FN ↑, D ↓	Venkatraman and Tucker-Kellogg, 2013; Hunt et al., 2019
Serotonin	Ca channel	D↓	Gatmaitan and Arias, 1993; Braet et al., 1995a

FN, fenestration number; D, fenestration diameter; ↑/↓, increase/decrease.

effect on maintenance of LSEC morphology *in vitro* (de Zanger et al., 1997). The effect was confirmed by co-administration of staurosporine, which inhibits PKC.

The effect of NO is complex and involves many different pathways. Besides cGMP signaling, NO can (competitively to O2) bind to complex IV in mitochondria, blocking the electron transport chain which results in an increased ROS production (Moncada and Erusalimsky, 2002). NO can then combine with ROS creating highly reactive peroxynitrate $ONOO^-$. NO production by NOS is calcium dependent but at the same time NO contributes to changes in intracellular calcium. Those mechanisms seem to work as a feedback loop gently steering the cell response, especially since NO is not a stable molecule so its influence is restricted to areas local to its synthesis. In LSEC, NO is required for fenestration maintenance. However, it is not sufficient alone, and other NO independent pathways are necessary. It has been shown that, besides NO production stimulated by VEGF, NO-independent VEGF signaling is needed also (Xie et al., 2012b). We propose two possible mechanisms: in endothelial cells VEGF can act through its membrane receptor on PLC, followed release of the Ca^{2+} from the endoplasmic reticulum (Rigor et al., 2013). Then, PKC enters a feedback loop of NO production leading to a decrease in Ca^{2+}. This would even further increase the NO production, but also would act as a balancing effect for calcium ions. NO can also induce protein *S*-nitrosilation, however it has been found not to affect fenestrations (Xie et al., 2012b). The other possibility is, reported in HUVEC, inhibition of Rho/ROCK pathway by VEGF receptors (Tagashira et al., 2018) which has been shown to play an important role in fenestration maintenance.

The cGMP pathway is a promising target for novel therapeutics for liver diseases and aging as restoration of cGMP levels can restore fenestrations in LSEC (Xie et al., 2012b). Drugs such as sildenafil influence cGMP by blocking its efflux by ABC transporters and degradation by phosphodiesterases (PDE) (Toque et al., 2008; Sager et al., 2012). Amlodipine, a blood pressure medication also affects fenestrations by acting through both cGMP and inhibition of Ca^{2+} channels (Berkels et al., 2004). Another drug used for lowering blood lipid levels – simvastatin, promotes NO production directly via the Akt pathway and through inhibition of Rho GTPases (de Sotomayor and Andriantsitohaina, 2001).

Regulation *via* ROS

There are many sources of ROS within the cell, such as the mitochondrial electron transport chain, NADPH and xanthine oxidase and, highly expressed in endothelium, eNOS when uncoupled (Widlansky and Gutterman, 2011; Jerkic and Letarte, 2015). ROS were initially considered mostly as cytotoxic, but recent reports summarize their positive regulatory roles both in physiological and pathological endothelium, reviewed in Widlansky and Gutterman (2011).

Recently the cytoprotective role of ROS through activation of autophagy signaling was shown in early ischemia injury (Bhogal et al., 2018). LSEC morphology is sensitive to ROS levels and many agents act through this mechanism, such as e.g., ethanol and acetaminophen causing the disappearance of fenestrations (Deaciuc et al., 1999). *In vivo* studies showed large gaps in LSEC caused by ROS, generated by xanthine oxidase and hypoxanthine suggesting destabilization of fenestrations which also prevent cells from closing those gaps (Deaciuc et al., 1999). Glutathione (GSH) is the main physiological countermeasure to free radicals such as ROS. Reducing agents such as NAC can reduce the depletion of GSH due to the presence of oxidative stress (Sun et al., 2014). The effect of ROS on fenestrations may come from different mechanisms based on the disturbance of the redox balance in the cell. Intracellularly, mitochondria are the main source of ROS while glycolysis is the main source of reducing agents such as GSH and NADH. Scavenging of ROS directly activates the Rho/ROCK signaling pathways (Popova et al., 2010) which may lead to promotion of stress fibers. By analogy, the reduction of ROS by antioxidants should lead to reduction of Rho/ROCK signaling, therefore promoting fenestration formation. This mechanism would explain the age-related defenestration associated with higher levels of ROS and reduced redox capabilities in the cells (Herrera et al., 2010).

In endothelial cells, ROS can act as a messenger molecule activating various signaling pathways. Besides the mitochondria, a second main ROS source are NAD(P)H oxidases which can be stimulated by various vasoactive agents (Griendling et al., 2000). It has been shown that LSEC morphology is sensitive to both vasodilators and vasoconstrictors, which was shown to increase and decrease the fenestration diameter respectively (**Table 2**). Moreover, LSEC lack underlying smooth muscles cells to emphasize the response to vasoconstrictors/dilators. There might exist more complicated cellular mechanisms in LSEC to compensate for this. Altogether, those findings suggest

that ROS may be part of signaling cascades activating redox-sensitive proteins.

CONCLUSION

Drug clearance mediated by the liver is heavily dependent on the proper phenotype of LSEC, including the transport through fenestrations. Individual drugs and stimulants have been reported to influence the porosity of LSEC. Some drugs show beneficial effects on LSEC phenotype, potentially allowing re-opening fenestration ("re-fenestration") which could be of benefit in the elderly. The role of LSEC senescence and "anti-aging" senolytic drugs, with regard to porosity, warrants further study. However, the background of polypharmacy (regular daily consumption of 4 or more medicines) in much of the elderly population needs to be considered in the refenestration context. Within this review we highlighted the areas of research which will be particularly beneficial for both physicians and researchers. LSEC research is growing in recent years and the latest stage of our knowledge about fenestrations is now facilitated with novel microscopic techniques. These super-resolution methods will continue to improve, so it is appropriate for the field to simultaneously improve sample status, for example to examine living LSEC, or "wet" fixed preparations of LSEC or whole liver mounts instead of dehydrated cells. The substrate upon which LSEC are typically cultured also likely needs to be re-worked – tissue culture plastic is considerably stiffer than the LSEC's natural surroundings, so other softer gel-based substrates should be considered, such as those described by Guixé-Muntet et al. (2020). Ultimately, *in vivo* imaging of LSEC fenestrations *in situ* would be the ideal real-time test of refenestration therapies, but the challenges (e.g., movement due breathing and heart beat) for this type of technology are rather significant. That said, existing technologies should allow for comprehensive studies and better understanding of these unique structures, and how they work, in the coming years.

AUTHOR CONTRIBUTIONS

KS, LK, and CH prepared the figures and tables. PM and BZ acquired the funding. All authors took part in conceptualization, analysis and writing of the manuscript, are responsible for all aspects of the manuscript and read and agreed to the submitted version of the manuscript.

FUNDING

This work received funding from the European Union's Horizon 2020 Research and Innovation Program under the Marie Skłodowska-Curie Grant Agreement No. 766181, project "DeLIVER," the Research Council of Norway Nano2021 program grant to "NanoChip" Grant No. 288565, and the Polish National Science Centre under the "SONATA 15" Project, Grant Agreement No.: UMO-2019/35/D/NZ3/01804.

ACKNOWLEDGMENTS

We would like to thank Professor Karen Kristine Sørensen from the University of Tromsø for sharing her SEM image of a liver sinusoid, and Mr. Eike Struck from University of Tromsø and Professor David Le Couteur from the ANZAC Research Institute in Sydney for the artwork in **Figure 2**. We would also like to thank Professor Bård Smedsrød from University of Tromsø for sharing his experience and knowledge about the history of LSEC.

REFERENCES

Alfaras, I., Mitchell, S. J., Mora, H., Lugo, D. R., Warren, A., Navas-Enamorado, I., et al. (2017). Health benefits of late-onset metformin treatment every other week in mice. *NPJ Aging Mechan. Dis.* 3:16. doi: 10.1038/s41514-017-0018-7

Álvarez-Santos, M. D., Álvarez-González, M., Estrada-Soto, S., and Bazán-Perkins, B. (2020). Regulation of myosin light-chain phosphatase activity to generate airway smooth muscle hypercontractility. *Front. Physiol.* 11:701. doi: 10.3389/fphys.2020.00701

Apte, R. S., Chen, D. S., and Ferrara, N. (2019). VEGF in signaling and disease: beyond discovery and development. *Cell* 176, 1248–1264. doi: 10.1016/j.cell.2019.01.021

Aronsen, L., Orvoll, E., Lysaa, R., Ravna, A. W., and Sager, G. (2014). Modulation of high affinity ATP-dependent cyclic nucleotide transporters by specific and non-specific cyclic nucleotide phosphodiesterase inhibitors. *Eur. J. Pharmacol.* 745, 249–253. doi: 10.1016/j.ejphar.2014.10.051

Asrani, S. K., Devarbhavi, H., Eaton, J., and Kamath, P. S. (2019). Burden of liver diseases in the world. *J. Hepatol.* 70, 151–171. doi: 10.1016/j.jhep.2018.09.014

Auvinen, K., Lokka, E., Mokkala, E., Jäppinen, N., Tyystjärvi, S., Saine, H., et al. (2019). Fenestral diaphragms and PLVAP associations in liver sinusoidal endothelial cells are developmentally regulated. *Sci. Rep.* 9:15698. doi: 10.1038/s41598-019-52068-x

Bacon, C. R., Cary, N., and Davenport, A. P. (1996). Endothelin peptide and receptors in human atherosclerotic coronary artery and aorta. *Circulation Res.* 79, 794–801. doi: 10.1161/01.RES.79.4.794

Bartolo, B. A. D., Cartland, S. P., Prado-Lourenco, L., Griffith, T. S., Gentile, C., Ravindran, J., et al. (2015). Tumor necrosis factor-related apoptosis-inducing ligand (TRAIL) promotes angiogenesis and ischemia-induced neovascularization via NADPH Oxidase 4 (NOX4) and Nitric Oxide-dependent mechanisms. *J. Am. Heart Assoc.* 4, 1–16. doi: 10.1161/JAHA.115.002527

Bender, A., and Beavo, J. A. (2006). Cyclic nucleotide phosphodiesterases: molecular regulation to clinical use. *Pharmacol. Rev.* 58, 488–520. doi: 10.1124/pr.58.3.5

Benowitz, N. L., and Burbank, A. (2016). Cardiovascular toxicity of nicotine: implications for electronic cigarette use neal. *Trends Cardiovasc. Med.* 26, 515–523. doi: 10.1016/j.tcm.2016.03.001

Berger, M., Gray, J. A., and Roth, B. L. (2009). The expanded biology of serotonin. *Annu. Rev. Med.* 60, 355–366. doi: 10.1146/annurev.med.60.042307.110802

Berkels, R., Taubert, D., Bartels, H., Breitenbach, T., Klaus, W., and Roesen, R. (2004). Amlodipine increases endothelial nitric oxide by dual mechanisms. *Pharmacology* 70, 39–45. doi: 10.1159/000074241

Bernier, M., Mitchell, S. J., Wahl, D., Diaz, A., Singh, A., Seo, W., et al. (2020). Disulfiram treatment normalizes body weight in obese mice. *Cell Metabolism* 32, 203.e4–214.e4. doi: 10.1016/j.cmet.2020.04.019

Bhandari, S., Li, R., Simón-Santamaría, J., McCourt, P., Johansen, S. D., Smedsrød, B., et al. (2020). Transcriptome and proteome profiling reveal complementary scavenger and immune features of rat liver sinusoidal endothelial cells and liver macrophages. *BMC Mol. Cell Biol.* 21:85. doi: 10.1186/s12860-020-00331-9

Bhogal, R. H., Weston, C. J., Velduis, S., Leuvenink, H. G. D., Reynolds, G. M., Davies, S., et al. (2018). The reactive oxygen species-mitophagy signalling

pathway regulates liver endothelial cell survival during Ischaemia/Reperfusion injury. *Liver Transplantation* 24, 1437–1452. doi: 10.1002/lt.25313

Blessing, W. W., and Seaman, B. (2003). 5-Hydroxytryptamine2A receptors regulate sympathetic nerves constricting the cutaneous vascular bed in rabbits and rats. *Neuroscience* 117, 939–948. doi: 10.1016/S0306-4522(02)00810-2

Bosma, E. K., Van Noorden, C. J. F., Schlingemann, R. O., and Klaassen, I. (2018). The role of plasmalemma vesicle-associated protein in pathological breakdown of blood-brain and blood-retinal barriers: potential novel therapeutic target for cerebral edema and diabetic macular edema. *Fluids Barriers CNS* 15:24. doi: 10.1186/s12987-018-0109-2

Braet, F. (2004). How molecular microscopy revealed new insights into the dynamics of hepatic endothelial fenestrae in the past decade. *Liver Int.* 24, 532–539. doi: 10.1111/j.1478-3231.2004.0974.x

Braet, F., De Zanger, R., Baekeland, M., Crabbé, E., Van Der Smissen, P., and Wisse, E. (1995a). Structure and dynamics of the fenestrae-associated cytoskeleton of rat liver sinusoidal endothelial cells. *Hepatology (Baltimore, Md.)* 21, 180–189.

Braet, F., De Zanger, R., Crabbe, E., and Wisse, E. (1995b). New observations on cytoskeleton and fenestrae in isolated rat-liver sinusoidal endothelial-cells. *J. Gastroenterol. Hepatol.* 10(Suppl. 1), S3–S7. doi: 10.1111/j.1440-1746.1995.tb01792.x

Braet, F., De Zanger, R., Jans, D., Spector, I., and Wisse, E. (1996a). Microfilament-disrupting agent latrunculin a induces an increased number of fenestrae in rat liver sinusoidal endothelial cells: comparison with cytochalasin B. *Hepatology* 24, 627–635. doi: 10.1053/jhep.1996.v24.pm0008781335

Braet, F., de Zanger, R., Sasaoki, T., Baekeland, M., Janssens, P., Smedsrød, B., et al. (1994). Assessment of a method of isolation, purification, and cultivation of rat liver sinusoidal endothelial cells. *Lab. Invest.* 70, 944–952.

Braet, F., de Zanger, R. B., Kalle, W., Raap, A. K., Tanke, H. J., and Wisse, E. (1996b). Comparative scanning, transmission and atomic force microscopy of the microtubular cytoskeleton in fenestrated liver endothelial cells. *Scanning Microscopy Suppl.* 10, 225–236.

Braet, F., de Zanger, R. B., Spector, I., and Wisse, E. (1997). The actin disrupting marine toxin latrunculin a induces an increased number of fenestrae in rat liver sinusoidal endothelial cells. *Kupffer Cell Foundation, Cells Hepatic Sinusoid* 6:82.

Braet, F., Kalle, W. H., De Zanger, R. B., De Grooth, B. G., Raap, A. K., Tanke, H. J., et al. (1996c). Comparative atomic force and scanning electron microscopy: an investigation on fenestrated endothelial cells in vitro. *J. Microscopy* 181(Pt 1), 10–17.

Braet, F., Muller, M., Vekemans, K., Wisse, E., and Le Couteur, D. G. (2003). Antimycin A-Induced defenestration in rat hepatic sinusoidal endothelial cells. *Hepatology* 38, 394–402. doi: 10.1053/jhep.2003.50347

Braet, F., Riches, J., Geerts, W., Jahn, K. A., Wisse, E., and Frederik, P. (2009). Three-dimensional organization of fenestrae labyrinths in liver sinusoidal endothelial cells. *Liver Int.* 29, 603–613. doi: 10.1111/j.1478-3231.2008.01836.x

Braet, F., Soon, L., Vekemans, K., Thordarson, P., and Spector, I. (2008). "Actin-Binding drugs: an elegant tool to dissect subcellular processes in endothelial and cancer cells," in *Actin-Binding Proteins and Disease. Protein Reviews*, Vol. 8, eds C. G. dos Remedios and D. Chhabra (New York, NY: Springer).

Braet, F., Spector, I., De Zanger, R., and Wisse, E. (1998). A novel structure involved in the formation of liver endothelial cell fenestrae revealed by using the actin inhibitor misakinolide. *Proc. Natl. Acad. Sci. U.S.A.* 95, 13635–13640. doi: 10.1073/pnas.95.23.13635

Braet, F., Spector, I., de Zanger, R. B., and Wisse, E. (1999). Fenestrae-Forming Center (FFC): a novel structure involved in the formation of liver sinusoidal endothelial cell fenestrae. *Kupffer Cell Foundation, Cells Hepatic Sinusoid.* 7:144.

Braet, F., Spector, I., Shochet, N., Crews, P., Higa, T., Menu, E., et al. (2002). The new anti-actin agent dihydrohalichondramide reveals fenestrae-forming centers in hepatic endothelial cells. *BMC Cell Biol.* 3:7. doi: 10.1186/1471-2121-3-7

Braet, F., and Wisse, E. (2002). Structural and functional aspects of liver sinusoidal endothelial cell fenestrae: a review. *Comparat. Hepatol.* 1:1. doi: 10.1186/1476-5926-1-1

Braet, F., and Wisse, E. (2012). AFM imaging of fenestrated liver sinusoidal endothelial cells. *Micron* 43, 1252–1258. doi: 10.1016/j.micron.2012.02.010

Braet, F., Wisse, E., Bomans, P., Frederik, P., Geerts, W., Koster, A., et al. (2007). Contribution of high-resolution correlative imaging techniques in the study of the liver sieve in three-dimensions. *Microscopy Res. Technique* 70, 230–242. doi: 10.1002/jemt.20408

Bravo, M., Raurell, I., Hide, D., Fernández-Iglesias, A., Gil, M., Barberá, A., et al. (2019). Restoration of liver sinusoidal cell phenotypes by statins improves portal hypertension and histology in rats with NASH. *Sci. Rep.* 9:20183. doi: 10.1038/s41598-019-56366-2

Brito, C., and Sousa, S. (2020). Non-muscle myosin 2A (NM2A): structure, regulation and function. *Cells* 9, 12–16. doi: 10.3390/cells9071590

Carpenter, B., Lin, Y., Stoll, S., Raffai, R. L., McCuskey, R., and Wang, R. (2005). VEGF is crucial for the hepatic vascular development required for lipoprotein uptake. *Development* 132, 3293–3303. doi: 10.1242/dev.01902

Charles, K., de Zanger, R. B., Van Bossuyt, H., Van Der Smissen, P., and Wisse, E. (1986). Influence of acute alcohol administration on endothelial fenestrae of rat livers: an invivo and in vitro scanning electron microscopic study. *Kupffer Cell Foundation, Cells Hepatic Sinusoid.* 1:497.

Cheluvappa, R., Jamieson, H. A., Hilmer, S. N., Muller, M., and Le Couteur, D. G. (2007). The effect of *pseudomonas aeruginosa* virulence factor, pyocyanin, on the liver sinusoidal endothelial cell. *J. Gastroenterol. Hepatol.* 22, 1350–1351. doi: 10.1111/j.1440-1746.2007.05016.x

Chen, K., Pittman, R. N., and Popel, A. S. (2008). Nitric oxide in the vasculature: where does it come from and where does it go? a quantitative perspective. *Antioxidants Redox Signal.* 10, 1185–1198. doi: 10.1089/ars.2007.1959

Chichili, G. R., and Rodgers, W. (2009). Cytoskeleton-membrane interactions in membrane raft structure. *Cell Mol. Life Sci.* 66, 2319–2328. doi: 10.1007/s00018-009-0022-6.Cytoskeleton-Membrane

Chong, T. J., Victorino, G. P., Schinco, M. A., and Coimbra, R. (2005). Cyclic nucleotide second messengers (CAMP and CGMP) play a central role in signal transduction and regulation of mesenteric postcapillary fluid leak. *J. Trauma - Injury, Infect. Crit. Care* 59, 302–307. doi: 10.1097/01.ta.0000180385.23675.98

Ciana, A., Achilli, C., Balduini, C., and Minetti, G. (2011). On the association of lipid rafts to the spectrin skeleton in human erythrocytes. *Biochim. Biophys. Acta - Biomembranes* 1808, 183–190. doi: 10.1016/j.bbamem.2010.08.019

Cluette-Brown, J., Mulligan, J., Doyle, K., Hagan, S., Osmolski, T., and Hojnacki, J. (1986). Oral nicotine induces an atherogenic lipoprotein profile. *Proc. Soc. Exp. Biol. Med.* 182, 409–413. doi: 10.3181/00379727-182-3-RC1

Cogger, V. C., Hilmer, S. N., Sullivan, D., Muller, M., Fraser, R., and Le Couteur, D. G. (2006). Hyperlipidemia and surfactants: the liver sieve is a link. *Atherosclerosis* 189, 273–281. doi: 10.1016/j.atherosclerosis.2005.12.025

Cogger, V. C., and Le Couteur, D. G. (2009). "Fenestrations in the liver sinusoidal endothelial cell," in *The Liver: Biology and Pathobiology*, 5th Edn, ed. I. M. Arias (Hoboken, NJ: Wiley Online Library), 389–406.

Cogger, V. C., McNerney, G. P., Nyunt, T., DeLeve, L. D., McCourt, P., Smedsrod, B., et al. (2010). Three-dimensional structured illumination microscopy of liver sinusoidal endothelial cell fenestrations. *J. Struct. Biol.* 171, 382–388. doi: 10.1016/j.jsb.2010.06.001

Cogger, V. C., Mitchell, S. J., Warren, A., De Cabo, R., and Le Couteur, D. G. (2014). Age-related loss of responsiveness to 2, 5-Dimethoxy-4-Iodoamphetamine in liver sinusoidal endothelial cells. *J. Gerontol. - Series A* 69, 514–518. doi: 10.1093/gerona/glt124

Cogger, V. C., Mross, P. E., Hosie, M. J., Ansselin, A. D., McLean, A. J., and Le Couteur, D. G. (2001). The effect of acute oxidative stress on the ultrastructure of the perfused rat liver. *Pharmacol. Toxicol.* 89, 306–311. doi: 10.1034/j.1600-0773.2001.d01-165.x

Cogger, V. C., Muller, M., Fraser, R., McLean, A. J., Khan, J., and Le Couteur, D. G. (2004). The effects of oxidative stress on the liver sieve. *J. Hepatol.* 41, 370–376. doi: 10.1016/j.jhep.2004.04.034

Cogger, V. C., O'Reilly, J. N., Warren, A., and Le Couteur, D. G. (2015). A standardized method for the analysis of liver sinusoidal endothelial cells and their fenestrations by scanning electron microscopy. *J. Visualized Exp.* 98:e52698. doi: 10.3791/52698

Cogger, V. C., Roessner, U., Warren, A., Fraser, R., and Le Couteur, D. G. (2013). A sieve-raft hypothesis for the regulation of endothelial fenestrations. *Computational Struct. Biotechnol. J.* 8, 1–9. doi: 10.5936/csbj.201308003

David, L., Mallet, C., Keramidas, M., Lamandé, N., Gasc, J. M., Dupuis-Girod, S., et al. (2008). Bone morphogenetic protein-9 is a circulating vascular quiescence factor. *Circulat. Res.* 102, 914–922. doi: 10.1161/CIRCRESAHA.107.165530

de Sotomayor, M. A., and Andriantsitohaina, R. (2001). Simvastatin and Ca2+ signaling in endothelial cells: involvement of Rho protein. *Biochem. Biophys. Res. Commun.* 280, 486–490. doi: 10.1006/bbrc.2000.4144

de Sotomayor, M. A., Pérez-Guerrero, C., Herrrera, M. D., Jimenez, L., Marín, R., Marhuenda, E., et al. (2005). Improvement of age-related endothelial dysfunction by simvastatin: effect on NO and COX pathways. *Br. J. Pharmacol.* 146, 1130–1138. doi: 10.1038/sj.bjp.0706420

de Zanger, R. B., Braet, F., Arnez Camacho, M. R., and Wisse, E. (1997). Prolongation of hepatic endothelial cell cultures by phorbol myristate acetate. *Kupffer Cell Foundation, Cells Hepatic Sinusoid.* 6:97.

Deaciuc, I. V., D'Souza, N. B., Sarphie, T. G., Schmidt, J., Hill, D. B., and McClain, C. J. (1999). Effects of exogenous superoxide anion and nitric oxide on the scavenging function and electron microscopic appearance of the sinusoidal endothelium in the isolated, perfused rat liver. *J. Hepatol.* 30, 213–221. doi: 10.1016/S0168-8278(99)80064-6

DeLeve, L. D. (2015). Liver sinusoidal endothelial cells in hepatic fibrosis. *Hepatology* 61, 1740–1746. doi: 10.1002/hep.27376

DeLeve, L. D., Ito, Y., Bethea, N. W., McCuskey, M. K., Wang, X., and McCuskey, R. S. (2003a). Embolization by sinusoidal lining cells obstructs the microcirculation in rat sinusoidal obstruction syndrome. *Am. J. Physiol. - Gastrointestinal Liver Physiol.* 284, 1045–1052. doi: 10.1152/ajpgi.00526.2002

DeLeve, L. D., and Maretti-Mira, A. C. (2017). Liver sinusoidal endothelial cell: an update. *Sem. Liver Dis.* 37, 377–387. doi: 10.1055/s-0037-1617455

DeLeve, L. D., McCuskey, R. S., Wang, X., Hu, L., McCuskey, M. K., Epstein, R. B., et al. (1999). Characterization of a reproducible rat model of hepatic veno-occlusive disease. *Hepatology* 29, 1779–1791. doi: 10.1002/hep.510290615

DeLeve, L. D., Wang, X., Kanel, G. C., Ito, Y., Bethea, N. W., McCuskey, M. K., et al. (2003b). Decreased hepatic nitric oxide production contributes to the development of rat sinusoidal obstruction syndrome. *Hepatology* 38, 900–908. doi: 10.1053/jhep.2003.50383

DeLeve, L. D., Wang, X., Kaplowitz, N., Shulman, H. M., Bart, J. A., and Van Der Hoek, A. (1997). Sinusoidal endothelial cells as a target for acetaminophen toxicity: direct action versus requirement for hepatocyte activation in different mouse strains. *Biochem. Pharmacol.* 53, 1339–1345. doi: 10.1016/S0006-2952(97)00048-8

Denninger, J. W., and Marletta, M. A. (1999). Guanylate cyclase and the .NO/CGMP signaling pathway. *Biochim. Biophys. Acta - Bioenerget.* 1411, 334–350. doi: 10.1016/S0005-2728(99)00024-9

Desroches-Castan, A., Tillet, E., Ricard, N., Ouarné, M., Mallet, C., Belmudes, L., et al. (2019a). Bone morphogenetic protein 9 is a paracrine factor controlling liver sinusoidal endothelial cell fenestration and protecting against hepatic fibrosis. *Hepatology* 70, 1392–1408. doi: 10.1002/hep.30655

Desroches-Castan, A., Tillet, E., Ricard, N., Ouarné, M., Mallet, C., Feige, J. J., et al. (2019b). Differential consequences of Bmp9 deletion on sinusoidal endothelial cell differentiation and liver fibrosis in 129/Ola and C57BL/6 Mice. *Cells* 8:1079. doi: 10.3390/cells8091079

Di Martino, J., Mascalchi, P., Legros, P., Lacomme, S., Gontier, E., Bioulac-Sage, P., et al. (2019). Actin depolymerization in dedifferentiated liver sinusoidal endothelial cells promotes fenestrae re-formation. *Hepatol. Commun.* 3, 213–219. doi: 10.1002/hep4.1301

Dobbs, B. R., Rogers, G. W. T., Xing, H. Y., and Fraser, R. (1994). Endotoxin-induced defenestration of the hepatic sinusoidal endothelium: a factor in the pathogenesis of cirrhosis? *Liver* 14, 230–233. doi: 10.1111/j.1600-0676.1994.tb00080.x

Elkadri, A., Thoeni, C., Deharvengt, S. J., Murchie, R., Guo, C., Stavropoulos, J. D., et al. (2015). Mutations in plasmalemma vesicle associated protein result in sieving protein-losing enteropathy characterized by hypoproteinemia, hypoalbuminemia, and hypertriglyceridemia. *Cellular Mol. Gastroenterol. Hepatol.* 1, 381–394. doi: 10.1016/j.jcmgh.2015.05.001

Fraser, R., Clark, S. A., Bowler, L. M., Murray, F. E. M., Wakasugi, J., Ishihara, M., et al. (1989). The opposite effects of nicotine and pantethine on the porosity of the liver sieve and lipoprotein metabolism. *Kupffer Cell Foundation, Cells Hepatic Sinusoid.* 2:335.

Fraser, R., Clark, S. A., Day, W. A., and Murray, F. E. (1988). Nicotine decreases the porosity of the rat liver sieve: a possible mechanism for hypercholesterolaemia. *Br. J. Exp. Pathol.* 69, 345–350.

Fraser, R., Cogger, V. C., Dobbs, B., Jamieson, H., Warren, A., Hilmer, S. N., et al. (2012). The liver sieve and atherosclerosis. *Pathology* 44, 181–186. doi: 10.1097/PAT.0b013e328351bcc8

Fraser, R., Dobbs, B. R., and Rogers, G. W. T. (1995a). Lipoproteins and the liver sieve: the role of the fenestrated sinusoidal endothelium in lipoprotein metabolism, atherosclerosis, and cirrhosis. *Hepatology* 21, 863–874. doi: 10.1016/0270-9139(95)90542-1

Fraser, R., Rogers, G. W. T., Bowler, L. M., Day, W. A., and Dobbs, B. R. (1991). Defenestration and vitamin a status in a rat model of cirrhosis. *Kupffer Cell Foundation, Cells Hepatic Sinusoid* 3:195.

Fraser, R., Rogers, G. W. T., Sutton, L. E., and Dobbs, B. R. (1995b). Single dose models of defenestration: tool to explore mechanisms, modulation and measurement of hepatic sinusoidal porosity. *Kupffer Cell Foundation, Cells Hepatic Sinusoid* 5:263.

Fredriksson, L., Li, H., and Eriksson, U. (2004). The PDGF family: four gene products form five dimeric isoforms. *Cytokine Growth Factor Rev.* 15, 197–204. doi: 10.1016/j.cytogfr.2004.03.007

Frenzel, H., Kremer, B., and Hucker, H. (1977). The liver sinusoids under various pathological conditions. A TEM and SEM study of rat liver after respiratory hypoxia, telecobalt-irradiation and endotoxin application. *Kupffer Other Liver Sinusoidal Cells* 213–222.

Fritzsche, M., Li, D., Colin-York, H., Chang, V. T., Moeendarbary, E., Felce, J. H., et al. (2017). Self-organizing actin patterns shape membrane architecture but not cell mechanics. *Nat. Commun.* 8:14347. doi: 10.1038/ncomms14347

Funyu, J., Mochida, S., Inao, M., Matsui, A., and Fujiwara, K. (2001). VEGF can act as vascular permeability factor in the hepatic sinusoids through upregulation of porosity of endothelial cells. *Biochem. Biophys. Res. Commun.* 280, 481–485. doi: 10.1006/bbrc.2000.4148

Furrer, K., Rickenbacher, A., Tian, Y., Jochum, W., Bittermann, A. G., Käch, A., et al. (2011). Serotonin reverts age-related capillarization and failure of regeneration in the liver through a VEGF-Dependent pathway. *Proc. Natl. Acad. Sci. U.S.A.* 108, 2945–2950. doi: 10.1073/pnas.1012531108

Gatmaitan, Z., and Arias, I. M. (1993). Hepatic endothelial cell fenestrae. *Kupffer Cell Foundation, Cells Hepatic Sinusoid* 4:3.

Gatmaitan, Z., Varticovski, L., Ling, L., Mikkelsen, R., Steffan, A. M., and Arias, I. M. (1996). Studies on fenestral contraction in rat liver endothelial cells in culture. *Am. J. Pathol.* 148, 2027–2041.

Gracia-Sancho, J., Caparrós, E., Fernández-Iglesias, A., and Francés, R. (2021). Role of liver sinusoidal endothelial cells in liver diseases. *Nat. Rev. Gastroenterol. Hepatol.* 18, 411–431. doi: 10.1038/s41575-020-00411-3

Griendling, K. K., Sorescu, D., Lassègue, B., and Ushio-Fukai, M. (2000). Modulation of protein kinase activity and gene expression by reactive oxygen species and their role in vascular physiology and pathophysiology. *Arteriosclerosis, Thrombosis, Vasc. Biol.* 20, 2175–2183. doi: 10.1161/01.ATV.20.10.2175

Grosse, L., Wagner, N., Emelyanov, A., Molina, C., Lacas-Gervais, S., Wagner, K. D., et al. (2020). Defined P16High senescent cell types are indispensable for mouse healthspan. *Cell Metabolism* 32, 87.e6–99.e6. doi: 10.1016/j.cmet.2020.05.002

Guixé-Muntet, S., Ortega-Ribera, M., Wang, C., Selicean, S., Andreu, I., Kechagia, J. Z., et al. (2020). Nuclear deformation mediates liver cell mechanosensing in cirrhosis. *JHEP Rep.* 2:100145. doi: 10.1016/j.jhepr.2020.100145

Hanchanale, V., and Eardley, I. (2014). Alprostadil for the treatment of impotence. *Exp. Opin. Pharmacother.* 15, 421–428. doi: 10.1517/14656566.2014.873789

Heerklotz, H. (2002). Triton promotes domain formation in lipid raft mixtures. *Biophys. J.* 83, 2693–2701. doi: 10.1016/S0006-3495(02)75278-8

Hepler, P. K. (2016). The cytoskeleton and its regulation by calcium and protons. *Plant Physiol.* 170, 3–22. doi: 10.1104/pp.15.01506

Herrera, M. D., Mingorance, C., Rodríguez-Rodríguez, R., and Alvarez de Sotomayor, M. (2010). Endothelial dysfunction and aging: an update. *Ageing Res. Rev.* 9, 142–152. doi: 10.1016/j.arr.2009.07.002

Herrnberger, L., Hennig, R., Kremer, W., Hellerbrand, C., Goepferich, A., Kalbitzer, H. R., et al. (2014). Formation of fenestrae in murine liver sinusoids depends on plasmalemma vesicle-associated protein and is required for lipoprotein passage. *PLoS One* 9:e115005. doi: 10.1371/journal.pone.0115005

Hide, D., Warren, A., Fernández-Iglesias, A., Maeso-Díaz, R., Peralta, C., Le Couteur, D. G., et al. (2020). Ischemia/Reperfusion injury in the aged liver: the

importance of the sinusoidal endothelium in developing therapeutic strategies for the elderly. *J. Gerontol. - Series A Biol. Sci. Med. Sci.* 75, 268–277. doi: 10.1093/gerona/glz012

Higashi, T., Friedman, S. L., and Hoshida, Y. (2017). Hepatic stellate cells as key target in liver fibrosis. *Adv. Drug Delivery Rev.* 121, 27–42. doi: 10.1016/j.addr.2017.05.007

Hilmer, S. N., Cogger, V. C., Fraser, R., McLean, A. J., Sullivan, D., and Le Couteur, D. G. (2005). Age-Related changes in the hepatic sinusoidal endothelium impede lipoprotein transfer in the rat. *Hepatology* 42, 1349–1354. doi: 10.1002/hep.20937

Hodgman, M., and Garrard, A. (2012). A review of acetaminophen poisoning. *Crit. Care Clin.* 28, 499–516.

Hojnacki, J., Mulligan, J., and Cluette-Brown, J. (1986). Oral nicotine impairs clearance of plasma low density lipoproteins. *Proc. Soc. Exp. Biol. Med.* 182, 414–418. doi: 10.3181/00379727-182-3-RC2

Holzer, P., Reichmann, F., and Farzi, A. (2012). Neuropeptide Y, Peptide YY and pancreatic polypeptide in the gut-brain axis. *Neuropeptides* 46, 261–274. doi: 10.1016/j.npep.2012.08.005

Horn, T., Christoffersen, P., and Henriksen, J. H. (1987). Alcoholic liver injury: defenestration in noncirrhotic livers-a scanning electron microscopic study. *Hepatology* 7, 77–82. doi: 10.1002/hep.1840070117

Hunt, N. J., Lockwood, G. P., Kang, S. W., Pulpitel, T., Clark, X., Mao, H., et al. (2020). The effects of metformin on age-related changes in the liver sinusoidal endothelial cell. *J. Gerontol. - Series A Biol. Sci. Med. Sci.* 75, 278–285. doi: 10.1093/gerona/glz153

Hunt, N. J., Lockwood, G. P., Warren, A., Mao, H., McCourt, P. A. G., Le Couteur, D. G., et al. (2019). Manipulating fenestrations in young and old liver sinusoidal endothelial cells. *Am. J. Phys. - Gastrointestinal Liver Physiol.* 316, G144–G154. doi: 10.1152/ajpgi.00179.2018

Hunt, N. J., McCourt, P. A. G., Le, D. G., and Cogger, V. C. (2018). Novel targets for delaying aging: the importance of the liver and advances in drug delivery. *Adv. Drug Delivery Rev.* 135, 39–49. doi: 10.1016/j.addr.2018.09.006

Imai, S., and Yoshino, J. (2013). The importance of NAMPT/NAD/SIRT1 in the systemic regulation of metabolism and ageing. *Diabetes, Obesity Metabolism* 15(Suppl. 3), 26–33. doi: 10.1111/dom.12171

Ito, Y., Abril, E. R., Bethea, N. W., McCuskey, M. K., Cover, C., Jaeschke, H., et al. (2006a). Mechanisms and pathophysiological implications of sinusoidal endothelial cell gap formation following treatment with Galactosamine/Endotoxin in mice. *Am. J. Physiol. - Gastrointestinal Liver Physiol.* 291, 211–218. doi: 10.1152/ajpgi.00312.2005

Ito, Y., Abril, E. R., Bethea, N. W., McCuskey, M. K., and McCuskey, R. S. (2006b). Dietary steatotic liver attenuates acetaminophen hepatotoxicity in mice. *Microcirculation* 13, 19–27. doi: 10.1080/10739680500383423

Ito, Y., Bethea, N. W., Abril, E. R., and McCuskey, R. S. (2003). Early hepatic microvascular injury in response to acetaminophen toxicity. *Microcirculation* 10, 391–400. doi: 10.1038/sj.mn.7800204

Iwasaki, M., Akiba, Y., and Kaunitz, J. D. (2019). Recent advances in vasoactive intestinal peptide physiology and pathophysiology: focus on the gastrointestinal system. *F1000Research* 8, 1–13. doi: 10.12688/f1000research.18039.1

Jerkic, M., and Letarte, M. (2015). Contribution of oxidative stress to endothelial dysfunction in hereditary hemorrhagic telangiectasia. *Front. Genet.* 5:34. doi: 10.3389/fgene.2015.00034

Ju, M., Ioannidou, S., and Munro, P. (2020). A Na,K-ATPase–Fodrin–Actin membrane cytoskeleton complex is required for endothelial fenestra biogenesis. *Cells* 9:1387. doi: 10.3390/cells9061387

Kalle, W. H. J., Braet, F., Raap, A. K., De Grooth, B. G., Tanket, H. J., and Wisse, E. (1997). Imaging of the membrane surface of sinusoidal rat liver endothelial cells by atomic force microscopy. *Kupffer Cell Foundation, Cells Hepatic Sinusoid* 6:94.

Kamegaya, Y., Oda, M., Yokomori, H., and Ishii, H. (2002). Role of endothelin receptors in endothelin-1-induced morphological changes of hepatic sinusoidal endothelial fenestrae: morphometric evaluation with scanning electron microscopy. *Hepatol. Res.* 22, 89–101. doi: 10.1016/S1386-6346(01)00147-4

Kapoor, K., Finer-Moore, J. S., Pedersen, B. P., Caboni, L., Waight, A., Hillig, R. C., et al. (2016). Mechanism of inhibition of human glucose transporter GLUT1 is conserved between cytochalasin B and Phenylalanine amides. *Proc. Natl. Acad. Sci. U.S.A.* 113, 4711–4716. doi: 10.1073/pnas.1603735113

Kaumann, A. J., and Levy, F. O. (2006). 5-Hydroxytryptamine receptors in the human cardiovascular system. *Pharmacol. Therapeutics* 111, 674–706. doi: 10.1016/j.pharmthera.2005.12.004

Kawanabe, Y., and Nauli, S. M. (2011). Endothelin. *Cellular Mol. Life Sci.* 68, 195–203. doi: 10.1007/s00018-010-0518-0

Kim, S. T., and Park, T. (2019). Acute and chronic effects of cocaine on cardiovascular health. *Int. J. Mol. Sci.* 20:584. doi: 10.3390/ijms20030584

Kim, W. K., Meliton, V., Kye, W. P., Hong, C., Tontonoz, P., Niewiadomski, P., et al. (2009). Negative regulation of hedgehog signaling by liver X receptors. *Mol. Endocrinol.* 23, 1532–1543. doi: 10.1210/me.2008-0453

Kirtland, S. J. (1988). Prostaglandin E1: a review. *Prostaglandins, Leukotrienes Essential Fatty Acids* 32, 165–174. doi: 10.1016/0952-3278(88)90168-8

Kiss, A., Erdődi, F., and Lontay, B. (2019). Myosin phosphatase: unexpected functions of a long-known enzyme. *Biochim. Biophys. Acta - Mol. Cell Res.* 1866, 2–15. doi: 10.1016/j.bbamcr.2018.07.023

Klappe, K., Hummel, I., Hoekstra, D., and Kok, J. W. (2009). "Lipid dependence of ABC transporter localization and function. *Chem. Phys. Lipids* 161, 57–64. doi: 10.1016/j.chemphyslip.2009.07.004

Kong, C., Bobe, S., Pilger, C., Lachetta, M., Øie, C. I., Kirschnick, N., et al. (2021). Multiscale and multimodal optical imaging of the ultrastructure of human liver biopsies. *Front. Physiol.* 12:637136. doi: 10.3389/fphys.2021.637136

Lapoint, J., Dargan, P. I., and Hoffman, R. S. (2013). "Chapter 7 - Synthetic amphetamine derivatives", in *Novel Psychoactive Substances* eds Paul I. Dargan and David M. Wood (Boston: Academic Press), 161–178. doi: 10.1016/B978-0-12-415816-0.00007-9

Le Couteur, D. G., Fraser, R., Cogger, V. C., and McLean, A. J. (2002). Hepatic pseudocapillarisation and atherosclerosis in ageing. *Lancet* 359, 1612–1615. doi: 10.1016/S0140-6736(02)08524-0

Le Couteur, D. G., Warren, A., Cogger, V. C., Smedsrød, B., Sørensen, K. K., De Cabo, R., et al. (2008). Old age and the hepatic sinusoid. *Anatomical Rec.* 291, 672–683. doi: 10.1002/ar.20661

Lesurtel, M., Graf, R., Aleil, B., Walther, D. J., Tian, Y., Jochum, W., et al. (2006). Platelet-derived serotonin mediates liver regeneration. *Science* 312, 104–107. doi: 10.1126/science.1123842

Leung, Y. Y., Hui, L. L. Y., and Kraus, V. B. (2015). Colchicine-update on mechanisms of action and therapeutic uses. *Semin. Arthritis Rheumatism* 45, 341–350.

Liu, D., Yovchev, M. I., Zhang, J., Alfieri, A. A., Tchaikovskaya, T., Laconi, E., et al. (2015). Identification and characterization of mesenchymal-epithelial progenitor-like cells in normal and injured rat liver. *Am. J. Pathol.* 185, 110–128. doi: 10.1016/j.ajpath.2014.08.029

MacDonald, J. A., and Walsh, M. P. (2018). Regulation of smooth muscle myosin light chain phosphatase by multisite phosphorylation of the myosin targeting subunit, MYPT1. *Cardiovasc. Hematol. Disord.-Drug Targets* 18, 4–13. doi: 10.2174/1871529x18666180326120638

Mak, K. M., and Lieber, C. S. (1984). Alterations in endothelial fenestrations in liver sinusoids of baboons fed alcohol: a scanning electron microscopic study. *Hepatology* 4, 386–391. doi: 10.1002/hep.1840040306

Mao, H., Diekmann, R., Liang, H. P. H., Cogger, V. C., Le Couteur, D. G., Lockwood, G. P., et al. (2019). Cost-efficient nanoscopy reveals nanoscale architecture of liver cells and platelets. *Nanophotonics* 8, 1299–1313. doi: 10.1515/nanoph-2019-0066

Maruthur, N. M., Tseng, E., Hutfless, S., Wilson, L. M., Suarez-Cuervo, C., Berger, Z., et al. (2016). Diabetes medications as monotherapy or metformin-based combination therapy for Type 2 diabetes: a systematic review and meta-analysis. *Ann. Int. Med.* 164, 740–751. doi: 10.7326/M15-2650

Maslak, E., Gregorius, A., and Chlopicki, S. (2015). Liver Sinusoidal Endothelial Cells (LSECs) function and NAFLD; NO-Based therapy targeted to the liver. *Pharmacol. Rep.* 67, 689–694. doi: 10.1016/j.pharep.2015.04.010

Mason, R. P., Jacob, R. F., Corbalan, J. J., Kaliszan, R., and Malinski, T. (2014). Amlodipine increased endothelial nitric oxide and decreased nitroxidative stress disproportionately to blood pressure changes. *Am. J. Hypertens.* 27, 482–488. doi: 10.1093/ajh/hpt202

Mateuszuk, L., Campagna, R., Kutryb-Zając, B., Kuś, K., Słominska, E. M., Smolenski, R. T., et al. (2020). Reversal of endothelial dysfunction by nicotinamide mononucleotide via extracellular conversion to nicotinamide

riboside. *Biochem. Pharmacol.* 178:114019. doi: 10.1016/j.bcp.2020.114019

McCuskey, R., and Reilly, F. (1993). Hepatic microvasculature: dynamic structure and its regulation. *Semin. Liver Dis.* 13, 1–12. doi: 10.1055/s-2007-1007333

McCuskey, R. S. (2006). Sinusoidal endothelial cells as an early target for hepatic toxicants. *Clin. Hemorheol. Microcirculation* 34, 5–10.

McCuskey, R. S., Bethea, N. W., Wong, J., McCuskey, M. K., Abril, E. R., Wang, X., et al. (2004). Ethanol binging exacerbates sinusoidal endothelial and parenchymal injury elicited by acetaminophen. *J. Hepatol.* 42, 371–377. doi: 10.1016/j.jhep.2004.11.033

McCuskey, R. S., Eguchi, H., Nishida, J., Krasovich, M. A., McDonell, D., Jolley, C. S., et al. (1993). Effects of ethanol and cocaine alone or in combination on the hepatic sinusoids of mice and rats. *Kupffer Cell Foundation, Cells Hepatic Sinusoid* 4:376.

Mehta, D., and Gunst, S. J. (1999). Actin polymerization stimulated by contractile activation regulates force development in canine tracheal smooth muscle. *J. Physiol.* 519, 829–840. doi: 10.1111/j.1469-7793.1999.0829n.x

Midão, L., Giardini, A., Menditto, E., Kardas, P., and Costa, E. (2018). Polypharmacy prevalence among older adults based on the survey of health, ageing and retirement in Europe. *Arch. Gerontol. Geriatrics* 78, 213–220. doi: 10.1016/j.archger.2018.06.018

Mills, K. F., Yoshida, S., Stein, L. R., Grozio, A., Kubota, S., Sasaki, Y., et al. (2016). Long-Term administration of nicotinamide mononucleotide mitigates age-associated physiological decline in mice. *Cell Metabolism* 24, 795–806. doi: 10.1016/j.cmet.2016.09.013

Mitchell, S. J., Huizer-Pajkos, A., Cogger, V. C., Mclachlan, A. J., Le Couteur, D. G., Jones, B., et al. (2011). Age-Related pseudocapillarization of the liver sinusoidal endothelium impairs the hepatic clearance of acetaminophen in rats. *J. Gerontol A Biol. Sci. Med. Sci.* 66, 400–408. doi: 10.1093/gerona/glq221

Mohamad, M., Mitchell, S. J., Wu, L. E., White, M. Y., Cordwell, S. J., Mach, J., et al. (2016). Ultrastructure of the liver microcirculation influences hepatic and systemic insulin activity and provides a mechanism for age-related insulin resistance. *Aging Cell* 15, 706–715. doi: 10.1111/acel.12481

Moncada, S., and Erusalimsky, J. D. (2002). Does nitric oxide modulate mitochondrial energy generation and apoptosis? *Nat. Rev. Mol. Cell Biol.* 3, 214–220. doi: 10.1038/nrm762

Mönkemöller, V., Øie, C., Hübner, W., Huser, T., and McCourt, P. (2015). Multimodal super-resolution optical microscopy visualizes the close connection between membrane and the cytoskeleton in liver sinusoidal endothelial cell fenestrations. *Sci. Rep.* 5:16279. doi: 10.1038/srep16279

Mori, T., Okanoue, T., Sawa, Y., Hori, N., Kanaoka, H., Itoh, Y., et al. (1993a). The change of sinusoidal endothelial cells in experimental liver cirrhosis - in vivo and in vitro study-. *Kupffer Cell Foundation, Cells Hepatic Sinusoid.* 4:280.

Mori, T., Okanoue, T., Sawa, Y., Hori, N., Ohta, M., and Kagawa, K. (1993b). Defenestration of the sinusoidal endothelial-cell in a rat model of cirrhosis. *Hepatology* 17, 891–897.

Namkoong, S., Lee, S. J., Kim, C. K., Kim, Y. M., Chung, H. T., Lee, H., et al. (2005). Prostaglandin E2 stimulates angiogenesis by activating the nitric Oxide/CGMP pathway in human umbilical vein endothelial cells. *Exp. Mol. Med.* 37, 588–600. doi: 10.1038/emm.2005.72

Oda, M., Azuma, T., Watanabe, N., Nishizaki, Y., Nishida, J., Ishii, K., et al. (1990). "Regulatory mechanism of hepatic microcirculation: involvement of the contraction and dilatation of sinusoids and sinusoidal endothelial fenestrae1," in *Proceeding of the Gastrointestinal Microcirculation. 9th Bodensee Symposium on Microcirculation, Bad Schachen/Konstanz, June/July 1989. Prog Appl Microcirc*, Vol. 17, eds K. Messmer and F. Hammersen (Basel: Karger), 103–128.

Oda, M., Kamegaya, Y., Yokomori, H., Han, J.-Y., Akiba, Y., Nakamura, M., et al. (1997). Roles of plasma membrane Ca2+-ATPase in the relaxation and contraction of hepatic sinusoidal endothelial fenestrae - effects of prostagrandin E1 and Endothelin1. *Kupffer Cell Foundation, Cells Hepatic Sinusoid* 6:313.

Oda, M., Kazemoto, S., Kaneko, H., Yokomori, H., Ishii, K., Tsukada, N., et al. (1993). Involvment of Ca2+-Calmodulin-Actomyosin system in contractility of hepatic sinusoidal endothelial fenestrae. *Kupffer Cell Foundation, Cells Hepatic Sinusoid* 4:174.

OECD/European Union (2020). *Health at a Glance: Europe 2020: State of Health in the EU Cycle*. Paris: OECD Publishing.

Owen, M. R., Doran, E., and Halestrap, A. P. (2000). Evidence that metformin exerts its anti-diabetic effects through inhibition of complex 1 of the mitochondrial respiratory chain. *Biochem. J.* 348(Pt 3), 607–614.

Pandey, E., Nour, A. S., and Harris, E. N. (2020). Prominent receptors of liver sinusoidal endothelial cells in liver homeostasis and disease. *Front. Physiol.* 11:873. doi: 10.3389/fphys.2020.00873

Poisson, J., Lemoinne, S., Boulanger, C., Durand, F., Moreau, R., Valla, D., et al. (2017). Liver sinusoidal endothelial cells: physiology and role in liver diseases. *J. Hepatol.* 66, 212–227. doi: 10.1016/j.jhep.2016.07.009

Popova, E. N., Pletjushkina, O. Y., Dugina, V. B., Domnina, L. V., Ivanova, O. Y., Izyumov, D. S., et al. (2010). Scavenging of reactive oxygen species in mitochondria induces myofibroblast differentiation. *Antioxidants Redox Signal.* 13, 1297–1307. doi: 10.1089/ars.2009.2949

Raines, S. M., Richards, O. C., Schneider, L. R., Schueler, K. L., Rabaglia, M. E., Oler, A. T., et al. (2011). Loss of PDGF-B activity increases hepatic vascular permeability and enhances insulin sensitivity. *Am. J. Physiol. - Endocrinol. Metabolism* 301, 517–526. doi: 10.1152/ajpendo.00241.2011

Rauch, S., and Fackler, O. T. (2007). Viruses, lipid rafts and signal transduction. *Signal Transduction* 7, 53–63. doi: 10.1002/sita.200600113

Reilly, F. D., Dimlich, R. V. W., Cilento, E. V., and McCuskey, R. S. (1982). Hepatic microvascular regulatory mechanisms. II. Cholinergic mechanisms. *Hepatology* 2, 230S–235S. doi: 10.1002/hep.1840020207

Rigor, R. R., Shen, Q., Pivetti, C. D., Wu, M. H., and Yuan, S. Y. (2013). Myosin light chain kinase signaling in endothelial barrier dysfunction. *Med. Res. Rev.* 33, 911–933. doi: 10.1002/med.21270

Rikitake, Y., and Liao, J. K. (2005). Rho GTPases, statins, and nitric oxide. *Circulat. Res.* 97, 1232–1235. doi: 10.1161/01.RES.0000196564.18314.23

Robbins, P. D., Jurk, D., Khosla, S., Kirkland, J. L., Lebrasseur, N. K., Miller, J. D., et al. (2021). Senolytic drugs: reducing senescent cell viability to extend health span. *Annu. Rev. Pharmacol. Toxicol.* 61, 779–803. doi: 10.1146/annurev-pharmtox-050120-105018

Roberts, W. G., and Palade, G. E. (1995). Increased microvascular permeability and endothelial fenestration induced by vascular endothelial growth factor. *J. Cell Sci.* 108, 2369–2379.

Rogers, G. W. T., Dobbs, B. R., and Fraser, R. (1992). Decreased hepatic uptake of cholesterol and retinol in the dimethylnitrosamine rat model of cirrhosis. *Liver* 12, 326–329. doi: 10.1111/j.1600-0676.1992.tb00581.x

Ruffolo, R. R., and Hieble, J. P. (1994). α-Adrenoceptors. *Pharmacol. Therapeutics* 61, 1–64. doi: 10.1016/0163-7258(94)90058-2

Rumberger, J. A., Napolitano, J., Azumano, I., Kamiya, T., and Evans, M. (2011). Pantethine, a derivative of vitamin B5 used as a nutritional supplement, favorably alters low-density lipoprotein cholesterol metabolism in low- to moderate-cardiovascular risk north American subjects: a triple-blinded placebo and diet-controlled investigation. *Nutr. Res.* 31, 608–615. doi: 10.1016/j.nutres.2011.08.001

Sager, G., Ørvoll, E. O., Lysaa, R. A., Kufareva, I., Abagyan, R., and Ravna, A. W. (2012). Novel CGMP efflux inhibitors identified by virtual ligand screening (VLS) and confirmed by experimental studies. *J. Med. Chem.* 55, 3049–3057. doi: 10.1021/jm2014666

Sakai, K. (1980). Coronary vasoconstriction by locally administered acetylcholine, carbachol and bethanechol in isolated, donor-perfused, rat hearts. *Br. J. Pharmacol.* 68, 625–632. doi: 10.1111/j.1476-5381.1980.tb10853.x

Sasaoki, T., Braet, F., de Zanger, R. B., Wisse, E., and Arii, S. (1995). The effect of endotoxin on liver sinusoidal endothelial cells. *Kupffer Cell Foundation, Cells Hepatic Sinusoid* 5:366.

Schreck, R., Meier, B., Mannel, D. N., Droge, W., and Baeuerle, P. A. (1992). Dithiocarbamates as potent inhibitors of nuclear factor Kb activation in intact cells. *J. Exp. Med.* 175, 1181–1194. doi: 10.1084/jem.175.5.1181

Shetty, S., Lalor, P. F., and Adams, D. H. (2018). Liver sinusoidal endothelial cells — gatekeepers of hepatic immunity. *Nat. Rev. Gastroenterol. Hepatol.* 15, 555–567. doi: 10.1038/s41575-018-0020-y

Shu, X., Li, N., Wu, Y., Li, W., Zhang, X., Li, P., et al. (2021). Mechanotransduction of liver sinusoidal endothelial cells under varied mechanical stimuli. *Acta Mechanica Sinica* 37, 201–217. doi: 10.1007/s10409-021-01057-3

Singh, Y., and Mikrou, P. (2018). Use of prostaglandins in duct-dependent congenital heart conditions. *Arch. Dis. Childhood: Educ. Practice Edn.* 103, 137–140. doi: 10.1136/archdischild-2017-313654

Somlyo, A. P., and Somlyo, A. V. (2000). Signal transduction by G-Proteins, Rho-Kinase and protein phosphatase to smooth muscle and non-muscle myosin II. *J. Physiol.* 522, 177–185. doi: 10.1111/j.1469-7793.2000.t01-2-00177.x

Sørensen, K. K., McCourt, P., Berg, T., Crossley, C., Le Couteur, D., Wake, K., et al. (2012). The scavenger endothelial cell: a new player in homeostasis and immunity. *Am. J. Physiol. - Regulat. Integrat. Comparat. Physiol.* 303, R1217–R1230. doi: 10.1152/ajpregu.00686.2011

Sørensen, K. K., Simon-Santamaria, J., McCuskey, R. S., and Smedsrød, B. (2015). Liver sinusoidal endothelial cells. *Comprehensive Physiol.* 5, 1751–1774. doi: 10.1002/cphy.c140078

Spector, I., Braet, F., Shochet, N. R., and Bubb, M. R. (1999). New anti-actin drugs in the study of the organization and function of the actin cytoskeleton. *Microscopy Res. Technique* 47, 18–37. doi: 10.1002/(SICI)1097-0029(19991001)47:1<18::AID-JEMT3>3.0.CO;2-E

Steffan, A. M., Gendrault, J. L., and Kirn, A. (1986). Phagocytosis and surface modulation of fenestrated areas - two properties of murine endothelial liver cells (EC) involving microfilaments. *Kupffer Cell Foundation, Cells Hepatic Sinusoid* 1:483.

Steffan, A. M., Gendrault, J. L., and Kirn, A. (1987). Increase in the number of fenestrae in mouse endothelial liver cells by altering the cytoskeleton with cytochalasin B. *Hepatology* 7, 1230–1238. doi: 10.1002/hep.1840070610

Straub, A. C., Clark, K. A., Ross, M. A., Chandra, A. G., Li, S., Gao, X., et al. (2008). Arsenic-Stimulated liver sinusoidal capillarization in mice requires NADPH oxidase-generated superoxide. *J. Clin. Investigat.* 118, 3980–3989. doi: 10.1172/JCI35092

Suh, J. J., Pettinati, H. M., Kampman, K. M., and O'Brien, C. P. (2006). The status of Disulfiram: a half of a century later. *J. Clin. Psychopharmacol.* 26, 290–302. doi: 10.1097/01.jcp.0000222512.25649.08

Sun, Y., Pu, L.-Y., Lu, L., Wang, X.-H., Zhang, F., and Rao, J.-H. (2014). N-Acetylcysteine attenuates reactive-oxygen-species- mediated endoplasmic reticulum stress during liver ischemia-reperfusion injury. *World J. Gastroenterol.* 20, 15289–15298. doi: 10.3748/wjg.v20.i41.15289

Svistounov, D., Warren, A., McNerney, G. P., Owen, D. M., Zencak, D., Zykova, S. N., et al. (2012). The relationship between fenestrations, sieve plates and rafts in liver sinusoidal endothelial cells. *PLoS One* 7:e46134. doi: 10.1371/journal.pone.0046134

Szafranska, K., Holte, C. F., Kruse, L. D., Mao, H., Øie, C. I., Szymonski, M., et al. (2021). Quantitative analysis methods for studying fenestrations in liver sinusoidal endothelial cells. A comparative study. *Micron* doi: 10.1016/j.micron.2021.103121

Tagashira, T., Fukuda, T., Miyata, M., Nakamura, K., Fujita, H., Takai, Y., et al. (2018). Afadin facilitates vascular endothelial growth factor-induced network formation and migration of vascular endothelial cells by inactivating Rho-Associated kinase through ARHGAP29. *Arteriosclerosis, Thrombosis, Vasc. Biol.* 38, 1159–1169. doi: 10.1161/ATVBAHA.118.310991

Takashimizu, S., Watanabe, N., Nishizaki, Y., Kawazoe, K., and Matsuzaki, S. (1999). Mechanisms of hepatic microcirculatory disturbances induced by acute ethanol administration in rats, with special reference to alterations of sinusoidal endothelial fenestrae. *Alcohol.: Clin. Exp. Res.* 23(Suppl. 4), 39S–46S. doi: 10.1111/j.1530-0277.1999.tb04532.x

Tamba-Lebbie, B., Rogers, G. W. T., Dobbs, B. R., and Fraser, R. (1993). Defenestration of the hepatic sinusoidal endothelium in the dimethylnitrosamine fed rat: is this process reversible? *Kupffer Cell Foundation, Cells Hepatic Sinusoid* 4:179.

Tanikawa, K., Noguchi, K., and Sata, M. (1991). Ultrastructural features of kupffer cells and sinusoidal endothelial cells in chronic ethanol-fed rats. *Kupffer Cell Foundation, Cells Hepatic Sinusoid* 3:445.

Tian, Y., Graf, R., El-Badry, A. M., Lesurtel, M., Furrer, K., Moritz, W., et al. (2011). Activation of serotonin Receptor-2B rescues small-for-size liver graft failure in mice. *Hepatology* 53, 253–262. doi: 10.1002/hep.23960

Toque, H. A., Teixeira, C. E., Priviero, F. B. M., Morganti, R. P., Antunes, E., and De Nucci, G. (2008). Vardenafil, but not sildenafil or tadalafil, has calcium-channel blocking activity in rabbit isolated pulmonary artery and human washed platelets. *Br. J. Pharmacol.* 154, 787–796. doi: 10.1038/bjp.2008.141

Tsukada, N., Oda, M., Yonei, Y., Honda, K., Aikawa, Y., Kiryu, Y., et al. (1986). Alterations of the hepatic sinusoidal endothelial fenestrae in response to vasoactive substances in the rat -in vivo and in vitro studies-. *Kupffer Cell Foundation, Cells Hepatic Sinusoid* 1:515.

Umetsu, Y., Tenno, T., Goda, N., Shirakawa, M., Ikegami, T., and Hiroaki, H. (2011). Structural difference of vasoactive intestinal peptide in two distinct membrane-mimicking environments. *Biochim. Biophys. Acta - Proteins Proteomics* 1814, 724–730. doi: 10.1016/j.bbapap.2011.03.009

Van Der Smissen, P., Van Bossuyt, H., Charles, K., and Wisse, E. (1986). The structure and function of the cytoskeleton in sinusoidal endothelial cells in the rat liver. *Kupffer Cell Foundation, Cells Hepatic Sinusoid* 1:517.

Venkatraman, L., and Tucker-Kellogg, L. (2013). The CD47-Binding peptide of thrombospondin-1 induces defenestration of liver sinusoidal endothelial cells. *Liver Int.* 33, 1386–1397. doi: 10.1111/liv.12231

Viola, A., and Gupta, N. (2007). Tether and trap: regulation of membrane-raft dynamics by actin-binding proteins. *Nat. Rev. Immunol.* 7, 889–896. doi: 10.1038/nri2193

Wachter, S. B., and Gilbert, E. M. (2012). Beta-Adrenergic receptors, from their discovery and characterization through their manipulation to beneficial clinical application. *Cardiology (Switzerland)* 122, 104–112. doi: 10.1159/000339271

Walker, R. M., Racz, W. J., and McElligott, T. F. (1983). Scanning electron microscopic examination of acetaminophen-induced hepatotoxicity and congestion in mice. *Am. J. Pathol.* 113, 321–330.

Wang, X.-K., and Peng, Z.-G. (2021). Targeting liver sinusoidal endothelial cells: an attractive therapeutic strategy to control inflammation in nonalcoholic fatty liver disease. *Front. Pharmacol.* 12:655557. doi: 10.3389/fphar.2021.655557

Warren, A., Cogger, V. C., Fraser, R., Deleve, L. D., McCuskey, R. S., and Le Couteur, D. G. (2011). The effects of old age on hepatic stellate cells. *Curr. Gerontol. Geriatrics Res.* 2011, 1–8. doi: 10.1155/2011/439835

Watanabe, N., Takashimizu, S., Nishizaki, Y., Kojima, S., Kagawa, T., and Matsuzaki, S. (2007). An endothelin a receptor antagonist induces dilatation of sinusoidal endothelial fenestrae: implications for endothelin-1 in hepatic microcirculation. *J. Gastroenterol.* 42, 775–782. doi: 10.1007/s00535-007-2093-1

Weaver, B. A. (2014). How Taxol/Paclitaxel kills cancer cells. *Mol. Biol. Cell* 25, 2677–2681. doi: 10.1091/mbc.E14-04-0916

Webb, R. C. (2003). Smooth muscle contraction and relaxation. *Am. J. Physiol. - Adv. Physiol. Educ.* 27, 201–206. doi: 10.1152/advan.00025.2003

White, J. D. (1993). Neuropeptide Y: a central regulator of energy homeostasis. *Regulat. Peptides* 49, 93–107. doi: 10.1016/0167-0115(93)90431-7

Widlansky, M. E., and Gutterman, D. D. (2011). Regulation of endothelial function by mitochondrial reactive oxygen species. *Antioxidants Redox Signal.* 15, 1517–1530. doi: 10.1089/ars.2010.3642

Wiley, S. R., Schooley, K., Smolak, P. J., Din, W. S., Huang, C. P., Nicholl, J. K., et al. (1995). Identification and characterization of a new member of the TNF family that induces apoptosis. *Immunity* 3, 673–682. doi: 10.1016/1074-7613(95)90057-8

Wilkinson, A. L., Qurashi, M., and Shetty, S. (2020). The role of sinusoidal endothelial cells in the axis of inflammation and cancer within the liver. *Front. Physiol.* 11:990. doi: 10.3389/fphys.2020.00990

Willy, P. J., Umesono, K., Ong, E. S., Evans, R. M., Heyman, R. A., and Mangelsdorf, D. J. (1995). LXR, a nuclear receptor that defines a distinct retinoid response pathway. *Genes Dev.* 9, 1033–1045. doi: 10.1101/gad.9.9.1033

Wisse, E. (1970). An electron microscopic study of the fenestrated endothelial lining of rat liver sinusoids. *J. Ultrasruct. Res.* 31, 125–150. doi: 10.1016/S0022-5320(70)90150-4

Wisse, E., Braet, F., Duimel, H., Vreuls, C., Koek, G., Damink, S. W. M. O., et al. (2010). Fixation methods for electron microscopy of human and other liver. *World J. Gastroenterol.* 16, 2851–2866. doi: 10.3748/wjg.v16.i23.2851

Wisse, E., Van Dierendonck, J. H., De Zanger, R. B., Fraser, R., and McCuskey, R. S. (1980). "On the role of the liver endothelial filter in the transport of particulate fat (Chylomicrons and Their Remnants) to parenchymal cells and the influence of certain hormones on the endothelial fenestrae," in *Proceeding of the Conference: Communications of Liver Cells*, eds H. Popper, L. Bianchi, F. Gudat, and W. Reutter (Lancaster: MTP Press Ltd), 195–200.

Xie, G., Choi, S. S., Syn, W.-K., Michelotti, G. A., Swiderska-Syn, M., Karaca, G., et al. (2012a). Hedgehog signaling regulates liver sinusoidal endothelial cell capillarisation. *Hepatol. Gut* 62, 299–309. doi: 10.1136/gutjnl-2011-301494

Xie, G., Wang, X., Wang, L., Wang, L., Atkinson, R. D., Kanel, G. C., et al. (2012b). Role of differentiation of liver sinusoidal endothelial cells in progression and

regression of hepatic fibrosis in rats. *Gastroenterology* 142, 918.e6–927.e6. doi: 10.1053/j.gastro.2011.12.017

Xing, Y., Zhao, T., Gao, X., and Wu, Y. (2016). Liver X receptor α is essential for the capillarization of liver sinusoidal endothelial cells in liver injury. *Sci. Rep.* 6:21309. doi: 10.1038/srep21309

Xu, B., Xiao-hong, L., Lin, G., Queen, L., and Ferro, A. (2002). Amlodipine, but not verapamil or nifedipine, dilates rabbit femoral artery largely through a nitric oxide- and kinin-dependent mechanism. *Br. J. Pharmacol.* 136, 375–382. doi: 10.1038/sj.bjp.0704753

Yamagishi, M. (1959). Electron microscope studies on the fine structure of the sinusoidal wall and fat-storing cells of rabbit livers. *Arch. Histol. Jpn.* 18, 223–261. doi: 10.1679/aohc1950.18.223

Yang, C., Sui, Z., Xu, T., Liu, W., Wang, X., and Zeng, X. (2018). Lipid raft-associated ß-Adducin participates in neutrophil migration. *Mol. Med. Rep.* 18, 1353–1360. doi: 10.3892/mmr.2018.9113

Yang, M., and Zhang, C. (2021). The role of liver sinusoidal endothelial cells in cancer liver metastasis ming. *Am. J. Cancer Res.* 11, 1845–1860.

Yokomori, H., Oda, M., Yoshimura, K., Nagai, T., Ogi, M., Nomura, M., et al. (2003). Vascular endothelial growth factor increases fenestral permeability in hepatic sinusoidal endothelial cells. *Liver Int.* 23, 467–475. doi: 10.1111/j.1478-3231.2003.00880.x

Yokomori, H., Yoshimura, K., Funakoshi, F., Nagai, T., Fujimaki, K., Nomura, M., et al. (2004). Rho modulates hepatic sinusoidal endothelial fenestrae via regulation of the actin cytoskeleton in rat endothelial cells. *Lab. Investigat.* 84, 857–864. doi: 10.1038/labinvest.3700114

Yokomori, H., Yoshimura, K., Ohshima, S., Nagai, T., Fujimaki, K., Nomura, M., et al. (2006). The Endothelin-1 receptor-mediated pathway is not involved in the endothelin-1-induced defenestration of liver sinusoidal endothelial cells. *Liver Int.* 26, 1268–1276. doi: 10.1111/j.1478-3231.2006.01365.x

Zapotoczny, B., Braet, F., Kus, E., Ginda-Mäkelä, K., Klejevskaja, B., Campagna, R., et al. (2019a). Actin-spectrin scaffold supports open fenestrae in liver sinusoidal endothelial cells. *Traffic* 20, 932–942. doi: 10.1111/tra.12700

Zapotoczny, B., Braet, F., Wisse, E., Lekka, M., and Szymonski, M. (2020). Biophysical nanocharacterization of liver sinusoidal endothelial cells through atomic force microscopy. *Biophys. Rev.* 12, 625–636. doi: 10.1007/s12551-020-00699-0

Zapotoczny, B., Szafranska, K., Kus, E., Braet, F., Wisse, E., Chlopicki, S., et al. (2019b). Tracking fenestrae dynamics in live murine liver sinusoidal endothelial cells. *Hepatology* 69, 876–888. doi: 10.1002/hep.30232

Zapotoczny, B., Szafranska, K., Kus, E., Chlopicki, S., and Szymonski, M. (2017a). Quantification of fenestrations in liver sinusoidal endothelial cells by atomic force microscopy. *Micron* 101, 48–53. doi: 10.1016/j.micron.2017.06.005

Zapotoczny, B., Szafranska, K., Owczarczyk, K., Kus, E., Chlopicki, S., and Szymonski, M. (2017b). Atomic force microscopy reveals the dynamic morphology of fenestrations in live liver sinusoidal endothelial cells. *Sci. Rep.* 7:7994. doi: 10.1038/s41598-017-08555-0

Zhang, J. X., Pegoli, W., and Clemens, M. G. (1994). Endothelin-1 induces direct constriction of hepatic sinusoids. *Am. J. Physiol. - Gastrointestinal Liver Physiol.* 266, 624–632. doi: 10.1152/ajpgi.1994.266.4.g624

Conflict of Interest: The authors declare that the research was conducted in the absence of any commercial or financial relationships that could be construed as a potential conflict of interest.

Publisher's Note: All claims expressed in this article are solely those of the authors and do not necessarily represent those of their affiliated organizations, or those of the publisher, the editors and the reviewers. Any product that may be evaluated in this article, or claim that may be made by its manufacturer, is not guaranteed or endorsed by the publisher.

Paper II

From fixed-dried to wet-fixed to live – comparative super-resolution microscopy of liver sinusoidal endothelial cell fenestrations

Szafranska K., Neuman T., Baster Z., Rajfur Z., Szelest O., Holte C., Kubisiak A., Kus E., Wolfson D.L., Chlopicki S., Ahluwalia B.S., Lekka M., Szymonski M., McCourt P., Zapotoczny B.

Nanophotonics
2022
https://doi.org/10.1515/nanoph-2021-0818

Research Article

Karolina Szafranska, Tanja Neuman, Zbigniew Baster, Zenon Rajfur, Oskar Szelest, Christopher Holte, Agata Kubisiak, Edyta Kus, Deanna L. Wolfson, Stefan Chlopicki, Balpreet S. Ahluwalia, Malgorzata Lekka, Marek Szymonski, Peter McCourt and Bartlomiej Zapotoczny*

From fixed-dried to wet-fixed to live – comparative super-resolution microscopy of liver sinusoidal endothelial cell fenestrations

https://doi.org/10.1515/nanoph-2021-0818
Received December 29, 2021; accepted April 6, 2022;
published online April 20, 2022

Abstract: Fenestrations in liver sinusoidal endothelial cells (LSEC) are transcellular nanopores of 50–350 nm diameter that facilitate bidirectional transport of solutes and macromolecules between the bloodstream and the parenchyma of the liver. Liver diseases, ageing, and various substances such as nicotine or ethanol can negatively influence LSECs fenestrations and lead to defenestration. Over the years, the diameter of fenestrations remained the main challenge for imaging of LSEC *in vitro*. Several microscopy, or rather nanoscopy, approaches have been used to quantify fenestrations in LSEC to assess the effect of drugs and, and toxins in different biological models. All techniques have their limitations, and measurements of the "true" size of fenestrations are hampered because of this. In this study, we approach the comparison of different types of microscopy in a correlative manner. We combine scanning electron microscopy (SEM) with optical nanoscopy methods such as structured illumination microscopy (SIM) or stimulated emission depletion (STED) microscopy. In addition, we combined atomic force microscopy (AFM) with SEM and STED, all to better understand the previously reported differences between the reports of fenestration dimensions. We conclude that sample dehydration alters fenestration diameters. Finally, we propose the combination of AFM with conventional microscopy that allows for easy super-resolution observation of the cell dynamics with additional chemical information that can be traced back for the whole experiment. Overall, by pairing the various types of imaging techniques that provide topological 2D/3D/label-free/chemical information we get a deeper insight into both limitations and strengths of each type microscopy when applied to fenestration analysis.

Keywords: atomic force microscopy (AFM); fenestration; liver sinusoidal endothelial cell (LSEC); scanning electron microscopy (SEM); stimulated emission depletion (STED) microscopy; structured illumination microscopy (SIM).

***Corresponding author: Bartlomiej Zapotoczny**, Department of Medical Biology, Vascular Biology Research Group, University of Tromsø (UiT), The Arctic University of Norway, Tromsø, Norway; and Institute of Nuclear Physics, Polish Academy of Sciences, Kraków, Poland, E-mail: bartlomiej.zapotoczny@ifj.edu.pl. https://orcid.org/0000-0003-2129-3714
Karolina Szafranska, Christopher Holte and Peter McCourt, Department of Medical Biology, Vascular Biology Research Group, University of Tromsø (UiT), The Arctic University of Norway, Tromsø, Norway. https://orcid.org/0000-0001-5072-4590 (P. McCourt)
Tanja Neuman, JPK BioAFM Business, Nano Surfaces and Metrology Division, Bruker Nano GmbH, Berlin, Germany
Zbigniew Baster, Zenon Rajfur, Agata Kubisiak and Marek Szymonski, Marian Smoluchowski Institute of Physics, Faculty of Physics, Astronomy and Applied Computer Sciences, Jagiellonian University, Krakow, Poland. https://orcid.org/0000-0003-1265-6480 (Z. Rajfur). https://orcid.org/0000-0003-1241-4035 (A. Kubisiak). https://orcid.org/0000-0002-3442-0543 (M. Szymonski)
Oskar Szelest, ICLab S.z.o.o, Krakow, Poland
Edyta Kus, Jagiellonian Centre for Experimental Therapeutics (JCET), Jagiellonian University, Krakow, Poland. https://orcid.org/0000-0003-3130-5854
Deanna L. Wolfson and Balpreet S. Ahluwalia, Department of Physics and Technology, UiT-The Arctic University of Norway, Tromsø, Norway. https://orcid.org/0000-0001-6059-2472 (D.L. Wolfson)
Stefan Chlopicki, Jagiellonian Centre for Experimental Therapeutics (JCET), Jagiellonian University, Krakow, Poland; and Chair of Pharmacology, Jagiellonian University Medical College, Krakow, Poland. https://orcid.org/0000-0002-2878-3858
Malgorzata Lekka, Institute of Nuclear Physics, Polish Academy of Sciences, Kraków, Poland. https://orcid.org/0000-0003-0844-8662

1 Introduction

The unique morphology of liver sinusoidal endothelial cells (LSEC) makes them an excellent platform for testing

drug responses [1], tracking the dynamics of the cytoskeleton [2] or even testing the resolution of novel microscopy techniques [3]. The LSEC fenestrations (also called fenestrae) are the main reason for an increasing interest in the research on LSEC morphology. Fenestrations are transcellular pores of 50–350 nm in diameter, typically clustered in groups of a few to a few hundred to form "sieve plates". Fenestration size is primarily below the resolution of standard optical microscopy, resulting in these pores not being visible in the microscope images. In addition, the thickness of the cell in the sieve plate regions is less than 200 nm, making them ideal test subjects to assess developing super-resolution techniques and data analysis algorithms [3–5]. However, fenestrations are interesting scientifically not only because of their structure but primarily because of their function. They facilitate extremely efficient passive bidirectional transport of solutes and macromolecules between blood and hepatocytes [6, 7]. The changes in fenestration size and/or number influence the efficiency of this bidirectional transport. The well-fenestrated morphology of LSEC is a marker for proper liver function. Decreased porosity, associated with ageing or liver diseases [8], affects not only the functioning of the liver but also general metabolism [9, 10]. Interestingly, fenestrations rapidly respond to different chemical agents [1, 11] opening a new field on re-opening fenestrations in defenestrated LSEC [2, 12]. Recently, several therapeutic approaches were reported to positively influence the number of fenestrations in young and old animals [12]. The detailed monitoring of fenestrated morphology under different experimental conditions has become an essential component of the research on LSEC. We have recently published a summary of all drugs and agents reported so far to affect fenestration size and/or number in [13].

To achieve proper quantification of the LSEC phenotype, several microscopy techniques have been recently introduced. The size of fenestrations is mainly below the diffraction limit of regular optical microscopy, so their imaging requires the use of super-resolution or nonoptical techniques. To date, scanning electron microscopy (SEM) [9, 14–16], transmission electron microscopy (TEM) [17, 18], atomic force microscopy (AFM) [9, 19–22], structured illumination microscopy (SIM) [23, 24], direct stochastic optical reconstruction microscopy (dSTORM) [1, 5, 23, 24], and stimulated emission depletion fluorescence microscopy (STED) [25, 26], were all successfully used to analyze fenestrations in fixed LSEC. Recent advances in AFM [2, 11] and STED [26] have opened new horizons for investigating fenestrations in live LSEC. However, the reported phototoxicity and sample bleaching connected with STED limits the imaging time; thus, AFM currently remains the only technique allowing for prolonged (>1 h) investigation of changes in porosity of LSEC. The abovementioned microscopy modalities require specific sample preparation. For example, high-resolution SEM requires sample dehydration and coating. Data coming from optical nanoscopy are based on formaldehyde (FA)-fixed samples, while AFM on glutaraldehyde (GA)-fixed samples. The influence of sample preparation on fenestrations in LSEC has not been discussed so far. Up to 2012, it was highlighted that fenestrations in wet-(GA)fixed LSEC are larger than in fixed-dried (dehydrated) LSEC [27]. However, the observed net-values of mean fenestration diameter varied largely from the values obtained using novel microscopy, indicating that an update in the comparison is needed.

Correlative imaging can be crucial for avoiding false or misleading conclusions. Several reports have indicated the advantages of coupling various super-resolution fluorescence microscope modalities in one device to provide information about the sample biochemical composition, with a detailed 3D topography provided by AFM [28–33]. In particular, AFM provided complementary information about the kinetics of amyloid aggregation, while data collected using only fluorescence microscopy (STED) fails to visualize all the products derived from the *in vitro* aggregation of misfolded proteins [32]. It highlights how labeling is a limiting factor in quantitative fluorescence imaging and how the results should ideally be supported with other techniques. Complementary imaging of LSEC was reported in the past, showing the differences in the porosity between the microscopy techniques in fixed-dried (chemically fixed and dehydrated) LSEC [15, 34, 35]. Recently developed photonic chips for correlative light and electron microscopy provide new possibilities for high-resolution imaging of LSEC [36]. So far, comparative imaging of fenestrations has been limited to fixed-dried samples [15, 37]. In particular, the mean fenestration size reported using different techniques varies more than 30% depending on the selected sample preparation method (Suppl. Table in [2]). Such differences may lead to incorrect conclusions about the filtration efficiency of particulate material through fenestrations. For example, large chylomicrons (>~350 nm) cannot pass the barrier of fenestrations, but chylomicron remnants, LDL or HDL particles can freely migrate through [38]. The reported increase or decrease in the diameter of fenestrations for newly discovered drugs determines their potential in treating liver diseases. It is important to find a way to understand the origins of those discrepancies, allowing for better comparison between reports. The variations might originate from differences between animals (species, age), different sample preparation protocols, imaging techniques, and analysis methods. Recently, we presented a report in which we compared different ways of image analysis allowing for

high throughput quantification of fenestrations size and number [39]. The differences between the novel optical microscopic methods for LSEC imaging have been discussed by Øie et al. [24] but the direct comparison including electron microscopy and AFM has not been reported so far. Despite the advantages, all techniques suffer from certain limitations [40, 41]. Optical nanoscopy requires the use of fluorescent labeling. The labeling density, distribution and bleaching all limit the resolution. It should be emphasized that fenestrations are "negative" structures in the context of fluorescence imaging. It means that we are looking at a lack of signal within the pores. Imaging a negative structure requires high density labeling of nearby positive objects (mainly by membrane dyes), and the efficiencies of the binding to those targets influences imaging. AFM is a label-free technique but requires tip-sample interaction, which (when cantilevers with sharpened, i.e., higher resolution tips are used) might alter the investigated structures [19, 42]. Both methods allow for measurements of wet-fixed LSEC or even live LSEC, while SEM needs sample dehydration.

Recent reports have provided great improvement in the imaging of fenestrations in LSEC. However, the direct comparison between them is lacking. Here, we present data from four comparative techniques, where the same cell was imaged using two selected techniques – SIM/SEM, STED/SEM, AFM/SEM, AFM/STED, and AFM/conventional confocal fluorescence. This article aims to discuss the differences between the fenestration diameters obtained by each method. Therefore, we introduced a novel method of correlative imaging in which the same individual fenestrations were measured using both techniques in a one-to-one manner. For accurate measurements we implemented recently introduced methods of image analysis [39]. Moreover, for the first time, we analyze the differences between wet-fixed and fixed-dried samples by comparing SIM/SEM, STED/SEM, and AFM/SEM techniques. We then focus on wet-fixed samples showing the first AFM and STED correlative images of LSEC and discussing the effect of the selected fixation method and permeabilization on LSEC morphology. Finally, we show the possibilities of combining non-super-resolution fluorescent microscopy with AFM for achieving live imaging with additional chemical information.

2 Materials and methods

2.1 Cell isolation

LSEC were isolated as previously described [20]. Briefly, livers were initially perfused to remove the blood and then digested using Liberase™ (*Roche*). After digestion, the cells were released from Glisson's capsule into a cold (4 °C) perfusion buffer containing 1% BSA. The obtained suspension of cells was subjected to several centrifugations (including 25–50% Percoll gradient separation for AFM/STED experiments) to separate hepatocytes, remaining blood cells, and nonparenchymal cells. Thereafter, LSEC and Kupffer cells were separated by immuno-magnetic separation using endothelium specific CD146 MicroBeads (*MACS*, *Miltenyi Biotec*, Germany). After isolation, cells were seeded on uncoated glass coverslips and incubated in 5% CO_2 at 37 °C in EGM-2 cell culture medium (*Lonza*) for 12–15 h for AFM/STED or on fibronectin-coated glass coverslips in RPMI-1640 (Sigma-Aldrich) for 4–6 h for SIM/SEM, STED/SEM, and AFM/SEM. Seeding conditions were optimized according to the specific microscopy requirements, using established methodology [39].

2.2 Sample handling

Large gaps, i.e., micron-sized holes in a membrane, were observed in freshly isolated LSEC after seeding. By comparing live and fixed LSEC, we noticed that no new gap formation occurred when LSEC were fixed with FA or GA. By monitoring LSEC morphology live, instead of fixed, when using AFM/conventional fluorescence microscopy, we showed that wet-fixation of cultured LSEC does not damage sieve plates. However, by investigating individual LSEC using AFM on each step of sample preparation, we noticed that thorough rinsing (pipetting) of samples with live or fixed cells could damage the delicate structure of fenestrations within sieve plates. We used warm (37 °C) buffers and fixative agents combined with slow aspiration and delicate rinsing to reduce gap formation.

2.3 Fixation

Wet-fixed LSEC. FA-fixed LSEC or GA-fixed LSEC terms are used in order to describe chemically fixed cells using aldehydes. In particular, after cell culture medium was removed and 3.6% FA added to LSEC for 15 min (FA-fixed LSEC) or 1% GA for 2 min (GA-fixed LSEC). Then the fixative was removed and cells were kept in phosphate buffered saline (PBS).
Fixed-dried LSEC. For 2 h, the sample was post-fixed in McDowell's solution (4% FA, 1% GA, pH 7.3) [44]. Samples were incubated for 1 h in freshly made 1% tannic acid in PHEM buffer, 1 h of 1% OsO_4 in H_2O, dehydrated in ethanol gradient (30, 60, 90% for 5 min each, then 4 times for 5 min in 100% ethanol), followed by two sets of incubation in hexamethyldisilane (HMDS) for 10 min. Finally, samples were left overnight to evaporate.

2.4 Staining of actin and cell membrane

3.6% FA-fixed cells were stained for 30 min in PBS using: phalloidin-Atto488 (*Sigma Aldrich*) 1:300, Invitrogen CellMask Deep Red Plasma membrane Stain (*Thermo Fisher Scientific*) 1:500, Invitrogen CellMask Green Plasma Membrane Stain (*Thermo Fisher Scientific*) 1:500; for 5 min using Hoechst 33258 (*Invitrogen*) 1 µg/ml. To avoid any additional effects of the dye on living cell, LSECs were stained after fixation. Cells were not permeabilized using detergent before staining.

2.5 Atomic force microscopy (AFM)

Live LSEC measurements were conducted in 25 mM HEPES buffered EGM-2 medium at 37 °C. Fixed cells (3.6% FA for 15 min or 1% GA for 2 min) were measured in PBS with Ca^{2+} and Mg^{2+} at 25 °C. Imaging was carried out in a BioCell™ (*Bruker Nano GmbH, Berlin, Germany*) under ambient atmosphere using Nanowizard 3 AFM system (*JPK Instruments*) and Nanowizard 4 (*Bruker Nano GmbH, Berlin, Germany*) for comparative AFM/STED and AFM/SEM measurements. All images were acquired using the force–distance curve-based imaging mode, a so called "Quantitative Imaging" (QI) (*Bruker Nano GmbH, Berlin, Germany*) according to [11]. Briefly, an independent, 300–800 nm force–distance curve was collected in each image pixel. It was further translated into the topography image, reconstructed for selected loading force, up to the maximal loading force used in the experiment [11]. We performed measurements using different types of commercially available cantilevers: (a) with tips of a radius of 25 nm on cantilevers with a spring constant of 0.1 N/m (SCM-PIC-V2, *Bruker Nano GmbH, Berlin, Germany*) (Figure 3, Supplementary Figures 4 and 5), (b) with tips of a radius of 20 nm on cantilevers with a spring constant of 0.7 N/m (ScanAsyst-Fluid, *Bruker Nano GmbH, Berlin, Germany*) (Figure 6), (c) with tips of a radius of 2–12 nm on cantilevers with a spring constant of 0.03 N/m (MSNL-10 D, *Bruker Nano GmbH, Berlin, Germany*) for AFM/SEM experiments (Figure 4, Supplementary Figure 3), and (d) with tips of a radius of 10 nm on cantilevers with a spring constant of 0.1 N/m (qp-BioAC) (Figure 5). The load force varied from 100 to 350 pN and was adjusted to obtain a clear image of fenestrations at 90% of the load force. The elasticity parameter (apparent Young's modulus) of LSEC (Figure 3A) was determined using gold-coated V-shaped colloidal probes (polystyrene, diameter 7.9 µm) with spring constants of 0.01 N/m (*Novascan*), as presented in [43]. 8×8 µm^2 areas over the cell nucleus were selected, and 8×8 matrices (total 64) of force-distance curves were acquired (Load force of 0.5 nN, load frequency 4 s). The value of the cell elasticity parameter was determined by fitting the Hertz model to each force-indentation curve. The obtained images of the topography, stiffness and elasticity were prepared using JPK Data Processing Software for further analysis.

2.6 Structured illumination microscopy (SIM)

Samples were prepared as previously described [19]. Briefly, cells were seeded on fibronectin-coated #1.5 glass-bottom MatTek dishes (*MatTek Corporation*, MA) and fixed for 15 min with 4% FA in PHEM buffer (60 mM PIPES, 25 mM HEPES, 10 mM EGTA, 4 mM $MgSO_4 \cdot 7H_2O$, pH 6.9). Samples were stored in PBS containing 0.1% FA at 4 °C. Before imaging, cells were stained using 10 µg/ml of CellMask Green (*ThermoFisher*) in PBS for 30 min. Images were obtained at room temperature using a commercial SIM microscope (OMX Blaze system, *GE Healthcare*) with a 60 × 1.42 NA oil-immersion objective (*Olympus*), using oil with a refractive index of 1.514 (*Cargille*) and a 488 nm laser. 3D-SIM image stacks of 1.5–2.0 µm were acquired with a *z*-distance of 125 nm and 15 raw images per plane (five phases, three angles). Raw datasets were computationally reconstructed using SoftWoRx software (*GE Healthcare*), and maximum intensity *z*-projections in *tiff* format were prepared for further analysis.

2.7 Stimulated emission depletion microscopy (STED)

Fixed samples were prepared as for SIM. STED imaging was performed at room temperature using a STEDYCON (Abberior compact line) mounted on an inverted optical microscope (Axio Observer, *Zeiss*) equipped with a 100× oil immersion objective with oil with refractive index 1.518. Images were acquired with the STEDYCON smart control software using the 640 nm excitation laser together with the 775 nm STED/depletion laser and 650–700 nm detection. The following parameters were set during STED measurements, dependent on the sample: excitation power: 1–6%, depletion laser power on sample: 210 mW, pixel dwell time: 10–50 µs with double signal accumulation, depletion pulse delay: 0 ns, depletion saturation power: 0.5–3.1%, gate delay: 1 ns, gate width: 6 ns, pinhole: 64 µm. The pixel size was 30 nm for AFM/STED and 39 nm for STED/SEM images. Furthermore, the STED setup was equipped with a Nanowizard 4 system for the complementary AFM investigation.

2.8 Scanning electron microscopy (SEM)

After STED, SIM or AFM measurements, the sample was prepared for SEM measurements according to the protocol described in *Methods*, point 2.3. Before imaging, samples were mounted on metal stubs using carbon tape and silver glue to reduce charging and sputter-coated with 10-nm gold/palladium. A commercial SEM system (Sigma HV0307, *Zeiss*) was used to image samples using a 2 kV electron beam. The image size was adjusted to the area measured with SIM, STED or AFM, with a 9–10 nm pixel size. For correlation purposes, slight adjustments (rotate and perspective tools) were performed with graphics software (*Gimp*, version 2.10.24) to obtain perfect matching based on landmarks.

2.9 Conventional confocal microscopy

Measurements on fixed LSECs were done using a ZEISS LSM 710 laser scanning confocal unit connected to an Axio Observer Z1 microscope with a 100×, 1.3 NA oil immersion objective. Images were acquired with ZEN 2012 SP1 Black Edition (version 8.1.0.484) software using the 488 and 633 nm excitation lasers. Comparative AFM/LSCM measurements were performed on two independent systems. Marked glass coverslips were used to localize the same position on a sample, which allowed measurements of the same cell with both techniques. AFM analysis was performed prior to confocal fluorescence microscopy measurements. The images were analyzed using Zeiss ZEN (blue edition). The scale and position of the AFM and confocal fluorescence microscopy images were adjusted manually using graphics software (*Gimp*, version 2.10.24).

2.10 Data analysis and statistics

For STED/SEM, SIM/SEM comparison, images were processed in Fiji/ImageJ software [44] and segmented using a semi-automated threshold-based method described in detail elsewhere [39]. Briefly, in each image the contrast was individually adjusted, then the image was converted into a binary mask. In particular, for optical nanoscopy the cut-off values were selected carefully, because of the uncertainty

connected with the point spread function (PSF) to reflect a point between the maximum intensity and full width at half maximum. After this every fenestration was measured. Parameters such as single fenestration area, fenestration diameter and roundness (ratio of min to max diameter assuming elliptical shape) were measured for each fenestra. This method was shown to be easily implemented and highly reproducible between the users in the assessments of fenestration diameters [39]. For STED/AFM and AFM/SEM an automated machine-learning method was selected, as described in the same report [39]. The advantage of this method is a precise identification of fenestrations at low-resolution (low number of pixels, big pixel size) and high-magnification images [39], here represented by AFM. After the binary mask was prepared, the fenestration measurements were performed using for semi-automated method. OriginPro software (OriginPro 2021, OriginLab Corp., Northampton, MA) was used for data analysis and graphical presentation.

It is important to note that the net values of fenestration size distributions differ between the methods. For example, the mean fenestrations size of SEM differs in SIM/SEM, STED/SEM, or AFM/SEM analyses. This is expected as the selection of analyzed sieve plates was performed in order to perform correlative imaging. To present the mean value of fenestrations in a biological group, several cells for each bio replicate are analyzed by measuring and counting all fenestrations from each cell. Here, we selected individual sieve plates, measured in the optimal conditions of each method. For example, in STED, it is difficult to obtain a high signal to noise ratio in the images of the whole cells and the thermal drift shifts the focus when imaging bigger areas. Therefore, individual sieve plates were measured and compared with SEM. Similarly to AFM measurements, the large view image was collected in the point to point resolution of ~80 nm to minimize thermal drift. However, 25–40 min per frame is needed. Individual sieve plates were then imaged in high resolution at 15–25 nm per pixel (with up to 15 min per image). Here, the main limiting factor was low throughput, but all techniques allow for comparing the same fenestrations in a one-to-one manner, and the differences between the selected microscopy techniques can be discussed.

3 Results

3.1 Wet-fixed versus fixed dried I. Comparative SIM/SEM imaging

SIM is a highly versatile optical microscopy method with double the resolution of diffraction limited microscopy. However, it is prone to image artefacts. To investigate this issue, we performed SEM on the same samples that were first examined by SIM. 488 nm excitation was selected to enable the highest optical resolution. In particular, LSEC

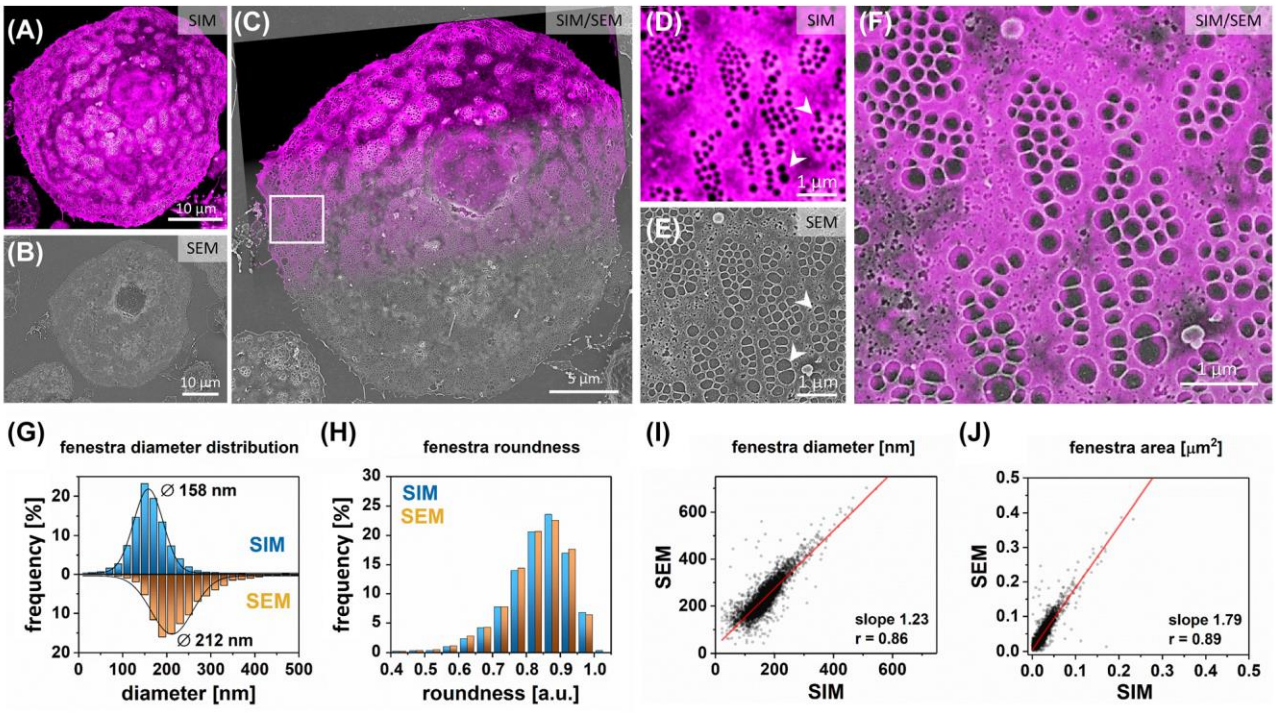

Figure 1: Correlative SIM and SEM imaging.
Firstly, SIM imaging was performed on wet-fixed LSEC labeled with CellMask Green; (A) A representative LSEC is presented (Magenta Hot Lookup was used to enhance the contrast of fenestrations in the image). (B) The sample was dehydrated, and the corresponding area was located (using landmarks) and imaged using SEM. (C) Both SIM and SEM images were then correlated. (D–F) High-magnification correlative imaging allows for precise identification of fenestrations within sieve plates using both techniques. Some fenestrations appear merged in SIM but not in SEM (white arrowheads). Fenestrations smaller than 100 nm can be distinguished in SIM (white arrows). 4942 fenestrations were detected and measured in a one-to-one manner using a semi-automated method. (G) Histogram of fenestration diameter distribution. The lines represent fitted Gaussian curves from which the mean values were calculated at the peak of the distribution (158 ± 40 nm and 212 ± 55 nm for SIM and SEM, respectively (n = 4942 fenestrations)). (H) Distribution of fenestration roundness measured by SIM (0.83 ± 0.09) and SEM (0.82 ± 0.09) (roundness = ratio of min to max diameter, assuming elliptical shape). A comparison of individual fenestration diameter I and area J indicate linear and even dilation of fenestrations in fixed-dried LSEC (linear regression slope of I = 1.23 (r = 0.83) and J = 1.79 (r = 0.89)). r – Pearson's coefficient.

were labeled with CellMask Green, allowing for detailed imaging of the cell membrane. A representative image of a single LSEC imaged using both SIM and SEM is presented in Figure 1.

The resolution of SIM images allowed for detailed identification of fenestrations in LSEC (Figure 1A). We selected 10–15 representative cells per sample and performed SIM imaging. Using such landmarks as cell shape and arrangement, the same cells were subsequently localized using SEM (Figure 1B). The correlation was performed using scales (calibration using representative scale bars) representative for both microscopes (Figure 1C and F). Using SEM, we identified several individual and small fenestrations located close to one another that appear as one fenestration in SIM (Figure 1D and E). Moreover, some fenestrations near the cell edge are distorted or merged in SEM but not in SIM. However, most of the fenestrations within the sieve plates were identified using both techniques, and the number of artefacts was not significant. The most prominent differences between the two techniques relate to the perinuclear regions of LSEC. In those areas some whole sieve plates were not visible or were dimly visible in SIM. The thick areas of the surrounding cell membrane hampered the proper identification of fenestrations in those sieve plates (Supplementary Figure 1). Therefore, the number of fenestrations per cell calculated with SEM will be larger than with SIM. The next prominent difference is connected with the diameter of the fenestrations. Fenestrations appear significantly larger in fixed-dried samples measured with SEM than in the wet-fixed samples measured with SIM (Figure 1D–F). To quantify this observation, we performed detailed measurements of corresponding fenestrations visualized with both techniques (Figure 1G–J). The analysis of almost 5000 individual fenestrations revealed that the mean fenestration size was 158 ± 40 nm using SIM compared to 212 ± 55 nm obtained from SEM. This corresponds to a 34% increase in diameter between SIM and SEM. There were no observed changes in fenestrations shape, which is reflected in the similar distribution of the roundness parameter – mean value for SEM: 0.82 ± 0.09, SIM = 0.83 ± 0.09 (Figure 1H). The linear relationship between the values of single fenestration area and diameter indicates that the fenestration diameter was evenly dilated for the analyzed group of pores, independently of their size (Figure 1I and J). The resolution of SIM is far lower than SEM, which, together with the possible artifacts from the SIM image reconstruction may affect the measurement of fenestration size. In fact, image reconstruction and processing allowed us for the identification of fenestrations down to 80 nm in diameter (Figure 1G), much smaller than the theoretical resolution of SIM (~110 nm). Still, those small fenestrations identified in SIM correspond to the fenestrations in SEM (Figure 1 white arrows). In order to achieve even higher spatial resolution, we performed similar experiments using STED – another optical nanoscopy technique which can achieve higher resolution than SIM.

3.2 Wet-fixed versus fixed dried II. Comparative STED/SEM imaging

We used CellMask Deep Red membrane stain to visualize the cell membrane surrounding fenestrations, as suggested in another report [26]. The advantages of STED microscopy cover the lack of reconstruction artifacts and the possibility of selecting small areas with a few sieve plates. It allows for decreased illumination time of LSEC and thus reduces bleaching of the surrounding area. The STED beam allows for precise illumination compared to the larger areas illuminated with the grid pattern in SIM; although the energy of the illumination is usually higher. Despite the growing number of new STED dyes, the selection is still somewhat limited. CellMask Deep Red provides both good dye density and resistance to bleaching allowing for detailed investigation of fenestrations. A representative STED image of LSEC shows the ultrastructure of fenestrations (Figure 2A).

Similarly to previous experiments, we used landmarks to localize the previously measured area on fixed-dried samples using SEM. The correlative image allowed identification of corresponding fenestrations using both imaging techniques (Figure 2C and F). Similarly to SIM/SEM, some artefacts were observed. We identified rupture and merging of some fenestrations (Supplementary Figure 2). Moreover, fenestrations in the perinuclear region or in the higher regions of cells (that are out of the plane of focus) can be omitted in STED analysis (Figure 2A–F). The detailed analysis of 1909 fenestrations detected by both techniques allowed for the direct comparison (Figure 2G–J). The mean fenestration diameter calculated for STED (124 ± 44 nm) and SEM (165 ± 64 nm) corresponds to an overall 33% increase in diameter and is similar to the SIM/SEM experiment. It is important to note that the net values obtained using SIM/SEM and STED/SEM differ. This is expected, as the fully random selection of the cells and the analysis of all cells' fenestrations was not applied for the analysis, however, all obtained images were used for analysis and no measurements were discarded afterwards; (see *Methods*).

The linear regression slope of 1.03 and r of 0.81 reflects the increase in fenestration diameters observed in SEM. Two groups of fenestrations were recognized: the majority of fenestrations were uniformly enlarged due to drying, but also some individual fenestrations enlarged to more than twice their STED-measured size and had an elongated shape. The shift in fenestrations shape in SEM can be observed in both mean roundness values – STED: 0.79 ± 0.11, SEM: 0.75 ± 0.13 and difference in the

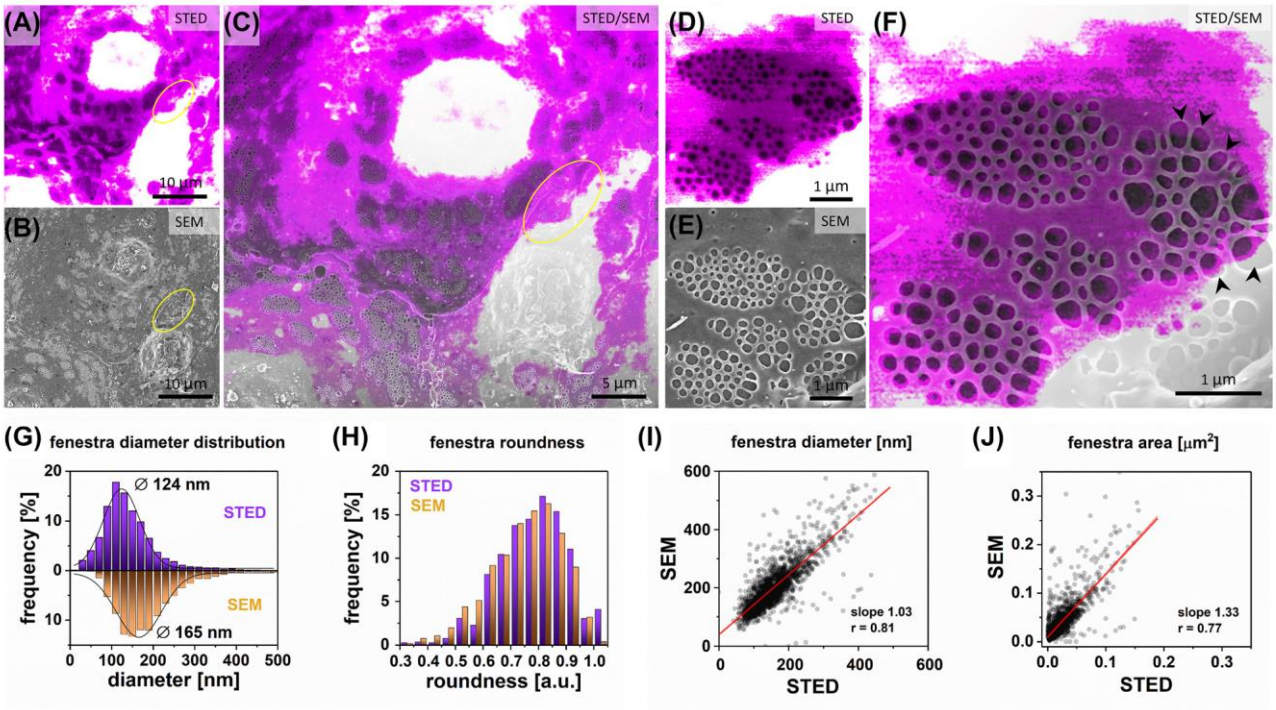

Figure 2: Correlative STED and SEM microscopy.
Firstly, STED measurements were performed for wet-fixed LSEC labeled with CellMask Deep Red; (A) A representative STED image of LSEC is presented. To achieve the highest possible contrast for fenestrated regions, areas corresponding to the cell nuclei were saturated (white) due to the high signal intensity. (B) The sample was dehydrated, the corresponding area was localized and measured with SEM. (C) Both STED and SEM images were then correlated. (D–F) High-magnification images allow for precise identification of all of the fenestrations within sieve plates. Fenestrations in the center of the sieve plate were less dilated than those on the edges (arrowheads). 1909 fenestrations were identified in the collected images and analyzed in a one-to-one manner. (G) Histogram of fenestration diameter distribution. The black lines represent fitted Gaussian curves from which the mean diameter was calculated at the peak of the distribution (STED 124 nm ± 44 nm, SEM 165 nm ± 64 nm). (H) Distribution of fenestration roundness measured by STED and SEM. A comparison of individual fenestration diameter *I* and area *J* indicate uniform dilation of fenestrations in SEM.

roundness distribution below 0.7. These deformed fenestrations are located at the edges of sieve plates and in the areas where the cell is either significantly thicker (nuclei region) or thinner (edge of the cell) than the average region with sieve plates (Figure 2F, arrowheads).

3.3 Wet-fixed versus fixed dried III. Comparative AFM/SEM imaging

3.3.1 From living to fixed LSEC – AFM study on sample preparation

In optical microscopy, the optimal fixation methods are limited by the autofluorescence of the agents and interactions with the fluorophores. Therefore, in most cases formaldehyde is the preferable fixative agent over for example, glutaraldehyde. Moreover, most antibody-based staining methods require a permeabilization step which can destabilize the cell membrane and affect fenestration measurement. To study those effects and investigate how different steps in sample preparations affect fenestrations we used the advantages of AFM. This label-free technique can be used in a wide range of environmental conditions and AFM images of LSEC have been reported for living, wet-fixed, and even fixed-dried cells. Therefore, before performing correlative imaging with AFM, we tested standard procedures in preparation of LSEC for microscopy, namely wet fixation using FA or GA and Triton X-100 permeabilization. The differences in fixation methods and their influence on the quality of super-resolution fluorescence imaging were discussed in detail by Whelan and Bell [45]. The authors presented optimized protocols for formaldehyde, glutaraldehyde, and methanol fixation, showing that the latter gives unsatisfactory results for actin staining. Because fenestrations are reported to consist of actin [23], we did not fix LSEC using alcohols. According to the Whelan and Bell protocols and our previous observations

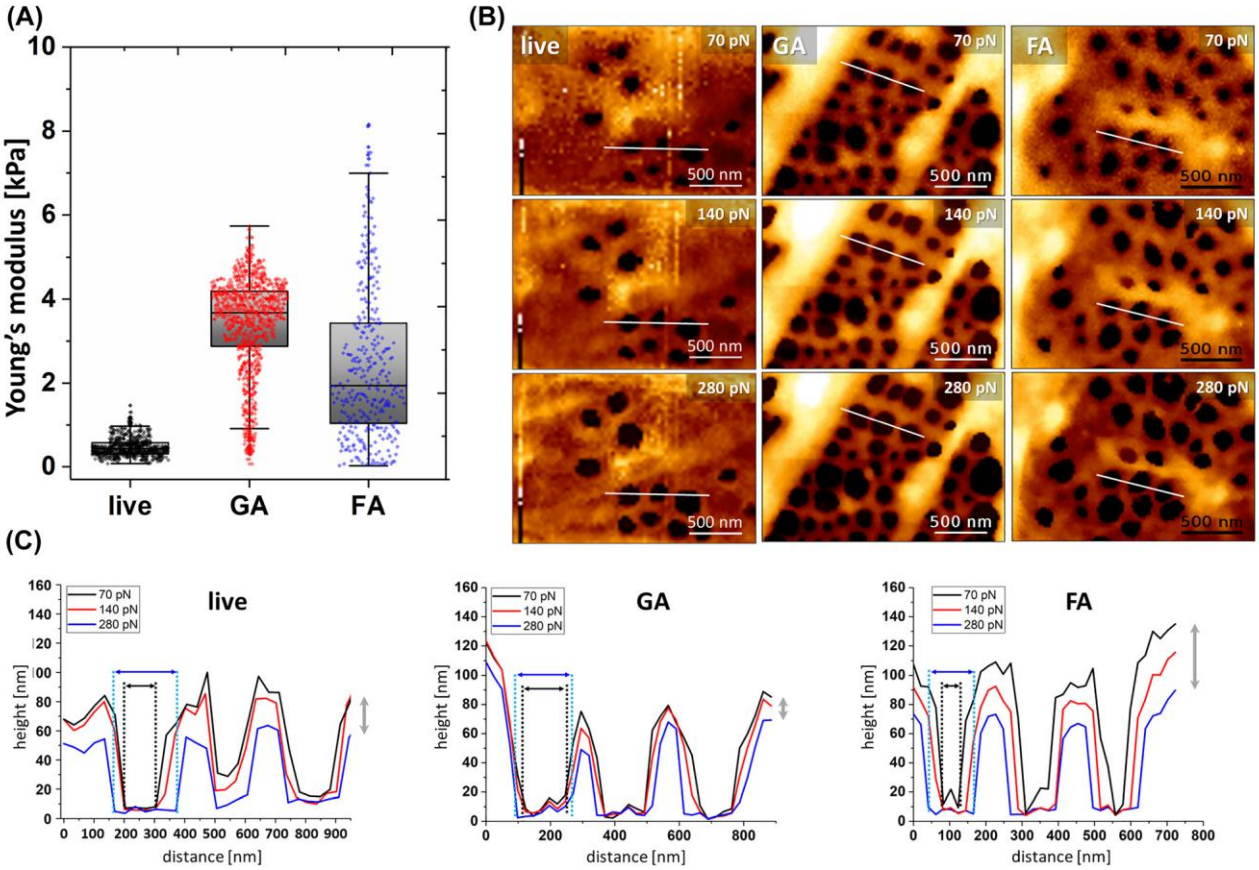

Figure 3: The difference in mechanical properties of LSEC and fenestrations in living, FA-fixed, and GA-fixed LSEC.
(A) The apparent Young's modulus of cells ($n \geq 15$ for each group, 64 curves per cell) was obtained for a colloidal cantilever for a load force of 200 pN. (B) Images of selected sieve plates measured using QI AFM reconstructed for a load force of 70 pN, 140 pN, and 280 pN. (C) The tip-induced enlargement of fenestrations presented as a cross-section of selected fenestrations collected for the same area of the images reconstructed for different load forces. Grey arrows indicate the tip-induced squeezing of the membrane surrounding fenestrations in the *z*-axis. Black and blue arrows indicate the boundaries of fenestration obtained for 70 and 280 pN, respectively.

[20], we selected 1% GA (2 min) and 3.6% FA (15 min) to investigate changes in the morphology of LSEC (Figure 3).

Firstly, we performed force mapping of live LSEC using a colloidal probe. Then, we analyzed the data for low loading force (200 pN), which corresponded to 50–200 nm indentation to uncouple the information about the elasticity of the deeper layer of the sample (e.g., cell nucleus, glass substrate) and to investigate only the cortical layer of the cell. We observed stiffening of the cortical layer for both fixatives compared to living cells (Figure 3A). The mean apparent Young's modulus of GA-fixed cells increased 7.2 fold, while a mean 5.2 fold increase was observed for FA-fixed LSEC. GA resulted in a narrower distribution of elasticity than FA. In the next step, using cantilevers with sharp tips, following the methodology described in [19], we investigated fenestration diameters of FA- and GA fixed samples. QI AFM enables image reconstruction for any load force: from near the contact point ("zero force") up to the maximum load force used in an experiment. In particular, to analyze the load force dependence for both fixative agents, we compared 70, 140 and 280 pN load forces applied in each pixel-point of the image (Figure 3B and C). The first point corresponds to near the contact point, where fenestrations can be distinguished. The following two points double the force, where the last point of 280 pN corresponds to 90% of the maximal indentation force used in the experiment and allows for stable imaging. FA-fixed LSEC requires slow-scanning using a minimal load force to avoid fenestration dilation. A >25% increase in the mean fenestration diameter in FA-fixed LSEC was observed with increasing load force. This effect corresponds with the deformation observed in the fenestration profile for both live and FA-fixed cells (Figure 3C). In contrast, GA-fixed LSEC presented much weaker load force

dependence resulting in less than 10% change of fenestration diameter when comparing load forces in the contact and maximal indentation points.

3.3.2 Combining AFM with SEM

In the final comparison between the wet-fixed and dehydrated samples, we performed AFM/SEM experiments. Neither requires sample labeling and both provide high resolution. Here we used GA fixation, as it shows stronger and more uniform fixative properties than FA and it is widely used in sample preparation protocols for SEM. We applied measurements using sharpened cantilevers (2–12 nm). It was reported that these provide high-resolution imaging with a steep cut-off on fenestrations boundaries, allowing for precise measurements [19]. We performed AFM/SEM experiments to verify whether the differences in fenestration size in SIM/SEM and STED/SEM experiments are due to the PSF (effectively reducing the measured fenestration diameter in SIM and STED) or dehydration and cell body shrinkage (effectively dilating fenestrations in SEM). The analysis of the AFM/SEM correlation is presented in Figure 4. Cytochalasin B treated LSEC were investigated to increase the number of fenestrations and imaging efficiency. Cytochalasins were reported to increase the number of fenestrations up to three times without any major influence on fenestration diameters [13, 25]. They disrupt the actin cytoskeleton, which lowers overall cell stiffness by removing stress fibers, but does not affect the AFM imaging in used QI (force-dependent) mode of GA-fixed LSEC (Supplementary Figure 5).

The correlation between the methods allowed for precise identification of fenestrations using both techniques. High magnification images of individual sieve plates allowed for one-to-one comparison of fenestrations dimensions. Analysis of 1081 fenestrations confirmed previously the observed enlargement of fenestrations in SEM. The mean fenestration size obtained using AFM was 131 ± 31 nm compared to 181 ± 48 nm for SEM (Figure 4G). This corresponds to a 38% increase in diameter after dehydration. As mentioned above, the net differences in mean size values correspond with the analysis of selected

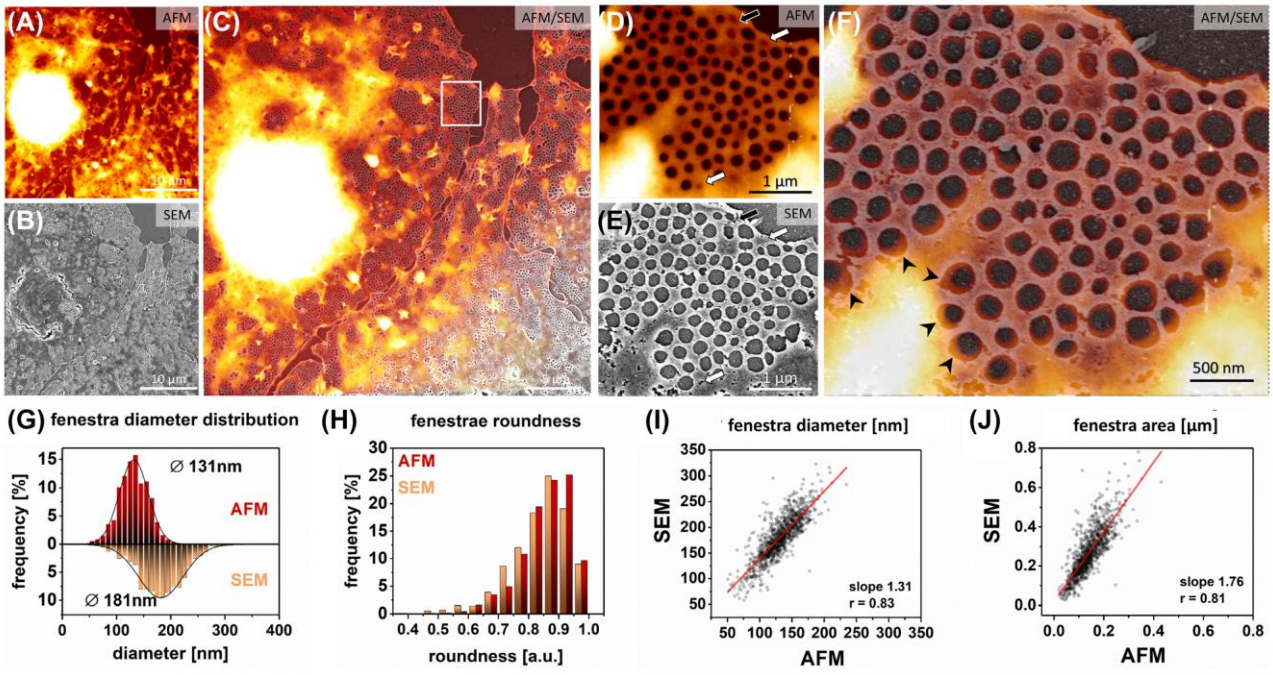

Figure 4: Correlative AFM and SEM microscopy of LSEC treated with cytochalasin B.
Firstly, AFM measurements were performed for GA wet-fixed LSEC; (A) A representative AFM image of LSEC is presented. (B) The sample was dehydrated, the corresponding area was localized and measured with SEM. (C) Both AFM and SEM images were then correlated. (D–F) High-magnification image allows for precise identification of all of the fenestrations within a sieve plate. Fenestrations in the center of the sieve plate were less dilated than those on the edges (arrowheads). Some closed fenestrations identified in AFM became open (black arrow) or are not distinguishable (white arrow) in SEM. 1081 fenestrations were identified in both methods and analyzed in a one-to-one manner. (G) Histogram of fenestration diameter distribution. The black lines represent fitted Gaussian curves from which the mean diameters were calculated at the peak of the distribution (AFM 131 nm ± 31 nm, SEM 181 nm ± 48 nm). (H) Distribution of fenestration roundness measured by AFM and SEM. A comparison of individual fenestration diameter *I* and area *J* indicate uniform dilation of fenestrations in SEM.

sieve plates (see *Methods*). Similarly to SIM/SEM and STED/SEM, we observed enlargement of the fenestrations at the edges of sieve plates after dehydration (Figure 4F, arrowheads). In addition, we observed that in some sieve plates located in the perinuclear zone – where the cell height is above 400 nm – the shape of fenestrations within is distorted (Supplementary Figure 3). Moreover in those areas, two layers of fenestra-like structures were observed forming structures resembling reported "fenestration labyrinths" [46]. Both techniques resolved even the smallest fenestrations and their number was preserved. The only detected difference can be connected with the open and closed (or fused) state of fenestrations, described recently in [1]. In an AFM image (Figure 4D), some fenestrations can be observed as just invaginations in the cell membrane (arrows), and not as transcellular pores. After dehydration for SEM imaging (Figure 4E), those close fenestrations either became open (black arrow) or remained closed but indistinguishable in the SEM image (white arrows). The newly opened fenestrations in SEM could be identified by the sharp edges and less circular shape. We observed a shift in the roundness distribution towards more circular in AFM (0.92 ± 0.09) compared to SEM (SEM: 0.85 ± 0.09) (Figure 4H). The linear relationship between the values of single fenestration area and diameter remains independent of their size (Figure 4I and J). This observation is similar in all tested methods.

3.4 Wet-fixed versus wet-fixed. Comparative AFM/STED imaging

AFM and STED comparative measurements of LSEC were performed on a single device. We investigated FA-fixed LSEC, as a standard fixation approach for STED measurements. We selected CellMask Deep Red staining to label the LSEC plasma membrane, which Di Martino et al. [26] previously suggested as suitable for fenestrations and Brunetti et al. established that it worked well with STED [47]. Permeabilization of the cell membrane prior to staining is not required for the selected dye. As for AFM/SEM experiment, we investigated cytochalasin B treated LSEC. Comparisons of AFM and STED of the same area shows a good correlation between obtained images (Figure 5).

Both techniques enabled precise measurements of the number and size of fenestrations. The cross-section in the same location showed a good correlation between both techniques. AFM provides much steeper boundaries between fenestrations, which allow easier analysis with lower error [39]. The fenestrations boundaries are less sharp for STED images due to the blurring related to the PSF. It results in low accuracy in identifying the smallest fenestrations (Figure 5, white circle). Nevertheless, we obtained similar fenestration diameter distributions using both techniques (Figure 5D). Analysis of 709 fenestrations resulted in a mean fenestration diameter of 173 ± 58 nm for STED and 188 ± 54 nm for AFM, which corresponds to a <10% increase due to deformation caused by AFM tip. The shape of fenestrations remains the same for both techniques which is indicated by the similar mean roundness values of 0.75 ± 0.11 and 0.76 ± 0.11 for STED and AFM, respectively. The slope in the single fenestration area comparison indicate that fenestration enlargement is the most prominent for large holes (Figure 5G).

3.5 AFM-based measurements combined with conventional fluorescence microscopy – a proposed approach for LSECs fenestrations imaging

Here, we present an experiment in which LSEC dynamics was tracked using AFM. The sample was finally fixed for additional non-super-resolution imaging, namely confocal fluorescence microscopy (Figure 6) at the end of the experiment. Such an approach combines super-resolution information about the dynamics of live LSEC with identifying biological structures arising from fluorescence microscopy. Even without super-resolution fluorescence imaging, such an approach can be beneficial for experiments on LSEC. Other optical techniques, such as deconvolution microscopy or spinning disk microscopy can be also used. In particular, we used landmarks such as cell shape and arrangement to identify the areas of interest when transferring samples between AFM and confocal microscope. At first, we performed an experiment in which live LSEC were measured using semi-stiff cantilevers. Such cantilevers allow for fast imaging with a load force of 1–2 nN, enabling visualization of the thick actin cytoskeleton beneath the cell membrane (Figure 6A). Afterwards, the sample was chemically fixed directly on an optical microscope. The high-resolution imaging was repeated in the same area (Figure 6B). Finally, the AFM measurements were followed by staining cells for actin and performing correlative fluorescence imaging of the same regions (Figure 6C and F).

We selected an area of the interconnection of three live cells, where fenestrated morphology was observed. The presented AFM image allowed visualization of sieve plates and fenestrations (Figure 6, white dotted-line circle). Thick stress fibers lining the cell can be easily distinguished as

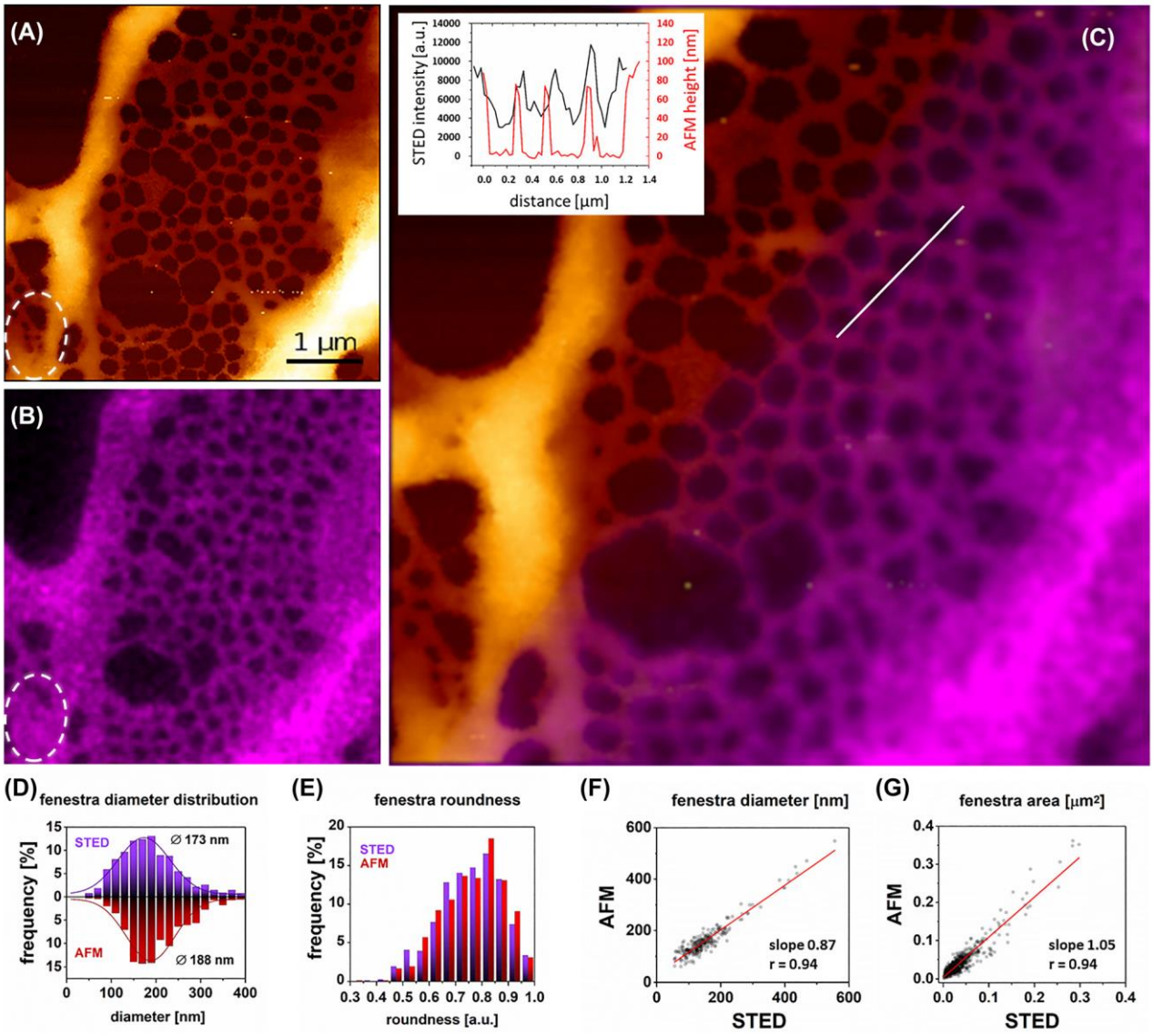

Figure 5: Correlative AFM and STED microscopy.
Comparative AFM and STED of FA-fixed LSEC treated with cytochalasin B using a device prototype that allows direct measurements using both techniques in one setup. Firstly, AFM measurements were performed for FA-fixed LSEC (load force 70 pN) labeled with CellMask Deep Red. (A) High-resolution image of a sieve plate in the LSEC periphery measured using AFM. (B) The corresponding area measured using STED. Fenestrations as small as 50 nm can be distinguished with AFM but not with STED (white dashed circle). (C) presents the correlative image of the same area measured using STED and AFM. The inset represents a cross-section of selected fenestrations (white line in (C)). 709 fenestrations were identified in the collected images and analyzed in a one-to-one manner. (D) Histogram of fenestration diameter distribution. The black lines represent fitted Gaussian curves from which the mean diameters were calculated at the peak of the distribution (STED 173 nm ± 58 nm, AFM 188 nm ± 54 nm). (E) Distribution of fenestration roundness measured by STED and SEM. A comparison of individual fenestration diameter *F* and area *G* indicate uniform and precise measurements of fenestrations using both techniques.

bright lines (Figure 6, arrowheads). After fixation, cells became stiffer and the AFM image corresponds more to the superficial topography of LSEC; fenestrations could still be noticed in the sieve plates, but most of the stress fibers were less prominent and partly covered with overlaying structures. The slight misalignment in AFM images for live and fixed cells is caused by the line-by-line acquisition of AFM in 20 min per frame. During this time, the cell cytoskeleton was continuously rearranging, resulting in, e.g., different sizes of individual sieve plates or changed positions of the gaps between images (Figure 6, white arrows), similar to previous reports [2, 11]. To reduce this effect, we measured and finally fixed LSEC after ~20 h post-seeding, where the rearrangement of the cellular cytoskeleton was shown to

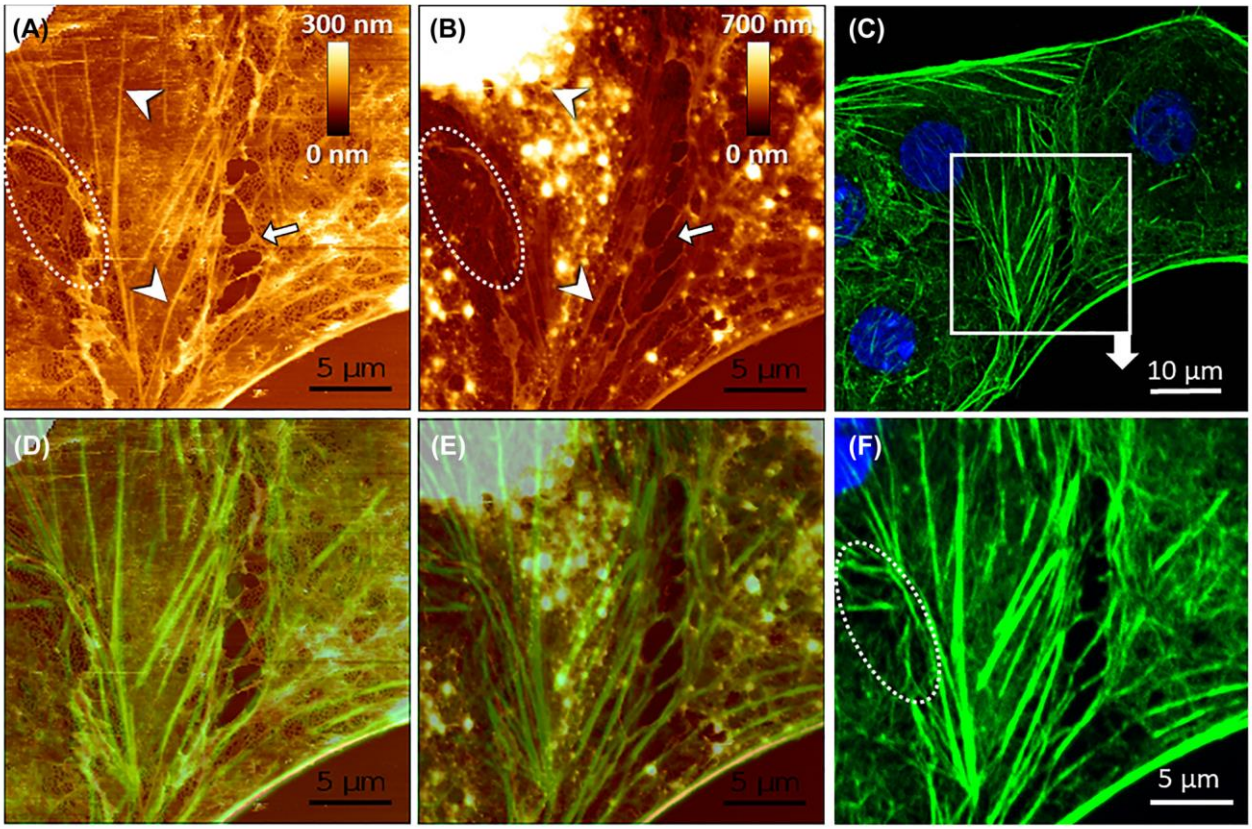

Figure 6: Correlative AFM and conventional fluorescence microscopy of LSEC.
(A) The topography of live cells was measured using AFM. (B) The same area measured after fixation with 1% GA. (C) LSEC were then labeled with phalloidin-Atto488 (green) for actin and Hoechst 33258 (blue) for cell nuclei, and the same area was localized using landmarks. (F) The area of interest corresponding to AFM measurements was selected. (D and E) present merged AFM and fluorescence microscopy images made, respectively, for live and fixed LSEC. Comparative data allow identifying actin stress fibers in live cells (white arrowheads), which visualization is hindered in fixed cells. Fenestrations can be identified as dark spots in AFM images of both live (A) and fixed (B) LSEC (dotted-line circle) but not in fluorescence microscopy images (F). Different sizes and position of gaps in live and fixed cells corresponds to cell migration prior to fixation (white arrows).

be relatively slow [11]. Finally, we stained cells using phalloidin-Atto488 for actin, and we observed a significant correlation of fluorescence and AFM images. Thick actin fibers remained in the exact positions as observed using AFM for live LSEC.

4 Discussion

In this report, we presented a first direct comparison of several super-resolution microscopy measurements of fenestrations in LSEC. Labeling the cell membrane is a well-established approach, allowing the comparison of the labeled cell and the lack of signal within the open, transcellular pore. Fenestrations can change their size in live LSEC *in vitro* by up to 200% [2], but the overall distribution of diameters is preserved after fixation. Still, different values of mean fenestrations sizes have been reported in various reports, with a pattern suggesting a dependence on the selected microscopy technique (SI_Table 1 in [2]). The accurate determination of fenestration size is crucial for understanding the filtration function, as only particles smaller than fenestrations can passively pass from the bloodstream into the space of Disse within the liver [38]. Here, we provided a detailed comparative analysis of fenestration diameters obtained using a combination of different types of microscopy. We want to emphasize that the presented mean fenestration size values are not absolute and do not describe mean fenestration size in the whole population of murine LSEC. The variations were observed because not all fenestrations from each cell were compared. The comparison occurs rather between individual sieve plates that were chosen in the context of efficient co-localization between techniques. Proper

investigations using individual techniques can be found elsewhere (AFM [19], SIM [48], STED [25], SEM [49], and TEM [50]). AFM and TEM independently showed similar data on fenestration size distribution. TEM however is not widely used in the evaluation of drug treatment and therefore is not included in this manuscript. TEM could be a perfect tool for the comparison of *in vitro* versus *in vivo* data on fenestrations, including their 3D structure [45]. The differences in the observation of fenestrations between cell culture and tissue are large (SI_Table 1 in [2]), probably because of complex sample preparation [16]. The use of novel TEM methods, including freeze-fraction sample preparation and FIB-SEM could be a part of a future study. We limited our EM studies in this paper to the SEM modality, where we selected individual well-fenestrated cells and compared fenestrations in a one-to-one manner. It allowed us to assess the origins of the discrepancies between the reports obtained using different microscopy modalities. Firstly, we showed that there are differences between fenestration diameter obtained for wet-fixed and fixed-dried LSEC. Our data are in contrast to that presented in [37] where an almost 30% reduction of fenestration diameter was reported for wet-fixed to fixed-dried fenestrations. However, that data was affected by the nascent and still developing AFM technique. The use of contact mode requires a relatively large load force; paired with limited microscope stability, it resulted in image artefacts as streaks and shadowing. The obtained mean fenestration diameter was 269 ± 44 nm using AFM, well above the values recently shown using gentler imaging modes of modern AFM microscopes [19, 42]. The influence of dehydration on fenestration diameters was also discussed in liver tissue [16]. The authors reported up to a 30% decrease in the size of small structures in tissue blocks measured with SEM and advised against the analysis of size using this technique. In tissue samples, dehydration causes collapse and shrinking of the tissue blocks, which results in the observed decrease of fenestration diameter. Our data comes from isolated LSEC measured *in vitro*, and the observed change in fenestration size is in the opposite direction. Cell surface integrins keep cells well-spread on the surface of the glass coverslip. When dehydrated, cells remained in the same shape and size, confirmed by our correlative imaging (Figures 1, 2 and 4). Individual fenestrations are kept in place by the actin cytoskeleton, which constitutes the stiff scaffold of fenestrations. The precise composition of the protein system that binds actin and the cell membrane is currently unknown in LSEC, but previous reports showed the involvement of spectrin [1] and myosin [51]. Together with the membrane composition [52], this structure regulates the fine-tuning of the fenestration size. As a result of cell body dehydration, the dilation was observed, suggesting that the connection between the cell membrane and the cytoskeleton scaffold may be affected by the created extra tension. The level of changes depends on the thickness of the surrounding cell. Thick areas consist of more water and after drying were affected much more than thin and flat areas within sieve plates (Figures 2F and 4F). Also, dehydration may create more tension close to the cell edges which sometimes results in stretched sieve plates with elongated fenestrations. Thereby, an overall 30–40% increase was observed compared to wet-fixed samples and those differences were documented independently using SIM, STED, and AFM. Altogether, small changes in fenestration diameters between the biological groups should be interpreted carefully, as the microscopy techniques combined with analysis methods (pixel size) are burdened with 10–20 nm error [39]. The correlation between fenestration diameter distributions between STED and AFM was within the margin of error. Furthermore, all wet techniques (SIM, STED, AFM) showed similar differences after preparation for SEM imaging. Therefore, in order to compare results between the methods we advise using a coefficient of $0.75 \times$ *mean fenestrations size in SEM* to calculate the expected mean fenestrations size for wet techniques, assuming a similar preparation protocol. Note that the elongation of fenestrations at the edges of sieve plates causes the standard deviation to be always wider in SEM.

Similarly, the differences in the porosity between the methods can be expected. Optical techniques would usually show lower values of fenestration frequency (the number of fenestrations per area) or porosity (the ratio of the total area covered with fenestrations to the area of cell/image), as those techniques have difficulties resolving fenestrations in the thick, perinuclear area. In contrast, both AFM and SEM showed to be much more efficient in visualizing fenestrations in these areas, including visualization of previously reported “fenestration labyrinths” [46]. Observation of the fenestration labyrinths in AFM indicates that these structures are not artificially induced after sample dehydration. Their biological role is not described yet, however, they have not been reported in LSECs *in vivo* so far.

For all described techniques, problems in the detection and measurement of fenestrations can be related to the difficulties in the detecting of fenestration edges. In label-free techniques, such as AFM and SEM, the exact edge of the fenestration can be easily defined. On the other hand, in label-dependent techniques, such as STED and SIM, blurring related to the point spread function is observed (Figure 5C, inset). Moreover, the size of fenestrations is

close to the achievable resolution of those techniques, which together with the PSF effects, may contribute to the lack of detection of some smaller pores. Small fenestrations (below 100 nm) may also be omitted due to the sampling problem – pixel size in the optical methods is usually scaled to the resolution and may result in undersampling.

Interestingly, we measured fenestrations with a size smaller than the theoretical resolution limit of our SIM system, but these results agree both with earlier SIM data shown by Cogger et al. [53], and, more importantly, with the underlying 'ground-truth', higher resolution correlative SEM images. The theoretical resolution of SIM in our setup (excitation/emission 488/525 nm, 1.42NA objective) calculated using the Rayleigh criterion is about 110 nm; however, less strict criteria such as the Abbe limit or Sparrow limit show our theoretical resolution closer to 80 nm, which aligns closer to our actual measurements. Demmerle et al. highlighted the difficulties in assessing the resolution in super-resolution imaging and in comparing between them [54]. In our case, there are several possible explanations for why we observed smaller than expected fenestrations, however, we are not certain of the definite cause here. Reconstruction of raw SIM data into super-resolution images requires a significant amount of post-acquisition image processing, and the final image is presented as a z projection, which in combination with not truly isotropic SIM data could make fenestrations appear smaller. The threshold used for image segmentation may also influence the measured diameters, as the exact location of the edge of a fenestration can be interpreted in multiple ways. Finally, it is possible that fenestrations may benefit from appearing as negative objects, with strong signal coming from the positively-stained objects (i.e., membrane) around them, as opposed to trying to image and measure weakly-fluorescent, isolated positive objects; having a better signal-to-noise ratio generally results in better reconstruction and resolution.

Our correlations were independent of cytochalasin B treatment. Other reports, applying STED and SEM individually, showed no changes in fenestration diameters of LSEC treated with cytochalasin B [26, 49]. It indicates that the level of actin polymerization does not additionally alter fenestration diameters during dehydration. Altogether, it allows us to conclude that the dehydration of samples in fixed-dried LSEC is significant, but constant, allowing for comparison between samples prepared, measured, and analyzed in the same way. We emphasize the need to analyze a large number of fenestrations (to avoid bias due to the large cell-to-cell differences). Recently developed automatic image analyses allow for the measurement of thousands of fenestrations a relatively quickly [39] or precise measurements of fenestrations in low-resolution images [55].

A comparison of STED and AFM provided further details. AFM resulted in less than 10% increase in mean fenestration size in comparison to STED. The effect might be ascribed to better AFM resolution – the PSF function causes blurring of the fenestration edges resulting in lower measured fenestration diameter. However, AFM imaging appeared to be prone to changes in mechanical properties. Data obtained using force tomography (a presentation of the image of the same area of LSEC reconstructed for increasing load force) showed load force dependence of fenestration size in living and FA/GA-fixed LSEC. The combined analysis of the elasticity and fenestration diameters for different loading forces indicate that increased cell rigidity aggravates tip-induced dilation of fenestrations. Cytochalasins reduce the Young's modulus of LSEC [43] and the effect can be translated into the fixed cells too [56]. Cytochalasin B is known to promote actin depolymerization but without affecting actin cross-linking proteins [57]. These findings suggest that the change in LSEC elasticity after cytochalasin B treatment is mainly due to the reduction of actin stress fibers rather than disruption of actin mesh. Fenestra-associated cytoskeleton rings (FACR) within actin mesh are preserved after cytochalasin B treatment and the changes of fenestration size within FACR depend on the (not fully known up to date) structure building membrane and actin [1]. These data is in agreement with most LSEC studies with cytochalasin B reporting no changes in the fenestration diameter [13]. Therefore, we assume no influence of cytochalasin B on fenestration diameter, but the decreased elastic modulus and lack of stress fibers should be taken into consideration and imaging with cantilevers of low spring constant and use of load force close to the contact point should be applied to minimize the tip-induced deformation.

In general, all presented methods have their advantages and limitations, summarized in Table 1. We recommend the selection of microscopy techniques depending on the planned experiment. SIM and SEM provide higher throughput measurements of single cells or even groups of LSEC. SEM provides unprecedented resolution in the whole range of image size from individual sieve plates up to several LSEC. However, it requires sample drying and a relatively long sample preparation procedure. Therefore, SIM can be a first-choice method to quickly assess the effect of various drugs or toxins of LSEC. The limited resolution and lack of the ability to resolve fenestration in the perinuclear areas should not prevent the observation of relatively large changes in the porosity when cells are flat and cultured at low confluence. Its limitation is the resolution and (together with STED) the

Table 1: Summary of presented microscopies.

	Wet fixed	Fixed dried	Fenestration size enlargement	Labeling	Live LSEC tracking	Applicability	Throughput	Measured feature size*	Accuracy
SEM	No	Yes	>30%	None	No	Whole cells and individual sieve plates	High 0.5–3 min/cell	<10 nm	Number of fenestrations
SIM	Yes[#]	–	None	Many dyes	Not reported yet	Whole cells and individual sieve plates	High 0.5–3 min/cell	~80 nm	Size of fenestrations
STED	Yes[#]	–	None	Limited dyes	Yes	Whole cells	Moderate high 5–8 min/cell	~50 nm	Size of fenestrations
						Individual sieve plates	High 10–30 s/area	~50 nm	Size of fenestrations
AFM	Yes[†]	Yes	+10%**	None	Yes	Whole cells	Low 25–40 min/cell	~80 nm	Number of fenestrations
						Individual sieve plates	Low 2–5 min/area	~30 nm	Number of fenestrations Size of fenestrations

*The theoretical resolution limit of SIM on our system is ~110 nm, but the combination with the thresholding of the image analysis yields a measurement size of ~80 nm; **For cantilevers with sharpened tip; dependent on the tip apex size; #FA fixation recommended; †GA fixation recommended.

ability to resolve and measure fenestrations in perinuclear areas. STED allows a balance between the throughput (sample preparation plus measurement time) and the accuracy of measurements. Moreover, the optical techniques allow for simultaneous colocalization with other structures that can be additionally labeled. Both STED and AFM are scanning techniques which make them relatively slow. Large images of the whole LSEC are possible to obtain with some limitations. AFM requires up to 40 min per high-resolution image of a single LSEC while during long STED measurements (up to 8 min per LSEC), bleaching and thermal drift might hamper the imaging. Moreover, performing additional high-magnification images using AFM is required to obtain a resolution comparable with SEM. Both STED and AFM should be the best choice when small images of part of LSEC are analyzed for size measurements. Moreover, both were reported to be applicable for live LSEC imaging.

SEM and AFM do not require sample labeling; hence the results provided by those techniques do not depend on the quality and density of labeling, making the analysis more reproducible. SIM can be used with almost all available dyes, while STED requires more specialized dyes. AFM can be used without any or with minimal sample preparation. We used this to our advantage to study the influence of each sample preparation step (required for other types of microscopies) on the topography of LSEC. Moreover, AFM remains the only technique showing fenestrations that are closed/fused within fenestrae-associated cytoskeleton rings (FACR) [58]. It also provides precise information about the height of investigated objects and allowing simultaneous assessment of the nanomechanical properties of investigated structures. Its main limitation is its low speed, which makes it impractical to use for large number of cells, as required, e.g., in screening of drug effects on LSEC morphology. On the other hand, AFM enables measurements of live LSEC and can be easily correlated with optical techniques. We therefore propose correlative live (AFM) and fixed (optical) imaging of LSEC. AFM lacks chemical information about investigated structures but provides unprecedented resolution for live LSEC imaging. The combination of AFM and fluorescence solves this problem. Here we propose that after the AFM experiment, when the dynamics of the structure of interest is captured, the sample can be fixed, labeled, and visualized using fluorescence microscopy. The resulting chemical information can be further extrapolated to the AFM data. We believe that such an approach in the near future would allow for a better understanding of the origin of fenestrations by disclosing the structure of fenestration-associated cytoskeletal structures as, e.g., fenestration-forming centers, defenestration centers, fenestration-associated cytoskeleton rings. Nowadays, the new dyes for live cell imaging are of great interest for researchers, but long-lasting fluorescence imaging options are limited.

The main problems are related to phototoxicity, bleaching and dye-sample interaction [25]. The latter issue is significant for LSEC imaging as limited responsiveness of LSEC is a major issue in tracking cell membrane dynamics. The presented approach, alongside with AFM, can be used for high-resolution imaging of fenestrations in live LSEC to test drug responses.

5 Conclusions

We compared several techniques (SEM, SIM, STED, AFM) allowing for visualization of fenestrations in LSECs *in vitro* at the resolution allowing calculation of the fenestration diameter. We provided the first direct comparison of fenestrations in wet-fixed and fixed-dried LSEC. We showed that fenestration diameters measured using SEM are >30% larger than with other wet techniques. We advise using SEM to describe the number of fenestrations per cell. Fenestration diameters should ideally be calculated using wet-fixed samples. AFM provides nanometer range resolution in living and fixed LSECs ensuring useful coupling with the optical microscopy. Moreover, the construction of the AFM head makes it an easily applicable extension for most optical nanoscopy modalities that are based on inverted geometry. We provided the first comparison of FA/GA fixation on LSEC diameters measured with AFM. Glutaraldehyde fixation is highly advised for AFM to minimize the uncertainty of tip-induced sample alterations. Independent use of all presented techniques can be applied for measurements of fenestrations. However, their combination can provide novel, additional information from the correlative perspective, particularly AFM and conventional fluorescence microscopy, which combines high-resolution topographical information with cellular protein identification.

Acknowledgments: The authors want to thank Abberior Instruments for providing access to a STEDYCON system located at JPK Headquarters in Berlin and Randi Olsen and Tom-Ivar Eilertsen from Advanced Microscopy Core Facility at UiT for their help with sample preparation and imaging with scanning electron microscopy.
Author contribution: All the authors have accepted responsibility for the entire content of this submitted manuscript and approved submission.
Research funding: This work is supported by the Polish National Science Centre under the "SYMFONIA 3" project, grant agreement no.: UMO-2015/16/W/NZ4/00070, the Research Council of Norway Nano2021 program grant to "NanoChip" Grant no. 288565, and the Polish National Science Centre under the "SONATA 15" Project, Grant Agreement No.: UMO-2019/35/D/NZ3/01804, and the European Union's Horizon 2020 research and innovation program under the Marie Sklodowska-Curie grant agreement no. 766181, project "DeLIVER".
Conflict of interest statement: The authors declare no conflicts of interest regarding this article.

References

[1] B. Zapotoczny, F. Braet, E. Kus, et al., "Actin-spectrin scaffold supports open fenestrae in liver sinusoidal endothelial cells," *Traffic*, vol. 20, no. 12, pp. 1–11, 2019.
[2] B. Zapotoczny, K. Szafranska, E. Kus, et al., "Tracking fenestrae dynamics in live murine liver sinusoidal endothelial cells," *Hepatology*, vol. 69, no. 2, pp. 876–888, 2019.
[3] R. Diekmann, Ø. I. Helle, C. I. Øie, et al., "Chip-based wide field-of-view nanoscopy," *Nat. Photonics*, vol. 11, no. 5, pp. 322–328, 2017.
[4] M. Müller, V. Mönkemöller, S. Hennig, W. Hübner, and T. Huser, "Open-source image reconstruction of super-resolution structured illumination microscopy data in ImageJ," *Nat. Commun.*, vol. 7, p. 10980, 2016.
[5] H. Mao, R. Diekmann, H. P. H. Liang, et al., "Cost-efficient nanoscopy reveals nanoscale architecture of liver cells and platelets," *Nanophotonics*, vol. 8, no. 7, pp. 1299–1313, 2019.
[6] V. C. Cogger, N. J. Hunt, and D. G. Le Couteur, "Fenestrations in the liver sinusoidal endothelial cell," in *The Liver: Biology and Pathobiology*, 6th ed. New Jersey, John Wiley & Sons Ltd., 2020, pp. 435–443.
[7] R. Fraser, V. C. Cogger, B. Dobbs, et al., "The liver sieve and atherosclerosis," *Pathology*, vol. 44, no. 3, pp. 181–186, 2012.
[8] D. G. Le Couteur, R. Fraser, V. C. Cogger, and A. J. McLean, "Hepatic pseudocapillarisation and atherosclerosis in ageing," *Lancet*, vol. 359, no. 9317, pp. 1612–1615, 2002.
[9] E. Kus, P. Kaczara, I. Czyzynska-Cichon, et al., "LSEC fenestrae are preserved despite pro-inflammatory phenotype of liver sinusoidal endothelial cells in mice on high fat diet," *Front. Physiol.*, vol. 12, p. 6, 2019.
[10] E. Maslak, A. Gregorius, and S. Chlopicki, "Liver sinusoidal endothelial cells (LSECs) function and NAFLD; NO-based therapy targeted to the liver," *Pharmacol. Rep.*, vol. 67, no. 4, pp. 689–694, 2015.
[11] B. Zapotoczny, K. Szafranska, K. Owczarczyk, E. Kus, S. Chlopicki, and M. Szymonski, "Atomic force microscopy reveals the dynamic morphology of fenestrations in live liver sinusoidal endothelial cells," *Sci. Rep.*, vol. 7, no. 1, p. 7994, 2017.
[12] N. J. Hunt, G. P. Lockwood, A. Warren, et al., "Manipulating fenestrations in young and old liver sinusoidal endothelial cells," *Am. J. Physiol. Gastrointest. Liver Physiol.*, vol. 316, no. 1, pp. G144–G154, 2019.

[13] K. Szafranska, C. F. Holte, L. D. Kruse, P. McCourt, and B. Zapotoczny, "The wHole story about fenestrations in liver sinusoidal endothelial cells," *Front. Physiol.*, vol. 12, pp. 1–25, 2021.
[14] M. Muto, M. Nishi, and T. Fujita, "Scanning electron microscopy of human liver sinusoids," *Arch. Histol. Jpn.*, vol. 40, no. 2, pp. 137–151, 1977.
[15] F. Braet, R. De Zanger, W. Kalle, A. Raap, H. Tanke, and E. Wisse, "Comparative scanning, transmission and atomic force microscopy of the microtubular cytoskeleton in fenestrated liver endothelial cells," *Scanning Microsc. Suppl.*, vol. 10, pp. 225–235, 1996, discussion 235-6.
[16] E. Wisse, "Fixation methods for electron microscopy of human and other liver," *World J. Gastroenterol.*, vol. 16, no. 23, pp. 2851–2866, 2010.
[17] F. Braet, R. De Zanger, and E. Wisse, "Drying cells for SEM, AFM and TEM by hexamethyldisilazane: a study on hepatic endothelial cells," *J. Microsc.*, vol. 186, no. Pt 1, pp. 84–87, 1997.
[18] F. Braet, R. De Zanger, M. Baekeland, E. Crabbé, P. Van Der Smissen, and E. Wisse, "Structure and dynamics of the fenestrae-associated cytoskeleton of rat liver sinusoidal endothelial cells," *Hepatology*, vol. 21, no. 1, pp. 180–189, 1995.
[19] B. Zapotoczny, K. Szafranska, E. Kus, S. Chlopicki, and M. Szymonski, "Quantification of fenestrations in liver sinusoidal endothelial cells by atomic force microscopy," *Micron*, vol. 101, pp. 48–53, 2017.
[20] B. Zapotoczny, K. Owczarczyk, K. Szafranska, E. Kus, S. Chlopicki, and M. Szymonski, "Morphology and force probing of primary murine liver sinusoidal endothelial cells," *J. Mol. Recogn.*, vol. 30, no. 7, pp. 1–8, 2017.
[21] F. Braet, C. Rotsch, E. Wisse, and M. Radmacher, "Comparison of fixed and living liver endothelial cells by atomic force microscopy," *Appl. Phys. Mater. Sci. Process*, vol. 66, pp. 575–578, 1998.
[22] F. Braet, R. De Zanger, S. Kämmer, and E. Wisse, "Noncontact versus contact imaging: an atomic force microscopic study on hepatic endothelial cells in vitro," *Int. J. Imag. Syst. Technol.*, vol. 8, no. 2, pp. 162–167, 1997.
[23] V. Mönkemöller, C. Øie, W. Hübner, T. Huser, and P. McCourt, "Multimodal super-resolution optical microscopy visualizes the close connection between membrane and the cytoskeleton," *Sci. Rep.*, vol. 5, p. 16279, 2015.
[24] C. I. Øie, V. Mönkemöller, W. Hübner, et al., "New ways of looking at very small holes - using optical nanoscopy to visualize liver sinusoidal endothelial cell fenestrations," *Nanophotonics*, vol. 7, no. 3, pp. 575–596, 2018.
[25] J. Di Martino, P. Mascalchi, P. Legros, et al., "Actin depolymerization in dedifferentiated liver sinusoidal endothelial cells promotes fenestrae re-formation," *Hepatol. Commun.*, vol. 3, no. 2, pp. 213–219, 2019.
[26] J. Di Martino, P. Mascalchi, P. Legros, et al., "STED microscopy: a simplified method for liver sinusoidal endothelial *fenestrae* analysis," *Biol. Cell.*, vol. 110, no. 7, pp. 1–10, 2018.
[27] F. Braet and E. Wisse, "AFM imaging of fenestrated liver sinusoidal endothelial cells," *Micron*, vol. 43, no. 12, pp. 1252–1258, 2012.
[28] L. M. Hirvonen and S. Cox, "STORM without enzymatic oxygen scavenging for correlative atomic force and fluorescence superresolution microscopy STORM without enzymatic oxygen scavenging for correlative atomic force and fluorescence superresolution microscopy," *Methods Appl. Fluoresc.*, vol. 6, no. 4, p. 045002, 2018.
[29] G. G. Qin, W.-H. Li, J.-C. Xu, et al., "Development of integrated atomic force microscopy and fluorescence microscopy for single-molecule analysis in living cells," *Chin. J. Anal. Chem.*, vol. 45, no. 12, pp. 1813–1823, 2017.
[30] P. Bondia, S. Casado, and C. Flors, "Correlative super-resolution fluorescence imaging and atomic force microscopy for the characterization of biological samples," in *Super-Resolution Microscopy*, vol. 1663, H. Erfle, Ed., New York, NY, Humana Press, 2017, pp. 105–113. Methods in Molecular Biology.
[31] B. Harke, J. V. Chacko, H. Haschke, C. Canale, and A. Diaspro, "A novel nanoscopic tool by combining AFM with STED microscopy," *Opt. Nanoscopy*, vol. 1, no. 1, pp. 1–6, 2012.
[32] M. Cosentino, C. Canale, P. Bianchini, and A. Diaspro, "AFM-STED correlative nanoscopy reveals a dark side in fluorescence microscopy imaging," *Sci. Adv.*, vol. 5, no. 6, pp. 1–8, 2019.
[33] A. I. Gómez-Varela, D. R. Stamov, A. Miranda, et al., "Simultaneous co-localized super-resolution fluorescence microscopy and atomic force microscopy: combined SIM and AFM platform for the life sciences," *Sci. Rep.*, vol. 10, no. 1, pp. 1–10, 2020.
[34] F. Braet, R. de Zanger, C. Seynaeve, and E. Wisse, "A comparative atomic force microscopy study on living skin fibroblasts and liver endothelial cells," *J. Electron. Microsc.*, vol. 50, no. 4, pp. 283–290, 2001.
[35] F. Braet, D. J. Taatjes, and E. Wisse, "Probing the unseen structure and function of liver cells through atomic force microscopy," *Semin. Cell Dev. Biol.*, vol. 73, pp. 13–30, 2018.
[36] J. C. Tinguely, A. M. Steyer, C. I. Øie, et al., "Photonic-chip assisted correlative light and electron microscopy," *Commun. Biol.*, vol. 3, no. 739, pp. 1–7, 2020.
[37] F. Braet, W. H. J. Kalle, R. B. De Zanger, et al., "Comparative atomic force and scanning electron microscopy: an investigation on fenestrated endothelial cells in vitro," *J. Microsc.*, vol. 181, no. 1, pp. 10–17, 1996.
[38] R. Fraser, B. R. Dobbs, and G. W. T. Rogers, "Lipoproteins and the liver sieve: the role of the fenestrated sinusoidal endothelium in lipoprotein metabolism, atherosclerosis, and cirrhosis," *Hepatology*, vol. 21, no. 3, pp. 863–874, 1995.
[39] K. Szafranska, C. F. Holte, L. D. Kruse, et al., "Quantitative analysis methods for studying fenestrations in liver sinusoidal endothelial cells. A comparative study," *Micron*, vol. 150, p. 103121, 2021.
[40] E. Wegel, A. Göhler, B. C. Lagerholm, et al., "Imaging cellular structures in super-resolution with SIM, STED and Localisation Microscopy: a practical comparison," *Sci. Rep.*, vol. 6, no. May, pp. 1–13, 2016.
[41] Y. F. Dufrêne, D. Martínez-Martín, I. Medalsy, D. Alsteens, and D. J. Müller, "Multiparametric imaging of biological systems by force-distance curve-based AFM," *Nat. Methods*, vol. 10, no. 9, pp. 847–854, 2013.
[42] P. Li, J. Zhou, W. Li, et al., "Characterizing liver sinusoidal endothelial cell fenestrae on soft substrates upon AFM imaging and deep learning," *Biochim. Biophys. Acta, Gen. Subj.*, vol. 1864, no. 12, p. 129702, 2020.

[43] B. Zapotoczny, F. Braet, E. Wisse, M. Lekka, and M. Szymonski, "Biophysical nanocharacterization of liver sinusoidal endothelial cells through atomic force microscopy," Biophys. Rev., vol. 12, no. 3, pp. 625–636, 2020.
[44] J. Schindelin, I. Arganda-Carreras, E. Frise, et al., "Fiji: an open-source platform for biological-image analysis," *Nat. Methods*, vol. 9, pp. 676–682, 2012.
[45] D. R. Whelan and T. D. M. Bell, "Image artifacts in single molecule localization microscopy: why optimization of sample preparation protocols matters," *Sci. Rep.*, vol. 5, pp. 1–10, 2015.
[46] F. Braet, J. Riches, W. Geerts, K. A. Jahn, E. Wisse, and P. Frederik, "Three-dimensional organization of fenestrae labyrinths in liver sinusoidal endothelial cells," *Liver Int.*, vol. 29, no. 4, pp. 603–613, 2009.
[47] R. M. Brunetti, G. Kockelkoren, P. Raghavan, et al., "WASP integrates substrate topology and cell polarity to guide neutrophil migration," *J. Cell Biol.*, vol. 221, no. 2, 2022. https://doi.org/10.1083/jcb.202104046.
[48] V. Mönkemöller, M. Schüttpelz, P. McCourt, K. Sørensen, B. Smedsrød, and T. Huser, "Imaging fenestrations in liver sinusoidal endothelial cells by optical localization microscopy," *Phys. Chem. Chem. Phys.*, vol. 16, no. 24, pp. 12576–12581, 2014.
[49] A. M. Steffan, J. L. Gendrault, and A. Kirn, "Increase in the number of fenestrae in mouse endothelial liver cells by altering the cytoskeleton with cytochalasin B," *Hepatology*, vol. 7, no. 6, pp. 1230–1238, 1987.
[50] E. Wisse, R. B. de Zanger, K. Charels, P. Van Der Smissen, and R. S. McCuskey, "The liver sieve: considerations concerning the structure and function of endothelial fenestrae, the sinusoidal wall and the space of Disse," *Hepatology*, vol. 5, no. 4, pp. 683–692, 1985.
[51] F. Braet and E. Wisse, "Structural and functional aspects of liver sinusoidal endothelial cell fenestrae: a review," *Comp. Hepatol.*, vol. 1, 2002. https://doi.org/10.1186/1476-5926-1-1.
[52] D. Svistounov, A. Warren, G. P. McNerney, et al., "The relationship between fenestrations, sieve plates and rafts in liver sinusoidal endothelial cells," *PLoS One*, vol. 7, no. 9, pp. 1–9, 2012.
[53] V. C. Cogger, G. P. McNerney, T. Nyunt, et al., "Three-dimensional structured illumination microscopy of liver sinusoidal endothelial cell fenestrations," *J. Struct. Biol.*, vol. 171, no. 3, pp. 382–388, 2010.
[54] J. Demmerle, E. Wegel, L. Schermelleh, and I. M. Dobbie, "Assessing resolution in super-resolution imaging," *Methods*, vol. 88, pp. 3–10, 2015.
[55] M. Giergiel, B. Zapotoczny, I. Czyzynska-Cichon, J. Konior, and M. Szymonski, "AFM image analysis of porous structures by means of neural networks," *Biomed. Signal Process Control J.*, vol. 71A, p. 103097, 2021.
[56] M. Targosz-Korecka, G. Daniel Brzezinka, J. Danilkiewicz, Z. Rajfur, and M. Szymonski, "Glutaraldehyde fixation preserves the trend of elasticity alterations for endothelial cells exposed to TNF-α," *Cytoskeleton*, vol. 72, no. 3, pp. 124–130, 2015.
[57] S. MacLean-Fletcher and T. D. Pollard, "Mechanism of action of cytochalasin B on actin," *Cell*, vol. 20, no. 2, pp. 329–341, 1980.
[58] F. Braet, R. De Zanger, E. Crabbe, and E. Wisse, "New observations on cytoskeleton and fenestrae in isolated rat liver sinusoidal endothelial cells," *J. Gastroenterol. Hepatol.*, vol. 10, pp. 3–7, 1995.

Supplementary Material: The online version of this article offers supplementary material (https://doi.org/10.1515/nanoph-2021-0818).

SUPPLEMENTARY INFORMATION

From fixed-dried to wet-fixed to live – comparative super-resolution microscopy of liver sinusoidal endothelial cell fenestrations

Karolina Szafranska[1], Tanja Neuman[2], Zbigniew Baster[3], Zenon Rajfur[3], Oskar Szelest[4], Christopher Holte[1], Agata Kubisiak[3], Edyta Kus[5], Deanna L. Wolfson[7], Stefan Chlopicki[5,6], Balpreet S. Ahluwalia[7], Malgorzata Lekka[8], Marek Szymonski[3], Peter McCourt[1], Bartlomiej Zapotoczny[1,8*]

[1] Department of Medical Biology, Vascular Biology Research Group, University of Tromsø (UiT), The Arctic University of Norway, Tromsø, Norway

[2] JPK BioAFM Business, Nano Surfaces and Metrology Division, Bruker Nano GmbH, Berlin, Germany

[3] Marian Smoluchowski Institute of Physics, Faculty of Physics, Astronomy and Applied Computer Sciences, Jagiellonian University, Krakow, Poland

[4] ICLab S.z.o.o, Krakow, Poland

[5] Jagiellonian Centre for Experimental Therapeutics (JCET), Jagiellonian University, Krakow, Poland

[6] Chair of Pharmacology, Jagiellonian University Medical College, Krakow, Poland

[7] Department of Physics and Technology, UiT-The Arctic University of Norway, Tromsø, Norway

[8] Institute of Nuclear Physics, Polish Academy of Sciences, Kraków, Poland

*Contact information

Corresponding author: Bartlomiej Zapotoczny. Tel.: +48 12 662 82 86.

e-mail address: bartlomiej.zapotoczny@ifj.edu.pl, (B. Zapotoczny).

Financial Support

This work is supported by the Polish National Science Centre under the “SYMFONIA 3” project, grant agreement no.: UMO-2015/16/W/NZ4/00070, the Research Council of Research Council of Norway Nano2021 program grant to “NanoChip” Grant no. 288565, and the Polish National Science Centre under the “SONATA 15” Project, Grant Agreement No.: UMO-2019/35/D/NZ3/01804, and the European Union’s Horizon 2020 research and innovation program under the Marie Sklodowska-Curie grant agreement no. 766181, project “DeLIVER”

1. Cell isolation and sample handling

Firstly, livers were initially perfused to remove the blood and then digested using Liberase TM (*Roche)*. After digestion, the cells were released from Glisson's capsule into a cold (4°C) perfusion buffer containing 1% BSA. The obtained suspension of cells was subjected to several centrifugations (including 25-50% Percoll gradient separation for AFM/STED experiments) to separate hepatocytes, remaining blood cells, and non-parenchymal cells. Thereafter, LSEC and Kupffer cells were separated by immuno-magnetic separation using endothelium specific CD146 MicroBeads (*MACS, Miltenyi Biotec*, Germany). After isolation, cells were seeded on uncoated glass coverslips and incubated in 5% CO_2 at 37°C in EGM-2 cell culture medium (*Lonza*) for 12-15 hours for AFM/STED or on fibronectin-coated glass coverslips in RPMI-1640 (Sigma-Aldrich) for 4-6 hours for SIM/SEM, STED/SEM, and AFM/SEM. Seeding conditions were optimized according to the specific microscopy requirements, using established methodology [1]. Large gaps, i.e. micron-sized holes in a membrane, were observed in freshly isolated LSEC after seeding. By comparing live and fixed LSEC, we noticed that no new gap formation occurred when LSEC were fixed with 3.6% formaldehyde (FA) for 15 minutes or 1% GA for 2 minutes. By monitoring LSEC morphology live, instead of fixed, when using AFM/conventional fluorescence microscopy, we showed that wet-fixation of cultured LSEC does not damage sieve plates. However, by investigating individual LSEC using AFM on each step of sample preparation, we noticed that thorough rinsing (pipetting) of samples with live or fixed cells could damage the delicate structure of fenestrations within sieve plates. We used warm (37°C) buffers and fixative agents combined with slow aspiration and delicate rinsing to reduce gap formation.

2. More about the observation in correlative imaging of LSEC

In both SIM/SEM and STED/SEM we observed that visualization of thick areas of LSEC with optical methods is hampered by such "thickness". Representative images are presented for SIM/SEM (**Supplementary figure 1**) and STED/SEM (**Supplementary figure 2**). The effect is a result of several factors. In contrast to SEM where imaging is done from the top, in both STED and SIM imaging is done in the inverted microscope setups with both excitation and emission beams coming from underneath the samples and cells. In STED, this forces the adjustment of the focal plane to the cell periphery area with fenestration (close to the substrate) and therefore fenestrations in the nuclear area are in the different focal plane, and thus not resolved properly. In SIM, the image reconstruction requires a series of z stacks at every 125 nm and then each plane is reconstructed. The images are not confocal so signal from the high/nuclear area where some fenestrations are observed are burdened with the signal from the rest of the cell body. For the final visualization we use projection images that average all z stacks which helps to improve signal to noise ratio and reduces background signal but it also disables observation of the objects that are not uniform throughout the whole cell. Another factor that causes this effect is the non-perpendicular orientation of those fenestrations, due to the slope from height difference between nucleus (2-3 µm) and cell periphery (0.3-0.5 µm).

Moreover, so called fenestration labyrinths are observed in these areas (**Supplementray figure 3**) which further interfere with imaging. As fenestrations are negative structures observed in optical techniques (i.e. we are looking for lack of a staining within fenestrations created by signal for the dye particles of the surrounding membrane), resolving fenestrations in these areas is overburdened with large errors.

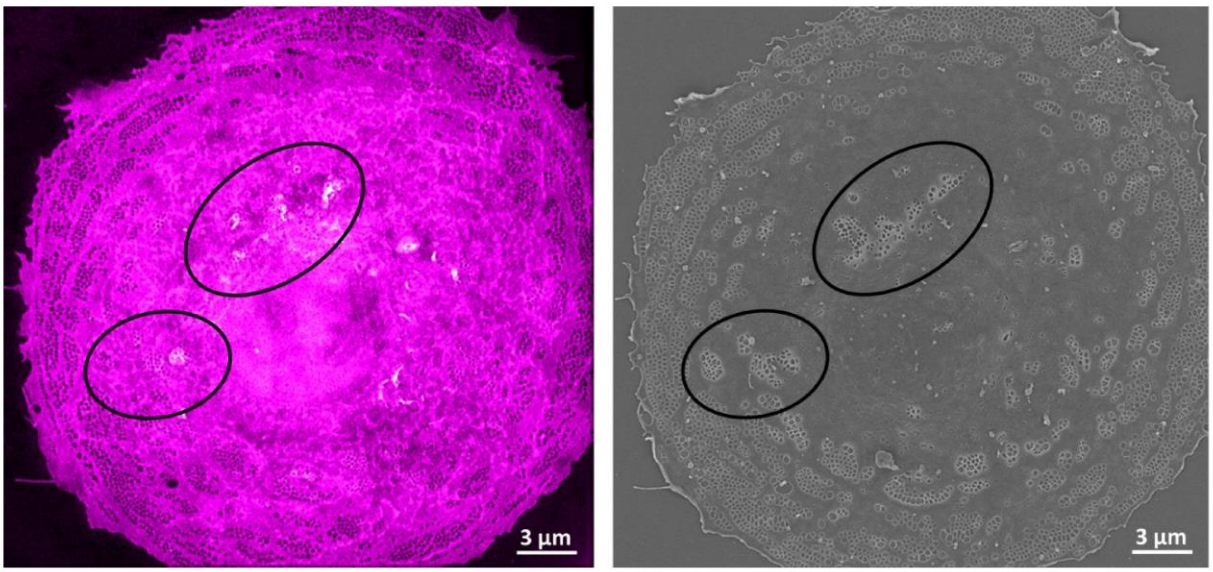

Supplementary Figure 1 | Correlative SIM and SEM microscopy of a liver sinusoidal endothelial cell. Images present a representative LSEC analysed in Figure 1. The perinuclear zone, where the cell is thick, hampers visualization of fenestrations (encircled area). As a result, the number of fenestrations is underestimated in SIM.

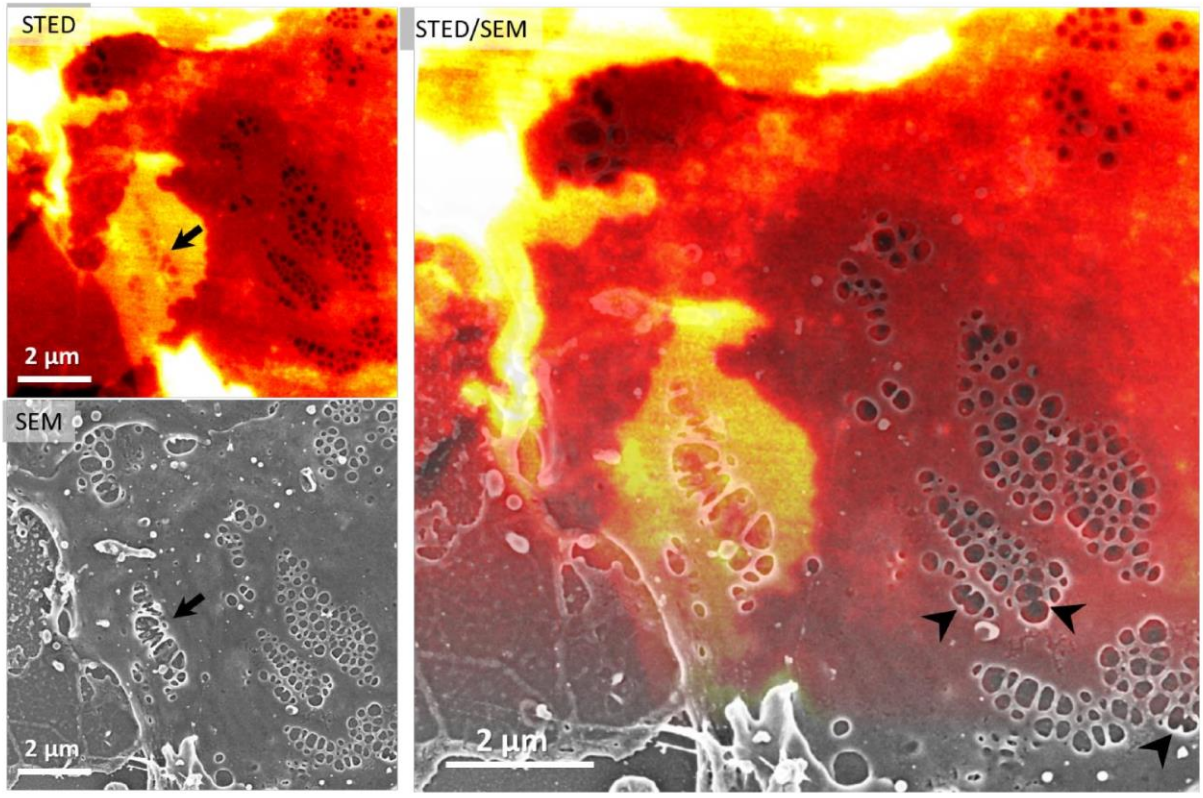

Supplementary Figure 2 | Correlative STED and SEM microscopy of part of a LSEC. Images present a sieve plate that was selected for the analysis in Figure 2. The area of LSEC where the cell is thick hampers visualization of fenestrations (**arrow**). The same area is distorted in SEM, as dehydration affects these areas more than the flatter areas. The coalescence of fenestrations is also observed in SEM but not in STED (**arrowheads**).

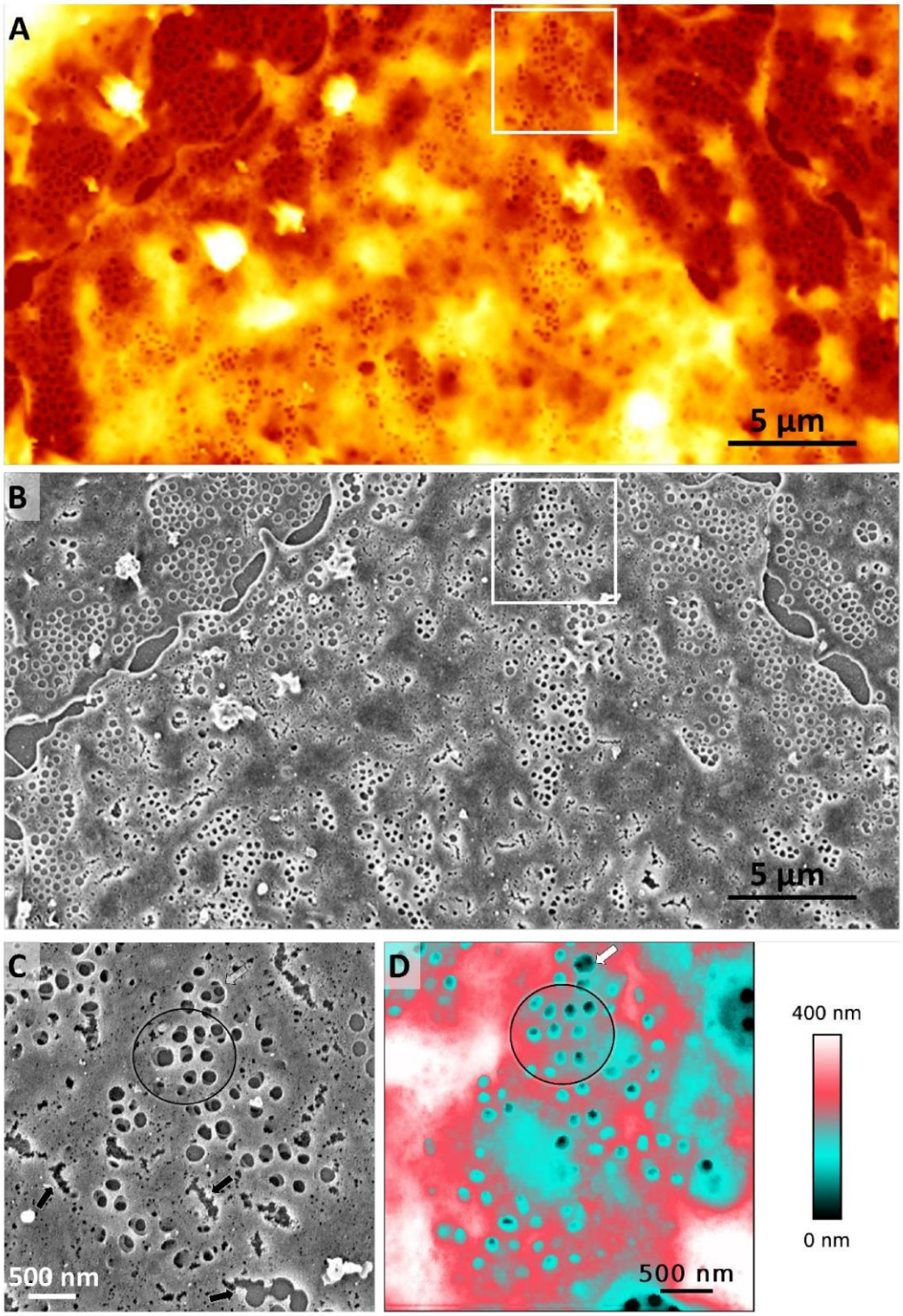

Supplementary Figure 3 | Correlative AFM and SEM microscopy of parts of LSECs. Images present an interconnection of cells that was selected for the analysis in Figure 4. Large view AFM image (**A**) allows for identification of fenestrations and assessment of cell height and comparison with the corresponding area in SEM (**B**). The pixel-point (as introduced in[2]) of 80 nm does not allow for precise measurement of fenestration diameter. High-resolution AFM image analysis was performed in the selected area of the SEM micrograph. After dehydration cracks in cells are often observed (**black arrows**). (**C**). Encircled area in SEM (**C**) and AFM (**D**) highlight fenestration labyrinths – the areas in which fenestration lie over other fenestrations. Transcellular regions, where AFM tip reached glass substrate are presented as black. Rounded cyan-coloured areas indicate fenestrations, for which cell membrane was observed within them. In particular, within one top fenestration more than one fenestration can be observed in the bottom layer (**white arrow**).

2. The effect of permeabilisation on LSEC fenestrations

In order to investigate the influence of staining procedures on LSEC morphology, we stained LSEC with CellMask Deep Red and with phalloidin-Atto488, both preceded by 5 min 0.1% Triton X-100 treatment. We found the morphology of LSEC to be unaltered after staining; however, we observed significant changes in the morphology of fenestrations in permeabilized LSEC (**Figure 4**).

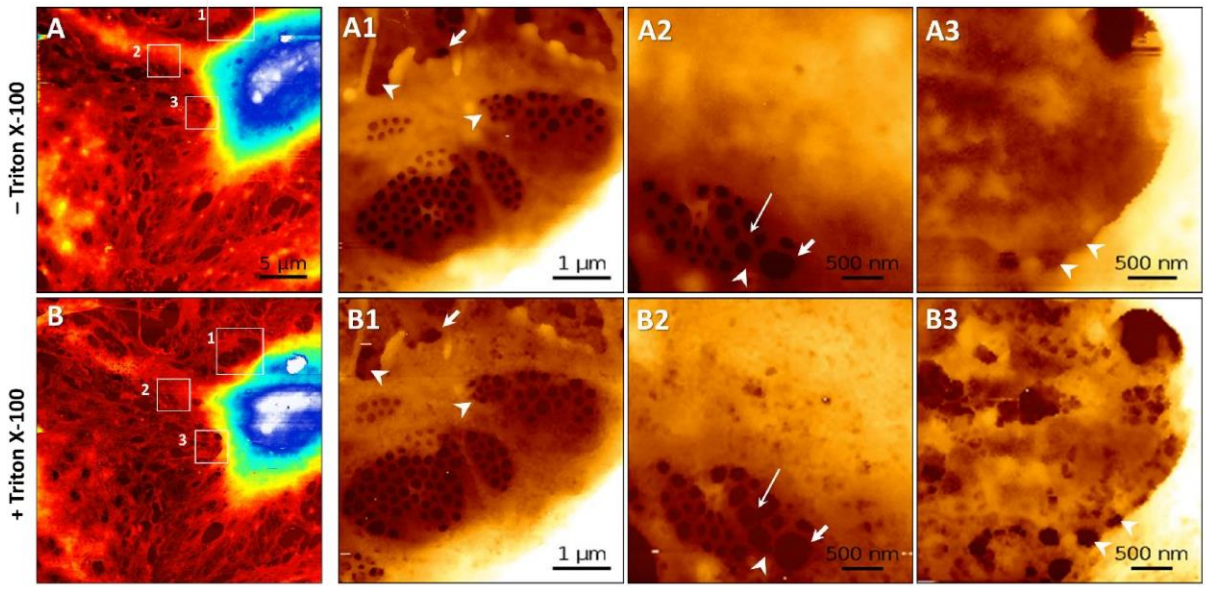

Supplementary Figure 4 | Changes in the topography of LSEC in response to Triton X-100 treatment measured using QI AFM. **A,B** FA-fixed LSEC. **A1-3** Areas of interest were selected and measured in high resolution. **B** the same area as A, measured after treatment with 0.1% Triton X-100 for 5 minutes. **B1-3** The same high-resolution images as in A1-3 were selected after permeabilization. The formation of new fenestrations (**arrowhead**), enlargement (**short arrow**) and fusion (**long arrow**) of existing fenestrations was indicated. The same area was scanned twice to exclude the effect of AFM tip altering the samples – no changes induced by the AFM tip were observed.

Triton X-100 is a widely used detergent for permeabilization of the cell membrane [3]. It enables dyes and antibodies to reach the interior of the cell. Triton X-100 does not change the cortical cytoskeleton, and the overall cell morphology remains unchanged [4]. Nevertheless, even the slightest changes may influence the calculated dimensions when investigating objects at the nanoscale, such as fenestrations in LSEC. Indeed, we observed several new openings in the cell cytoplasm, and some of them were the size of fenestrations (**Figure 4, arrowhead**). Moreover, occasionally an enlargement in individual fenestrations was noticed, mainly due to coalescence of fenestrations (**Figure 4, arrows**). Similarly to another report [5], we did not observe any significant changes in cell elasticity after 0.1% Triton X-100 treatment.

The smooth cell membrane visualized with AFM for fixed cells became rough and distorted after 5 minutes of 0.1% Triton X-100 treatment. The merging of individual fenestrations and the formation of new open fenestrations were observed. However, the overall porosity seems to be only slightly affected, as most of the fenestrations gathered in sieve plates can be clearly identified. Nevertheless, we recommend using non-permeabilized cells when a detailed analysis of fenestration diameter is performed.

3. The effect of formaldehyde (FA) fixation on imaging of fenestrations in LSEC using AFM

Cytochalasin B was reported to not affect fenestration diameters. Here, we observed an increase in FA-fixed cells treated with cytochalasin B for the same load force used in the experiment (**Supplementary figure 5**). We observed higher load-force-dependence for cytochalasin B treated cells than for the control. Since the fenestration scaffold is made of actin [1],[6] and cytochalasin disrupts actin, the effect is expected for large load force values (here we used 350 pN). In **Figure 3** we showed that GA provides better crosslinking of proteins than FA resulting in higher apparent Young's modulus values. When we analysed LSEC treated with cytochalasin B and fixed using GA the enlargement vanished. Therefore, we advise using GA-fixed LSEC (**Figure 4**), or use of minimal load force of < 100 pN (close to the contact point) (**Figure 5**), when fenestration diameters are analysed with AFM

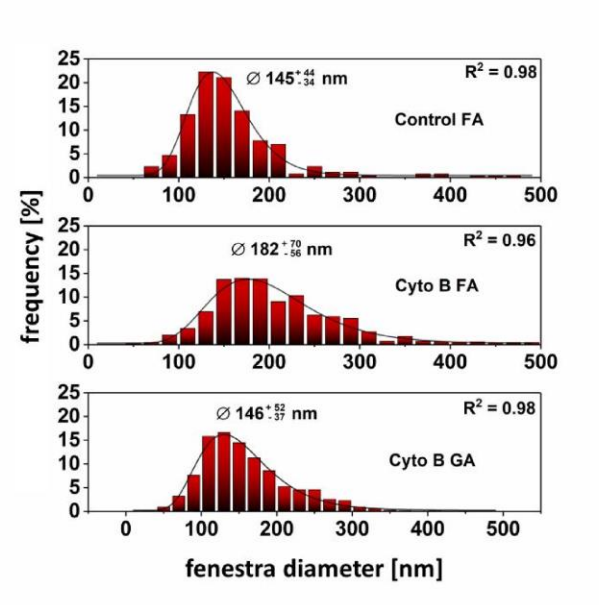

Supplementary Figure 5 | The distribution of fenestration diameters obtained as a result of AFM measurements and analysis of LSEC fixed with glutaraldehyde (GA) and formaldehyde (FA), both control and treated with 21 µM cytochalasin B for 30 minutes prior to fixation. The load force of 350 pN was applied in all measurements (k=0.1, tip apex 25 nm). Mean values and standard deviation were presented above corresponding plot, resulting from log-normal fit.

Supplementary bibliography

[1] K. Szafranska et al., “Quantitative analysis methods for studying fenestrations in liver sinusoidal endothelial cells. A comparative study,” Micron, p. 103121, 2021, doi: https://doi.org/10.1016/j.micron.2021.103121.

[2] B. Zapotoczny, K. Szafranska, K. Owczarczyk, E. Kus, S. Chlopicki, and M. Szymonski, “Atomic Force Microscopy Reveals the Dynamic Morphology of Fenestrations in Live Liver Sinusoidal Endothelial Cells,” Sci. Rep., vol. 7, no. 1, p. 7994, 2017, doi: 10.1038/s41598-017-08555-0.

[3] M. Le Maire, P. Champeil, and J. V. Møller, “Interaction of membrane proteins and lipids with solubilizing detergents,” Biochim. Biophys. Acta - Biomembr., vol. 1508, no. 1–2, pp. 86–111, 2000, doi: 10.1016/S0304-4157(00)00010-1.

[4] X. Zhang, Q. Tang, L. Wu, J. Huang, and Y. Chen, “AFM visualization of cortical filaments/network under cell-bound membrane vesicles,” Biochim. Biophys. Acta - Biomembr., vol. 1848, no. 10, pp. 2225–2232, 2015, doi: 10.1016/j.bbamem.2015.06.025.

[5] K. B. Grimm, H. Oberleithner, and J. Fels, “Fixed endothelial cells exhibit physiologically relevant nanomechanics of the cortical actin web,” Nanotechnology, vol. 25, no. 21, 2014, doi: 10.1088/0957-4484/25/21/215101.

[6] V. Mönkemöller, C. Øie, W. Hübner, T. Huser, and P. McCourt, “Multimodal super-resolution optical microscopy visualizes the close connection between membrane and the cytoskeleton in liver sinusoidal endothelial cell fenestrations.,” Sci. Rep., vol. 5, p. 16279, 2015, doi: 10.1038/srep16279.

Paper III

Quantitative analysis methods for studying fenestrations in liver sinusoidal endothelial cells. A comparative study

Szafranska K., Holte C.F., Kruse L.D., Mao H., Øie C.I., Szymonski M., Zapotoczny B., McCourt P.A.G.

Micron
2021, vol. 150 article 103121
https://doi.org/10.1016/j.micron.2021.103121

Micron 150 (2021) 103121

Contents lists available at ScienceDirect

Micron

journal homepage: www.elsevier.com/locate/micron

Quantitative analysis methods for studying fenestrations in liver sinusoidal endothelial cells. A comparative study

K. Szafranska [a,b,*], C.F. Holte [a], L.D. Kruse [a], H. Mao [a], C.I. Øie [a], M. Szymonski [b], B. Zapotoczny [a,c], P.A.G. McCourt [a]

[a] Department of Medical Biology, Vascular Biology Research Group, University of Tromsø (UiT), The Arctic University of Norway, Norway
[b] Centre for Nanometer-Scale Science and Advanced Materials, NANOSAM, Faculty of Physics, Astronomy, and Applied Computer Science, Jagiellonian University, Krakow, Poland
[c] Institute of Nuclear Physics, Polish Academy of Sciences, 31-342, Krakow, Poland

ARTICLE INFO

Keywords:
Quantitative analysis of LSEC porosity
Machine learning
Fenestrations
Liver sinusoidal endothelial cells
Atomic force microscopy
Super-resolution microscopy

ABSTRACT

Liver Sinusoidal Endothelial Cells (LSEC) line the hepatic vasculature providing blood filtration via transmembrane nanopores called fenestrations. These structures are 50−300 nm in diameter, which is below the resolution limit of a conventional light microscopy. To date, there is no standardized method of fenestration image analysis. With this study, we provide and compare three different approaches: manual measurements, a semi-automatic (threshold-based) method, and an automatic method based on user-friendly open source machine learning software. Images were obtained using three super resolution techniques – atomic force microscopy (AFM), scanning electron microscopy (SEM), and structured illumination microscopy (SIM). Parameters describing fenestrations such as diameter, area, roundness, frequency, and porosity were measured. Finally, we studied the user bias by comparison of the data obtained by five different users applying provided analysis methods.

1. Introduction

Liver Sinusoidal Endothelial Cells (LSEC) are the interface between the blood stream and the surrounding hepatocytes in the liver. Filtration is maintained by LSEC nanopores which are also known as fenestrations. Their diameter of 50−300 nm is crucial for size dependent passive transport of plasma soluble molecules (e.g., albumin, glucose, drugs) and small nanoparticles such as chylomicron remnants (Braet and Wisse, 2002). These nanopores are typically found in groups of 5–100 called sieve plates which are located mostly in the area outside the nuclear region. Fenestrations are dynamic structures that can react to various stimuli such as drugs or change in local environment (Braet and Wisse, 2002) and adapt their diameter and/or number within minutes or even seconds (Zapotoczny et al., 2019, 2017). Along with the passive transport of macromolecules via fenestrations, LSEC also participate in the clearing of circulating waste through active uptake via scavenging receptors. A diverse array of macromolecular waste material is constantly removed from the blood circulation by clathrin-mediated endocytosis (Sørensen et al., 2012). LSEC also play an active role in the clearance of circulating polyoma virus (Simon-Santamaria et al., 2014) and bacteriophages (Øie et al., 2020).

Both the number and diameter of fenestration are important for proper liver function. Defenestration – the loss of porous morphology is an early indication of liver fibrosis, which can cause atherosclerosis due to lack of filtration of lipoproteins from the blood stream (Rogers et al., 1992). It has been reported that porosity decreases in ageing and can be a main factor contributing for the need of increasing doses of drugs targeting hepatocytes (e.g. statins) that have to pass through the pores to reach their target (Le Couteur et al., 2002; Hunt et al., 2018a). Conversely, hepatocyte mediated detoxification of drugs from the plasma, requires porous LSEC – age related loss of porosity can result in drug doses, otherwise safe for young people, being toxic for the elderly. Moreover, hepatocytes regulate the glucose plasma concentration and LSEC are responsible for the passage of insulin (via fenestrations) to facilitate glucose disposal (Tsuchiya and Accili, 2013). All these aspects confirm that the lack of a healthy LSEC phenotype plays an important role in the development of many diseases. However, recent work has shown that the ageing related loss of LSEC fenestrations may be

* Corresponding author at: Vascular Biology Research Group (VBRG), University of Tromsø (UiT), Hansine Hansens veg 18, 9019 Tromsø, Norway.
E-mail addresses: szafranska.k.j@gmail.com, karolina.szafranska@uit.no (K. Szafranska).

https://doi.org/10.1016/j.micron.2021.103121
Received 28 March 2021; Received in revised form 1 July 2021; Accepted 14 July 2021
Available online 28 July 2021

reversible by repurposing a number of existing medicines (Hunt et al., 2018b, a). In addition, new nanomedicines show promise in this regard (Hunt et al., 2020b, 2021).

To date, in almost every article describing LSEC, the fenestration size is typically shown as a histogram of diameter distribution and/or mean value of fenestration diameter. Other parameters describing LSEC's porous morphology are fenestration frequency (number of fenestrations per area, less often per cell) and porosity (percentage of cell area covered by fenestrations). Altogether, these three features allow for complete evaluation and comparison between the LSEC phenotype in health and diseases, as well as after challenge with various drugs, with ageing, etc. However, the methods by which researchers obtain these data are often vaguely described. The lack of standardization results in cumbersome comparisons between the separate experiments conducted by different researchers.

Only a few studies proposed to standardize and automate the analysis of fenestrations using images obtained by different microscopy techniques. In 2015, Cogger et al. (2015) proposed a method for isolation, sample preparation and analysis using scanning electron microscopy (SEM). The authors suggested to manually mark the cell surface area and then measure the longest fenestration diameter using free access software such as Fiji/ImageJ (Schindelin et al., 2012). Although this method can be precise, it is time consuming and requires an assumption of fenestration circularity, which may bias the results. The magnification or pixel size issues resulted from poor image resolution are not discussed in the protocol. In 2018, Di Martino et al. (2018) proposed the analysis method for STED (Stimulated Emission Depletion) microscopy images of fenestrations using contour trace and macro programming to obtain semi-automatization of the process. The brief description suggests also that some manual steps are required. The authors made assumptions about fenestration circularity, but the exact roundness parameters for exclusion were not specified. Kong and Bobe (2021) proposed a well described semi-automated processing of human LSEC images obtained by Structured Illumination Microscopy (SIM). A Python based automated image processing macro utilizes an adaptive thresholding process and segmented images are further analysed to calculate both the number and diameter of fenestration. In 2017, we proposed the quantitative method for atomic force microscopy (AFM) image analysis of LSEC (Zapotoczny and Szafranska, 2017). Fenestration diameters were manually measured from high magnification images and, together with the manually counted fenestration number, then converted into porosity. The proposed method was precise, yet time consuming similarly to the other methods described above that involve manual measurements.

Recent developments in machine learning resulted in new possibilities for automatization or semi-automatization of the LSEC morphology analysis. Li et al. (2020) proposed an in house developed image recognition program based on a fully convolutional network for fenestration analysis. Unfortunately, many algorithms require programming skills in various programming languages, which is the main obstacle for the wide use of machine learning in biology. Recently, new software was developed with user friendly interfaces such as Weka Segmentation (Arganda-Carreras et al., 2017) or Ilastik (Berg et al., 2019). The combination of machine learning, basic image analysis and manual adjustments offers new ways to optimize the previously proposed methods and adjust them to sample size and precision needed for future experiments.

In this article we compare three different methods of image analysis: fully manual, semi-automatic (thresholding using ImageJ/Fiji) and automatic – machine learning (based on Ilastik software). We apply all three analysis methods for images obtained using each type of microscopy – AFM, SEM, and SIM. For clarity, both methods and results sections are divided according to the three imaging techniques. Finally, user bias is discussed based on the cross-correlation of image analysis performed independently by five researchers.

2. Materials and methods

2.1. Cell isolation

The cells were isolated as described in Zapotoczny and Szafranska (2017) for AFM and SIM (mouse LSECs) and in Mönkemöller et al. (2018) for SEM (cryopreserved rat LSEC). The experiments followed protocols approved by the local Animal Care and User Committees. Briefly, mice/rats were anesthetized using a mix of ketamine/xylazine and liver was perfused to remove blood and digested using Liberase™ (Roche, Germany). Thereafter, parenchymal cells were removed by a series of centrifugations. Mouse LSECs were isolated using immunomagnetic separation and CD146 conjugated magnetic beads (MACS, MiltenyiBiotec, Germany) while rat LSEC were separated by density gradient centrifugation (50/25 % Percoll gradient) followed by selective adherence to remove stellate cells and Kupffer cells, respectively. After separation, cells were seeded on glass coverslips and washed with media after 1 h incubation in 37 °C, 5 % CO_2, 5 % O_2 (cell culture media and surface coating specified for each technique below).

2.2. Sample preparation, imaging, and quantitative analysis

The differences in properties of the images obtained by each microscopy modality affect the analysis strategies. Therefore, each quantitative analysis is described separately for each imaging technique. For more detailed examples of the analysis see Supplementary Materials. The list of the parameters of interest can be found in Table 1.

2.2.1. Atomic Force Microscopy (AFM)

2.2.1.1. Sample preparation and imaging. In our analysis, we used images of samples prepared according to Zapotoczny and Szafranska (2017) and Mönkemöller et al. (2018). LSEC were cultured for 12−16 h on uncoated glass coverslips in EGM-2 full media (Lonza) and fixed for 2 min in 1 % glutaraldehyde in PBS and stored in PBS (with Mg^{2+}, Ca^{2+}) until imaging for up to two weeks. The measurements were performed using a JPK Nanowizard 3 AFM system (JPK Instruments AG, Germany) in PBS (with Mg^{2+}, Ca^{2+}) in a commercial liquid cell with the temperature control (25 °C). High magnification images were obtained using Quantitative Imaging mode with semi-soft (k = 0.03−0.06 N/m) triangular cantilevers with sharpened tips (radius <12 nm); low

Table 1
Parameters used for description of LSEC morphology.

Parameter	Definition	Unit
Cell area	(SEM/SIM) area of single cell surface (AFM) area of all cells in the image reduced by nuclei region of height above 700nm	nm^2 (μm^2)
Fenestration diameter	Max diameter – the longest diameter of single fenestration Min diameter – the shortest diameter of single fenestration For (semi-)automatic methods max and min diameter are calculated with the assumption of elliptical shape	nm
Roundness	$\frac{\text{min diameter}}{\text{max diameter}}$	0–1, unitless
Single fenestration area	(circularity assumption) $\pi \times \text{diameter}^2$ (elliptical assumption) $\pi \times \text{min diameter} \times \text{max diameter}$	nm^2
Total area of fenestrations	(Manual method, SI2) Number of fenestrations x fenestration diameter distribution ((Semi-)automatic methods) total detected area of fenestration	nm^2 (μm^2)
Porosity	$\frac{\text{total area of fenestrations}}{\text{cell area}} \times 100\%$	%
Fenestration frequency	$\frac{\text{number of fenestrations}}{\text{cell area}}$	$\frac{\text{No. of fen.}}{\mu m^2}$

magnification images of whole cells were imaged with contact mode and semi-soft triangular cantilevers with a regular tip (radius <60 nm). Precise imaging description and parameters such as loading force can be found in our previous work (Zapotoczny and Szafranska, 2017). Collected data were processed with JPK Data Processing Software and converted to tiff format for further analysis using ImageJ/Fiji.

2.2.1.2. Quantitative analysis.

1 Fenestration diameters

Single fenestration diameters were measured in three different ways from 26 high magnification images displaying a total of 625 fenestrations. A representative image is presented in Fig. 1A.

I Manual quantification was performed as follows: First, images were scaled to the scale bar individually for every image. Then, the shortest and the longest diameter of each fenestration were measured (minor and major axis respectively, assuming an elliptical shape of fenestration). Finally, the area of every pore was calculated with the assumption of an elliptical shape. The roundness parameter was defined as a ratio between the minor and major axes measured. Every fenestration was assigned with a number for further identification and comparison with another two methods. Holes on the edge of the image or clearly distorted i.e., not having a round shape or merged due to imaging or sample preparation artifacts were excluded.

II The semi-automatic method is based on the difference in contrast between the inside of fenestration and LSEC membrane. A simple threshold tool in Fiji was used to manually set cut off values for every independent image to ensure maximal precision (image from same imaging conditions are recommended when applying the same thresholding value to reduce bias). Next, the image was converted into a binary mask and then every fenestration was measured. Parameters such as fenestration area, fenestration diameter (min, max, mean), and roundness were calculated automatically (under "Analyze particles" tool in Fiji, size and circularity were set the same for all the images) and assigned to each fenestration according to the previously established order (for fenestration-by-fenestration analysis). Similarly to the manual quantification, the scale bar was used to adjust the scale for every image.

III The automatic method for the measurement of fenestrations is based on machine learning. Presented results were analyzed with Ilastik software. The algorithm was trained on a set of four representative images. A user teaches the software by marking parts of the image indicating the areas of fenestrations and the rest of the cell body area. Training is simple and takes about 30 min. Then, batch processing was applied to all 26 images to create simple segmentation binary masks (Fig. 1A, top). Finally, masks were analyzed using ImageJ/Fiji similarly to the semi-automatic method.

All 625 fenestrations were independently assigned with area, diameter (min, max, mean) and roundness obtained from three different quantitative methods and then compared.

2 Fenestration frequency and porosity

The fenestration frequency and porosity (see Table 1 for definitions) were measured from low magnification images of whole cells (Fig. 1B). 27 images of 40 μm × 40 μm size were analyzed. Initially, the image size was artificially converted (from 1024 × 1024 pixels to 2048 × 2048 pixels) with linear interpolation to digitally increase the resolution of an image ("Adjust Size" tool in Fiji). Artificially increased resolution does not bring any new information, however smaller pixel size is beneficial for better fenestration detection in all 3 analysis methods.

I Manual quantification was utilized in a two-step process. First, fenestrations were counted manually for the whole AFM images. Second, the cell area was calculated, excluding the background and nuclei areas. To achieve this, by using the 3D information about the topography of cells, regions of heights above 0.7–1.0 μm were excluded from analysis, by image contrast adjustment. We assumed that fenestrations can be formed only in flat areas of LSEC. Finally, the total area occupied by fenestrations, fenestration frequency, and porosity were calculated using the number of holes and mean diameter distribution measured from high magnification images (detailed description of calculation can be found in Supplementary information SI.1.).

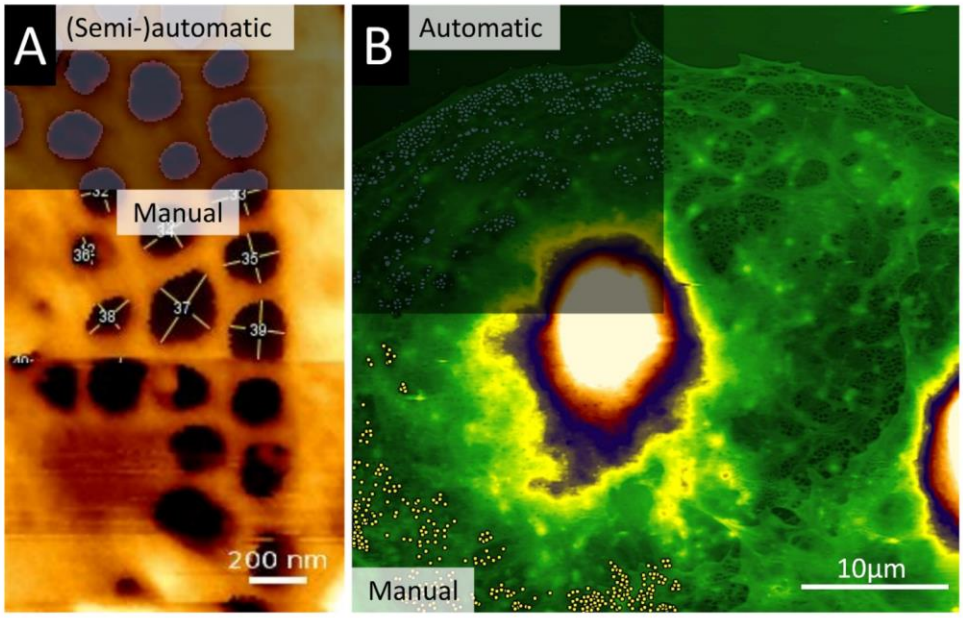

Fig. 1. Representation of the AFM image analysis. (A) High magnification AFM image of the sieve plate. Overlaid mask of fenestrations detected by (semi-)automatic methods and manually measured diameters are presented. Fixed cells were imaged using QI AFM mode and a sharp MSCT tip. (B) Low magnification AFM image of LSEC. Overlaid mask of detected fenestrations from the automatic method and marker points from manual fenestration counting are shown. Fixed cells were imaged using AFM contact mode and the MLCT tip.

II Simple thresholding could not be used for low magnification images due to the artefacts of AFM measurements that make the height (topography) images look curved/tilted. Built in image corrections are not sufficient and images require cumbersome analysis. Therefore, the semi-automatic method could not be applied to the low magnification AFM images.

III Automatic image analysis was successfully applied to measure fenestration number and area from low magnification AFM images. First, the program was trained on sets of four images (training time of around 1 h) and then all 27 images were analyzed using batch processing. Next, images were converted into simple segmentation binary masks and analyzed in ImageJ/Fiji. To avoid fenestrations merged together the watershed tool was used followed by particle analysis to exclude objects from outside of the fenestration range of 50−300 nm and circularity below 0.4. The remaining objects were automatically counted, and the total area measured to calculate porosity and fenestration frequency.

2.2.2. Nanoscopy – Structured Illumination Microscopy (SIM)

2.2.2.1. Sample preparation and imaging. Samples were prepared as previously described (Zapotoczny and Szafranska, 2017; Mönkemöller et al., 2018). Briefly, cells were seeded on fibronectin coated coverslips in RPMI-1640 medium (Sigma-Aldrich) and then fixed for 10 min with 4 % formaldehyde (FA) in PBS and stored in PBS containing 0.1 % FA. Before imaging, cells were stained using CellMask Green (ThermoFisher) 1:1000 dilution in PBS for 30 min and then mounted onto glass slides using Vectashield antifading mounting media (Vector Labs). Images were obtained using a commercial SIM microscope (OMX Blaze system, GE Healthcare) with a 60x 1.42NA oil-immersion objective (Olympus). 3D-SIM image stacks of 2−3 μm were acquired with a z-distance of 125 nm and with 15 raw images per plane (five phases, three angles). Raw datasets were computationally reconstructed using SoftWoRx software (GE Healthcare) and z-projections in tiff format were prepared for further analysis.

2.2.2.2. Quantitative analysis (Fenestration diameter, fenestration frequency and porosity). Initially, the image size was converted from 1024 × 1024 pixels to 2048 × 2048 pixels, with linear interpolation, using the adjust size tool in Fiji to digitally increase the resolution of the image.

I The scale was adjusted to the size of the image of 40.96 μm × 40.96 μm and 300 fenestrations were manually measured from the top right quarter of each of 20 images. For every fenestration, both the smallest and the largest diameters were measured to calculate mean values. For calculation of fenestration frequency, the cell area was measured using the threshold tool in ImageJ/Fiji (fenestrations area including) and fenestrations were manually counted (Fig. 2 Manual). Porosity was calculated using fenestration diameter distribution and the number of fenestrations individually for every image (for detailed calculations see Supplementary information SI.1.).

II For the semi-automatic method, images were converted into binary masks using the threshold tool with manually adjusted values for each image. A watershed function was then applied to avoid exclusion of merged fenestrations, and only objects within the fenestration size range were saved ("Analyse particles" Fiji tool, 50−300 nm diameter and circularity above 0.4). Finally, fenestration diameter, the total area and number of fenestrations were measured and used to calculate porosity and fenestration frequency (Fig. 2 Semi-automatic).

III The machine learning based automatic method was used for fast image processing. After training on four images (training time of about 1 h) all 20 images were processed and converted into simple segmentation binary masks in tiff format (Fig. 2 Automatic). Further analysis was the same as for the semi-automated method described above (analyse particles, size dependent object exclusion).

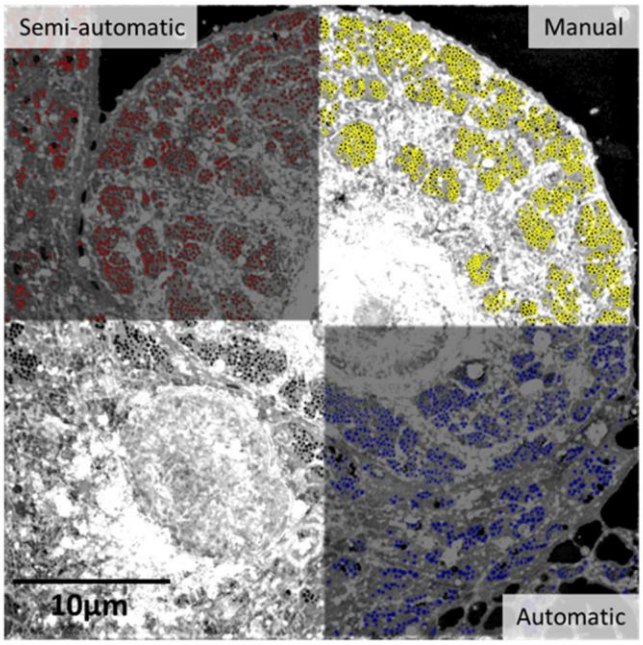

Fig. 2. Representative analysis of SIM image of LSEC stained with CellMask Green. Red - fenestrations detected by semi-automatic method, blue – fenestrations detected by automatic machine learning method, yellow marks – fenestrations counted manually.

2.2.3. Scanning Electron Microscopy (SEM)

2.2.3.1. Sample preparation and imaging. Samples were prepared as previously described (Mönkemöller et al., 2018). LSEC were seeded for 3 h on fibronection covered glass coverslips in RPMI-1640 medium (Sigma-Aldrich) and then fixed and stored in a mix of 4 % formaldehyde and 2.5 % glutaraldehyde in cacodylic buffer. Samples were then processed with 1 h treatment with freshly made 1 % tannic acid in PHEM buffer, 1 h of 1 % OsO_4 in H_2O, dehydrated in ethanol gradient (30 %, 60 %, 90 % for 5 min each, 5 times for 4 min in 100 % ethanol, and incubated twice for 10 min in hexamethyldisilane (HMDS), then left overnight to evaporate. Before imaging, samples were mounted on metal stubs using carbon tape and silver glue to reduce charging and then sputter coated with 10 nm gold/palladium. A commercial SEM system (Sigma, Zeiss) was used for imaging with a 2 kV electron beam. Low magnification images (Fig. 3B) were obtained from 5 different areas of the sample with 20 images of single cells in total. High magnification images (Fig. 3A, ~6.5 nm/pixel) were taken for each of the 20 cells.

2.2.3.2. Quantitative analysis.

1. Fenestration diameters

Contrast and brightness were adjusted for every image and the scale was set according to the scale bar.

I Fenestrations were manually measured from 20 high magnification images; assuming elliptical shape, both the smallest and the largest diameter (along minor and major axis respectively) were measured and then used for the calculation of the area and roundness.

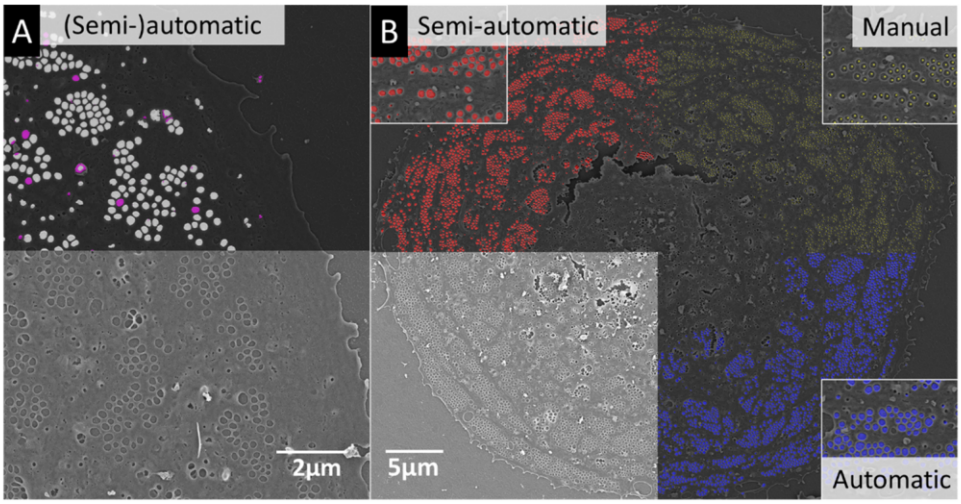

Fig. 3. Representation of the SEM image analysis. (A) High magnification of LSEC imaged using SEM. The upper panel of the image represents the overlaid mask of detected fenestration by semi- and automatic methods (white) or automatic only (magenta). (B) Low magnification of LSEC imaged using SEM. Red - fenestrations detected by semi-automatic method, blue – fenestrations detected by the automatic machine learning method, yellow – fenestrations counted manually.

II The second semi-automatic method based on the Fiji threshold function consists of few steps (detailed example in Supplementary information SI.2.). First, the contrast was adjusted to better visualize the edges of fenestrations and the image was inverted. Next, the threshold was manually set using the Huang algorithm to the point where single fenestrations but not their surrounding edges were covered. Images were then converted into binary masks and objects larger than 300 nm or smaller than 50 nm and with roundness below 0.4 were excluded. Every fenestration was then automatically measured and parameters such as area, diameters (min, max, mean) and roundness were calculated.

III For fast image processing, machine learning was applied. First, the algorithm was trained using four images (training time of about 2 h) and then all 20 images were processed and converted into simple segmentation binary images. Fenestrations were then measured the same way as described for the semi-automated method.

2. Porosity and fenestration frequency

I Fenestrations were manually counted (Fig. 3B, yellow) and the cell area was calculated from the manually marked cell shape. The total area of fenestrations was calculated using fenestration number and previously measured diameter distribution from high magnification images (details in SI.1.).

II The semi-automatic method was applied with parameters adjusted for every image individually as for the high magnification images described above (contrast adjustment, inversion, threshold and particle analysis exclusion by size) (Fig. 3B red). The total area and number of fenestrations were automatically measured after scale adjustment and used for the calculation of porosity and fenestration frequency.

III For automatic analysis, the algorithm was trained using five low magnification SEM images and then all 20 images were processed. Simple segmentation binary images were then analyzed using ImageJ/Fiji similarly to the semi-automated method.

2.3. User comparison

Five individual users with different experience with image analysis were asked to analyze one high magnification SEM and nine SIM images. For the SEM image, each user was asked to manually measure the same 700 marked fenestrations, set the scale by measuring the scale bar and perform analysis using semi-automatic and automatic methods according to the descriptions above. Then each of the 700 marked fenestrations were assigned with parameters (area of single fenestration, fenestration diameters (min, max, mean), and fenestration roundness). For SIM images, all participants were asked to manually count fenestrations from nine whole images and then analyze all images using semi-automatic and automatic methods as described above. The parameters were measured by five different users using three different analysis methods. Results were cross-correlated between each other (every single user with every other user).

2.4. Statistics

All statistical analyses were performed using OriginPro software (OriginPro 2021, OriginLab Corp., Northampton, MA). The total numbers of analysed cells and fenestrations are summarized in the Table 2. For porosity and frequency parameters, the comparison between the methods was based on the relation between the (semi-) automatic methods and manual (standard) approach. The linear correlation is necessary for the method to be useful in the experiments with expected changes in selected parameters. Therefore, linear regression was fitted to the data with the R^2 coefficient describing linearity (the closer to 1 the more linear) and slope (tangent of the angle) describing the correlation between the values. A slope of 1 is preferred as the change in porosity/frequency measured by the (semi-) automatic and manual methods would remain the same even if the absolute values vary. Slopes lower or higher than 1 mean under- or over-estimation, respectively.

Table 2
Total number of analysed images per imaging technique.

Imaging technique	Image Magnification	Number of images/cells	Number of measured fenestrations	Pixel size [nm]
AFM	High	26	(M,S-A, A) 625	4–6
	Low	27		20
SIM	Low	20	(M) 6 000 (S-A) 60 000 (A) 63 000	20
SEM	High	20	(M) 8 100 (S-A, A) 16 000	6–7
	Low	20		18–20

M – manual, S-A- semi-automatic, A - automatic.

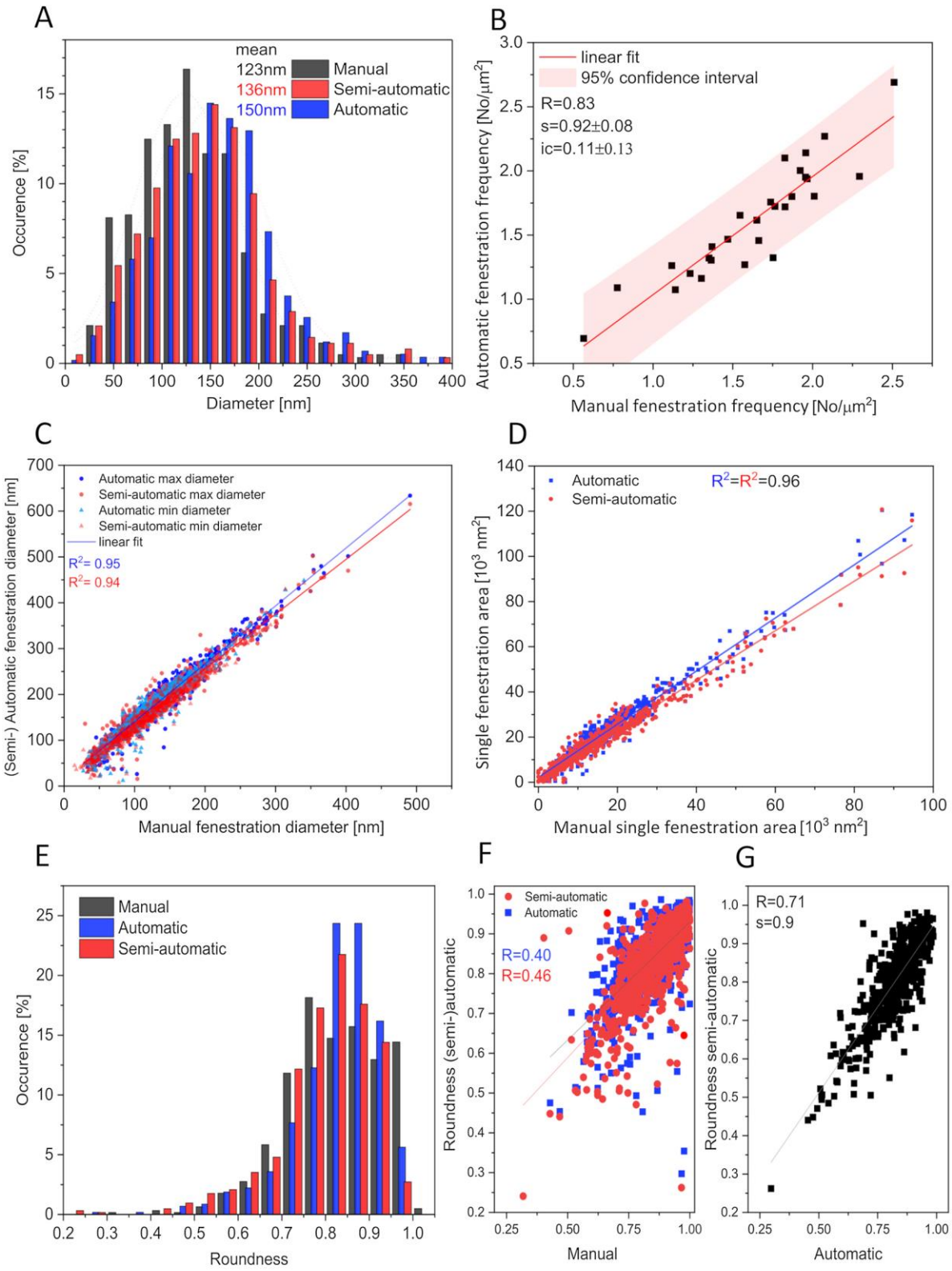

Fig. 4. Analysis of AFM images. (A) Histogram of fenestration diameter distribution. The dotted lines represent fitted Gaussian curves from which the mean values were calculated. Data comes from 625 fenestrations from 26 high magnification images of sieve plates (see Fig. 1A). (B) Correlation of fenestration frequency calculated using Automatic and Manual counting. Each dot represents a single image (see Fig. 1B), 27 images in total. S - slope of the fitted linear function, ic - intercept. (C) comparison of single fenestration diameter measured manually and automatically with the assumption of elliptical fenestration shape. Max, min diameter – major and minor axis of the ellipse. (D) comparison of single fenestration area measured manually and automatically. (C, D) each dot represents a single fenestration measured by 3 different techniques. (E) Distribution of fenestration roundness measured by different techniques (roundness = ratio of min to max diameter). (F, G) correlation of roundness parameter between manually and automatically measured fenestrations.

3. Results and discussion

In this section, the terms Manual, Semi-automatic and Automatic are used for the 3 quantitative analysis methods described in detail in the Materials and Methods section

3.1. AFM image analysis

Fenestration diameter distribution obtained from 26 high magnification AFM images show differences between the three analysis methods (Fig. 4A). Gaussian curves were fitted to calculate the mean diameter and the width of the distribution. The smallest mean diameter of 123 nm was obtained from manually measured data, semi- and automatic methods gave values of 136 nm and 150 nm, respectively. The larger diameter for non-manual methods may be related to the fenestration edge detection. Manual measurement is based on contrast and user judgement and may vary between the images. For semi- and automatic methods, the diameter is calculated back from the measured areas of single fenestrations with the assumption of circularity. Moreover, the detection of fenestrations by machine learning may require detection of the edge of the hole and it could therefore increase the total area and diameter of fenestration. This issue is related to the pyramidal shape of the AFM tip which may influence the intensity gradient corresponding with the height on the fenestration edge (more information about the AFM tip shape problems for fenestration measurement can we found in Zapotoczny and Szafranska (2017)). A pixel size of 4–6 nm would explain that difference of 13/27 nm, which correlates with 2–4 pixels between the manual and (semi-)automatic methods (Fig. 4A).

Individual analysis of each of the 625 fenestrations provides a comparison of each of the three analysis techniques for each pore. Fig. 4C shows the linear relation between the manually measured min and max diameters and the (semi-)automatic method calculated data. The fitted linear regression presents a good correlation of $R^2 = 0.94$ and 0.95 for the automatic and semi-automatic methods, respectively. The slope of the regression for both methods was 1.2 and the intercepts of 16 nm and 10 nm for the automatic and semi-automatic methods, respectively. Both the slope above 1 and the intercept values confirm that the non-manual methods detect fenestrations as larger than the manual data, however, the good linear correlation makes the measurement comparable between the samples with differences in fenestration size. The same results have been observed for fenestration-by-fenestration analysis of the areas of single pores (Fig. 4D). The linear regression slope of 1.1 and $R^2 = 0.96$ show a good linear correlation.

Most of the previously published articles dealing with the measurement of LSEC morphology assumed circularity of fenestrations. Here we show that the roundness parameter – the ratio between minimum and maximum diameter, concentrates about the value of ~0.85 for all methods (Fig. 4E). Interestingly the distribution of the manual measurements is wider and the number of nearly circular fenestrations (0.95-1) is much higher than for (semi-)automatic methods. Moreover, the comparison of roundness of single fenestrations between the three methods shows a correlation between automatic and semi-automatic (Fig. 4G) but not between manual and automatic methods (Fig. 4F). This result may suggest the user bias towards a more circular shape as the choice of min/max diameter is subjective. The roundness distribution from the automatic and semi-automatic methods is very similar and a slight increase towards more round fenestrations correlates well with the assumption that the machine learning algorithm detects the edges of the holes equally enlarging both min and max diameters and therefore increasing the roundness parameter.

The fenestration frequency calculated using automatic methods shows good correlation with the manual measurement (Fig. 4B). Almost all measured data lay within 95 % confidence interval and slope of 0.92 with $R^2 = 0.83$ indicate linear correlation.

3.2. SIM image analysis

Twenty LSEC SIM images were analyzed in three different ways. The comparison between the manual method and the (semi)automatic methods (Fig. 5A) showed a linear correlation with R^2 values of 0.85 and 0.82, respectively. The correlation for SIM is similar to the AFM images which it is enough to be useful for comparison of data from different treatment groups. There are no significant differences in the measured numbers of fenestration per image between various analysis methods (Fig. 5B). Fenestration frequency was not calculated due to difficulties in the detection of cell boundaries. The Cell Mask dyes are a group of cell membrane dyes that provide great contrast needed for detection of fenestrations but further analysis and calculations can be optimized for single cells only on non-confluent samples where only a single cell is visible in the field of view of the microscope. Alternatively, cells can be separated manually. For samples with tight cell monolayers, the cell area can be normalized according to the visible number of cells for porosity/fenestration frequency calculations by subtraction of the mean area of nuclei (10 μm is a good approximation of diameter of LSEC nuclei).

Fig. 5C shows the differences in the distribution of diameters. The semi-automatic method shifted distribution towards a larger apparent fenestration size with a mean value of 178 nm. Automatic and manual methods gave similar results with mean diameters of 138 nm and 130 nm, respectively. Machine learning showed a high number of small pores below 75 nm which may be an artifact of the detection algorithm and can be optimized by the increased training time. For all methods objects smaller than 50 nm were excluded. A pixel size of 20 nm is not sufficient for the detection of holes below 50 nm due to Nyquist's sampling criterion. The mean diameter values were calculated as centers of the fitted Gaussian distribution curves to compensate for this. The difference between semi-automatic and the other methods can be biased by the manual adjustments of the cut-off intensity value. The threshold must be set individually for every image so changes towards both smaller and larger diameters can be introduced by the users. It is not possible to use a fixed value as the intensity in the perinuclear area varies between the cells and would induce artifacts that influence the segmentation more than the manual adjustment.

Similarly to the data from the AFM images, the roundness parameter was calculated with the assumption of fenestration elliptical shape. The shift towards a more circular shape can be observed for manual measurements which is consistent with the previous observation, most probably resulting from the user bias. Also, the roundness values concentrate around a value of 0.9 for SIM images compared to 0.82 for AFM images. This difference is connected with the imaging technique – raw SIM images require reconstruction which will make small objects at the edge of achievable resolution appear more round in shape due to Wiener filtering (part of the SIM reconstruction algorithm). Adjustment of the image size using bilinear interpolation makes the shape even more circular. Nevertheless, the benefits of the decreased pixel size, which allows better precision of the quantitative analysis, outweigh the downsides.

3.3. SEM image analysis

Twenty high magnification SEM images were quantitatively analyzed using three different methods. Comparisons between manual and (semi)automatic techniques showed differences in the shape of mean diameter distribution (Fig. 6A). Mean fenestration size was calculated from the manually measured min and max diameters or for (semi-)automatic methods calculated from the detected areas, assuming circularity of holes. Only manually measured values had a simple Gaussian distribution with the center at 175 nm. The other two methods show the results with at least double Gaussian shape peaks; the first one being within the regular fenestration size range with centers at 178 nm and 191 nm for semi-automatic and automatic methods respectively,

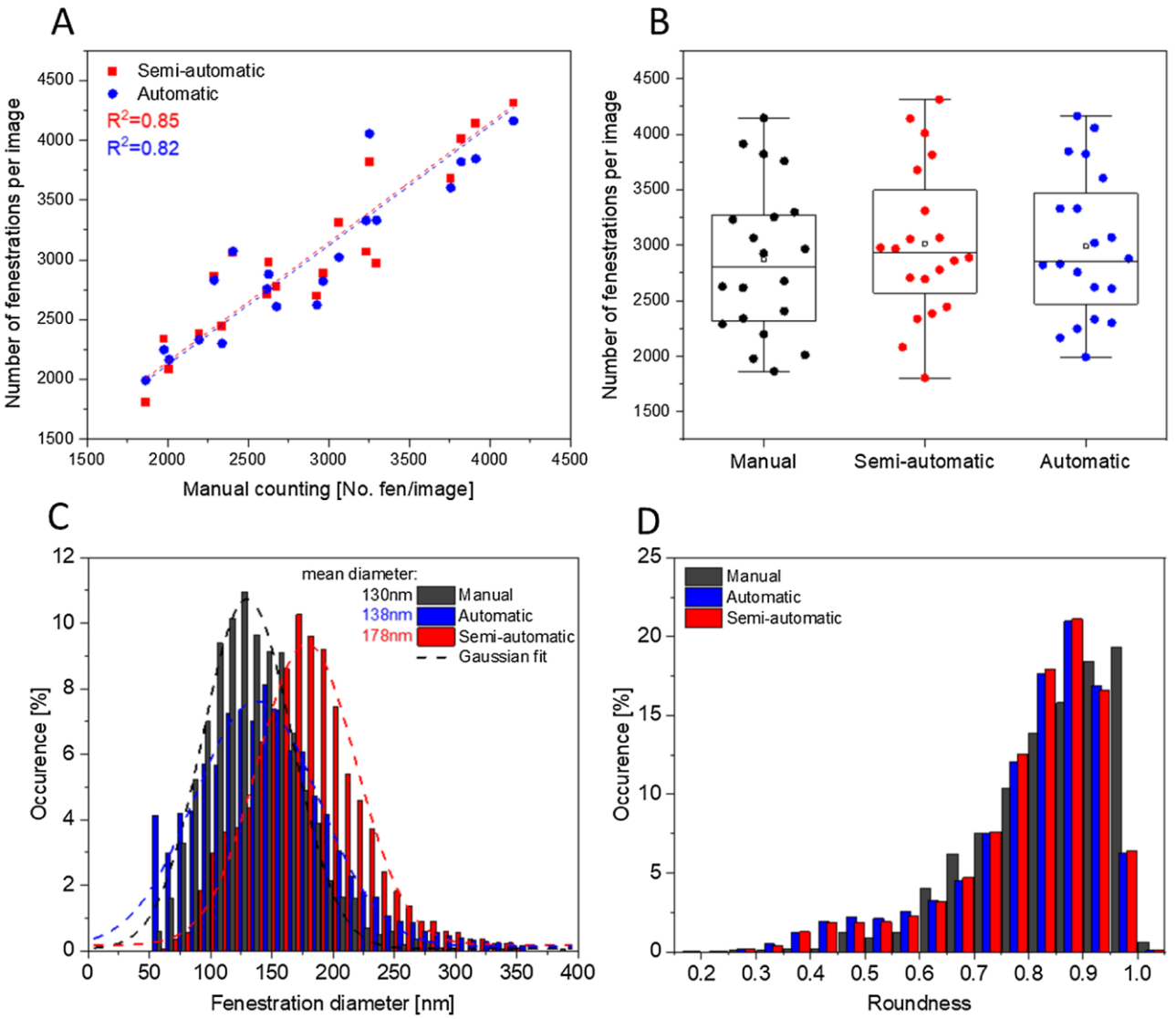

Fig. 5. Analysis of SIM images. (A) Correlation between manually and automatically counted fenestrations. Each dot represents a single image (see Fig. 2), 20 images in total. (B) Comparison of fenestration frequency between the studied groups. (C) Distribution of fenestration diameter. The dashed line represents fitted Gaussian curve from which the average value was calculated (tip of the curve). Fenestrations smaller than 50 nm were excluded due to a pixel size of 20 nm. The total number of fenestrations measured – 6 000, 60 000, 63 000 from manual, semi-automatic and automatic methods respectively. (D) Distribution of the roundness parameter calculated from measured fenestrations.

and the second maximum with centers at 100 nm and 120 nm. The additional detected objects are identified on the images as non-transmembrane protrusions in the cell membrane, most probably endocytic vesicles arising from the prominent endocytic properties of LSECs. Their size and contrast, being similar to fenestrations, make them impossible to be separated from fenestrations using threshold or Ilastik analysis, however, they can be removed from further calculations and analysis using the multi-peak Gaussian curve fitting or by cutting off all the objects below a certain size. The first approach requires more time as it should be adjusted for every cell/image but interferes less with the data. The second approach can be automated to a cut-off value set in the middle of the two maxima, but it can significantly affect the results if changes in fenestration diameters towards smaller values are expected (two peaks overlapping).

Fenestration-by-fenestration analysis with three different methods shows a good linear correlation between manual and (semi)automatic measurements with $R^2 = 0.95–0.96$ and a slope of 1. The automatic compared to the semi-automatic approach causes a 16 nm shift towards larger apparent fenestration size and area of 2300 nm^2. Similarly to the analysis of the AFM images, the machine learning algorithm is detecting the edge of the holes resulting in the systematic error with the value connected to the pixel size. This error would not affect the comparison between the treatment groups with expected changes in diameter but should be taken into consideration for comparison between data calculated with different methods of analysis.

Porosity and fenestration frequency were calculated from low magnification images. Both semi-automatic and automatic methods show a linear correlation of the values of porosity when compared with manual measurements, $R^2 = 0.89$ and 0.91 (Fig. 6D). However, the slopes of the linear regression are 0.63 and 0.9 respectively. The difference in slope suggests that the semi-automatic method is underestimating the value of calculated porosity. The difference in slope values between the methods can be more pronounced with the increase of cell porosity due to drug treatment. As a result, smaller changes in cell porosity can be wrongly assigned as not significant. The smaller intercept of linear regression of the semi-automatic compared to the automatic method makes it more similar to manual measurement, however, the difference in slope is more important for the usefulness as a tool for

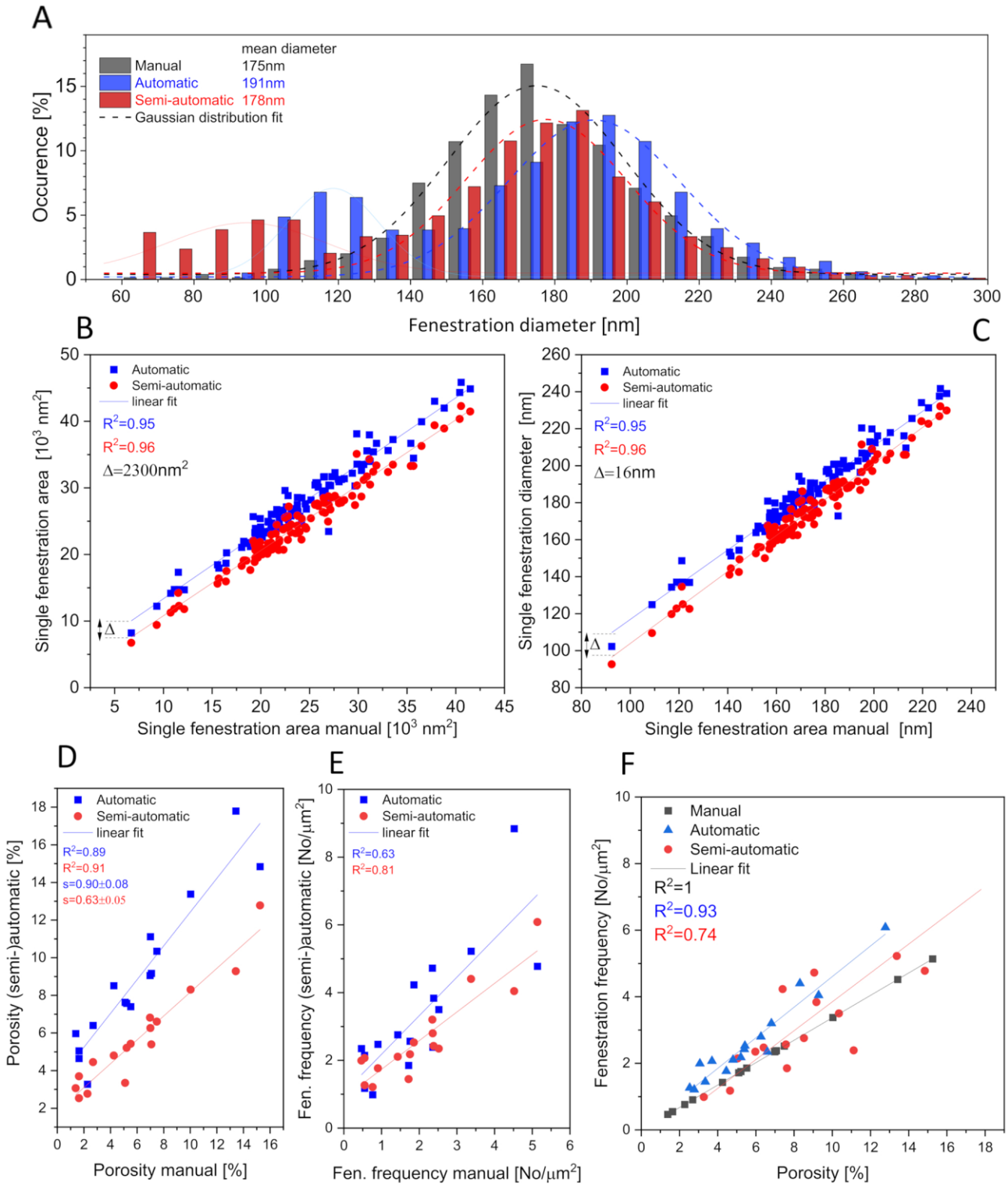

Fig. 6. Analysis of SEM images. (A) Fenestration diameter distribution measured from high magnification SEM images (see Fig. 3A). The dashed line represents fitted Gaussian curves, for semi-automatic and automatic methods a multi-peak fit was used to exclude the non-fenestration objects (thin line Gaussian curve). The total number of fenestrations measured – 8 100 from 20 images/cells for manual measurement and 16 000 from 20 images/cells for (semi-)automatic methods. Correlation of single fenestration area (B) and diameter (C) between manual and automatic methods. Δ – intercept between fitted linear functions. Comparison of porosity (D) and fenestration frequency (E) between manual and automatic methods. Each point represents a single image (see Fig. 3B), total number of images – 18. (F) the relation between frequency and porosity measured using different methods.

comparison between treatment groups.

Fenestration frequency showed a weaker linear correlation than porosity with $R^2 = 0.63$ and 0.81 for Ilastik and threshold respectively (Fig. 6E). These results correlate with the detection of the small fenestration-like objects shown as a second maximum on diameter distribution (Fig. 6A). Because of the small size of these structures, they do not significantly affect porosity, but their number is significant compared to detected fenestrations and this influences fenestration

Table 3
Parameters of fenestrations measured by 3 different methods from SEM images.

Parameter		Manual	Semi-automatic	Automatic
Area	Average [nm^2]	26,926 ± 2140	26,818 ± 443	26,488 ± 3767
	User comp. [%]	1.25 ± 12	0.10 ± 1.8	3.45 ± 22.6
Max diameter	Average [nm]	199 ± 7	201 ± 1.8	200 ± 13
	User comp. [%]	0.34 ± 5.25	0.03 ± 0.86	0.79 ± 10.29
Min diameter	Average [nm]	168 ± 7	166 ± 1.4	165 ± 12
	User comp. [%]	0.46 ± 6	0.03 ± 1	1.10 ± 12
Mean	Average [nm]	184 ± 7	184 ± 1.4	182 ± 13
	User comp. [%]	0.30 ± 5.7	0.02 ± 0.87	0.8 ± 10.9
Roundness	Average	0.849 ± 0.011	0.828 ± 0.001	0.830 ± 0.009
	User comp. [%]	0.000 ± 0.015	0.000 ± 0.001	0.000 ± 0.019

±SD; user comp. = comparison between users.

frequency. The above proposed approaches of removing these structures may help to reduce the effect on fenestration frequency and enable comparison between the groups if changes in frequency are expected to be independent of porosity changes (for example changes in fenestration diameter may compensate for the difference in fenestration number and show no changes in porosity). The comparison between porosity and fenestration frequency among the studied methods (Fig. 6F) shows a good correlation for manual measurement due to the direct connection between these parameters – the fenestrated area used to calculate porosity is calculated from the number of fenestrations. The automatic method shows a good linear correlation with R^2 of 0.93 while the semi-automatic method presents R^2 of 0.74 which points to the influence of detected fenestration-like objects in the calculation of fenestration number.

3.4. User comparison

To compare the differences between users and study user bias, sets of SIM and SEM images were analyzed by five researchers with different levels of imaging experience, from beginner to advanced user.

3.4.1. SEM

Firstly, 700 fenestrations from Fig. 3A were individually measured (fenestration-by-fenestration) by five users using the three studied methods and then the parameters were cross-correlated between all the users. Next, mean values were calculated for every user and the average was calculated for each method. Interestingly, the average values of parameters were similar for all techniques (Table 3). However, differences between the users (Fig. 7) and SD values of the cross-correlation show significant differences among the users. The biggest deviation is observed with the automatic method; the cross-correlation parameter for a single fenestration area was only 3.5 %, but the standard deviation of over 20 % suggested significant differences between the users. One of the main reasons for that may be the specificity of the machine learning algorithm. Each user trained the software independently and small differences can lead to different ways of detecting fenestrations. Every fenestration on a SEM image has a visible, high contrast edge which can be included or excluded from the detected area. Differences between the calculated mean values of the diameter (Fig. 7B) for manual and automatic methods are of about 6−7 nm which is similar to the pixel size of this image - 6.5 nm. The semi-automatic method is intensity and contrast based and therefore, less sensitive to user preferences about the fenestration edge. Fenestrations are detected due to high contrast edges characteristic for SEM images - steep edges give a higher signal compared to a flat cell surface or substrate in the fenestration lumen. This hypothesis was confirmed by merging binary images of detected fenestration from automatic and semi-automatic methods showing rings around the holes (see Supplementary information SI.3). Small differences in fenestration roundness among the users using the semi-automatic method (Fig. 7C) also suggest that the shape of the detected holes is the least biased by this method. A shift towards a more circular shape (roundness value closer to 1) is observed for manual measurements which (consistent with previous observations) confirms the influence of the assumption of circularity by the users.

3.4.2. SIM

Nine SIM images were analyzed independently by five users with the three methods. Each image was then cross-correlated between all users and (semi-)automatic methods were compared with manual counting.

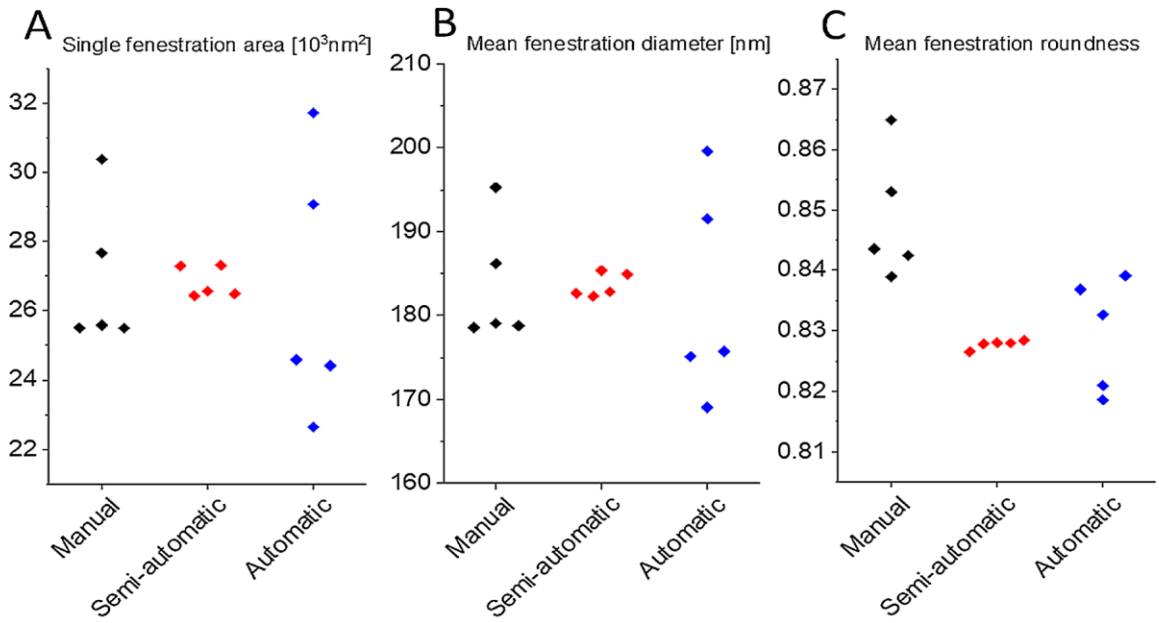

Fig. 7. Comparison of analysis methods between the users. Each point represents one user and the mean value of the presented parameter calculated from 700 measured fenestrations from SEM image.

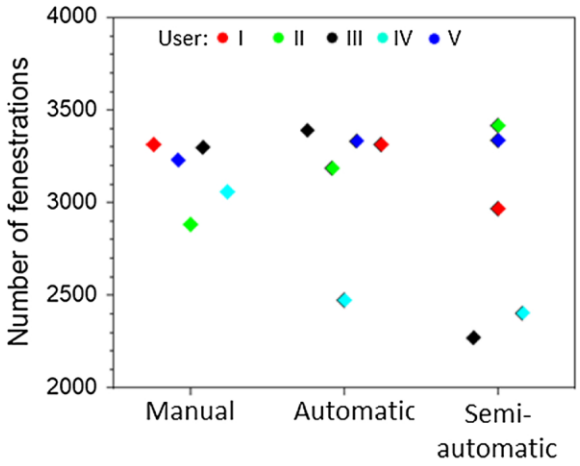

Fig. 8. Comparison between users' measurements of fenestrations number using three different techniques for one of the analysed SIM images.

Table 4
Comparison of fenestration number between the users and analysis methods for SIM images.

Change in fenestration number compared to manual counting [%]			
User	Semi-automatic	Automatic	Manual
I	10.1 ± 13	10.2 ± 12	
II	18.5 ± 9	8 ± 11	
III	−7.4 ± 15	−5.9 ± 11	
IV	−4.8 ± 13	−11.5 ± 12	
V	−4.5 ± 14	3.5 ± 13	
Cross correlation between users [%]	1.9 ± 9.5	3.3 ± 12	0.17 ± 11

The mean value of fenestration number per image was similar among the users (0.2–3.3 %), however, the difference between users within one method was about 10−12 %. An example of one of the analyzed images (Fig. 8) shows the differences between the users and methods. Manual counting has the smallest variation while (semi-)automatic methods present a wider range of calculated numbers. The main source of differences between the users using (semi)automatic methods is the large pixel size which causes the merging of fenestrations within one sieve plate during segmentation. Lowering the threshold or retraining the machine learning software leads to the presence of undetected fenestrations while the watershed function, used to split the merged holes, leads to splitting single fenestrations which causes an elevated number of detected objects (Table 4). The decision is made by each user and if it is standardized, the error can be minimized.

3.5. Discussion

In this study we investigated the use of three methods for quantitative analysis of LSEC images: manual measurement or counting of fenestrations, a semi-automatic threshold-based method and an automatic machine learning-based method. All three techniques have their advantages and disadvantages, mainly time efficiency at the cost of accuracy. The manual method was, until recently, the standard way of fenestration analysis due to the lack of proper software to semi-automate or automate the process. It was considered to be the gold standard, but the lack of scoring description prevents a proper comparison between results from different studies. Recently, attempts to apply home-made algorithms and machine learning have been reported (Di Martino et al., 2018; Kong and Bobe, 2021; Li et al., 2020), but their application requires a certain level of programming skills not available to every researcher. Here we report two methods which can be easily applied to experimental data where differences in fenestration diameter and/or number are expected.

The efficiency of each method depends mainly on the number of samples which is directly correlated with the time needed for analysis. This can be optimized in each study by designing experiments that would give minimum but sufficient sets of data for statistical analyses. The most time consuming is the manual method but the poor image quality or high number of artifacts may prevent the use of other, faster techniques. User comparison showed also that there is significant user bias for manual measurements so all analyses should be performed by one single user, ideally blind to the sample id. If there is a need for data analysis to involve more than a single person, the threshold method would introduce the smallest bias for fenestration size measurements. Fenestration frequency and porosity show similar differences among the users for all three methods so the choice can be based on to the quality of the images.

The data from all three imaging techniques suggests that the precision of both (semi-)automatic methods is similar and linear correlation allows us to use them for comparison of the parameters between experimental groups. All experiments where changes in fenestration size and/or number are expected can be analyzed using the semi-automatic or automatic method. However, the porosity calculated from SEM images using the semi-automatic method may seem underestimated. The comparison between the manual and semi-automatic methods shows a linear correlation with a slope below 1, which indicates that some fenestrated areas are not detected in the cells with higher porosity/higher number of fenestrations

The machine learning software includes a batch processing feature where, after training, tens or even hundreds of images can be automatically analyzed. The only limitation is the computer processing power which affects the speed. The main disadvantage of this approach is the requirement of images with similar contrast and brightness. In practice, each sample or group of samples may require adjustments for these parameters, and depending on the number of samples, this may reduce the time advantage over the semi-automatic method. Although, the threshold-based approach requires manual adjustment of the cut-off value for each image segmentation but still, the large number of fenestrations is analyzed for each manual step. It is a significant advantage over the fully manual approach, where single manual step gives information about only one fenestration.

For fenestration size measurements, both (semi-)automatic methods showed a systematic error that needs to be taken into consideration. The source of this error was identified and connected with the edge of the fenestration detection, related to the pixel size of the image. For the automatic method, the batch processing of all images using the same trained algorithm would solve this problem. For manual and semi-automatic methods inclusion/exclusion must be decided before the analysis.

4. Conclusions

All three proposed methods can be applied for fenestration analyses, but the best method should be selected based on the following criteria: the available imaging technique, the achievable quality of the images, the time for the analysis and the predicted outcome in measured

Table 5
Comparison of properties of the three methods of quantitative analysis.

Property	Manual	Semi-automatic	Automatic
Speed	− − − −	+	++
User bias	−/+	+	−/+
Accuracy - fenestration number	++	−	+
Accuracy - porosity	+/−	+	+
Accuracy - diameter	+/−	++	+
Artifacts sensitive	++	− −	−/+
Image quality sensitive	++	− −	−/+
User friendly	++	++	+

parameters. The pros and cons of the three selected methods are listed in Table 5.

We emphasize the need for small-scale pilot experiments to assess both the best imaging technique as well as the predicted range of changes in the LSEC morphology parameters. The time invested in the analysis of preliminary results will lead to the best possible protocol for further analysis. The combination of more than one analysis method can also be beneficial, for example, the best accuracy of diameter measurement was shown with the semi-automatic method while the number of fenestrations is most precisely detected manually.

The main limiting factor – time – can be overcome by automation, which is getting easier with the developments of new and more precise software and ongoing advancements in the field of microscopy. The results of this study show that the semi-automatic and automatic methods can be a timesaving alternative for the standard manual approach, but considerations of suitable methods are needed prior to application.

The choice of the best analysis method has to be based on the quality of every experimental data set. We suggest to first focus on obtaining the best possible image quality, within reasonable imaging time. For the fenestration size measurements, we recommend use of semi-automatic or automatic method. Automatization allows measurement of thousands of fenestrations at the same time compared to manual measurement of tens of fenestrations; it provides a better statistical overview and removes user bias manifesting as an increase in the roundness parameter. For the porosity and fenestration frequency measurements we recommend the use of the automatic method as it is the most time efficient simultaneously processing of many images. If the image quality is poor, and artifacts do not allow the use of automatic methods, the manual approach may be necessary. When using (semi-)automatic methods we recommend using the manual method for small data sets as a reference, especially if the changes in porosity or fenestration frequency between the experimental groups are small.

The above strategies for scoring LSEC porosity using SEM, SIM and AFM imaging can also be applied to other super resolution imaging modalities applied to LSEC, e.g. dSTORM (Mönkemöller et al., 2014; Mao et al., 2019) or STED (Di Martino et al., 2018). These latter two methods have the highest reported optical resolution, at 10−20 nm. (Semi-)Automation of the LSEC porosity scoring process, in combination with current and new developments in super-resolution imaging, will accelerate the evaluation of LSECs in health, disease and aging, thus aiding to development of therapies that reverse the effects on LSEC defenestration, a key phenotypic feature in various diseases and ageing.

Declaration of Competing Interest

The authors declare no competing interest.

Acknowledgements

This work received funding from the European Union's Horizon 2020 research and innovation programme under the Marie Sklodowska-Curie grant agreement no. 766181, project "DeLIVER" and Research Council of Norway, Grant no. 288565 "NANO2021". This work was supported by the Polish National Science Centre under the "SYMFONIA 3" project, grant agreement no. UMO-2015/16/W/NZ4/00070.

The authors would like to thank Randi Olsen and Tom-Ivar Eilertsen from Advanced Microscopy Core Facility at UiT for the electron microscopy expertise and Deanna Wolfson for the help with SIM imaging.

Appendix A. Supplementary data

Supplementary material related to this article can be found, in the online version, at doi:https://doi.org/10.1016/j.micron.2021.103121.

References

Arganda-Carreras, I., et al., 2017. Trainable Weka Segmentation: a machine learning tool for microscopy pixel classification. Bioinformatics 33 (15). https://doi.org/10.1093/bioinformatics/btx180.

Berg, S., et al., 2019. Ilastik: interactive machine learning for (Bio)Image analysis. Nat. Methods 16 (12). https://doi.org/10.1038/s41592-019-0582-9.

Braet, F., Wisse, E., 2002. Structural and functional aspects of liver sinusoidal endothelial cell fenestrae: a review. Comp. Hepatol. 1 (1) https://doi.org/10.1186/1476-5926-1-1.

Cogger, V.C., et al., 2015. A standardized method for the analysis of liver sinusoidal endothelial cells and their fenestrations by scanning electron microscopy. JoVE 98. https://doi.org/10.3791/52698.

Di Martino, J., et al., 2018. STED microscopy: a simplified method for liver sinusoidal endothelial fenestrae analysis. Biol. Cell 110 (7). https://doi.org/10.1111/boc.201800016.

Hunt, N.J., et al., 2018a. Novel targets for delaying aging: the importance of the liver and advances in drug delivery. Adv. Drug Deliv. Rev. 135 https://doi.org/10.1016/j.addr.2018.09.006.

Hunt, N.J., et al., 2018b. Manipulating fenestrations in young and old liver sinusoidal endothelial cells. Am. J. Physiol. – Gastrointest. Liver Physiol. 316 (1) https://doi.org/10.1152/ajpgi.00179.2018.

Hunt, N.J., et al., 2020a. The effects of metformin on age-related changes in the liver sinusoidal endothelial cell. J. Gerontol. - Ser. A Biol. Sci. Med. Sci. 75 (2) https://doi.org/10.1093/gerona/glz153.

Hunt, N.J., et al., 2020b. Rapid intestinal uptake and targeted delivery to the liver endothelium using orally administered silver sulfide quantum dots. ACS Nano 14 (2). https://doi.org/10.1021/acsnano.9b06071.

Hunt, N.J., et al., 2021. Quantum dot nanomedicine formulations dramatically improve pharmacological properties and alter uptake pathways of metformin and nicotinamide mononucleotide in aging mice. ACS Nano 15 (3). https://doi.org/10.1021/acsnano.0c09278.

Kong, C., Bobe, S., et al., 2021. Multiscale and multimodal optical imaging of the ultrastructure of human liver biopsies. Front. Physiol. 12 https://doi.org/10.3389/fphys.2021.637136.

Le Couteur, D.G., et al., 2002. Hepatic pseudocapillarisation and atherosclerosis in ageing. Lancet 359 (9317). https://doi.org/10.1016/S0140-6736(02)08524-0.

Li, P., et al., 2020. Characterizing liver sinusoidal endothelial cell fenestrae on soft substrates upon AFM imaging and deep learning. Biochim. Biophys. Acta 1864 (12). https://doi.org/10.1016/j.bbagen.2020.129702.

Mao, H., et al., 2019. Cost-efficient nanoscopy reveals nanoscale architecture of liver cells and platelets. Nanophotonics 8 (7). https://doi.org/10.1515/nanoph-2019-0066.

Mönkemöller, V., et al., 2014. Imaging fenestrations in liver sinusoidal endothelial cells by optical localization microscopy. Phys. Chem. Chem. Phys. 16 (24) https://doi.org/10.1039/C4CP01574F.

Mönkemöller, V., et al., 2018. Primary rat LSECs preserve their characteristic phenotype after cryopreservation. Sci. Rep. 8 (1) https://doi.org/10.1038/s41598-018-32103-z.

Øie, C.I., et al., 2020. Liver sinusoidal endothelial cells contribute to the uptake and degradation of entero bacterial viruses. Sci. Rep. 10 (898) https://doi.org/10.1038/s41598-020-57652-0.

Rogers, G.W.T., et al., 1992. Decreased hepatic uptake of cholesterol and retinol in the dimethylnitrosamine rat model of cirrhosis. Liver 12 (5). https://doi.org/10.1111/j.1600-0676.1992.tb00581.x.

Schindelin, J., et al., 2012. Fiji: an open-source platform for biological-image analysis. Nat. Methods 9. https://doi.org/10.1038/nmeth.2019.

Simon-Santamaria, J., et al., 2014. Efficient uptake of blood-borne BK and JC polyomavirus-like particles in endothelial cells of liver sinusoids and renal Vasa recta. PLoS One 9 (11). https://doi.org/10.1371/journal.pone.0111762.

Sørensen, K.K., et al., 2012. The scavenger endothelial cell: a new player in homeostasis and immunity. Am. J. Physiol. 303 (12) https://doi.org/10.1152/ajpregu.00686.2011.

Tsuchiya, K., Accili, D., 2013. Liver sinusoidal endothelial cells link hyperinsulinemia to hepatic insulin resistance. Diabetes 62 (5). https://doi.org/10.2337/db12-1296.

Zapotoczny, B., Szafranska, K., et al., 2017. Quantification of fenestrations in liver sinusoidal endothelial cells by atomic force microscopy. Micron 101. https://doi.org/10.1016/j.micron.2017.06.005.

Zapotoczny, B., et al., 2017. AFM reveals dynamic morphology of fenestrations in living liver sinusoidal endothelial cells. Sci. Rep. 7 (7994) https://doi.org/10.1038/s41598-017-08555-0.

Zapotoczny, B., et al., 2019. Tracking fenestrae dynamics in live murine liver sinusoidal endothelial cells. Hepatology 69 (2). https://doi.org/10.1002/hep.30232.

Quantitative analysis methods for studying fenestrations in liver sinusoidal endothelial cells. A comparative study, **Supplementary Information**

Supplementary information

SI1. Porosity calculation from fenestration diameter distribution and number of fenestrations:

Table S1. Fenestration diameter distribution data

bin center [nm]	counts	cumulative sum	cumulative percent	frequency	Partial area [nm²] (1000 fenestrations)
10	3	3	0.48	0.48	376.8
30	13	16	2.56	2.08	14695.2
50	34	50	8	5.44	106760
70	45	95	15.2	7.2	276948
90	61	156	24.96	9.76	620589.6
110	78	234	37.44	12.48	1185412.8
130	80	314	50.24	12.8	1698112
150	90	404	64.64	14.4	2543400
170	82	486	77.76	13.12	2976468.8
190	59	545	87.2	9.44	2675154.4
210	29	574	91.84	4.64	1606298.4
230	18	592	94.72	2.88	1195963.2
250	9	601	96.16	1.44	706500
270	7	608	97.28	1.12	640936.8
290	7	615	98.4	1.12	739407.2
310	3	618	98.88	0.48	362104.8
330	0	618	98.88	0	0
350	5	623	99.68	0.8	769300
370	0	623	99.68	0	0
390	2	625	100	0.32	382075.2

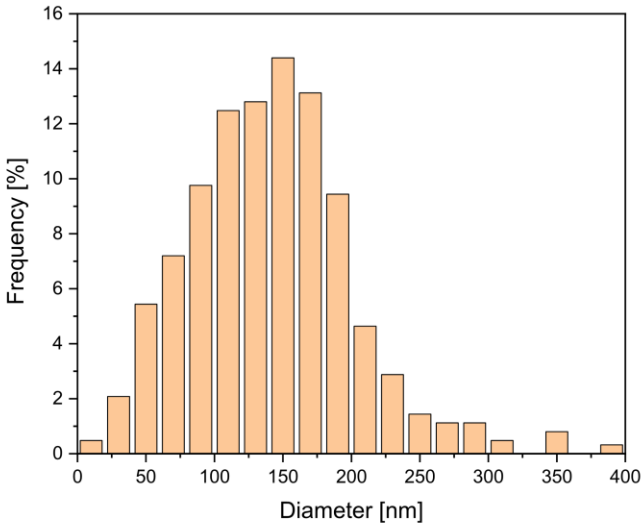

Fig. S1. Distribution of fenestration diameter

Frequency is the percentage of fenestration with certain size, which can be used to calculate the total area of fenestrations for each cell. For example, 14.4% of the fenestrations are in the range of 120-140 nm diameter (bin center 130).

Partial area is the total area of fenestrations of certain size, calculated using separately for each bin and the sum of partial areas is the total area of fenestrations for selected cell.

$$Partial\ Area\ [nm^2] = \pi * \left(\frac{bin\ center}{2}\right)^2 * Frequency[\%] * 0{,}01 * number\ of\ fenestration\ per\ cell$$

$$Total\ area\ of\ fenestrations\ [nm^2] = \sum Partial\ area\ [nm^2]$$

$$Porosity = 100 * \frac{Total\ area\ of\ fenestrations\ [nm^2]}{Cell\ area\ [nm^2]}\ [\%]$$

Cell area [nm^2]	Number of fenestrations	Total area of fenestration [nm^2]	Porosity
370010064	1000	18500503.2	5%

SI2. Semi-automatic method protocol

- Adjust scale
- Enchance contrast

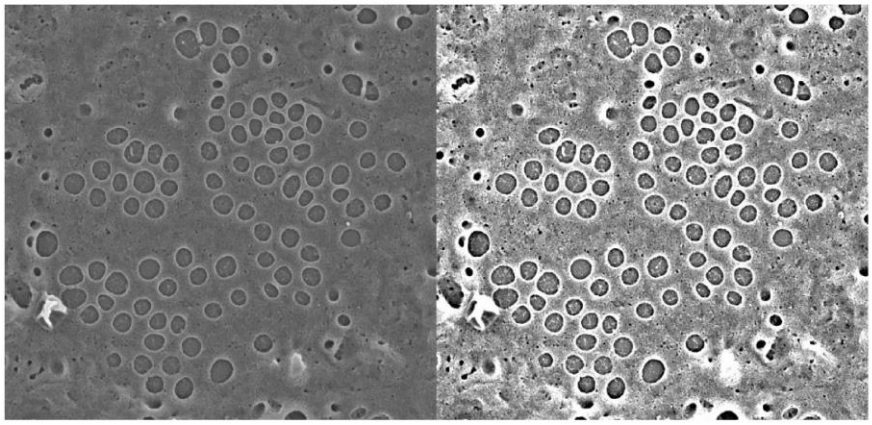

- Set threshold using Huang algorithm, every fenestration should be filled and separated. Apply – image is now binary (black and white)

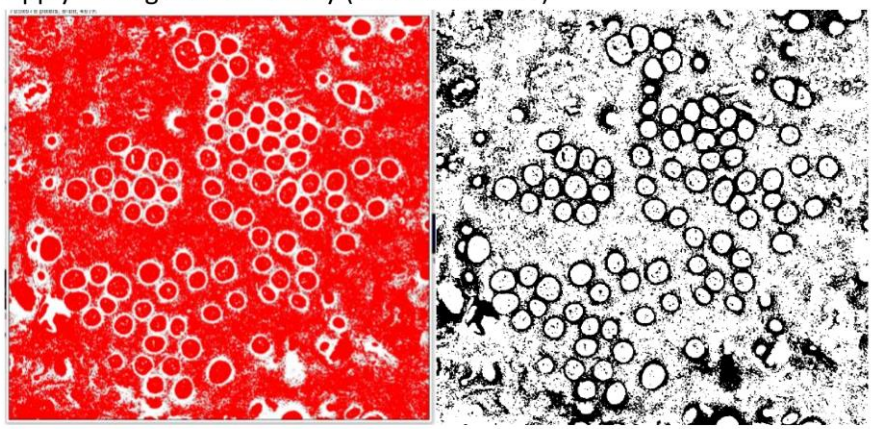

- Use Analyze particles in Fiji set to selected size range (50-400 nm, 1 900 – 125 000 nm^2, roundness 0.4-1.0). Fill holes option can be use to ensure that whole fenestration area is covered

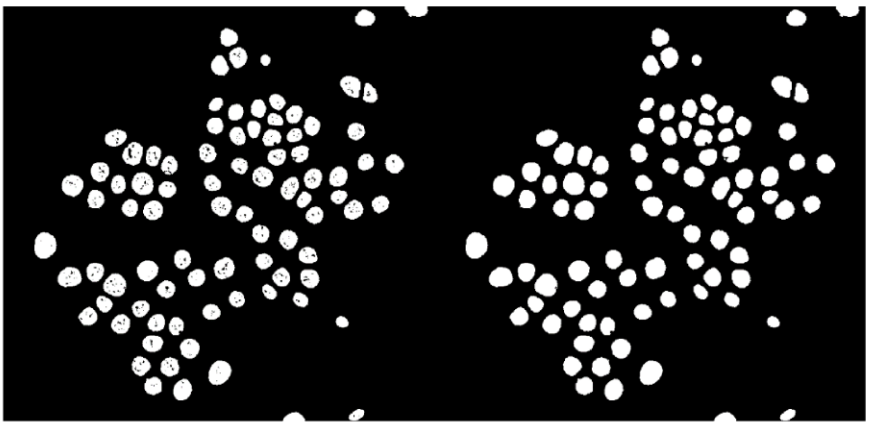

SI3. Difference in fenestration size for automatic methods

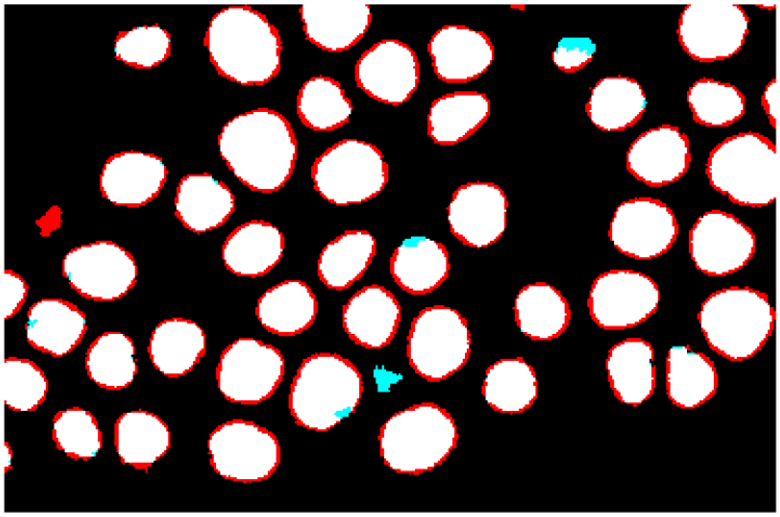

Fig. S2 Mask of fenestration detected by semi-automatic methods (white) and automatic/machine learning method (red).

Difference in diameter distribution between automatic and semi-automatic methods are related to the edge detection (Fig.S2). This difference can be removed by retraining of machine learning software or adjustment of threshold value in semi-automatic method.

Paper IV

Effect of caffeine and other xanthines on liver sinusoidal endothelial cell ultrastructure

Mao H., Szafranska K., Kruse L.D., Holte C.F., Wolfson D.L., Ahluwalia B.S., Whitchurch C.B., Cole L., Lockwood G.P., Diekmann R., Le Couteur D., Cogger V.C., McCourt P.A.G.

Nutrients (under review)

Article

Effect of caffeine and other xanthines on liver sinusoidal endothelial cell ultrastructure

Hong Mao[1,2,*,†], Karolina Szafranska[1,*, †], Larissa Kruse[1], Christopher Holte[1], Deanna L. Wolfson[2], Balpreet Singh Ahluwalia[2], Cynthia B. Whitchurch[3], Louise Cole[3], Glen P. Lockwood[4], Robin Diekmann[5,6], David Le Couteur[4], Victoria C. Cogger[4], Peter A.G. McCourt[1,4]

1 Vascular Biology Research Group, Department of Medical Biology, Faculty of Health Sciences, University of Tromsø, The Arctic University of Norway, Tromsø, Norway
2 Optical Nanoscopy Research Group, Department of Physics and Technology, Faculty of Science and Technology, University of Tromsø, The Arctic University of Norway, Tromsø, Norway
3 Microbial Imaging Facility. the ithree institute, University of Technology Sydney, Ultimo, NSW, Australia
4 Centre for Education and Research and ANZAC Research Institute, Concord Repatriation General Hospital, Concord, NSW, Australia; and The Faculty of Medicine and Health, University of Sydney,, Sydney, NSW, Australia
5 Cell Biology and Biophysics Unit, European Molecular Biology Laboratory (EMBL), Heidelberg, Germany
6 LaVision BioTec GmbH, Bielefeld, Germany
* Correspondence: Hong Mao, hong.mao@uit.no, Karolina Szafranska, karolina.szafranska@uit.no, szafranska.k.j@gmail.com, Vascular Biology Research Group, Department of Medical Biology, Faculty of Health Sciences, University of Tromsø-The Arctic University of Norway, 9037 Tromsø, Norway,

†These authors have contributed equally to this work and share first authorship

Abstract: (200 words) Xanthines such as caffeine and theobromine are among the most consumed psychoactive stimulants in the world, either as natural components of coffee, tea and chocolate, or as food additives. The present study assessed if xanthines affect liver sinusoidal endothelial cells (LSEC). Cultured primary rat LSEC were challenged with xanthines at concentrations typically obtained from normal consumption of xanthine-containing beverages, food or medicines; and at higher concentrations below the *in vitro* toxic limit. The fenestrated morphology of LSEC were examined with scanning electron and structured illumination microscopy. All xanthine challenges had no toxic effects on LSEC ultrastructure as judged by LSEC fenestration morphology, or function as determined by endocytosis studies. All xanthines in high concentrations (150 μg/mL) increased fenestration frequency but in physiologically relevant concentrations, only theobromine (8 μg/mL) showed an effect. LSEC porosity was influenced only by high caffeine doses which also shifted fenestration distribution towards smaller holes. Moreover, we noted some responses varied significantly between the individual rats. Differences between animal responses to the treatments were noted. If these compounds induce similar changes *in vivo*, age-related reduction of LSEC porosity can be targeted by oral treatment with theobromine or with other xanthines using targeted delivery.

Keywords: Coffee, caffeine, xanthines, liver, liver sinusoidal endothelial cell, fenestration

1. Introduction

Coffee is one of the most widely consumed beverages meaning that any potential effects related to coffee intake will have significant global implications. Furthermore, most people drink coffee daily due to its stimulating effects. The main active ingredient in coffee – caffeine, can be found also in other beverages (tea, soft and energy drinks), food (guarana berries, chocolate), dietary supplements or even painkillers [1]. Formulations consisting of caffeine and either aspirin (a non-steroidal anti-inflammatory drug, NSAID) or paracetamol, are effective treatments for headaches [2] and sore throats [3] and caffeine has been shown to have an analgesic effect alone [4]. Many studies have investigated the

associations between caffeine or coffee intake and health/diseases. Recently, the correlation between increased coffee consumption and improved neurocognitive functioning parameters was elicited in patients infected with human immunodeficiency virus (HIV) and hepatitis C virus (HCV) [5]. A different study showed that a sub-group of patients suffering from multiple sclerosis (MS) benefitted from additional coffee intake [6]. Interestingly, in a meta-analysis of studies about the effects of caffeine on Parkinson's disease (PD) caffeine appeared to both lower the rate of PD progression in patients suffering from the disease as well as decrease the risk of developing PD in the healthy population [7]. On the other hand, several studies have noted that an adjustment may be needed for an individual's caffeine dosage in relation to their age, sex and health conditions to maximize the positive and limit negative effects [8] [9].

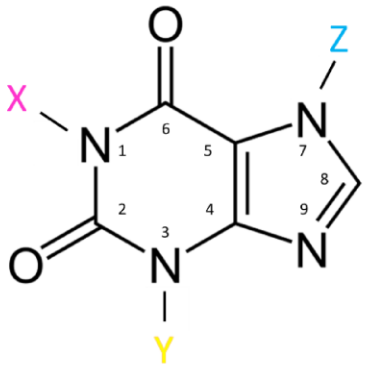

	X	Y	Z
Caffeine	CH_3	CH_3	CH_3
Theobromine	H	CH_3	CH_3
Theophylline	CH_3	CH_3	H
Paraxanthine	CH_3	H	CH_3

Figure 1 Figure 1 Chemical structure of xanthines. Caffeine (1,3,7-trimethylxanthine) is metabolized by demethylation in the liver to 3 main compounds: theobromine (3,7-dimethylxanthine), theophylline (1,3-dimethylxanthine) and paraxanthine (1,7-dimethylxanthine) [10]

Caffeine is primarily metabolized in the liver to theobromine, theophylline and paraxanthine (Figure 1). The demethylation process occurs in the hepatocytes via the cytochrome P450 enzyme system [10]. Overall, more than 25 metabolites have been identified in humans deriving from caffeine metabolism [11] [12], with paraxanthine accounting for approximately 80% of the metabolites in the human liver [13][14]. In rats and mice, however, all three main metabolites of caffeine are present in similar amounts [15][16]. All the aforementioned primary metabolites are pharmacologically active and their plasma concentration may exceed that of caffeine in some stages due to their respective rate of metabolism and clearance [10], especially paraxanthine [16] [17].

The liver, the body's largest internal organ, has the major role of detoxifying various metabolites in the human body. Liver sinusoidal endothelial cells (LSEC), which are located in hepatic sinusoids, play a fundamental role in maintaining the homeostasis and metabolic integrity of the liver [18]. LSEC are the most effective scavengers of blood-borne waste [19], regulate sinusoidal blood flow [20], trigger liver regeneration and contribute to hepatic complications, such as liver fibrosis and liver metastasis [21][22][18]. The distinct dynamic morphological features of LSEC – called fenestrations/fenestrae, enable bidirectional size-based transfer between the blood and the underlying hepatocytes. Fenestrations are non-diaphragmed nano-pores with diameters of 50-350 nm [23][24], and they are typically grouped in clusters called sieve plates [25][26]. The structural integrity of fenestrations is vital for the maintenance of regular exchange between the liver and the blood, and alterations in fenestrations can affect hepatocytes and liver function [26]. The regulation of fenestration size and frequency is not yet fully understood, but some signaling pathways have been shown to influence the formation of fenestrations [24]. For example, sildenafil (the active constituent of Viagra) was shown to improve porosity in both young and old mice [27], presumptively via regulation of intracellular cGMP levels (via nitric oxide) and/or vascular endothelial growth factor (VEGF)-related/(VEGF)-independent pathways [28][29]. It should be noted however that other pathways may also be involved

in the regulation of fenestration size and number (e.g. those mediated by calcium, regulated by myosin light chain (MLC) [24] or by alpha/beta-adrenergic receptors among others [30]).

Even though caffeine is primarily metabolized in hepatocytes, LSEC regulate transportation between the plasma and hepatocytes. Fenestrations create a dynamic barrier that can adapt to environmental conditions in a matter of seconds [31]. Caffeine intake is generally considered to be safe in moderate amounts (≤ 400 mg /day) in healthy adults [32][33], and with normal consumption the plasma concentrations are usually between 2-10 μg/mL (approximately 10-50 μM), rarely exceeding this [34]. Toxic effects occur for plasma concentrations of >40 μg/mL [34] [35]. The adverse effects of large doses of caffeine have been noted from early times, and these include nervousness, anxiety, insomnia, irregular heartbeats, excess stomach acid and heartburn [36]. However, it is important to understand that the liver can be exposed to far greater concentrations of caffeine and related compounds because the uptake takes place in the gastrointestinal (GI) tract. All the venous blood from the GI tract is collected into the portal vein, which then provides 75% of the blood inflow to the liver. This is the first-pass effect whereby the initial local concentration in the liver can be much higher while systemic plasma concentrations of the studied compound are lower [37].

The commercially available products rarely lead to toxic plasma concentrations of xanthines. A single standard cup of black coffee can yield a peak plasma caffeine concentration of about 2 μg/mL, while caffeine supplements can yield up to 10 μg/mL [38]. However, somewhat higher concentrations (8-20 μg/mL) are needed for the therapeutic effect of the caffeine metabolite theophylline in controlling asthma in adult humans [39][40]. Life-threatening effects were reported for the theophylline serum concentrations above 30 ug/mL [41]. Chocolate contains two methylated xanthine derivatives (caffeine and theobromine), which may contribute to its reinforcing effects [42]. It was reported that 370 mg theobromine from 82g chocolate (40-80g of dark chocolate or 110g of regular milk chocolate, roughly the size of a chocolate bar) was rapidly absorbed in humans and produces a plasma concentration of 8 μg/mL after 2 hours [43][44][45]. In humans, paraxanthine plasma levels are usually higher than caffeine and can remain at a high level for a longer time due to the slower clearance and ongoing metabolism of caffeine [17].

Although coffee, chocolate, and other caffeinated substances such as tea are widely used all over the world, the effects of caffeine and its metabolites on LSEC have not been investigated. Here, we study the influence of xanthines on rat LSEC in both physiologically achievable concentrations as well as in higher concentrations that can simulate the first-pass effect.

2. Materials and Methods

2.1. Rat LSEC production and cell culture

Sprague Dawley male rats (Animal Resource Centre, Murdoch, Western Australia) were kept under standard conditions and fed standard chow *ad libitum* (Glen Forrest, Western Australia). The experimental protocols were approved by the ethics committee of the Sydney Local Health District Animal Welfare Committee (Approval 2017/012A). All experiments were performed in accordance with relevant approved guidelines and regulations.

Rats (body weight 300-400 g, age 2-3 months) were anesthetized with a mixture of 10 mg/kg Xylazine (Bayer Health Care, California, USA) and 100 mg/kg ketamine (Ketalar, Pfizer, New York,USA), and LSEC were isolated and purified as described Smedsrød et al. [46]. Several fractions of cells were frozen and prepared for each of the methodologies as described previously [47].

Reagents included caffeine (Cat No. C0750; Sigma-Aldrich, Oslo, Norway), sildenafil citrate (Cat No. PHR1807, Sigma-Aldrich, Oslo, Norway), theobromine (Cat No. T4500; Sigma-Aldrich, Oslo, Norway), theophylline (Cat No. T1633; Sigma-Aldrich, Oslo, Norway), and paraxanthine (Cat No. P6148; Sigma-Aldrich, Oslo, Norway). Fibronectin was isolated from human plasma using GelatinSepharose 4B (Cat No. 17-0956-01, GE

Healthcare, Sydney, Australia) according to the manufacturer's instructions. All reagents were dissolved in serum-free RPMI media (Sigma-Aldrich, Sydney, Australia/Oslo, Norway). All experiments were performed in triplicate, using cells isolated from 3 different rats. *In vitro* treatment of LSEC with caffeine was at 8 and 150 μg/mL. Metabolites of caffeine: theobromine (8 and 150 μg/mL), theophylline [40] (20 and 150 μg/mL), paraxanthine (8 and 150 μg/mL) were applied at physiologically relevant and high concentrations in the same manner as for caffeine. Sildenafil was used at 0.06 and 0.6 μg/mL concentrations, based on previous studies [27][48], for the purpose of method validation.

2.2. Scanning electron microscopy (SEM)

For SEM preparation, cryopreserved rat LSEC were used, the thawing and culturing protocols are described in our previous study [47]. Cells were plated on 0.2 mg/mL fibronectin coated coverslips and cultured (37°C, 5% CO_2) for 3 h in serum-free RPMI-1640 (with 10,000 U/mL Penicillin, 10 mg/mL Streptomycin, 1:100) (Sigma-Aldrich, Sydney, Australia) at a density of 0.2×10^6 cells/cm2. The LSEC were treated with various agents for 30 min to determine their effects on fenestrations, then fixed using McDowell's solution (4 % formaldehyde and 2.5 % glutaraldehyde in PHEM buffer pH 7.2) for 15 min and stored in McDowell's solution until preparation for SEM. After washes with PHEM, the coverslips containing the cells were treated with freshly made 1% tannic acid in 0.15 mol/l PHEM buffer for 1 hour, 1% OsO_4 in water for 1 hour, dehydrated in ethanol (30%, 60%, 90% for 5 minutes each, 5 times 100% ethanol for 4 minutes each), and incubated twice in hexamethyldisilazane for 2 minutes (Sigma-Aldrich, Oslo, Norway), before coating with 10-nm gold/palladium alloys. Imaging and image analysis was performed blind to the sample ID. Coded specimens were examined using a commercial SEM (Sigma HV0307, Zeiss) at 2kV. Large fields of view (magnification of 1k) containing several/individual cells were randomly acquired to determine cell culture condition and cell size, and high-resolution SEM images of cell at magnification of 15k were selected blindly to assess fenestration size.

Fenestration size, porosity and frequency were assessed in SEM images from each cell culture selected from different areas. Open pores with diameters between 50–350 nm were defined as fenestrations and holes larger than 350 nm as gaps. Porosity was defined as the sum area of fenestrations per total area of the cell in the micrographs. Frequency was denoted as the total number of fenestrations per sum area of the cell excluding the sum area of gaps [49].

2.3. Structured illumination microscopy (SIM)

After fixation, the cells were stained with CellMask Green (1:1000 in phosphate buffered saline (PBS)) for 10 minutes, washed 3 times in PBS and then mounted in Vectashield antifade mounting medium (Vectro Laboratories, Burlingame, California) and imaged using a commercial super-resolving SIM (DeltaVision/OMXv4.0 BLAZE, GE Healthcare) with a 60X 1.42NA oil-immersion objective (Olympus). 3D-SIM image stacks of 1 μm were acquired with a z-distance of 125 nm and with 15 raw images per plane (five phases, three angles). Raw datasets were computationally reconstructed using SoftWoRx software (GE Healthcare). The datasets were further analyzed using the pixel classification workflow in the freely available machine learning image processing software Ilastik [51]. Fenestration detection steps were described in our previous study [50], notably, the detected objects with diameters below 50 nm and above 300 nm were excluded prior to binning for SIM images.

2.4. Endocytosis and degradation assay.

For quantitative studies of endocytosis and degradation, fully confluent cultures of cryopreserved rat LSEC (approx. $0.25–0.3 \times 10^6$ cells/cm^2) established in 24-well culture dishes coated with fibronectin, were pretreated with different agents for 30 minutes (at 37 °C, 5% CO_2), subsequently incubated in 0.2 mL serum-free RPMI containing 1% human serum albumin and ~20000 cpm ^{125}I-FSA for 2 h (total incubation time with drugs was 2.5

h). Thereafter, the cell-associated and degraded FSA fractions were assayed as described previously [50]. The radioactivity was measured using a Cobra II, Auto-Gamma detector (Packard Instruments, Laborel, Oslo, Norway).

2.4. Data analysis and statistics

We selected image analysis methods according to our previous study [49]. Fenestration diameters were measured from SEM images using a threshold-based semi-automated method. This approach allowed us to greatly improve both the number of analysed fenestrations as well as the precision of measurement. Mean fenestration diameters were calculated from the single fenestration areas obtained from the segmented images (See supplementary information Figure S2). Fenestration frequency was obtained from the manually counted fenestrations from each cell. This reduced the influence of any imaging artifacts including differences in image quality between the samples. Porosity was calculated as a combination of both fenestration number and size distribution (details can be found in the supplementary information of [49]).

All graphs were prepared using OriginPro software (OriginPro 2021, OriginLab Corp., Northampton, Massachusetts) and image analysis was performed using the free, open-source software Fiji/Image J [51]. Significance was assessed using a two-tailed student T-Test for porosity and fenestration frequency parameters. Fenestration diameters and endocytosis experimental data were analyzed with one-way ANOVA performed using the GraphPad Prism 8 (La Jolla, USA, www.graphpad.com), and the post hoc tests were used with Dunnett's multiple comparisons test for each treatment with control. The results were considered significant if $p<0.05$ (*) or described as trends for $p<0.1$ (#).

3. Results and discussion

3.1. Endocytosis

LSEC are the main scavenger cells in the body, clearing various compounds from the blood [18]. A well-established method for validation of LSEC functional viability is a measurement of their endocytic capacity of denatured or modified proteins such as formaldehyde-treated serum albumin (FSA) [52]. To assess the possible toxic effects of xanthines and sildenafil, we measured the uptake and degradation of radiolabeled FSA. The data show no significant effects on endocytosis (Figure 2) except with a high (150 µg/mL) dose of caffeine where a 22% decrease in the degraded fraction was observed. Evaluation of cell morphology on SEM images did not reveal any apparent morphological disruptions characteristic for LSEC (Figure 3) (indicated by e.g. large gaps >400 nm, cell shrinkage or disrupted cell edges). The additional morphological assessment was performed using structured illumination microscopy (SIM) (Figure 6). Nevertheless, this small decrease of degradation of FSA could be related to the toxic effects of the compound, suggesting that a concentration of 150 µg/mL is just on the edge of the *in vitro* toxic dose of caffeine for LSEC.

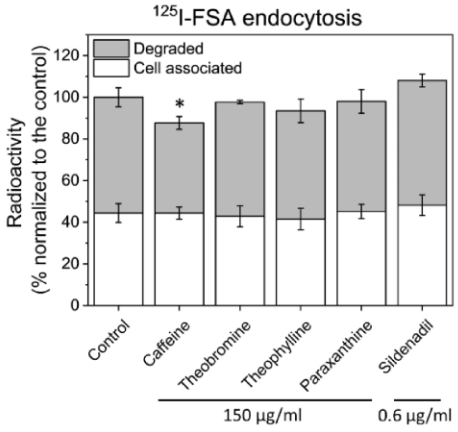

Figure 2 ^{125}I-FSA uptake in LSEC after treatments with high doses of xanthines and sildenafil. Incubation time with ^{125}I-FSA – 2h. Bars indicate mean ± SD, n = 3-4, *$p<0.05$

3.2. LSEC morphology

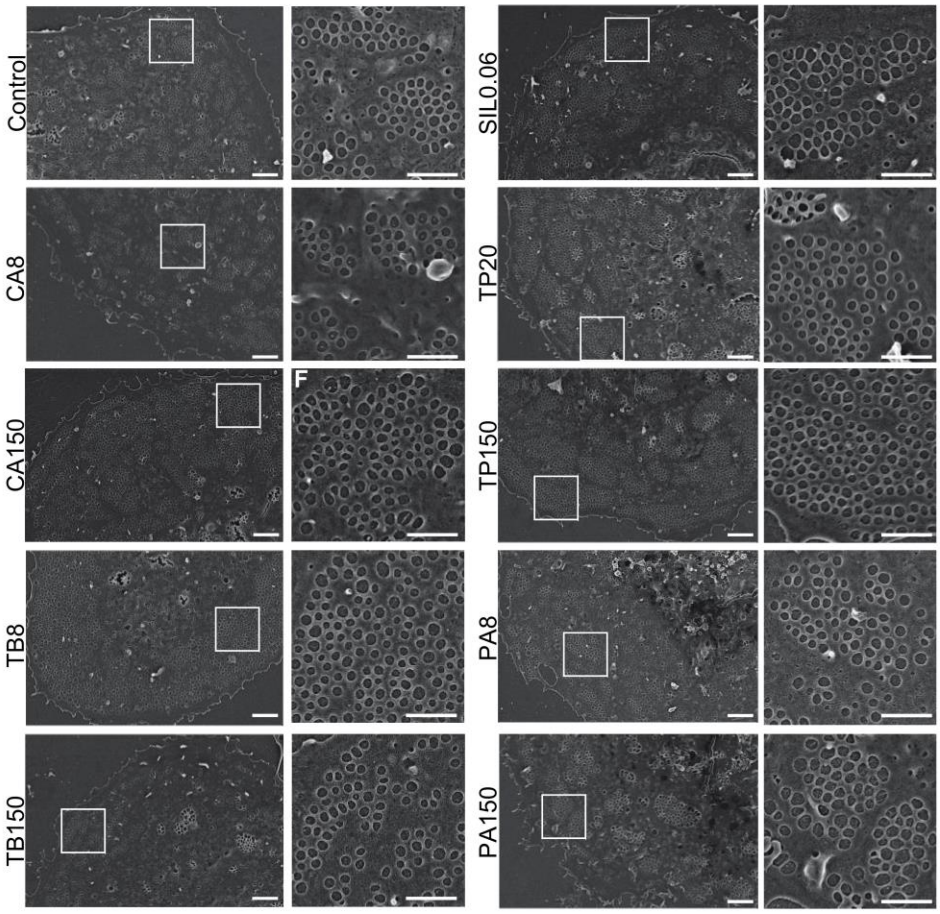

Figure 3 Representative scanning electron microscopy (SEM) images following xanthines and sildenafil treatment of rat liver sinusoidal endothelial cell (LSEC) fenestration. Scale bar size: overview images 2 μm, inset 1 μm. CA - caffeine, TB - theobromine, TP – theophylline, PA - paraxanthine, SIL – sildenafil. Indicated concentrations are μg/ml.

A typical flat, well-spread morphology was observed in all samples, and cell culture purity was assessed based on the presence of the unique morphological feature of LSEC—fenestrations (Figure 3). SEM data with the analyzed number of cells as well as fenestration diameter, porosity (i.e. percentage of the cell surface covered by fenestrations) and frequency (i.e. the number of fenestrations per cell area) following various treatments are summarized in Table 1. The fenestration diameter after different treatments remains within the range of 179 to 203 nm, which is consistent with previously reported data [23] [24]. Roughly 7200-69000 "holes" were analyzed for each treatment group to calculate fenestration diameters. Fenestration frequency and porosity were measured for 60 cells total from 3 individual animals.

The cell morphology from different treatment groups was observed after 30 minutes incubation. No drastic changes and signs of toxicity were noticed. Only the high dose (150 μg/mL) of theobromine showed possible early signs of toxicity in some cells – namely irregular cell edges and shrinking.

3.3. Quantitative effects on fenestrations

Table 1 Changes in the parameters describing LSEC fenestrated morphology. Measurements were extracted from SEM images using semi-automatic (diameter) and manual methods (frequency).

Treatment		No. fenestrations measured	No. cells	Diameter [nm] ± SD	Porosity [%] ± SD	Frequency [No./μm²] ± SD	No. cells measured
Drug	Concentration [μg/mL]						
Control	-	68829	157	190 ± 51	7.50 ± 4.24	2.52 ± 1.33	51
Caffeine	8	7235	33	176 ± 46*	7.04 ± 3.27	2.72 ± 1.27	49
	150	18844	34	179 ± 53*	9.13 ± 3.91*	3.07 ± 1.38*	60
Theobromine	8	12771	20	185 ± 48*	7.50 ± 3.29	3.32 ± 1.42*	55
	150	7029	17	177 ± 58*	7.65 ± 3.48	3.15 ± 1.43#	49
Theophylline	20	13496	27	188 ± 51*	8.15 ± 3.36	2.61 ± 1.14	54
	150	20311	33	178 ± 47*	8.97 ± 3.45#	3.23 ± 1.39*	60
Paraxanthine	8	15210	21	178 ± 46*	8.61 ± 3.71#	2.80 ± 1.28	60
	150	16766	36	190 ± 55	8.79 ± 4.27#	2.88 ± 1.40#	56
Sildenafil	0.06	13857	29	191 ± 52	7.56 ± 3.81	2.31 ± 1.20	60
	0.6	16443	33	180 ± 56*	6.44 ± 3.36	2.45 ± 1.23	60

SD – standard deviation. *p<0.05, #p<0.1.

Changes in fenestration size in combination with differences in fenestration number may also influence the average cell porosity. Fenestration frequency is a parameter describing the number of fenestrations per cell which in combination with fenestration size can be translated into porosity – the percentage of the cell area covered in fenestrations. The diameter of fenestrations is responsible for (size-dependent) selectivity of passive transport between the bloodstream and hepatocytes, while the number of fenestrations per cell/area relates to the rate of liver filtration [53].

Some of the xanthines elicited changes in the fenestration frequency (Figure 4, Table 1): a significant increase was observed for the high doses (150 μg/mL) of caffeine and theophylline and lower dose (8 μg/mL) of theobromine, (22%, 28% and 32%, respectively). Also, high doses of theobromine and paraxanthine show increasing trends in fenestration number. The less prominent effect of high versus low dose of theobromine may be a result of early toxic effects suggested by the visual examination of the cell images - some cells treated with the high dose showed signs of irregular cell edges or reduced cell area. The trend after paraxanthine treatment may suggest that exposure to the drug longer than used here 30 minutes, may improve LSEC morphology. In humans, paraxanthine is the main metabolite of caffeine and its concentration in the plasma can reach higher values than caffeine itself and remain at this high level for a prolonged period, up to a few hours [17]. Our treatments of adult rat LSEC with 0.06 and 0.6 μg/ml sildenafil showed no significant changes in fenestration frequency or porosity, whereas Hunt et al. [27] also reported no changes after 0.6 μg/ml sildenafil treatment in young mice but increased porosity in old mice. They also reported a decrease in fenestration diameter of about 10 nm in mice after treatment with 0.3 μg/ml sildenafil, while in our study we observed similar effects but with 0.6 μg/ml treatment of rat LSEC (Table 1). This suggests a dose and/or species dependence of sildenafil which should be investigated further.

Even though we did not observe large changes in the mean fenestration diameters, the porosity parameter shows the influence of the diameter distribution (Table 1). A significant increase (22%) in porosity was observed only in the high dose of caffeine. The high dose of caffeine did not affect the mean fenestration diameter, so the effect is visible

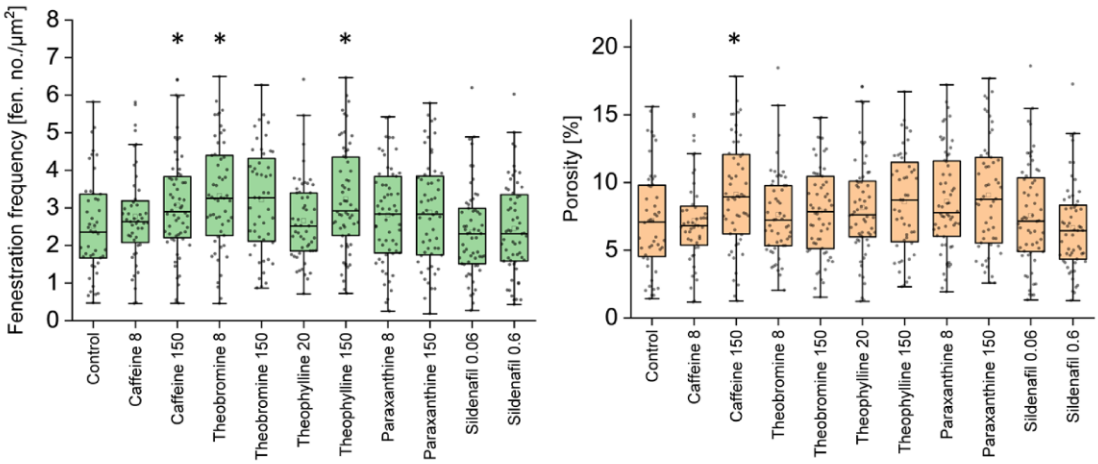

Figure 4 Fenestration frequency and porosity of LSEC treated with xanthines and sildenafil. The graphs present combined data from 3 studied animals, data from separate animals can be found in figure S4. Each dot represents analyzed SEM image of a single cell. * $p<0.05$

in both parameters. On the other hand, the high dose of both theobromine and theophylline caused a decrease in fenestration size which counteracted the influence of increased fenestration number. *In vivo*, such an occurrence would suggest faster filtration of the smaller molecules in the liver. For the sildenafil treatment, we observed a decrease in the porosity in the 0.6 µg/ml dose due to the decrease in the fenestration size. This finding correlates with the findings of Hunt et al. [27] where a similar effect was observed but for 0.3 µg/ml dose in young mice. Paraxanthine for both concentrations and high dose theophylline treatments also showed an increasing trend in porosity.

To further understand the changes in fenestration diameter after the various treatments, we studied the whole distribution of fenestration size, instead of just average values. We observed shifts in the diameter histograms, and to better visualize that data we separated fenestrations into 3 size groups: small (S) - <100 nm, medium (M) – 100-200 nm, large (L) - >200 nm. These groups can be related to the filtration of different molecules that are metabolized by hepatocytes – HDL and LDL have a diameter below 100 nm, while chylomicron remnants are usually above 100 nm in diameter [54]. Already in 1970, Wisse pointed out that fenestration size may play a role in liver filtration [20] and later in 1995, Fraser et al. [55] proposed the barrier function of LSEC that is chylomicron remnant clearance, namely that LSEC fenestration diameter dictates which chylomicron remnants can be removed from the circulation. Changes in the distribution of fenestrations between those groups relative to control can be found in Figure 5.

We observed a decrease in the large fenestrations after treatment with all xanthines with the exception of the high paraxanthine dose. The high dose of theophylline and lower dose of paraxanthine showed a 33% decrease in the number of large fenestrations. The high dose of caffeine also was responsible for an almost 22% reduction in the large fenestration number. The medium size fenestration fraction was increased by low doses of caffeine and paraxanthine and high dose of theophylline by 29%, 26% and 25%, respectively. The remaining treatments show little to no effects in this size range. Interestingly, high doses of caffeine and theobromine cause a large increase in the detectable number of small fenestrations, of 48% and 95%, respectively. The high dose of paraxanthine also resulted in a 23% increase in small fenestrations, but unlike caffeine or theobromine it had very little impact on either medium or large pores. Sildenafil treatment showed an increase of 15% and 71% in small fenestrations for both low and high doses, respectively, with only minimal effect on the number of medium and large pores.

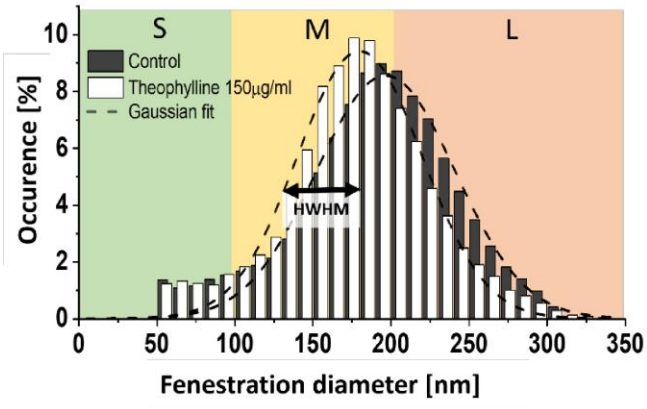

Changes in the distributions of fenestration diameter

Treatment	Dose [μg/ml]	Fenestration diameter			
		S (<100 nm)	M (100-200nm)	L (>200nm)	Gaussian mean ± HWHM
Caffeine	8	2.9% ↑	28.6% ↑	37.8 ↓	179 ± 45*
	150	48.3% ↑	9.4% ↑	21.9% ↓	187 ± 49*
Theobromine	8	1.5% ↑	11.6% ↑	15.5% ↓	192 ± 40*
	150	94.5% ↑	2.4% ↓	14.8% ↓	188 ± 61*
Theophylline	20	6.6% ↑	3.7% ↑	6.7% ↓	195 ± 42*
	150	1.3% ↑	25.0% ↑	33.5% ↓	180 ± 43*
Paraxanthine	8	4.2% ↓	26.3% ↑	33.7% ↓	182 ± 42*
	150	22.6% ↑	5.3% ↓	1.9% ↑	198 ± 49
Sildenafil	0.06	14.5% ↑	10.8% ↓	11.2% ↑	203 ± 43
	0.6	71.2% ↑	0.5% ↓	12.5% ↓	193 ± 45*
Control	-	-	-	-	197 ± 48

HWHM – half width at half maximum

Figure 5 Fenestration distribution in LSEC treated with xanthines and sildenafil. The graph presents the control group and theobromine (high concentration) treatement as an example (all histograms can be found in supplementary materials (Figure S1). S (small)/M (medium)/L (large) represent the fractions of fenestrations according to their size. Changes in the fenestration distribution are presented in the table as relative to the control/untreated samples. Gaussian mean is calculated as a center of Gaussian fit. The data was obtained from SEM images using semi-automated method.

The detailed analysis of the fenestration size distribution reveals some additional information about the changes in the liver sieve. To date, most studies reported changes in fenestration size as just a difference in the mean value but a Gaussian-like distribution of fenestration was confirmed in multiple studies [26][56][49]. Here, we show that the fenestration distribution shape can remain as a Gaussian distribution with little to no changes to the mean value while changes in specific fractions, reflected in the distribution width, can be significant and have biological implications. For example, low dose paraxanthine results in over 20% increase in <100 nm fenestrations with only 5% increase in medium-size holes without a change in the mean fenestration value – 197 nm and 198 nm in control and after treatment. Meanwhile, such a change *in vivo* can lead to increased availability of VLDL, HDL and other small molecules to hepatocytes, therefore increasing filtration from the bloodstream. On the other hand, a decrease in the large fenestration fraction (such as after low doses of caffeine and paraxanthine or high dose of theophylline) can lead to reduced filtration of some fractions of larger chylomicron remnants. Changes in transportation between plasma and hepatocytes can therefore have both positive and negative effects. Lower filtration can have a protective role against reducing the exposure of some agents to hepatocytes, but it also can increase lipoprotein fractions in the blood which may contribute to cardiovascular diseases. Wright et al. [57] showed that smaller liver fenestrations observed in rabbits can be a cause of their susceptibility to arteriosclerosis. This theory is supported by the increase of fenestration size in rabbits reported after pantethine treatment, which reduced their sensitivity to dietary cholesterol [58]. The chylomicron remnants size varies from 100 to even 1000 nm, so the reduction in large or medium fenestrations could correspondingly affect/lower the filtration of certain fractions of chylomicrons containing different amounts of triglycerides and cholesterols.

To validate our findings, we also assessed the fenestrations with some treatments on SIM (Figure 6, caffeine 150 μg/mL and theophylline 30 μg/mL are shown for comparison). Similar to the SEM observations, LSECs featured numerous fenestrations which were clustered as sieve plates. Further assessment of the diameter of fenestrations was conducted in a machine learning assisted workflow, as was used in a previous study [48]. By comparing the mean fenestration diameter in our dehydrated SEM result with wet-fixed SIM data, the latter resulted in a 15% smaller size for the control groups [59]. The SIM data

confirmed the increase in fenestration frequency and changes in diameter distribution induced by the high dose of caffeine and theophylline (Figure 6).

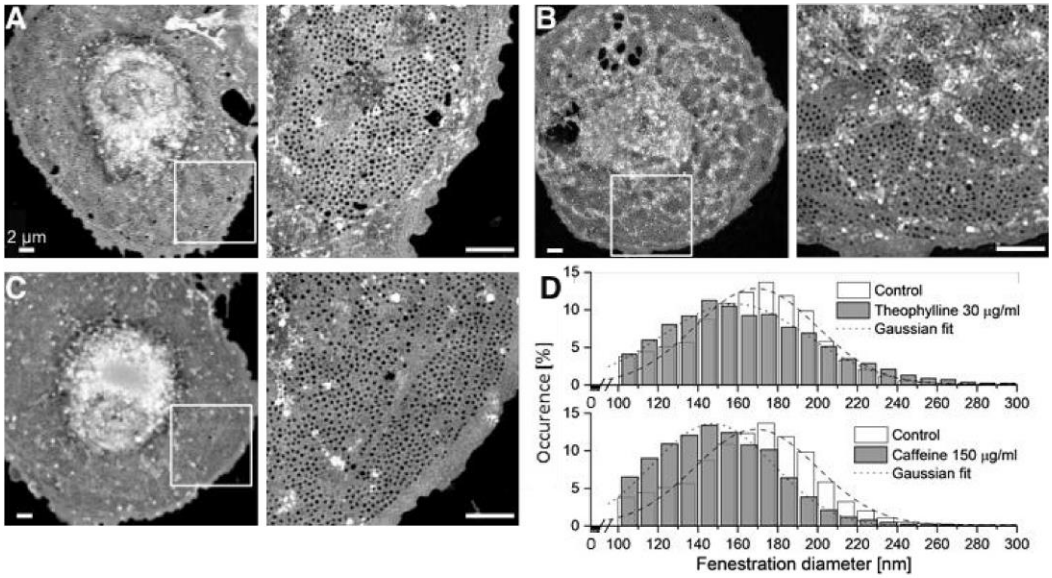

Figure 6 Maximum intensity z-projections of 3D-SIM images show fenestrations grouped in sieve plates (inset) following treatments - A: Control; B: Theophylline (30 µg/mL); C: Caffeine (150 µg/mL); D: Fenestration size distribution after treatments. Mean diameter calculated from Gaussian fits ± HWHM: Control 169±35 nm, theoplylline 159±43 nm, caffeine 148±35 nm. Scale bars: 2 µm

Though not as high resolution as SEM, the SIM technique gives a resolution double that obtained via conventional light microscopy. The average diameter of fenestrations is well discerned within the regular observed size range. For SIM, the samples can be studied while wet, thus avoiding the artifacts from dehydration required for SEM. 3D-SIM was used in our study to image fenestrations in fixed rat LSECs in Vectashield mounted samples. Importantly, a limitation of the linear SIM is that only fenestrations with a diameter around 100 nm or more are resolved. As mentioned above, by comparing the results of the control group from both methods, the mean fenestration diameter was larger in SEM processed samples, which might be due to the dehydration step during SEM preparation. Notably, due to the resolution limit of SIM being around 100 nm, the diameter analyzed from SIM images was of the same magnitude (Figure 6D). Furthermore, the analysis of porosity of SIM images at such magnitude is not as accurate when compared with SEM results.

3.4. Individual animal differences

To further analyze the effects of xanthines and sildenafil on LSEC morphology, we investigated the influence on individual animals (bio-replicates). The data from each individual animal is presented in Figure 7. For some treatments, significant changes among the bio-replicates were found for both fenestration frequency and porosity. Primary LSEC morphology can be studied only for a short time after isolation, so small but non-significant differences between the untreated control groups are the norm. Overall, the individual differences tend to be dose-related i.e. the more significant differences among bio-replicates were observed in the high dose versus the low dose groups. For instance, caffeine and theophylline in low doses did not show differences between individuals whereas high doses of these elicited significant changes. Notably, cells from rats II and III responded more to both treatments (150 µg/mL caffeine and theophylline) than rat I, even when taking into consideration of the difference in control samples. The low dose of theobromine also revealed that rat III showed a higher increase in fenestration frequency than other rats. 150 µg/mL paraxanthine treatment resulted in an increase in both porosity and

fenestration frequency in rat II but not in rats I and III. Interestingly, both sildenafil treatments affected cells from animal I rather more than animals II and III which is even more significant when considering the low control values for the animal. These individual differences are not apparent when data from all animals are pooled together.

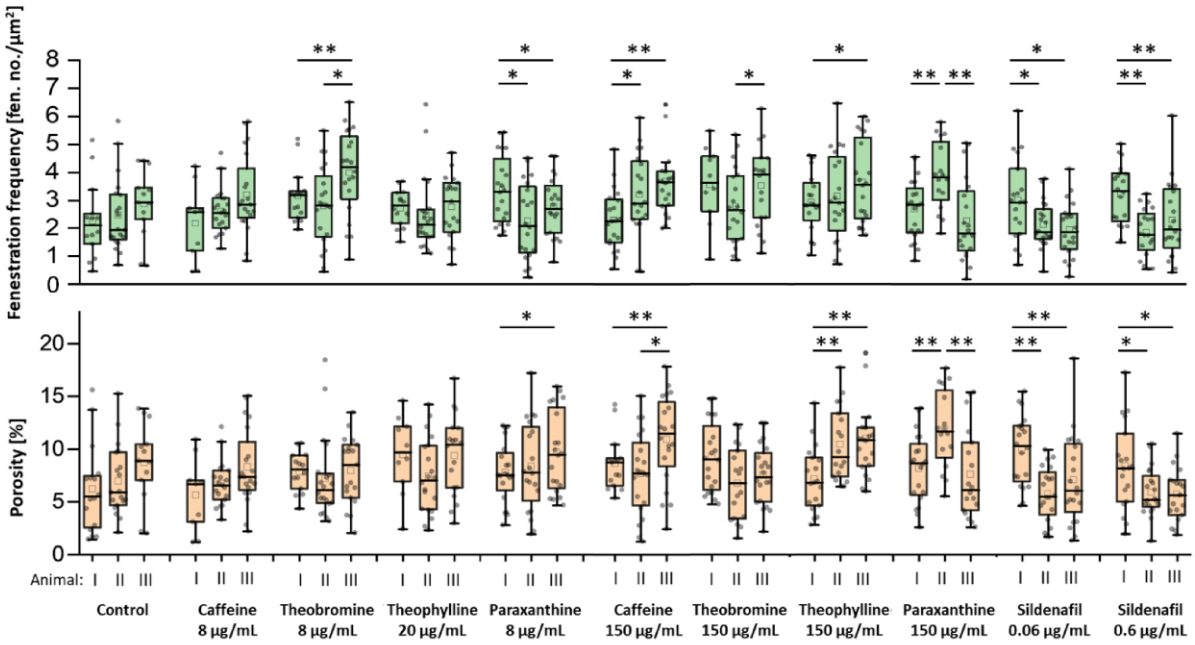

Figure 7 Individual differences in fenestration frequency and porosity between the studied animals after treatments. Each dot represents the analyzed image of a single cell. Indicated significance is within the treatment group * $p<0.05$, ** $p<0.01$

In this study, we used cells isolated from male Sprague Dawley rats, which is one of the most widely used outbred rat stock. Even though the animals are nearly identical, a recent study of the whole genotypes obtained from these rats, even when from the same breeding facility, showed differences between animals [60]. This may account, at least in part, for the different responses to xanthines observed on LSEC. Further to this, caffeine is metabolized in hepatocytes mainly by the CYP1A2 enzyme and the coding gene of this enzyme varies between humans [61]. The differences in this gene cause the differences in the caffeine metabolism which affects clearance time and therefore results in the different total stimulating effects of caffeine. Another study conducted on twins subjected to oral caffeine intake showed that although genetic factors play the main role in differences in caffeine metabolism, environmental factors also can influence the activity of the CYP1A2 enzyme c. In humans, this phenomenon manifests as different sensitivity to coffee/caffeine.

3.5. Translational relevance

Even though LSEC do not express CYP1A2 [62] nor metabolize caffeine *per se*, here we show that xanthines can affect their morphology. The exact mechanism is not known but there are several receptors and pathways present in LSEC that can be influenced. Based on our extensive review of mechanisms behind the structure and functioning of LSEC fenestration, some possible mechanisms of action can be proposed [24]. For example, changes in intracellular cGMP are associated with fenestration regulation [27] and cGMP levels are mainly controlled by various phosphodiesterases (PDE) as well as ABC transporters, whereas both caffeine and theophylline are non-specific PDE inhibitors [63][64]. Caffeine and paraxanthine can also act through nonselective antagonizing of adenosine receptors [65], which could influence fenestrations via reduction of cAMP. This mechanism has not been confirmed in LSEC yet, however, the effects of adenosine receptors in the liver are currently under investigation [66].

Daily consumption of 40-80 g of dark chocolate or 110 g of regular milk chocolate yields a plasma theobromine concentration of 4-8 μg/mL in humans, which is within the region that elicits increased porosity in rat LSEC *in vitro*. Our study demonstrated theobromine, in physiologically relevant concentration, may increase the fenestrations frequency in LSEC, which may further affect hepatocyte metabolism and xenobiotic detoxification. If the results in this study translate to the *in vivo* context, the theobromine induced increase in fenestration number could improve liver function by enhancing the bi-directional exchange of substrates between the plasma and the hepatocytes, for example in the elderly who have reduced LSEC porosity. On the other hand, due to fenestration loss associated with ageing, some hepatocyte-targeting drug dosages should be adjusted for elderly people [67]. The otherwise positive effect or re-fenestration (induced reappearance of fenestrations) after xanthine treatment could lead to toxic effects due to the sudden increase of drug levels to which hepatocytes are exposed. This effect may be even more relevant for the people taking multiple drugs at the time as polypharmacy (daily intake of 5 or more drugs) is steadily increasing in recent years [68].

The positive effects of high doses of caffeine and theophylline are however harder to translate into useful intervention for the benefit of liver health as this concentration (150 μg/mL) is within the toxic range for those compounds. Recent studies have suggested the high plasma concentration needed for effect can be avoided if therapies are directly delivered to LSECs via nanoparticles and may result in similar *in vivo* effects as observed *in vitro* [69][70]. Further studies are clearly required to determine if xanthines affect fenestrations *in vivo*. Previous studies investigated the possibility of using rates of caffeine clearance as a guide to deteriorating liver function in cirrhosis. The results could be explained by the effect on LSEC fenestrations as the caffeine clearance did not correlate with conventional liver function tests [37]. These findings suggest that the development of the new tests of hepatic function should take into consideration also possible effects of the agents on the LSEC barrier, and not only hepatocyte metabolism.

4. Conclusions

In conclusion, we have shown *in vitro* xanthine treatments with caffeine, theobromine, theophylline and paraxanthine elicit changes in fenestration size, porosity and frequency in rat LSEC. Caffeine and theophylline in high doses increase fenestration frequency and the number of smaller-sized fenestrations in LSEC. A high dose of caffeine has an inhibitory impact on the uptake of soluble macromolecules. Theobromine at a physiologically relevant dose also increases fenestration frequency in rat LSEC. Although similar findings remain to be confirmed *in vivo,* if theobromine elicits these effects in animal studies, it might prove to be a useful (and simple) intervention (via chocolate) to improve LSEC porosity in elderly people. Concomitant to this, caffeine and theophylline could be used for the improvement of LSEC fenestration number; however, a drug delivery system targeting LSEC would be required to avoid systemic side effects.

Author Contributions: Conceptualization, DLW, HM, KS, PM; image acquisition, HM, KS, CFH, CBW, LC; data analysis, KS, HM, LDK, CFH; methods optimization, CBW, RD, DLC, VCC; cell preparation, GL, HM, KS; figures and graphics preparation, KS, HM, DLW; writing—original draft preparation, HM, KS.; writing—review and editing, all authors; funding acquisition, PM, BSA. All authors have read and agreed to the published version of the manuscript.

Funding: This study was supported by grants from the Tromsø Research Foundation/Trond Mohn, the University of Tromsø-The Arctic University of Norway, the Research Council of Norway FRIMED grant no. 262538, FRIMED2/FORSKER21 grant no. 325446, Nano2021 grant no. 288565 and Marie Sklodowska-Curie Grant Agreement No. 766181, project: DeLIVER, and the Engelhorn Foundation (Postdoctoral Fellowship to RD).

Acknowledgments: The authors would like to thank Randi Olsen and Tom-Ivar Eilertsen from Advanced Microscopy Core Facility at UiT for the electron microscopy expertise.

Conflicts of Interest: The authors declare no conflict of interest

References

1. Heckman, M.A.; Weil, J.; de Mejia, E.G. Caffeine (1, 3, 7-Trimethylxanthine) in Foods: A Comprehensive Review on Consumption, Functionality, Safety, and Regulatory Matters. *J. Food Sci.* **2010**, *75*, 77–87, doi:10.1111/j.1750-3841.2010.01561.x.
2. Pini, L.A.; Del Bene, E.; Zanchin, G.; Sarchielli, P.; Di Trapani, G.; Prudenzano, M.P.; LaPegna, G.; Savi, L.; Di Loreto, G.; Dionisio, P.; et al. Tolerability and Efficacy of a Combination of Paracetamol and Caffeine in the Treatment of Tension-Type Headache: A Randomised, Double-Blind, Double-Dummy, Cross-over Study versus Placebo and Naproxen Sodium. *J. Headache Pain* **2008**, *9*, 367–373, doi:10.1007/s10194-008-0071-5.
3. Schachtel, B.; Fillingim, J.M.; Lane, A.C.; Thoden, W.R.; Baybutt, R.I. Caffeine as an Analgesic Adjuvant A Double Blind Stody Comparing Aspirin with Caffeine to Aspirin and Placebo in Patients With Sore Throat. *Arch Intern Med* **1991**, *151*, doi:10.1001/archinte.151.4.733.
4. Ward, N.; Whitney, C.; Avery, D.; Dunner, D. The Analgesic Effects of Caffeine in Headache. *Pain* **1991**, *44*, 151–155, doi:10.1016/0304-3959(91)90129-L.
5. Antwerpes, S.; Protopopescu, C.; Morlat, P.; Marcellin, F.; Michel, L.; Carrieri, M.P.; Hepavih, C.O.; Group, S. Coffee Intake and Neurocognitive Performance in HIV/HCV Coinfected Patients (ANRS CO13 HEPAVIH). *Nutrients* **2020**, *12*, doi:10.3390/nu12092532.
6. Herden, L.; Weissert, R. The Effect of Coffee and Caffeine Consumption on Patients with Multiple Sclerosis-Related Fatigue. *Nutrients* **2020**, *12*, doi:10.3390/nu12082262.
7. Hong, C.T.; Chan, L.; Bai, C. The Effect of Caffeine on the Risk and Progression of Parkinson's Disease: A Meta-Analysis. *Nutrients* **2020**, *12*, doi:10.3390/nu12061860.
8. Nowaczewska, M.; Wicinski, M.; Kazmierczak, W. The Ambiguous Role of Caffeine in Migraine Headache: From Trigger to Treatment. *Nutrients* **2020**, *12*, doi:10.3390/nu12082259.
9. Jee, H.J.; Lee, S.G.; Bormate, K.J.; Jung, Y.S. Effect of Caffeine Consumption on the Risk for Neurological and Psychiatric Disorders: Sex Differences in Human. *Nutrients* **2020**, *12*, doi:10.3390/nu12103080.
10. Arnaud, M.J. Metabolism of Caffeine and Other Components of Coffee. *Caffeine, Coffee Heal.* **1993**, 43–95.
11. Somani, S.; Gupta, P. Caffeine: A New Look at an Age-Old Drug. *Int. J. Clin. Pharmacol. Ther. Toxicol.* **1988**, *26*, 521–533.
12. Carrillo, J.A.; Benitez, J. Clinically Significant Pharmacokinetic Interactions between Dietary Caffeine and Medications. *Clin. Pharmacokinet.* **2000**, *39*, 127–153, doi:10.2165/00003088-200039020-00004.
13. Sawynok, J.; Yaksh, T. Caffeine as an Analgesic Adjuvant: A Review of Pharmacology and Mechanisms of Action. *Pharmacol Rev* **1993**, *45*.
14. Arnaud, M.J. Pharmacokinetics and Metabolism of Natural Methylxanthines in Animal and Man. In *Handbook of Experimental Pharmacology*; 2011; Vol. 200, pp. 471–478 ISBN 9783642134425.
15. Arnaud, M. Comparative Metabolic Disposition of [1-Me14C] Caffeine in Rats , Mice , and Chinese Hamsters. **1985**, *13*.
16. Orrú, M.; Guitart, X.; Karcz-Kubicha, M.; Solinas, M.; Justinova, Z.; Barodia, S.K.; Zanoveli, J.; Cortes, A.; Lluis, C.; Casado, V.; et al. Psychostimulant Pharmacological Profile of Paraxanthine, the Main Metabolite of Caffeine in Humans. *Neuropharmacology* **2013**, *67*, 476–484, doi:10.1016/j.neuropharm.2012.11.029.
17. Committee on military nutrition research *Caffeine for the Sustainment of Mental Task Performance: Formulations for Military Operations*; NATIONAL ACADEMY PRESS, 2001; ISBN 978-0-309-08258-7.
18. Sørensen, K.K.; McCourt, P.; Berg, T.; Crossley, C.; Le Couteur, D.; Wake, K.; Smedsrød, B. The Scavenger Endothelial Cell: A New Player in Homeostasis and Immunity. *Am. J. Physiol. - Regul. Integr. Comp. Physiol.* **2012**, *303*, R1217-30, doi:10.1152/ajpregu.00686.2011.
19. Bhandari, S.; Larsen, A.K.; McCourt, P.; Smedsrød, B.; Sørensen, K.K. The Scavenger Function of Liver Sinusoidal Endothelial Cells in Health and Disease. *Front. Physiol.* **2021**, *12*, 1–23, doi:10.3389/fphys.2021.757469.
20. McCuskey, R.S. Morphological Mechanisms for Regulating Blood Flow through Hepatic Sinusoids. *Liver* **2000**, *20*, 3–7, doi:10.1034/j.1600-0676.2000.020001003.x.

21. Deleve, L.D. Liver Sinusoidal Endothelial Cells in Hepatic Fibrosis. *Hepatology* **2015**, *61*, 1740–1746, doi:10.1002/hep.27376.
22. Poisson, J.; Lemoinne, S.; Boulanger, C.; Durand, F.; Moreau, R.; Valla, D.; Rautou, P. Liver Sinusoidal Endothelial Cells: Physiology and Role in Liver Diseases. *J. Hepatol.* **2017**, *66*, 212–227, doi:10.1016/j.jhep.2016.07.009.
23. Braet, F.; Wisse, E. Structural and Functional Aspects of Liver Sinusoidal Endothelial Cell Fenestrae: A Review. *Comp. Hepatol.* **2002**, *1*, 1, doi:10.1186/1476-5926-1-1.
24. Szafranska, K.; Holte, C.F.; Kruse, L.D.; McCourt, P.; Zapotoczny, B. The WHole Story about Fenestrations in Liver Sinusoidal Endothelial Cells. *Front. Physiol.* **2021**, *12*, doi:doi: 10.3389/fphys.2021.735573.
25. Wisse, E. An Electron Microscopic Study of the Fenestrated Endothelial Lining of Rat Liver Sinusoids. *J. Ultrasructure Res.* **1970**, *31*, 125–150, doi:10.1016/S0022-5320(70)90150-4.
26. Wisse, E.; de Zanger, R.B.; Charels, K.; Van Der Smissen, P.; McCuskey, R.S. The Liver Sieve: Considerations Concerning the Structure and Function of Endothelial Fenestrae, the Sinusoidal Wall and the Space of Disse. *Hepatology* **1985**, *5*, 683–692, doi:10.1002/hep.1840050427.
27. Hunt, N.J.; Lockwood, G.P.; Warren, A.; Mao, H.; McCourt, P.A.G.; Le Couteur, D.G.; Cogger, V.C. Manipulating Fenestrations in Young and Old Liver Sinusoidal Endothelial Cells. *Am. J. Physiol. - Gastrointest. Liver Physiol.* **2019**, *316*, G144–G154, doi:10.1152/ajpgi.00179.2018.
28. Svistounov, D.; Warren, A.; Mcnerney, G.P.; Owen, D.M.; Zencak, D.; Le, D.G.; Zykova, S.N.; Crane, H.; Huser, T.; Quinn, R.J.; et al. The Relationship between Fenestrations, Sieve Plates and Rafts in Liver Sinusoidal Endothelial Cells. *PLoS One* **2012**, *7*, 1–9, doi:10.1371/journal.pone.0046134.
29. Xie, G.; Wang, X.; Wang, L.L.L.; Wang, L.L.L.; Atkinson, R.D.; Kanel, G.C.; Gaarde, W.A.; DeLeve, L.D. Role of Differentiation of Liver Sinusoidal Endothelial Cells in Progression and Regression of Hepatic Fibrosis in Rats. *Gastroenterology* **2012**, *142*, 918-927.e6, doi:10.1053/j.gastro.2011.12.017.
30. Gatmaitan, Z.; Varticovski, L.; Ling, L.; Mikkelsen, R.; Steffan, A.M.; Arias, I.M. Studies on Fenestral Contraction in Rat Liver Endothelial Cells in Culture. *Am. J. Pathol.* **1996**, *148*, 2027–2041.
31. Zapotoczny, B.; Szafranska, K.; Kus, E.; Braet, F.; Wisse, E.; Chlopicki, S.; Szymonski, M. Tracking Fenestrae Dynamics in Live Murine Liver Sinusoidal Endothelial Cells. *Hepatology* **2019**, *69*, 876–888, doi:10.1002/hep.30232.
32. Curatolo, P.; Robertson, D. The Health Consequences of Caffeine. *Ann. Intern. Med.* **1983**, *98*, 641–653, doi:https://doi.org/10.7326/0003-4819-98-5-641.
33. Nawrot, P.; Jordan, S.; Eastwood, J.; Rotstein, J.; Hugenholtz, A.; Feeley, M. Effects of Caffeine on Human Health. *Food Addit. Contam.* **2003**, *20*, 1–30, doi:10.1080/0265203021000007840.
34. Fredholm, B.B.; Bättig, K.; Holmén, J.; Nehlig, A.; Zvartau, E.E. Actions of Caffeine in the Brain with Special Reference to Factors That Contribute to Its Widespread Use. *Pharmacol Rev* **1999**, *51*.
35. Kulkarni, P.; Dorand, R. Caffeine Toxicity in a Neonate. *Pediatrics* **1979**, *64*, doi:10.1542/peds.64.2.254.
36. Sepkowitz, K.A. Energy Drinks and Caffeine-Related Adverse Effects. *JAMA - J. Am. Med. Assoc.* **2013**, *309*, 243–244, doi:10.1001/jama.2012.173526.
37. Cheng, W.S.C.; Murphy, T.L.; Smith, M.T.; Cooksley, W.G.E.; Halliday, J.W.; Powell, L.W. Dose-Dependent Pharmacokinetics of Caffeine in Humans: Relevance as a Test of Quantitative Liver Function. *Clin. Pharmacol. Ther.* **1990**, *47*, 516–524, doi:10.1038/clpt.1990.66.
38. Bonati, M.; Latini, R.; Galletti, F.; Young, J.; Tognoni, G.; Garattini, S. Caffeine Disposition after Oral Doses. *Clin. Pharmucol. Ther* **1982**, *32*, 98–106.
39. Blanchard, J.; Harvey, S.; Morgan, W. Variability of the Serum Protein Binding of Theophylline in Patients with Asthma and Cystic Fibrosis. *Br. J. Clin. Pharmacol.* **1992**, *33*, 653–656, doi:10.1111/j.1365-2125.1992.tb04096.x.
40. Rowe, D.J.F.; Watson, I.D.; Williams, J.; Berry, D.J. The Clinical Use and Measurement of Theophylline. *Ann. Clin. Biochem.* **1988**, *25*, 4–26, doi:10.1177/000456328802500102.
41. Geib, A.-J. Theophylline and Other Methylxanthines. In *Critical Care Toxicology: Diagnosis and Management of the Critically*

Poisoned Patient; 2017; pp. 1–3058 ISBN 9783319179001.

42. Baggott, M.J.; Childs, E.; Hart, A.B.; De Bruin, E.; Palmer, A.A.; Wilkinson, J.E.; De Wit, H. Psychopharmacology of Theobromine in Healthy Volunteers. *Psychopharmacology (Berl).* **2013**, *228*, 109–118, doi:10.1007/s00213-013-3021-0.
43. Mayorga-Gross, A.L.; Esquivel, P. Impact of Cocoa Products Intake on Plasma and Urine Metabolites: A Review of Targeted and Non-Targeted Studies in Humans. *Nutrients* **2019**, *11*, doi:10.3390/nu11051163.
44. Mumford, G.K.; Benowitz, N.L.; Evans, S.M.; Kaminski, B.J.; Preston, K.L.; Sannerud, C.A.; Silverman, K.; Griffiths, R.R. Absorption Rate of Methylxanthines Following Capsules, Cola and Chocolate. *Eur. J. Clin. Pharmacol.* **1996**, *51*, 319–325, doi:10.1007/s002280050205.
45. Resman, B.H.; Blumenthal, H.P.; Jusko, W.J. Breast Milk Distribution of Theobromine from Chocolate. *Pediatr. Pharmacol. Ther.* **1977**, *97*, 477–480, doi:10.1016/S0022-3476(77)81329-2.
46. Smedsrød, B.; Pertoft, H. Preparation of Pure Hepatocytes and Reticuloendothelial Cells in High Yield from a Single Rat Liver by Means of Percoll Centrifugation and Selective Adherence. *J. Leukoc. Biol.* **1985**, *38*, 213–230, doi:10.1002/jlb.38.2.213.
47. Mönkemöller, V.; Mao, H.; Hübner, W.; Dumitriu, G.; Heimann, P.; Levy, G.; Huser, T.; Kaltschmidt, B.; Kaltschmidt, C.; Øie, C.I. Primary Rat LSECs Preserve Their Characteristic Phenotype after Cryopreservation. *Sci. Rep.* **2018**, *8*, 1–10, doi:10.1038/s41598-018-32103-z.
48. Mao, H.; Diekmann, R.; Liang, H.P.H.; Cogger, V.C.; Le Couteur, D.G.; Lockwood, G.P.; Hunt, N.J.; Schüttpelz, M.; Huser, T.R.; Chen, V.M.; et al. Cost-Efficient Nanoscopy Reveals Nanoscale Architecture of Liver Cells and Platelets. *Nanophotonics* **2019**, *8*, 1299–1313, doi:10.1515/nanoph-2019-0066.
49. Szafranska, K.; Holte, C.F.; Kruse, L.D.; Mao, H.; Øie, C.I.; Szymonski, M.; Zapotoczny, B.; McCourt, P.A.G. Quantitative Analysis Methods for Studying Fenestrations in Liver Sinusoidal Endothelial Cells. A Comparative Study. *Micron* **2021**, 103121, doi:https://doi.org/10.1016/j.micron.2021.103121.
50. Blomhoff, R.; Eskild, W.; Berg, T. Endocytosis of Formaldehyde-Treated Serum Albumin via Scavenger Pathway in Liver Endothelial Cells. *Biochem. J.* **1984**, *218*, 81–86, doi:10.1042/bj2180081.
51. Schindelin, J.; Arganda-Carreras, I.; Frise, E.; Kaynig, V.; Longair, M.; Pietzsch, T.; Preibisch, S.; Rueden, C.; Saalfeld, S.; Schmid, B.; et al. Fiji: An Open-Source Platform for Biological-Image Analysis. *Nat. Methods* **2012**, *9*, 676–682.
52. Simon-Santamaria, J.; Malovic, I.; Warren, A.; Oteiza, A.; Le Couteur, D.; Smedsrod, B.; McCourt, P.; Sorensen, K.K. Age-Related Changes in Scavenger Receptor-Mediated Endocytosis in Rat Liver Sinusoidal Endothelial Cells. *Journals Gerontol. Ser. a-Biological Sci. Med. Sci.* **2010**, *65*, 951–960, doi:DOI 10.1093/gerona/glq108.
53. Wisse, E.; Van Dierendonck, J.H.; De Zanger, R.B.; Fraser, R.; McCuskey, R.S. On the Role of the Liver Endothelial Filter in the Transport of Particulate Fat (Chylomicrons and Their Remnants) to Parenchymal Cells and the Influence of Certain Hormones on the Endothelial Fenestrae. **1980**, 195–200.
54. Fraser, R.; Cogger, V.C.; Dobbs, B.; Jamieson, H.; Warren, A.; Hilmer, S.N.; Le Couteur, D.G. The Liver Sieve and Atherosclerosis. *Pathology* **2012**, *44*, 181–186, doi:10.1097/PAT.0b013e328351bcc8.
55. Fraser, R.; Dobbs, B.R.; Rogers, G.W.T. Lipoproteins and the Liver Sieve: The Role of the Fenestrated Sinusoidal Endothelium in Lipoprotein Metabolism, Atherosclerosis, and Cirrhosis. *Hepatology* **1995**, *21*, 863–874, doi:10.1016/0270-9139(95)90542-1.
56. Jacobs, F.; Gordts, S.C.; Muthuramu, I.; De Geest, B. The Liver as a Target Organ for Gene Therapy: State of the Art, Challenges, and Future Perspectives. *Pharmaceuticals* **2012**, *5*, 1372–1392, doi:10.3390/ph5121372.
57. Wright, P.L.; Smith, K.F.; Day, W.A.; Fraser, R. Small Liver Fenestrae May Explain the Susceptibility of Rabbits to Atherosclerosis. **1983**.
58. Fraser, R.; Clark, S.A.; Bowler, L.M.; Murray, F.E.M.; Wakasugi, J.; Ishihara, M.; Tomikawa, M. The Opposite Effects of Nicotine and Pantethine on the Porosity of the Liver Sieve and Lipoprotein Metabolism. *Kupffer Cell Found. Cells Hepatic Sinusoid, Vol. 2* **1989**, 335.
59. Szafrańska, K. From Fixed-Dried to Wet-Fixed to Live – Comparative Super-Resolution Microscopy of Fenestrations in Liver Sinusoidal Endothelial Cells in Vitro. **2021**, *4*, 6.

60. Gileta, A.F.; Fitzpatrick, C.J.; Chitre, A.S.; St. Pierre, C.L.; Joyce, E. V.; Maguire, R.J.; McLeod, A.M.; Gonzales, N.M.; Williams, A.E.; Morrow, J.D.; et al. Genetic Characterization of Outbred Sprague Dawley Rats and Utility for Genome-Wide Association Studies. *bioRxiv* **2018**, 0–61, doi:10.1101/412924.
61. Nehlig, A. Interindividual Differences in Caffeine Metabolism and Factors Driving Caffeine Consumption. *Pharmacol. Rev.* **2018**, *70*, 384–411, doi:10.1124/pr.117.014407.
62. Bhandari, S.; Li, R.; Simón-Santamaría, J.; McCourt, P.; Johansen, S.D.; Smedsrød, B.; Martinez-Zubiaurre, I.; Sørensen, K.K. Transcriptome and Proteome Profiling Reveal Complementary Scavenger and Immune Features of Rat Liver Sinusoidal Endothelial Cells and Liver Macrophages. *BMC Mol. Cell Biol.* **2020**, *21*, 1–25, doi:10.21203/rs.2.24396/v1.
63. Van Staveren, W.C.G.; Markerink-van Ittersum, M.; Steinbusch, H.W.M.; De Vente, J. The Effects of Phosphodiesterase Inhibition on Cyclic GMP and Cyclic AMP Accumulation in the Hippocampus of the Rat. *Brain Res.* **2001**, *888*, 275–286, doi:10.1016/S0006-8993(00)03081-X.
64. Schultz, C.; Vaskinn, S.; Kildalsen, H.; Sager, G. Cyclic AMP Stimulates the Cyclic GMP Egression Pump in Human Erythrocytes: Effects of Probenecid, Verapamil, Progesterone, Theophylline, IBMX, Forskolin, and Cyclic AMP on Cyclic GMP Uptake and Association to inside-out Vesicles. *Biochemistry* **1998**, *37*, 1161–1166, doi:10.1021/bi9713409.
65. Benowitz, N.L.; Jacob, P.; Mayan, H.; Denaro, C. Sympathomimetic Effects of Paraxanthine and Caffeine in Humans. *Clin. Pharmacol. Ther.* **1995**, *58*, 684–691, doi:10.1016/0009-9236(95)90025-X.
66. Mandili, G.; Alchera, E.; Merlin, S.; Imarisio, C.; Chandrashekar, B.R.; Riganti, C.; Bianchi, A.; Novelli, F.; Follenzi, A.; Carini, R. Mouse Hepatocytes and LSEC Proteome Reveal Novel Mechanisms of Ischemia/Reperfusion Damage and Protection by A2aR Stimulation. *J. Hepatol.* **2015**, *62*, 573–580, doi:10.1016/j.jhep.2014.10.007.
67. Le Couteur, D.G.; Fraser, R.; Hilmer, S.; Rivory, L.P.; McLean, A.J. The Hepatic Sinusoid in Aging and Cirrhosis: Effects on Hepatic Substrate Disposition and Drug Clearance. *Clin. Pharmacokinet.* **2005**, *44*, 187–200, doi:10.2165/00003088-200544020-00004.
68. Midão, L.; Giardini, A.; Menditto, E.; Kardas, P.; Costa, E. Polypharmacy Prevalence among Older Adults Based on the Survey of Health, Ageing and Retirement in Europe. *Arch. Gerontol. Geriatr.* **2018**, *78*, 213–220, doi:10.1016/j.archger.2018.06.018.
69. Sano, N.; Tamura, T.; Toriyabe, N.; Nowatari, T.; Nakayama, K.; Tanoi, T.; Murata, S.; Sakurai, Y.; Hyodo, M.; Fukunaga, K.; et al. New Drug Delivery System for Liver Sinusoidal Endothelial Cells for Ischemia-Reperfusion Injury. *World J. Gastroenterol.* **2015**, *21*, 12778–12786, doi:10.3748/wjg.v21.i45.12778.
70. Hunt, N.J.; Lockwood, G.P.; Le Couteur, F.H.; McCourt, P.A.G.; Singla, N.; Kang, S.W.S.; Burgess, A.; Kuncic, Z.; Le Couteur, D.G.; Cogger, V.C. Rapid Intestinal Uptake and Targeted Delivery to the Liver Endothelium Using Orally Administered Silver Sulfide Quantum Dots. *ACS Nano* **2020**, *14*, 1492–1507, doi:10.1021/acsnano.9b06071.

Supplementary information

S1. Fenestration size distributions

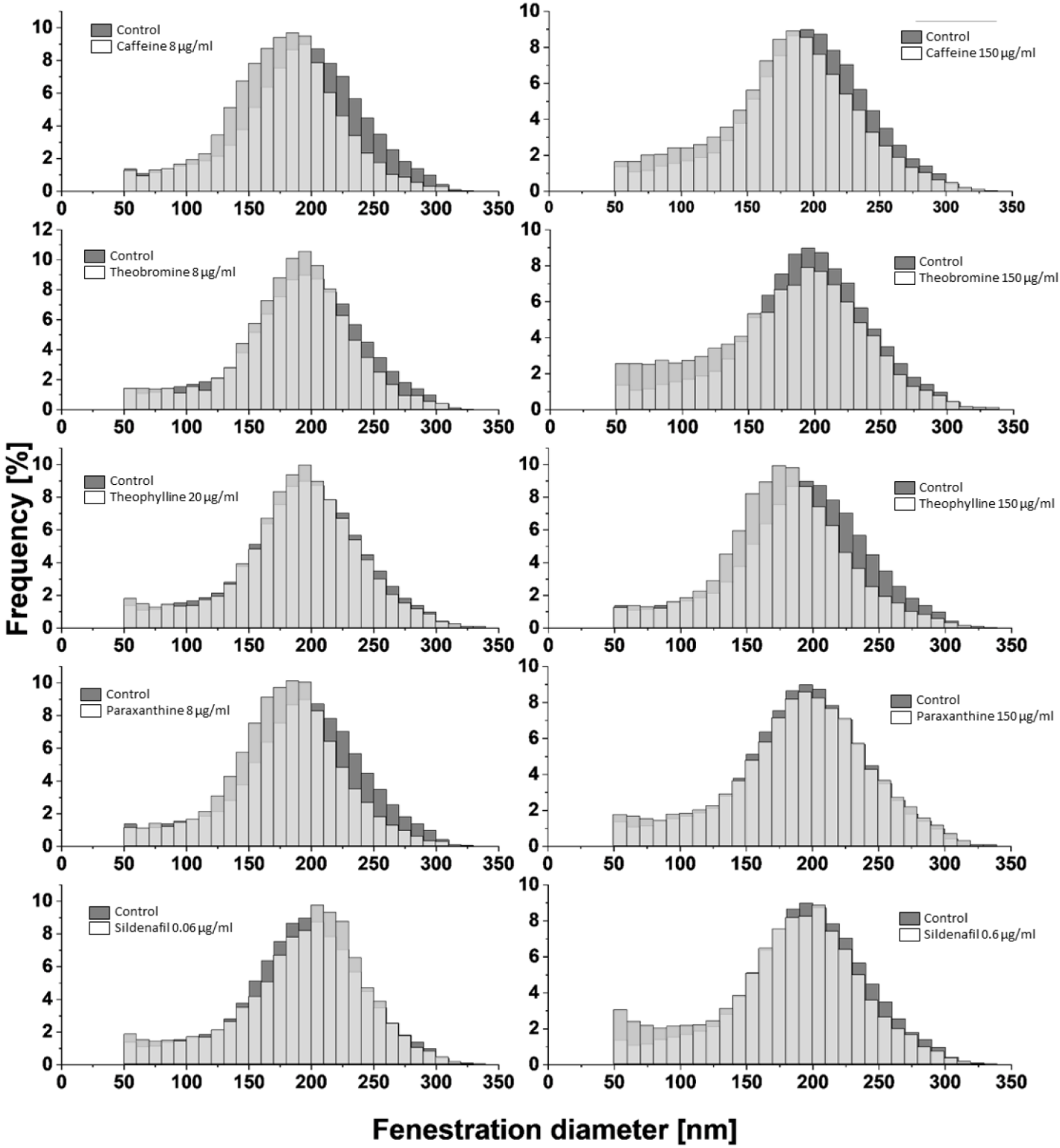

Figure S1. Distribution of fenestration size after treatments in comparison with the control/untreated samples

S2. Image analysis data

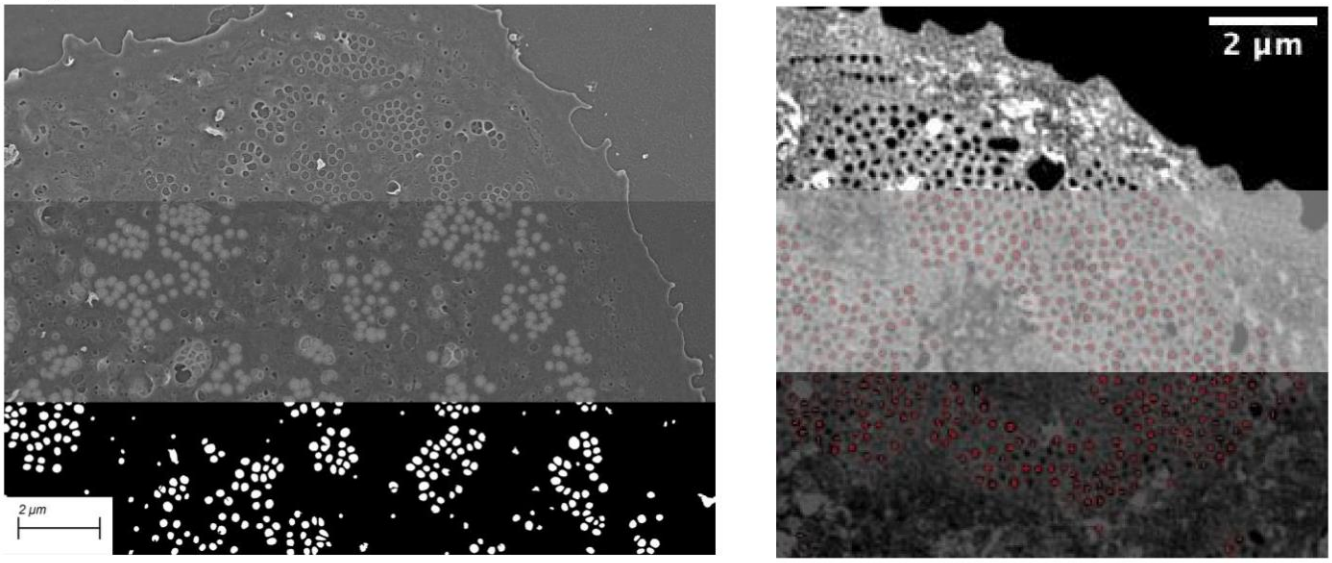

Figure S2. Examples of the images used for measurement of fenestration diameters. The top part is a raw SEM(left)/SIM(right) image, bottom part presents the binary mask used for quantitative analysis, and the middle part shows the overlay used to identify fenestrations.